

Optogenetic chloride loading in neurons: implications for epilepsy

Hannah Alfonsa

Thesis submitted for the degree of
Doctor of Philosophy

Institute of Neuroscience
Newcastle University

February, 2015

Abstract

Altered inhibitory function is an important facet of epileptic pathology. A key concept is that GABAergic activity can become excitatory, if intraneuronal chloride $[Cl^-]_i$ rises. It has proved difficult, however, to separate out the role of raised $[Cl^-]_i$ from other contributory factors in complex network phenomena such as epileptic pathology. To address this, in this thesis I used Halorhodopsin to load clusters of pyramidal cells artificially with Cl^- , to explore the implication of raised $[Cl^-]_i$ in the generation of epileptic activity and seizure initiation.

Brief Halorhodopsin activation caused substantial positive shifts in the GABAergic reversal potential (E_{GABA}). At the network level, these positive shifts in E_{GABA} produced a transient rise in network excitability, with many distinctive features of epileptic foci, including high frequency oscillations with evidence of out-of-phase firing. Such firing patterns can arise from quite small shifts in the mean $[Cl^-]_i$ level, within heterogeneous neuronal populations. Notably, however, chloride-loading by itself did not trigger full ictal events, even with additional electrical stimulation to the underlying white matter. In contrast, when performed in combination with low, sub-epileptic levels of 4-aminopyridine, Halorhodopsin activation rapidly induced full ictal activity. These results suggest that in vitro, chloride-loading has an adjunctive role in ictogenesis.

Additionally, in this thesis an optogenetic approach to extrude Cl^- was also explored, as a potential way to correct the raised $[Cl^-]_i$ issue in epilepsy. A strategy that was proved to be successful was the combination of ArchaeorhodopsinT (ArchT) hyperpolarizing effect and the opening of light activated Cl^- channel (ChloC), which together provides a driving force and a conductance for an outward Cl^- flow. Co-activation of the two opsins consistently induced a negative shift in E_{GABA} indicative of Cl^- extrusion mechanism, which in the future could be tested as a new optogenetic approach to control epilepsy.

Acknowledgment

My biggest thanks to my supervisor Dr. Andrew J. Trevelyan, the one who introduced me to the Neuroscience world, who has been my biggest inspiration, and who made me fall in love with this field. Thanks for the brilliant PhD project ideas, limitless support, and guidance for these last 4 years. I never knew science could be fun until I met you. Thanks for members of Trevelyan's lab (Dr. Ryley Parrish, Dr. Rolando Berlinguer-Palmini, Neela Codadu, Partow Yazdani, Christoforos Papasavvas, Edward Merricks, and Emma Craddock), who have been a family to me in the UK. Thank you for the constant encouragement and for making these 4 years not only educative but also fun. Special thanks to Neela Codadu, the one who has spent really long hours, chatting and working with me in the lab, to make things work. I will not have made it without you.

I also like to thank Professor Robert Lightowlers who has always been the best advisor for the molecular biology part of the project, who always been happy to proof read all the cDNA sequence of every constructs and to Professor Jeremy Lakey who has been my main source of knowledge about protein structure. Thank you for teaching me that science is not only about positive results but more importantly is about addressing scientific questions appropriately. Thank you for Dr. Claudia Racca, who enthusiastically taught me how to do immunolabelling. All the pretty pictures in this thesis are especially dedicated for you. Thank you for teaching me to always be passionate in what you do. I would like to thank the Institute of Neuroscience Newcastle University, for funding me throughout my PhD, thanks for the big opportunity. Thank you for Dr. Elizabeth Stoll for helping me with the virus making, for Dr. Richard McQuade for helping me with the injection process, and for Dr. Mark Cunningham for helping us setting up the interface chamber rig. Thank you for sharing the tips and tricks, this project would have been far more difficult otherwise.

Last but not least, thank you for my parents, my sister and my brother, who always get my back, and who always believe in me. Also big thanks for Dr. Andrei Ilie, for all the stimulating conversation we had for these last 3 years. You have been the cure for my lack of confidence. Thank you, you made me fall in love even more deeply with Neuroscience.

Table of Contents

Abstract.....	ii
Acknowledgment	iii
Table of Contents	iv
List of figures	viii
Chapter 1. Introduction.....	1
1.1 GABA inhibition at a single neuron level.....	3
1.2 Chloride regulation at neuronal level.....	5
1.2.1 Chloride-coupled co-transporters' activity regulate intraneuronal Cl ⁻ level	6
1.2.2 Developmental shift from depolarizing GABA to hyperpolarizing GABA ...	6
1.2.3 Possible effect of local impermeant anions in regulating intraneuronal Cl ⁻	7
1.2.4 Activity dependent disinhibition	8
1.2.5 Summary	9
1.3 The main inhibitory interneurons in the cortex	9
1.3.1 Somatostatin positive interneuron	10
1.3.2 Parvalbumin positive interneuron	10
1.4 The role of PV interneurons in gamma-oscillation.....	11
1.5 Altered inhibition function in Epilepsy	12
1.5.1 Depletion of GABA neurotransmitter	12
1.5.2 Depolarization block of interneurons	12
1.5.3 Raised intraneuronal Cl ⁻	13
1.6 Raised intraneuronal chloride in Epilepsy	13
1.6.1 Increased Cl ⁻ uptake by NKCC1	13
1.6.2 Reduced Cl ⁻ extrusion by KCC2.....	14
1.6.3 Cl ⁻ accumulation due to intense GABA _A activation	14
1.6.4 High intraneuronal Cl ⁻ and depolarizing GABA contributes to the generation of epileptic afterdischarge.....	15

1.6.5	Summary	15
1.7	The need for new treatment	16
1.8	Optogenetics	17
1.9	Optogenetics in epilepsy	19
1.10	The rationale of this thesis	22
1.11	The aim of this thesis	23
Chapter 2. Material and methods		24
2.1	Dissociated neuronal culture	24
2.2	Calcium phosphate transfection	24
2.3	Lentivirus Production and Transfection	25
2.4	Electroporation.....	26
2.5	Patch clamp experiments	27
2.5.1.	Whole cell patch.....	27
2.5.2.	Perforated gramicidin patch	27
2.6	Cortical expression of optogenetic proteins	30
2.7	Brain slices experiments.....	31
2.8	Optogenetic illumination.....	32
2.9	Molecular biology.....	33
2.9.1.	Enzyme digestion	33
2.9.2.	Electrophoresis.....	33
2.9.3.	Ligation.....	33
2.9.4.	Bacterial transformation	34
2.9.5.	Plasmid prep.....	34
2.9.6.	Different constructs preparation	35
2.10	Immunofluorescence staining	37
2.11	Analysis	37
2.11.1.	E_{GABA} measurement	37
2.11.2.	Afterdischarge terminating oscillation.....	38
2.11.3.	Assessment of GABA modulation in I_{Clamp} recording	38
Chapter 3. Characterisation of halorhodopsin chloride pump		39
3.1	Introduction.....	39
3.2	Results	40
3.2.1	Halorhodopsin activation causes a transient chloride loading effect	40

3.2.2	Blue light stabilizes halorhodopsin current	45
3.2.3	Designing HR illumination system for field recording in the interface chamber	49
3.3	Discussion	53
3.4	Summary.....	56
Chapter 4.	Characteristics of epileptic network activity arising from raised intraneuronal chloride	57
4.1.	Introduction.....	57
4.1.1.	High frequency activity in epileptic networks.....	57
4.1.2.	Seizure termination.....	58
4.2.	Methods	60
4.2.1.	High frequency oscillation analysis	60
Control analysis for spectral leak	61	
4.2.2.....		61
4.3.	Results	63
4.3.1.	Raised intraneuronal chloride induces high frequency oscillation.....	63
4.3.2.	In a pro-epileptic state focal raised intraneuronal chloride initiates ictal activity	75
4.3.3.	Characteristic seizure terminating pattern.....	78
4.4.	Discussion	83
4.4.1.	HR chloride loading as a model for high $[Cl^-]_i$	83
4.4.2.	Heterogeneity of $[Cl^-]_i$ explains the out-of-phase firing in the HFO.....	84
4.4.3.	HR Cl^- loading and how ictogenic it is	87
4.4.4.	Afterdischarge terminating oscillation	90
Chapter 5.	Designing a new optogenetic tool to correct raised intraneuronal chloride in epilepsy	92
5.1.	Introduction.....	92
5.1.1.	Reversal of light activated Cl^- pump - Halorhodopsin.....	92
5.1.2.	Light activated Cl^- channel: iClC2 and ChloC.....	99
5.2.	Results	101
5.2.1.	The effect of Cl^- concentration gradient on HR current	101
5.2.2.	The reversal of HR by altering the distribution of charged residues	102
5.2.3.	Reversion of HR by protein anchoring	109
5.2.4.	Co-expression of light activated Cl^- channel and ArchT to extrude Cl^- ...	112

5.3. Discussion	131
5.3.1. Attempts to reverse the orientation of HR	131
5.3.2. Light activated Cl ⁻ channel as a tool to extrude Cl ⁻	132
5.3.3. Reverse HR strategy versus ArchT-ChloC co-activation strategy.....	138
Chapter 6. General Discussion	140
6.1. Summary of experimental findings	140
6.2. HR chloride loading effect as a model of raised intraneuronal chloride	142
6.3. The role of raised [Cl ⁻] _i in generation of high frequency oscillation	143
6.4. The adjunctive role of raised [Cl ⁻] _i in seizure initiation	148
6.5. After discharge terminating oscillation	150
6.6. The use of HR to control epilepsy	155
6.7. A novel use of optogenetic tools to extrude Cl ⁻	156
6.8. The prospect of gene therapy and optogenetics as a treatment for epilepsy 160	
6.9. Conclusion	163
Appendix	164
Sequence of ChloC-T2A-ArchT_GFP.....	164
References.....	165

List of figures

Figure 1.1 Chloride regulations in immature and mature neurons.	7
Figure 1.2 Different excitatory and inhibitory optogenetic proteins.	18
Figure 2.1 Voltage ramps protocol to measure GABA reversal potential.	29
Figure 2.2 Tetrode configuration of extracellular electrodes – from Neuronexus.	32
Figure 3.1 Halorhodopsin chloride loading effect.	41
Figure 3.2 Estimation of the changes in $[Cl^-]_i$ induced by HR activation.....	42
Figure 3.3 HR Cl^- loading effect in acute brain slices taken from adult mice.	43
Figure 3.4 Furosemide prolonged the decay of HR chloride loading effect.	44
Figure 3.5 Intermittent illumination of blue and orange light optimizes HR Cl^- loading effect.	47
Figure 3.6 Co-illumination of both 561 nm and 491nm light optimizes halorhodopsin current.....	48
Figure 3.7 Network activity recording arrangement.	50
Figure 3.8 Halorhodopsin current suppresses electrically evoked event.....	52
Figure 4.1 Measurement of half-width indices to quantify the increased jitter and out-of-phase firing.	61
Figure 4.2 Spectral leak from a delta-function.	62
Figure 4.3 Experimental protocols for HR priming and ArchT priming.....	63
Figure 4.4 Halorhodopsin chloride loading induced high frequency oscillations.....	65
Figure 4.5 Frequency analysis of HR-priming versus ArchT-priming experiments.....	66
Figure 4.6 When expressed under synapsin promoter, HR priming failed to induce high frequency oscillation.	67
Figure 4.7 HR priming failed to induce high frequency oscillation in the presence of 100 μ M furosemide.....	68
Figure 4.8 Neuronal Cl^- loading triggered out-of-phase firing during spontaneous bursts of activity.....	69
Figure 4.9 Different spike time distributions of HR priming data sets.	71
Figure 4.10 Half-width indices from baseline, HR primed, and ArchT primed periods. .	72
Figure 4.11 Control analyses for spectral leak: spike amputation and time shifted.	73
Figure 4.12 Spike time histograms and half-width indices derived after control analyses.	74

Figure 4.13 Epileptic escalation by HR priming in the presence of 20 μ M 4-AP.	76
Figure 4.14 Rapid ictal event induction by HR priming in conjunction with 20 μ M 4-AP.	77
Figure 4.15 Afterdischarge terminating oscillation (ATO).	78
Figure 4.16 ATO was recorded following a long series of repeated HR priming, and is associated with a subsequent period of neuronal suppression.	80
Figure 4.17 ATO was initiated in the Cl^- loaded area.	81
Figure 4.18 Propagation of HR priming induced ictal discharge and the associated ATO.	82
Figure 4.19 Heterogeneity in levels of intracellular Cl^- can explain the appearance of out-of-phase population firing.	86
Figure 5.1 Altering the distribution of charged residues strategy.	95
Figure 5.2 Protein anchoring strategy.	98
Figure 5.3 The size of HR current is affected by chloride concentration.	102
Figure 5.4 Charged amino acid substitutions of HR to reverse its orientation.	104
Figure 5.5 mutHR-EYFP and mutHR-IRES-EYFP expression and electrophysiology recording.	108
Figure 5.6 Expression of lepA-GFP-HR construct.	109
Figure 5.7 Neuronal expression of CD8-GFP, CD8-GFP-HR, and CD8-HR-IRES-EYFP.	110
Figure 5.8 Immunofluorescence staining against HR in CD8-GFP-HR and CD8-HR-IRES-GFP construct.	111
Figure 5.9 Whole cell recording of i_{ClC2} and slow-ChloC light activated current.	112
Figure 5.10 Co-expression of slowChloC and ArchT on dissociated neuronal culture.	113
Figure 5.11 Co-activation of slowChloC and ArchT induced a negative shift in E_{GABA}	114
Figure 5.12 Transient effect of ArchT-ChloC co-activation in extruding Cl^-	116
Figure 5.13 Pooled data of E_{GABA} shift introduced by co-activation of ArchT-ChloC.	117
Figure 5.14 Co-expression of ChloC and ArchT on dissociated neuronal culture.	118
Figure 5.15 Protocol to assess the Cl^- clearance effect of ChloC-ArchT Cl^- when cells were Cl^- loaded prior to the optogenetic activation.	119
Figure 5.16 Hyperpolarizing and depolarizing initial E_{GABA} gave a different effect on the successive E_{GABA} during repetitive activation of GABA_A receptor.	120
Figure 5.17 Co-activation of ChloC and ArchT rescued the E_{GABA} to a more hyperpolarised level post repetitive GABA activation.	122

Figure 5.18 E_{GABA} measurements for baseline, post repetitive GABA activation, and with optogenetic activation of ArchT and ChloC.	123
Figure 5.19 Activation of ArchT or ChloC alone does not induce a negative shift in E_{GABA} in a mature neuron.	124
Figure 5.20 Co-expression of ChloC and ArchT using 2A peptide technique.	127
Figure 5.21 Pooled data of E_{GABA} shift by light activation from cells transfected with ChloC-2A-ArchT_GFP.....	127
Figure 5.22 Current clamp recording of ChloC-ArchT co-activation effect on GABA activity using the T2A co-expression system.	129
Figure 5.23 Pooled data of current clamp recording showing GABA modulation by ChloC-ArchT co-activation expressed using T2A peptide system.....	130
Figure 5.24 Co-expression of ChloC and Arch to extrude chloride.....	136
Figure 6.1 Striking resemblance between spontaneous epileptic HFO and HR priming tissue.	144
Figure 6.2 Hypothetical underlying mechanism of ATO that terminates an ictal discharge.	153
Table 5-1 Amino acids sequence of wild-type HR and 4 different mutants HR. Amino acid substitutions and insertions introduced by site-directed mutagenesis are shown in red.	105

Chapter 1. Introduction

The brain is one of the most complex machineries ever to have existed, comprising over 100 billion neurons, each making hundreds to thousands of connections to other neurons (Shepherd, 2004; Buzsaki, 2006). It is only fair to begin with a sincere acknowledgment that there is too much that we do not yet understand. To begin teasing apart how a complex system works, there is not much option than to start with investigating the simpler components of the system. All brain functions ultimately depend on the processing at the level of neuronal networks and single neurons, where there is a permanent interplay between excitation and inhibition. This is mediated by excitatory and inhibitory neurotransmitters respectively; with glutamate being the main excitatory one and gamma amino butyric acid (GABA) and glycine being the main inhibitory ones. Excitatory neurotransmitters are released by the principal cells that account for approximately 80% of the neuronal population in cortical networks, whereas the inhibitory neurotransmitters are released mainly by the remaining 20% of the population called the interneurons (Hendry *et al.*, 1987).

Healthy brain function requires precise combinations and adequate levels of both excitation and inhibition. When precise interplay between excitation and inhibition breaks down, pathological states can arise, such as an epileptic seizure. The International League Against Epilepsy (ILAE) defines an epileptic seizure as a transient occurrence of signs and or symptoms due to abnormal excessive or synchronous neuronal activity in the brain (Fisher *et al.*, 2014). Epileptic seizures have been extensively described and studied from as early as the 17th century by prominent neurologists and scientists such as John Hughlings Jackson (Jackson, 1879). However, even today, how an epileptic seizure is initiated and terminated is still a puzzling question without a definitive answer. A more comprehensive understanding of these phenomena is still acutely needed as this might help the development of new treatment options for the approximately 30% of patients with epilepsy, who remain resistant to current anti-epileptic medication (Moshé *et al.*, 2014).

One of the most important facets of epilepsy pathophysiology is the altered GABA inhibition as the main mechanism that controls the spread of activity in the brain. Fast-acting GABA inhibition works by opening GABA_A channels that are mainly permeable to Cl⁻. Consequently Cl⁻ distribution across the membrane becomes an important determinant of GABA inhibitory activity. There is an increasing evidence showing that Cl⁻ dysregulation could be a key pathology in epilepsy (Huberfeld *et al.*, 2007c; Ellender *et al.*, 2014; Pallud *et al.*, 2014). Accordingly, studying the role of Cl⁻ in the modulation of GABA inhibitory activity, both at the neuronal level and at the network level, could provide an important insight into understanding how epileptic seizures are initiated.

Considering the involvement of Cl⁻ dysregulation in epilepsy, a way to manipulate neuronal Cl⁻ concentration is desired, both as a research tool, but also as a possible way to control epileptic seizures. To achieve this, the potential use of different optogenetic proteins will be explored. Optogenetics is a technique that allows cell-type specific manipulation of neuronal activity using light. This is made possible by expressing channels or pumps of bacterial or algae origin, which are activated by light (Deisseroth *et al.*, 2006). This technique has allowed neuroscientists to artificially trigger a depolarizing or hyperpolarizing current in a neuron or neuronal population using light activation.

I will start this chapter by describing how GABA inhibition works in the brain and how Cl⁻ regulation is such an important determinant for GABAergic activity. I will also describe how alterations in Cl⁻ regulation have been linked to hyperexcitability states in the epileptic brain. I will then review the potential use of optogenetics as a way of controlling epileptic seizure activity. Lastly I will list the aims of my PhD project, which will be explored in the following chapters of this thesis.

1.1 GABA inhibition at a single neuron level

GABA neurotransmitter is produced and released by inhibitory interneurons pre-synaptically. GABA will then bind to its receptors in the post-synaptic cells and induce a conformational change in the receptors necessary to conduct ionic flow. GABA mainly affects 2 different types of receptors, namely GABA_A and GABA_B. GABA inhibitory activity via GABA_A receptors works in 2 different modes of action: fast-acting and tonic inhibition. Fast-acting inhibition is exerted by the opening of GABA_A receptors that are expressed at the synapses. The GABA_A receptor is a ligand operated ion channel, mainly permeable to Cl⁻ and to a lesser extent to bicarbonate (HCO₃⁻) (Bormann *et al.*, 1987). GABA_A activation at the synapse allows a sudden flow of Cl⁻ into the cells that generate an instantaneous inhibitory post-synaptic potential (IPSP) (Nicoll *et al.*, 1990). In contrast, tonic inhibition is mediated by the opening of extra-synaptic GABA_A receptors, which gives rise to a tonic current that influences the basal excitability of the cells over long time scales (Farrant & Nusser, 2005). Additionally, GABA can also activate extra synaptic GABA_B receptors, which are G-protein coupled receptors (Bowery *et al.*, 1980; Craig & McBain, 2014). GABA activation of GABA_B receptors reduces cell excitability both pre-synaptically and post-synaptically. This is mediated by the inhibition of voltage-gated calcium channel that consequently reduces neurotransmitter release from the pre-synaptic neuron and by activation of inward rectifying potassium channels on the post-synaptic neuron (Gassmann & Bettler, 2012; Craig & McBain, 2014).

Fast-acting GABA_A-mediated inhibition has 2 facets of inhibitory effect namely shunting inhibition and hyperpolarising inhibition. The shunting inhibition effect on post-synaptic neurons is mainly due to the reduction of the membrane input resistance by GABA_A channels opening, which makes the cell membrane more 'leaky' and hence 'short-circuiting' the incoming excitatory input to the cell (Coombs *et al.*, 1955; Staley & Mody, 1992). In contrast, the hyperpolarising effect of GABA is due to the anion inward flow that brings the membrane potential to a more negative level, hence more excitation is needed to depolarise the cell (Kahle *et al.*, 2008). This could be measured as the inhibitory postsynaptic current (IPSC) that based on the Ohm's law is equal to V/R , which can also be formulated as a function of conductance (g_{IPSC}) x driving force (Jack *et al.*, 1975).

$$IPSC = g_{IPSC} \times \text{driving force}$$

$$\text{driving force} = E_m - E_{GABA}$$

The strength of GABA hyperpolarising current (IPSC) is therefore directly proportional to the g_{IPSC} and the driving force for its corresponding permeable ion. The g_{IPSC} represents the individual conductance for each GABA_A receptors and the number of GABA_A channels opening at the membrane that is affected by 3 factors: the number of neurotransmitter molecules released pre-synaptically, the number of functional channels expressed post-synaptically, and the sensitivity of the channel to its ligand (Thompson & Gahwiler, 1989b). The driving force for GABA on the other hand is set by the electrochemical gradient for the main permeable ions, namely Cl⁻. This could be calculated as the difference between the membrane potential (E_m) and the Cl⁻ reversal potential (E_{Cl^-}) (Thompson & Gahwiler, 1989a).

By definition, ion reversal potential is the point of equilibrium for both ion fluxes driven by concentration gradient and electric charge gradient, whereby no net ion flux will take place and this follows the thermodynamics principle as described in the Nernst equation. The two variables involve in the Nernst equation are the temperature and the ratio between ion outside and inside the cell. As temperature tends to remain constant, the ion reversal potential is mostly dependent on the distribution of ions inside and outside the cell.

$$E_{ion} = \frac{RT}{zF} \log e \frac{[ion \text{ outside cell}]}{[ion \text{ inside cell}]}$$

R = universal gas constant, T = temperature (K),

z = valence of the ionic species, F = Faraday's constant

Accordingly, the driving force of GABA activity is therefore largely affected by the basal distribution of Cl^- inside and outside the cell. It should be noted however that the GABA_A channel is also permeable to HCO_3^- hence $E_{\text{HCO}_3^-}$ also has an effect on the GABA activity. In mature neurons $E_{\text{HCO}_3^-}$ is around -10 mV and this is due to a nearly unlimited supply of HCO_3^- within the neuron that is dependent on the carbonic anhydrase (CA) activity, as part of the pH buffer mechanism of the cell (Kaila *et al.*, 1993; Rivera *et al.*, 2005). Extracellularly, HCO_3^- concentration is relatively low, favouring an outward flow of the ion. Despite the bicarbonate depolarising reversal potential, GABA is still very often hyperpolarising as GABA_A channels is permeable to chloride 3.3-5 times more than to bicarbonate (Bormann *et al.*, 1987), and since Cl^- tends to be kept low inside the cells and high outside, it gives a relatively hyperpolarising reversal potential. Interestingly when CA is blocked, reducing the outward flow of bicarbonate through GABA_A channel, inward flow of chloride is attenuated. This suggests that bicarbonate outward flow could actually assist the inward flow of Cl^- for its hyperpolarising effect (Kaila *et al.*, 1997). Although there seems to be a delicate interaction between Cl^- and HCO_3^- and consequently between pH and inhibition, further discussion of this thesis will focus only on Cl^- in GABA inhibition.

1.2 Chloride regulation at neuronal level

The Cl^- driving force is dependent on the E_{Cl^-} that is determined by the Cl^- distribution inside and outside the cell; and the E_m which depends on the resting membrane potential (E_{Rest}) that is affected by the expression of all ion channels in the membrane and synaptic events. When E_{Cl^-} is more negative than E_m , Cl^- will enter the cell, while when it is more positive than E_m , Cl^- will leave the cell. Accordingly, the polarity of GABA events become hugely dependent on Cl^- regulation of the post-synaptic cell that determines the E_{Cl^-} .

1.2.1 Chloride-coupled co-transporters' activity regulate intraneuronal Cl⁻ level

The main mechanism that sets basal intraneuronal Cl⁻ has traditionally been considered to be the activity of co-transporters (Rivera *et al.*, 1999; Yamada *et al.*, 2004; Kaila *et al.*, 2014). Neurons express different types of chloride-coupled co-transporters. The main importer of Cl⁻ is the sodium potassium chloride co-transporter (NKCC1) that brings 2 Cl⁻ together with 1 potassium ion (K⁺) and 1 sodium ion (Na⁺) into the cell (Plotkin *et al.*, 1997). NKCC1 uses the driving force from Na⁺ concentration gradient that is actively maintained to be low inside and high outside by Na⁺/K⁺ATPase (Plotkin *et al.*, 1997; Pfeiffer *et al.*, 2009). To extrude Cl⁻ on the other hand, neurons express potassium chloride co-transporter (KCC2) that brings a single Cl⁻ out together with a single K⁺, driven by the concentration gradient of K⁺ that is high inside and low outside (Rivera *et al.*, 1999). On top of these, neurons also express sodium chloride bicarbonate co-transporter and chloride bicarbonate co-transporter that could also contribute to the basal intraneuronal level of Cl⁻ (Somjen, 2004).

1.2.2 Developmental shift from depolarizing GABA to hyperpolarizing GABA

Neuronal Cl⁻ regulation changes throughout development. In immature neurons, [Cl⁻]_i is found to be higher compared to the mature neuron (Rivera *et al.*, 2005). This is consistent with the tendency of GABA_A activation to give an outward flow of Cl⁻, hence exerting a depolarising effect, in immature neurons. On the other hand, in mature neurons [Cl⁻]_i is maintained low, that consequently results in a GABA hyperpolarising effect (Rivera *et al.*, 1999). These differences could be explained by the developmental up-regulation of KCC2 that is part of neuronal differentiation during maturation (Rivera *et al.*, 1999). Immature neurons dominantly express NKCC1 over KCC2, which consequently promotes Cl⁻ influx (figure 1.1A). However, as the neurons mature, KCC2 is drastically up-regulated while NKCC1 is only slightly if at all up-regulated, explaining the developmental shift from depolarizing GABA towards hyperpolarizing GABA (Rivera *et al.*, 2005; Kaila *et al.*, 2014). During development depolarizing GABA together with glutamatergic drive is thought to be essential in the development of neuronal connection especially in somatosensory cortex (Balakrishnan *et al.*, 2003; Luhmann *et al.*, 2014b). While in a mature brain, low [Cl⁻]_i is preferable to provide a driving force for GABA hyperpolarizing current.

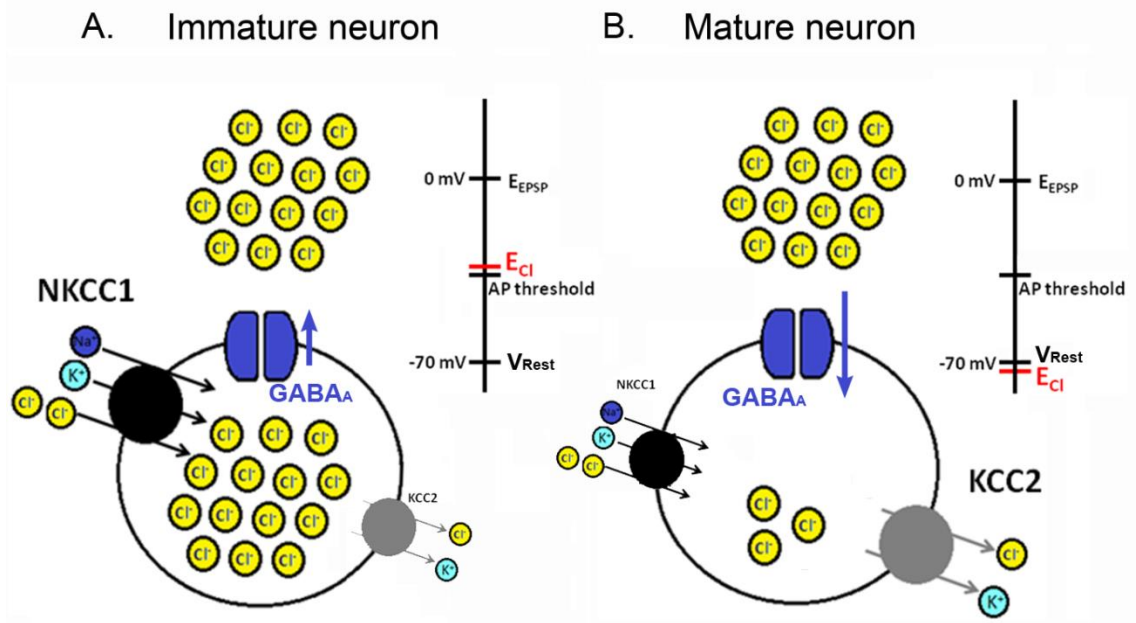


Figure 1.1 Chloride regulations in immature and mature neurons. A. In immature neurons, NKCC1 activity dominates $[Cl^-]_i$ regulation due to the low expression of KCC2. This results in a relatively high amount of Cl^- inside the cell that consequently gives a depolarizing E_{GABA_A} , allowing outward Cl^- flow (depolarizing) when GABA_A channel opens (blue). B. During maturation, KCC2 is up-regulated to outnumber NKCC1 favouring Cl^- extrusion to maintain low $[Cl^-]_i$. This gives a more negative E_{GABA_A} that allows Cl^- to move into the cells (hyperpolarizing) when GABA_A channel opens.

1.2.3 Possible effect of local impermeant anions in regulating intraneuronal Cl^-

A recent study has claimed that intraneuronal Cl^- could actually be regulated by the local impermeant anion concentration inside $[A^-]_i$ and outside the cell $[A^-]_o$; this mainly arises from the phosphate group of the DNA backbone and the negative charges associated in the extracellular matrix respectively (Glykys *et al.*, 2014a). This suggestion was based on the Gibbs-Donnan effect that explains how charged particles sometimes cannot be distributed evenly across a semi-permeable membrane due to the presence of impermeable charged particles that introduced an imbalance of electrical charges across the membrane (Ricka & Tanaka, 1984).

In this case, Cl^- as a permeable charged particle is distributed unevenly across cell membrane with low $[\text{Cl}^-]_i$ and high $[\text{Cl}^-]_o$ due to the imbalance of negative charges across the membrane set by the ratio between impermeable anions inside and outside the cell. Glykys et al (2014) suggested that $[\text{Cl}^-]_i$ is actually determined by the ratio between the local $[\text{A}^-]_i$ and $[\text{A}^-]_o$ to maintain the Gibbs-Donnan equilibrium, while co-transporters only assists the transport of Cl^- when there is transient change of the $[\text{Cl}^-]_i$ away from the baseline. This however is still a matter of debate (Glykys *et al.*, 2014b; Luhmann *et al.*, 2014a; Voipio *et al.*, 2014) and further studies are needed for clarification.

1.2.4 Activity dependent disinhibition

Although a cell's preferred $[\text{Cl}^-]_i$ is mainly set by co-transporter activity or possibly by the Gibbs-Donnan effect introduced by the impermeable anions, in actual fact neuronal $[\text{Cl}^-]_i$ is dynamic. $[\text{Cl}^-]_i$ could change at any given time depending on the ongoing synaptic activities. A neuron that is involved in a network activity will be exposed to both glutamatergic synapses as well as GABAergic synapses. Glutamatergic activity exerts a strong depolarization in a neuron that brings its E_m towards 0 mV ($E_{\text{glutamate}}$). Positive value of E_m will create a big driving force for Cl^- uptake by the cell when the conductance is increased by the opening of GABA_A channel (Buzsáki *et al.*, 2007). Indeed, neurons are equipped with Cl^- extrusion mechanism such as KCC2 that will clear Cl^- back towards its initial $[\text{Cl}^-]_i$, however this process is not as fast as synaptic events (Jin *et al.*, 2005). Study by Thompson and Gahwiler in 1989 showed that after repetitive electrical stimulations, the amplitude of GABA mediated IPSPs were significantly reduced (Thompson & Gahwiler, 1989a). They then showed that this is mainly due to an accumulation of Cl^- intracellularly by GABA conductance that shifts E_{Cl} to a more depolarized level hence reducing the driving force of Cl^- inward flow. This sometimes even results in a switch of GABA polarity from hyperpolarizing to depolarizing. This phenomenon is also known as activity dependent disinhibition.

1.2.5 Summary

To summarize, studies have shown that neuron $[Cl^-]_i$ is set by NKCC1 and KCC2 activity, however $[Cl^-]_i$ is dynamic depending on the on-going synaptic events. When exposed to both glutamate and GABA repetitively, neuron will undergo an activity dependent disinhibition that could be explained by the accumulation of Cl^- intracellularly.

1.3 The main inhibitory interneurons in the cortex

In the network level, inhibition system also depends on the connections or synapses between principal cells and the interneurons (Shepherd, 2004; Klausberger & Somogyi, 2008). Inhibition then becomes even more complex due to a wide variability of interneuronal subclasses that differ not only in their connectivity with the principal cells but also in their firing behaviour (Buzsáki *et al.*, 2007; Klausberger & Somogyi, 2008). In neocortex, the two main subclasses of interneurons are the parvalbumin positive interneuron (PV) and somatostatin positive interneuron (SOM), which accounts for ~40% and ~30% of the interneuronal population respectively (Markram *et al.*, 2004; Rudy *et al.*, 2011; Pfeffer *et al.*, 2013). The remaining ~30% of the interneurons were found to express 5-hydroxytryptamine-3a (5HR3aR) in which 40% of them are vasointestinal peptide (VIP) positive (Rudy *et al.*, 2011).

In neocortex, PV positive cells mainly consist of basket cells and chandelier cells interneuron while SOM positive cells are mainly Martinotti cells (Markram *et al.*, 2004). These two subclasses differ in both their synapses target onto the post-synaptic cells and their firing pattern that equips them to serve different functions in the system.

1.3.1 Somatostatin positive interneuron

SOM positive interneurons make synapses on the dendritic shaft or dendritic spines of the post-synaptic neurons (Markram *et al.*, 2004). Their axon could project into a distant column horizontally, hence providing inhibition across cortical columns (Markram *et al.*, 2004). As dendrites are the site of most excitatory synapses, by gating the excitatory inputs in the dendrites, SOM inhibitory effect could significantly shift the input-output function of a neuron (Lovett-Barron *et al.*, 2012; Pouille *et al.*, 2013). Excitatory synapses onto SOM interneurons are known to be facilitating (Rudy *et al.*, 2011), meaning that with repeated activation, the post-synaptic effect will increase supralinearly, resulting in an increase of inhibition onto the post-synaptic pyramidal cells (Kapfer *et al.*, 2007). This makes SOM interneurons best activated when there is an increasing activity of the network.

1.3.2 Parvalbumin positive interneuron

In contrast, PV positive basket cells are known to target the soma and proximal dendrites of pyramidal cells and interneurons, while the chandelier cells are known to specifically target the axon initial segment (AIS) (Markram *et al.*, 2004). The strategic location of PV synapses on pyramidal cells enables them to directly suppress the output of the pyramidal cell (Pouille *et al.*, 2013). Excitatory synapses on PV interneurons however tend to be depressing (Rudy *et al.*, 2011); or in other words multiple excitatory inputs onto PV will not result in a proportional output of PV cells.

PV cells also have been termed fast-spiking as they are capable to sustain high frequency trains of action potential. The fast-spiking characteristic could be explained by the ion-channel profiles that are expressed by these cells (Markram *et al.*, 2004). For instance, PV interneurons are known to express powerful delayed rectifying voltage-gated potassium channel Kv3.1 and Kv3.2, more densely than PV negative interneurons or pyramidal cells (Martina *et al.*, 1998; Rudy & McBain, 2001). These allow a stronger repolarisation after each action potential enabling the generation of successive action potentials with only a very short delay. These potassium channels are sensitive to the potassium channel blocker 4-aminopyridine (4-AP), which triggers intense firing of these cells (Martina *et al.*, 1998).

PV cells especially basket cells make a highly divergent contact to pyramidal cells but also to other PV interneurons in which 1 basket cell could make synapses with more than 1500 pyramidal cells and 60 other PV interneurons (Sik *et al.*, 1995). Furthermore PV cells are also known to be electrically coupled to each other via gap junction (Galarreta & Hestrin, 1999; Gibson *et al.*, 1999; Tamas *et al.*, 2000). This means that activity in one PV cell could spread to other PV cell in close proximity without having to make synapses. Consequently PV interneuron activity could impose a widespread impact in the network. The divergent connectivity and the electrically coupled PV cells network allow synchronization of different PV interneurons activity in the network and also the post-synaptic pyramidal cells (Tamas *et al.*, 2000).

1.4 The role of PV interneurons in gamma-oscillation

With all these characteristics, PV interneurons have been implicated in the synchronization of cortical network activity, playing an important role as a pacemaker in the generation of networks oscillations especially in the gamma frequency range (30 – 90 Hz) (Traub *et al.*, 2004; Bartos *et al.*, 2007; Cardin *et al.*, 2009). These studies have shown that basket cells are highly active during gamma oscillation with firing rates that lie close to the frequency of the gamma oscillation itself. Furthermore, basket cells are firing action potentials that are phase-locked to the gamma oscillation (Bragin *et al.*, 1995; Hájos *et al.*, 2004), suggesting a correlation between basket cells outputs and the rhythm of the oscillation. Both synaptic and electrical coupling between basket cells synchronize their outputs that down the line impose a synchronizing effect on the post-synaptic pyramidal cells as well (Tamas *et al.*, 2000). Basket cells' outputs impose a time constraint for the firing of pyramidal cells, which can only occur when the basket cells are in the refractory period. This entrainment of pyramidal cells firing, together with the synchronizing effect of basket cells on the network, results in the generation of gamma oscillation (Traub *et al.*, 1999).

1.5 Altered inhibition function in Epilepsy

Altered inhibition has long been associated with epileptic seizures, a transient episode of abnormal excessive or synchronous neuronal activity in the brain (Fisher *et al.*, 2014). In a simple in vitro model of epilepsy, pyramidal cells are bombarded with inhibitory inputs just before the ictal wave (Trevelyan *et al.*, 2006b; Trevelyan *et al.*, 2007a). Similar activity has also been recorded in vivo (Prince & Wilder, 1967b; Dichter & Spencer, 1969; Schwartz & Bonhoeffer, 2001) and also in human epileptic tissues recorded by implanted microelectrode (Schevon *et al.*, 2012). This inhibitory mechanism, also known as the inhibitory restraint, appears to suppress the intense excitatory drives. It is believed that recruitment of new territories occurs when the local restraint fails. This may only happen many seconds after the glutamatergic barrages start, thus highlighting the important role of inhibition at this time. Based on this, it is important to investigate the mechanism of how the inhibitory restraint fails in order to understand how a seizure starts and spreads.

1.5.1 Depletion of GABA neurotransmitter

There are several possibilities of how the inhibitory restraint could fail. The first possible mechanism is by a decreased GABA conductance after a period of inhibitory restraint against the glutamatergic barrages. There was a suggestion that seizures could be preceded by reduced GABA release from the pre-synaptic cells that consequently cause a reduction of GABA activation in the post-synaptic pyramidal cells (Zhang *et al.*, 2012). However, many other studies show otherwise that GABA conductance exists even throughout the seizure (Fujiwara-Tsukamoto *et al.*, 2006; Ellender *et al.*, 2014).

1.5.2 Depolarization block of interneurons

A second possibility is a depolarization block phenomenon that could affect interneurons especially the fast-spiking interneurons, hindering them from firing during seizure activity. Depolarization block is a situation where cells are so strongly depolarized that it reaches a membrane potential in which voltage gated sodium channels fails to de-inactivate (Somjen, 2004). Consequently the cells are left incapable of generating action potentials until the membrane potential is recovered back to normal (Bragin *et al.*, 1997). It has been shown that in a model of focal epilepsy where

NMDA was applied locally, ictal event only started invading wider territory once PV interneurons entered a depolarising block (Cammarota *et al.*, 2013). It should be noted that in this study, 4-AP was used in the bath, and this is known to block potassium channels Kv3.1 and Kv3.2 typically expressed in PV cells. These potassium channels are important to strongly hyperpolarize the cell after an action potential to be ready to fire another action potential. With these channels compromised, PV cells become more susceptible to depolarization block due to its fast-spiking behaviour. Whether PV depolarization block happens in other epilepsy models or in naturally occurring seizures still requires further investigation.

1.5.3 Raised intraneuronal Cl⁻

Lastly, inhibitory restraints could also fail when there is an intraneuronal Cl⁻ accumulation, which causes a reduction of Cl⁻ driving force or even a switch of GABA polarity from hyperpolarizing to depolarizing such as explained earlier. Evidence that shows the involvement of Cl⁻ in epilepsy will be elaborated in the next section.

1.6 Raised intraneuronal chloride in Epilepsy

There is good evidence that the phenomenon of compromised inhibition due to high intraneuronal chloride could be a key pathology in epilepsy. Intracellular Cl⁻ accumulation or a depolarizing shift in E_{GABA} has been shown both by gramicidin perforated patch (Fujiwara-Tsukamoto *et al.*, 2006) and Cl⁻ imaging (Isomura *et al.*, 2003; Dzhalala *et al.*, 2010b), in several different models of epilepsy such as the post-tetanic stimulation seizures, spontaneous seizures developed by organotypic culture, 0 Mg²⁺ and 4-AP induced seizures (Fujiwara-Tsukamoto *et al.*, 2006; Ilie *et al.*, 2012; Lillis *et al.*, 2012).

1.6.1 Increased Cl⁻ uptake by NKCC1

Several mechanisms could contribute to intracellular Cl⁻ accumulation in epilepsy. First is by Cl⁻ uptake by NKCC1. This is particularly important in neonatal seizures in which NKCC1 activity dominates the Cl⁻ regulation system of neurons (Nardou *et al.*, 2011; Kaila *et al.*, 2014). Evidence has shown that during seizures, NKCC1 activity contributes

to intracellular Cl^- accumulation. This is particularly strong after repeated seizures (Dzhala *et al.*, 2010b).

1.6.2 Reduced Cl^- extrusion by KCC2

Secondly, Cl^- could accumulate inside the cell due to a compromised Cl^- extrusion activity of KCC2. This could happen firstly via down-regulation of KCC2 expression. It has been shown that there is a reduction of KCC2 protein in human epileptic tissue resected from patients with mesial temporal lobe epilepsy or with glioma associated seizures, as detected by immunostaining against KCC2 (Huberfeld *et al.*, 2007c; Pallud *et al.*, 2014). Reduction of KCC2 expression was directly correlated with a more depolarizing IPSP recorded from pyramidal cells during interictal activity (Huberfeld *et al.*, 2007c).

KCC2 reduction could also be observed at the mRNA level (Huberfeld *et al.*, 2007c), which suggests that there is a down-regulation of KCC2 production even at the pre-translational level of epileptic tissue. It should be noted that this observation was made from resected human epileptic tissues that has been exposed to multiple number of seizures for a long period of time.

Another mechanism that could lead to a compromised KCC2 activity is the post-translational modification of KCC2, triggered by epileptic activities (Kaila *et al.*, 2014). For instance, a recent study has shown that repetitive interictal discharges in vitro, could lead to a reduction of KCC2 activity. This is due to dephosphorylation of KCC2 at serine 940 that triggered calpain-mediated cleavage of the protein, leaving the remaining part of KCC2 dysfunctional (Puskarjov *et al.*, 2012). Others have shown that seizure activity could rapidly trigger endocytosis of KCC2 from the membrane and proteolysis of the protein that results in the loss of hyperpolarizing effect of GABA (Rivera *et al.*, 2004; Kaila *et al.*, 2014).

1.6.3 Cl^- accumulation due to intense GABA_A activation

Lastly, Cl^- could also accumulate due to intense GABA_A activation that seems to dominate the activity of pyramidal cells just before the ictal wave (Trevelyan *et al.*, 2006a). Supporting evidence comes from a Cl^- imaging study done in post-tetanic

seizure model (Isomura *et al.*, 2003). In this study it was shown that Cl^- rapidly rises within the neurons post-tetanic stimulation, which also resulted in a seizure like activity. Cl^- accumulation was markedly reduced by approximately 75% when GABA_A was blocked using bicuculline, which also abolished the seizure activity post-tetanic stimulation (Isomura *et al.*, 2003). However, bicuculline did not completely abolish the Cl^- influx (Isomura *et al.*, 2003) indicating that there is indeed some other mechanism that could facilitate Cl^- entry during seizure other than GABA_A activation.

1.6.4 High intraneuronal Cl^- and depolarizing GABA contributes to the generation of epileptic afterdischarge

During seizures, high intraneuronal Cl^- , and so depolarizing GABA, has been implicated in the generation of epileptic afterdischarges. It has been shown that in a post-tetanic seizure model, local GABA application during seizure was actually triggering bursts of action potentials rather than inducing an IPSP (Fujiwara-Tsukamoto *et al.*, 2006). A recent study also showed a similar phenomenon using an optogenetic approach, in a post-tetanic seizure model (Ellender *et al.*, 2014). Ellender et al specifically targeted PV cells for expression of either channelrhodopsin (ChR2) for PV cells activation or archaerhodopsin (Arch) for PV cell inhibition. During ictal activity, PV cell activation using ChR2 led to an increased frequency of afterdischarges when recording from a pyramidal cell. In contrast, when PV cells were inhibited by Arch activation, a reduced number of afterdischarges was observed.

1.6.5 Summary

Together, it could be concluded that epileptic tissues are found to be associated with co-transporters dysregulation, which introduces a depolarizing shift in E_{GABA} that compromises GABA inhibitory activity. More Cl^- then accumulates inside the cells during epileptic activity such as interictal or ictal discharges due to GABA_A activation. During ictal activity, depolarizing GABA has been suggested to contribute to the generation of afterdischarges or the clonic phase of ictal discharges. Conversely, repetitive epileptic activities such as interictal and ictal discharges could also contribute to the alteration of co-transporter regulation that further leads to the depolarizing shift of E_{GABA} .

1.7 The need for new treatment

Despite the increasing number of new anti-epileptic drugs being developed in the last decade, the number of patients with epilepsy resistant to the current anti-epileptic medication remains remarkably constant at around 30% (Moshé *et al.*, 2014). Patients with drug resistant focal epilepsy sometimes could undergo surgery to remove the epileptic foci. This option however is highly dependent on the location of the epileptic focus, as surgery cannot be done in the eloquent region of the cortex that is important for sensory and movement processing for example. Surgery also does not guarantee sustained seizure freedom as about 42% of patients with intractable epilepsy who underwent surgery ended up developing seizures again later in life (Wiebe *et al.*, 2001; Moshé *et al.*, 2014).

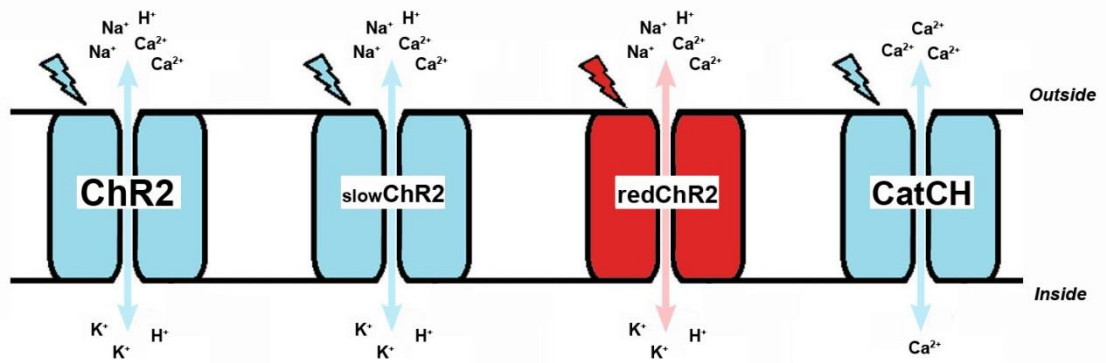
Other alternative treatment for drug resistant epilepsy, which is not suitable for surgery, is neurostimulation. The most common approach is vagal nerve stimulation, that indeed showed a reduction of seizure frequency by approximately 50% in half the number of treated patients (Englot *et al.*, 2011). However, in most of the cases, vagal nerve stimulation did not result in seizure freedom (Moshé *et al.*, 2014). Another approach is by deep brain stimulation that is more invasive than vagal nerve stimulation. This is only applied as a last resort for drug resistant patients with severe epilepsy. Similarly, patients treated with deep brain stimulation showed some seizure reduction but with relatively small seizure free rate (Fisher *et al.*, 2010; Moshé *et al.*, 2014). The mechanism of neurostimulation techniques as a treatment for epilepsy is still not clear and so future improvement for these approaches is not a simple matter. Based on the low seizure-free rate of the available treatment options, new approaches for drug-resistant epilepsy treatment are still desperately needed.

1.8 Optogenetics

Recent technology that has been considered as a new candidate for epilepsy treatment is optogenetics. Optogenetics has been widely used as a research tool to manipulate neuronal activity using light. This is achieved by expressing light sensitive proteins, from algae and bacteria, in neurons (Deisseroth *et al.*, 2006). When these proteins are expressed in neurons, temporally controlled depolarization or hyperpolarization could be induced by light illumination. Furthermore, different types of neuron could be targeted using cell-type specific promoter for optogenetic protein expression, allowing cell-specific modulation of neuronal activity (Peron & Svoboda, 2011).

Optogenetic proteins are divided into 2 main categories, those with excitatory and those with inhibitory actions. The most common excitatory protein being used is channelrhodopsin (ChR2), an algae derived channel that allows non-specific cations flow when illuminated with blue light (Cardin *et al.*, 2010). Several genetic modifications of ChR2 have resulted in a variety of different ChR2 variants with certain characteristic properties such as slow-kinetic ChR2, which stays open for longer than the light illumination (Haikala *et al.*, 2013), calcium specific channel known as CatCh (Kleinlogel *et al.*, 2011a), and a red-shifted ChR2 that is activated by red light rather than blue light (Zhang *et al.*, 2008).

Excitatory optogenetic proteins



Inhibitory optogenetic proteins

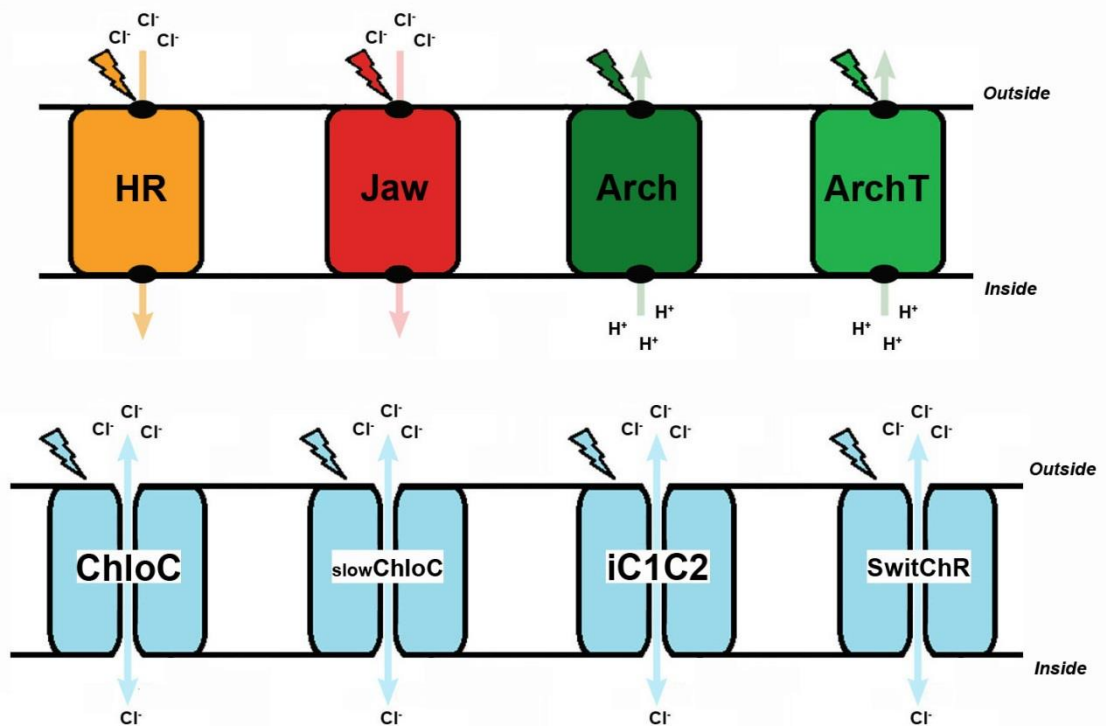


Figure 1.2 Different excitatory and inhibitory optogenetic proteins.

Inhibitory optogenetic proteins available are the bacterial origin inward Cl^- pump halorhodopsin (HR) that is activated by orange light (Gradinaru *et al.*, 2008) and the red-activated Cl^- pump known as Jaw (Chuong *et al.*, 2014), the outward proton pumps archaerhodopsin (Arch) and the high-light sensitivity version archaerhodopsinT (ArchT) (Chow *et al.*, 2010; Han *et al.*, 2011), and also the light activated Cl^- channel that is a genetically modified ChR2 namely iC1C2 and the slow-kinetic version of it called SwitChR (Berndt *et al.*, 2014) and ChloC and the slow-kinetic version of it called slow-ChloC (Wietek *et al.*, 2014).

1.9 Optogenetics in epilepsy

Due to the transient and unpredictable nature of epileptic seizure, there is a need for an on-demand seizure control with high temporal precision. The possibility for cell type-specific targeting and the high temporal precision where light induced responses could be triggered within milliseconds, make optogenetics a promising new therapeutic candidate.

Several different groups have conducted studies using different strategies of optogenetic application to control epilepsy, both in vitro and also in vivo models of epilepsy. The two main strategies that have been explored so far are the expression of the inhibitory protein HR in pyramidal cells under CamKII promoter in either neocortex, hippocampus, or thalamus (Tønnesen *et al.*, 2009; Krook-Magnuson E *et al.*, 2012; Wykes *et al.*, 2012; Paz *et al.*, 2013) and the expression of the excitatory protein ChR2 in the interneurons (Krook-Magnuson E *et al.*, 2012; Ledri *et al.*, 2014). Furthermore, globally targeting all interneurons under GAD promoter and specifically targeting only parvalbumin positive interneurons or somatostatin positive interneurons have also been investigated (Ledri *et al.*, 2014).

A direct comparison between the two approaches was made by Krook-Magnuson et al (2012). Kainate was injected into the hippocampus of mice as a model of temporal lobe epilepsy. Injected mice started developing spontaneous seizures after several weeks. In the same mice, they expressed either HR in pyramidal cells or ChR2 in PV interneurons, locally to where the kainate injection was made. Optogenetic activation

and recording were made in vivo. Both approaches showed seizure suppressive effect of optogenetic activation as measured in a reduction of seizure duration by $57 \pm 14\%$ and $43 \pm 11\%$ for HR on pyramidal cells and ChR2 on PV interneurons group respectively (Krook-Magnuson E *et al.*, 2012).

Indeed optogenetic activation by light has shown effective seizure suppression in comparison to no light activation in the kainate acid epilepsy model. However with HR expressed on pyramidal cells and ChR2 expressed on PV interneurons, seizure duration was remain longer than 10 s in approximately 20% and 60% of the total recorded seizures respectively, even when optogenetic activation was done (Krook-Magnuson E *et al.*, 2012). This suggests that there is still room for improvement that could enhance the effectivity of this technique as a tool to control epileptic seizures.

Optogenetics is essentially an artificial way of altering certain ion/ions level inside and outside the cells. Inevitably, there could be some consequences on the neuronal system that are naturally regulated by a certain balanced state of the manipulated ions. This should be taken into consideration when designing the best strategy to apply optogenetics in epilepsy. One possible issue, for instance, is the effect of HR activation on neuronal Cl^- level. As HR hyperpolarises the cells by pumping Cl^- into the cell, there is a danger of inducing a positive shift in the E_{Cl^-} that makes GABA activity more depolarising as intracellular Cl^- level rises (Raimondo *et al.*, 2012). This is also consistent with their observation that HR activation significantly increased the firing probability of pyramidal cells in healthy tissue (Raimondo *et al.*, 2012).

The same effect could also take place indirectly when activating ChR2 in the interneuronal population. As interneurons activation by ChR2 increases the release of GABA neurotransmitter, this too will eventually accumulate Cl^- on the post-synaptic neurons through the activation of GABA_A receptors. This has been observed by Ledri and colleagues, who showed that when ChR2 was expressed under interneuronal promoters such as GAD, SOM or PV, light activation briefly initiates action potentials firing on the CA3 pyramidal cells (Ledri *et al.*, 2014); although this could also be explained by a reduced GABA release from the interneurons when a sustained activation of interneurons was introduced by long illumination of ChR2.

Rebound firing, following HR activation on pyramidal cells or ChR2 on interneurons activation could also be attributed to the I_H current by the hyperpolarization-activated cyclic nucleotide-gated (HCN) channels. HCN channels are activated by hyperpolarization and the opening of these channels result in a depolarizing current (I_H) due to an inflow of cations (Maccaferri *et al.*, 1993; He *et al.*, 2014). In their study, Raimondo et al has shown that I_H contribution to the rebound firing post HR activation on pyramidal cells is rather weak, at least in a single cell level of organotypic cultures on post- natal day 14-17.

This was shown by activating Arch optogenetic protein (outward H^+ pump) that does not have chloride loading effect on cells but should still affect I_H , and observing that the spike probability of a neuron does not increase significantly before and after Arch activation (Raimondo *et al.*, 2012). It should be noted however that this effect could be marginally amplified when assessing multiple cells in the network level, as synchronized hyperpolarisation such those imposed by optogenetics could also synchronise the rebound firing of different cells and hence amplify its impact on the network excitability.

The success of optogenetics will also depend on the illumination paradigm. Depending on the dynamic of the seizure activity, even with the Cl^- loading effect, the illumination strategy could potentially undermine the issue. To give one instance, Chuong et al in their recent paper successfully reduced the rebound firing post HR activation by about 60% simply by ramping down the light when terminating the light illumination, instead of using the standard square pulse light paradigm (Chuong *et al.*, 2014). Another interesting question is whether extra Cl^- loading from HR activation could do further harm once a seizure has been initiated, as intraneuronal Cl^- is already high at the start of a seizure (Lillis *et al.*, 2012). If no is the answer, then HR application will be safe if it is only activated when seizure has been initiated. The recent advance that allows this is the development of the close-loop optogenetic stimulation technique where illumination is set to be triggered by a computer algorithm that recognizes when a seizure is being initiated (Krook-Magnuson E *et al.*, 2012; Armstrong *et al.*, 2013).

In conclusion, optogenetics has shown promise as an on-demand control for seizures in various animal models of epilepsy. However, there are some issues that could be

further improved such as the possibility of HR Cl⁻ loading effect that could compromise GABA inhibition during seizure. The use of different optogenetic proteins and tailoring the illumination paradigm should be considered to further optimize the effectivity and efficiency of optogenetic application in epilepsy.

1.10 The rationale of this thesis

The maintenance of low [Cl⁻]_i in neurons is important for hyperpolarising GABA inhibition. It has been shown that Cl⁻ accumulation inside the cell that promotes depolarising activity of GABA, contributes to epileptic pathophysiology. Although the implication of high [Cl⁻]_i state during seizure is well recognized, its effect on seizure initiation is unknown.

Considering the intraneuronal Cl⁻ accumulation issue as one possible mechanism that could lead to the failure of inhibitory restraint, correcting high intracellular Cl⁻ level to restore GABA inhibitory activity in epilepsy theoretically would be beneficial, both during the course of a seizure, and also during pre-ictal discharges, to prevent the onset of subsequent seizures. One possibility is by limiting the influx of Cl⁻ for instance by using bumetanide, a NKCC1 blocker. Potential anti-epileptic effect of bumetanide is still being assessed on an on-going clinical trial, targeting neonatal epilepsy in which NKCC1 activity is relatively high. However, there was a suggestion that bumetanide effect could be limited, as it was shown to be inefficient in blocking the generation and propagation of kainate induced ictal discharges in vitro (Nardou *et al.*, 2009). This could be the case as NKCC1 blockers are often not specific and it has a blocking effect on KCC2 too; beside the entry of Cl⁻ during the ictal event is largely facilitated through GABA_A channels (Isomura *et al.*, 2003). Additionally, there is also some issue that bumetanide only poorly penetrates the blood-brain-barrier (Töllner *et al.*, 2014).

Another possible mean of correcting high [Cl⁻]_i is by boosting the activity of KCC2 in extruding Cl⁻. Recently a KCC2 enhancer drug namely CLP257 has been developed (Gagnon *et al.*, 2013). CLP257 has been shown to successfully rescue the membrane expression level of KCC2 and thereby reduce [Cl⁻]_i (Gagnon *et al.*, 2013), however the potential anti-epileptic effect of this drug has not been tested. A possible issue that could arise from using CLP257 in epilepsy would be the systemic effect of this agent

that would affect the $[Cl^-]_i$ of all types of neurons in the brain and also other cell types that expresses KCC2.

An alternative approach that could provide a more localized effect and cell-specific manipulation of neuronal Cl^- level is optogenetic. However, so far this is only possible in an inward direction as to load cells with $[Cl^-]_i$ by using HR Cl^- pump. A novel use of optogenetic tools to extrude Cl^- could be beneficial in epilepsy to restore the hyperpolarizing effect of GABA as a natural inhibition in the brain.

1.11 The aim of this thesis

Accordingly, the general aim of this thesis is to investigate the effect of high intraneuronal Cl^- in network activity, especially related to epilepsy, and to design optogenetic tools to extrude Cl^- that could have a therapeutic effect in epilepsy.

The specific aims of this thesis are as follows

1. To characterize halorhodopsin Cl^- pump and to assess the possibility of using halorhodopsin as a tool to artificially load population of cells with Cl^- .
2. To investigate the implication of a high intraneuronal Cl^- state in the generation of specific pattern of epileptic activity and seizure initiation.
3. To design a novel use of optogenetic proteins as a tool to extrude Cl^- and assess the therapeutic effect of Cl^- extrusion in epilepsy.

Chapter 2. Material and methods

2.1 Dissociated neuronal culture

Pregnant rats were ordered with a specified gestation day from Charles River laboratories. Primary neuronal cultures were prepared from rat pups at embryonic day 18-20. The pregnant rat was sacrificed by cervical dislocation; a sagittal incision was made in the abdominal area to remove the pups. Generally, cortices and hippocampi from 8 pups were isolated. Dissection was conducted in the dissection media (Na₂SO₄ 82 mM, K₂SO₄ 30 mM, MgCl₂ 5.8 mM, CaCl₂ 0.25 mM, Hepes 1 mM, Glucose 20 mM, KyMg 0.2 mM, phenol red), pH was adjusted using 0.2 M NaOH until the color of the solution became red. Collected tissues were then digested twice using papain solution (60 units/30 ml papain latex - Sigma Aldrich) for 20 minutes by incubation at 37° C heat bath. Tissues were then washed twice with the dissection medium (2 mL each time) and twice with the growing media 2mL each time (Neurobasal A, 2% B-27 supplement, 1% of FBS, 0.5% glutamate, and 0.5% antibiotic-antimicotic, all from GIBCO Invitrogen).

Cells were then dissociated within the growing media by gentle agitation using a pipette gun with a 10 ml tip. Cells were counted using a haemocytometer and then diluted to the desired density in Opti-MEM containing 20µM glucose. Cells were plated on previously coated coverslips using poly-L-lysine with 1:10 dilution for overnight in room temperature (Sigma Aldrich). For calcium phosphate and viral transfection cells were plated in 100.000 cells/ml density as it was found to be the best for cells' survival post- transfection. Cells were allowed to attach to the coverslips by incubating at 37°C, O₂ (95%), CO₂ (5%), for 2.5 hours. At that time, the media was changed to growing media and cells were maintained in the incubator for at least 2 weeks, with medium changed every 3 days, before doing the transfection (technique was adopted from Prof Hardingham's group, Edinburgh University).

2.2 Calcium phosphate transfection

Some of the earlier wild type HR transfections were done using the calcium phosphate precipitation technique, under the sterile tissue culture hood as follows. 2 x HBS buffer

was prepared, aliquoted, and stored in -20°C (NaCl 274 mM, KCl 10 mM, Na_2HPO_4 1.4mM, glucose 15 mM, Hepes 42 mM; pH: 7.05). The medium on the plate was changed to DMEM 30 minutes prior to transfection. For 1 plate of 12 wells, the transfection reaction A (600 μl of 2 x HBS solution) and B (50 mg of plasmid, 120 μl of 2.5 M CaCl_2 , H_2O to make up 600 μl mixture) were prepared.

B was added to A drop by drop while vortexing using a low power until all mixed. The mixture was incubated in the dark at room temperature for 30 minutes. 100 μl of transfection mix was then added to each well drop by drop. The cells were incubated at 37°C for 20 minutes before washing away the transfection reaction. All coverslips were rinsed three times with pre-warmed DMEM and a fresh growth medium was added to the wells. Cells were grown for at least four days before doing any experiments to allow the cells to produce and express sufficient amount of protein. This protocol is adapted from (Jiang & Chen, 2006).

2.3 Lentivirus Production and Transfection

Later experiments used lentiviral transfection, because of its higher transfection rates. This protocol was adapted from (Zhang *et al.*, 2010) and done as follows. Lentivirus vector was produced using HEK293FT cell line. Low passage cells (<P:10) were grown in D-10 (DMEM, 10% FBS, glutamate 6mM, 1% penicillin-streptomycin) medium containing 500 $\mu\text{g}/\text{ml}$ geneticin until it reached 90% confluency. Cells were then split into four T-75 flasks and grown in geneticin free D-10 medium overnight.

On the next day, cells were transfected using the calcium phosphate method. Plasmid DNA of pLenti-eNpHR3.0-EYFP (80 μg), pCMVR8.74 (80 μg), and pMD2.G (52 μg) were prepared using recombinant deficient StbI3 E.Coli strand (Invitrogen) and QIAGEN maxi prep kit. Plasmid DNAs were mixed thoroughly with CaCl_2 to a final concentration of 0.25 M and water was added to make up a 2 ml solution. 2 ml of BBS (borate buffer saline) was added and mixed by inverting the tube three times. Transfection mixture was incubated for 30 minutes at room temperature, and then added to each flask (1 ml for 1 T-75) drop by drop. Cells were incubated at 37°C , 3% CO_2 incubator for 18 hours. Medium was discarded and replaced with a fresh D-10 media. The first and

second collections of the virus-containing media were done at 24 hours and 48 hours after the initial media changing. Collected media was spun down for 10 minutes (2200 RPM) and filtered using 0.45 µm pore filter (Millipore).

Virus was concentrated by ultracentrifugation using a Beckman SW28 rotor and Beckman-358156 adaptor. Virus containing media was loaded into a conical ultracentrifuge tube Beckman-358126 (26000 RPM, 4°C, 2 hours) on top of a 4 ml 20% sucrose cushion. Supernatant was discarded and the pellet was resuspended in 100 µl PBS by gently swirling the tube. Virus was transferred to a 1 ml eppendorf, spun for 5 minutes (7000 RPM), and aliquoted into 10 µl stocks to be stored in -80°C. Culture transduction was done by diluting 1 µl of lentivirus in 100 µl growing medium and added 10 µl of that to each well (12 wells plate). Medium was changed 24 hours post transduction and experiments were conducted at least 4 days afterwards.

2.4 Electroporation

For my experiments with newly engineered protein sequences, electroporation became the favoured way of transfection as it had a better transfection rate than calcium phosphate technique and virus making was too time consuming for the testing process. Dissociated neuronal cells were prepared as explained above. Rat Neuron Nucleofactor kit (Lonza Amaxa) was used for electroporation. Plates with pre-coated coverslips using poly-L-lysine with 1:10 dilution were prepared a day before. Before starting the electroporation process, growing media (2 ml per well for 6 wells plate or 1 ml per well for 12 wells plate) was loaded into each well and plates were placed in the incubator. For one electroporation, five million cells were collected by centrifugation with 80 RCF for 5 minutes. Cells pellet was resuspended in 100 µl nucleofactor solution. 1-2 µg of plasmid DNA was added and mixed thoroughly. Cells were then transferred to an electroporation cuvette, and cuvette was placed in the electroporater. G-013 was used as the appropriate electroporation program for rat cortical neurons transfection and start button was pressed to initiate the process. Once finished, 500 µl of the pre-incubated growing medium was added to the cuvette and mixed with the cells. Finally, cells were distributed equally to every well of 6 well or 12 well culture plates. Medium was changed 3 hours and 24 hours post-plating.

Imaging / electrophysiological experiments were conducted at least 7 days post transfection.

2.5 Patch clamp experiments

Recordings were made using a laser spinning disc confocal microscope (Visitech) fitted with Patchstar micromanipulators (Scientifica) mounted on a Scientifica movable top plate. Electrophysiological data was collected using a Multiclamp 700B amplifier (Molecular Devices) and Digidata acquisition boards connected to Dell desktop computers running pClamp software (Molecular Devices). During the entire recording, cells were bathed in circulating oxygenated (95% O₂/ 5% CO₂) ACSF solution (perfusion at 1–3 ml/min) heated to 33–37°C by a sleeve heater element (Warner Instruments) around the inflow tube.

2.5.1. Whole cell patch

Whole cell recordings were made using 3-7M Ω pipettes made of borosilicate glass (Harvard apparatus). Electrode filling solution used was either low Cl⁻ (K-methyl-SO₄ 125 mM, Hepes 10 mM, Mg-ATP 2.5 mM, NaCl 6mM; 290 mOsM and pH 7.35) or high Cl⁻ (KCl 135 mM, Na₂ATP 4 mM, Na₃GTP 0.3 mM, MgCl₂ 2mM, and Hepes 10 mM; 290 mOsM and pH 7.35). Assessment of all modified HR proteins and experiment assessing Cl⁻ concentration gradient on the wild-type HR were done by whole cell patch using high Cl⁻ electrode filling solution whereas the initial exploration of iClC2 versus slowChloC current was done using low Cl⁻ electrode filling solution.

During the assessment of Cl⁻ concentration gradient on wild-type HR current, cells were perfused with oxygenated ACSF (NaCl 125 mM, KCl 3.5 mM, NaHCO₃ 26 mM, NaH₂PO₄ 1.26 mM, glucose 10 mM, MgCl₂ 1 mM, and CaCl₂ 2 mM) and low Cl⁻ ACSF (Na isethionate 125 mM, KCl 3.5 mM, NaHCO₃ 26 mM, NaH₂PO₄ 1.26 mM, glucose 10 mM, MgCl₂ 1 mM, and CaCl₂ 2 mM).

2.5.2. Perforated gramicidin patch

Assessment of the chloride-loading effect of HR activation or the ArchT-ChloC Cl⁻ extrusion effect was performed by doing perforated gramicidin patch. Gramicidin is a

chemical that creates a pore in cell membrane that is impermeable to Cl^- . Cations can flow through and so high quality of intracellular recordings can be made but importantly Cl^- cannot pass through. This type of patch is necessary to ensure that the Cl^- internal milieu of the cells are intact and not affected by the electrode filling solution in the patching pipette hence giving a more accurate measurement of the E_{Cl^-} (Ebihara *et al.*, 1995).

Cells were constantly perfused with oxygenated ACSF. Gramicidin perforated patch recordings were made using 3–7M Ω pipettes (borosilicate glass; Harvard Apparatus) filled with a high Cl^- electrode filling solution (KCl 135 mM, Na_2ATP 4mM, Na_3GTP 0.3 mM, MgCl_2 2 mM, and Hepes 10 mM; 290 mOsM and pH 7.35), so that the integrity of the cell membrane could be monitored. If the patch breaks through, equivalent to a whole cell mode, the high Cl^- in the patching pipette will diffuse into the cell instantaneously giving an extremely depolarized E_{GABA} . Fresh Gramicidin (Sigma Aldrich, G5002) stock was made daily with 5 mg/mL concentration in dimethylsulfoxide (DMSO). Gramicidin stock was added to the high Cl^- electrode filling solution with 1:5 dilution to achieve a final concentration of 0.1 mg/ml and mixed by 40 s vortexing and 5 s sonication. Gramicidin electrode filling solution was then filtered using a 0.45 millipore filter and used for patching straight away. Experiments were conducted when series resistance had stabilized (below 100 M Ω , approximately 30 minute after patching).

Recordings were made in voltage-clamp mode, with a baseline holding potential of -70mV, and repeated 200ms duration test ramps (triangular up-down function; peak -50mV; trough -90mV; slope $\pm 400\text{mV/s}$; figure 1.1). GABA_A currents were induced by muscimol (100 μM) application delivered close to the recorded neuron through a patch pipette coupled to a picospritzer (Parker Instrumentation) delivering 10ms pressure pulses (10-20 PSI), and timing was coordinated with the illumination (optogenetic activation) via the pClamp software coupled to a Digitimer box. Test voltage ramps were applied at baseline and also at close to the peak of GABA_A current (I_{GABA}).

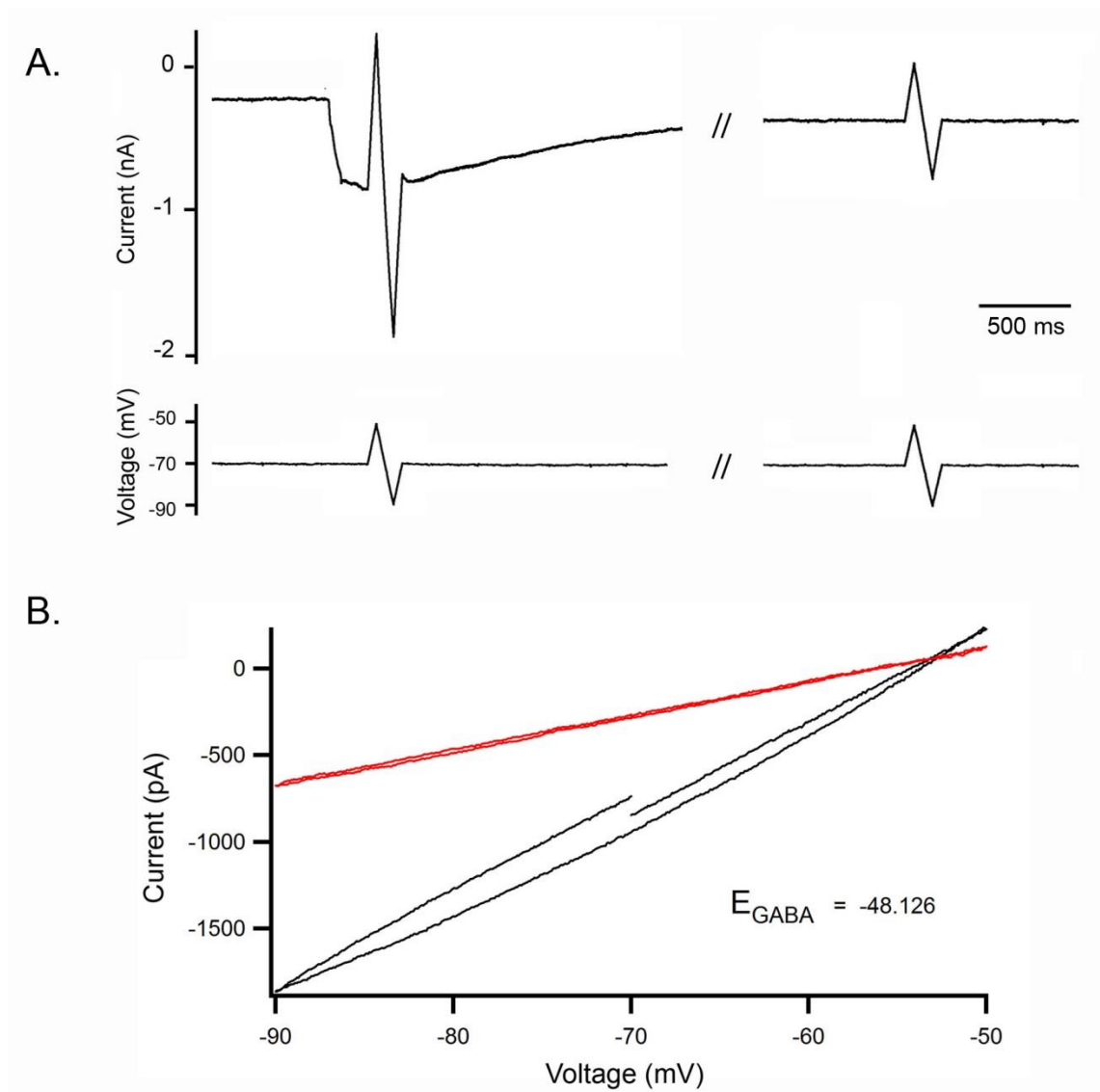


Figure 2.1 Voltage ramps protocol to measure GABA reversal potential. A. E_{GABA} was measured in voltage clamp configuration with a V_{Hold} of -70 mV (top trace). Plus and minus 20 mV voltage ramps that lasted for 200 ms were introduced; one at the peak of muscimol event and one at the baseline period (bottom trace). B. Voltage and current relationship (I-V curve) was derived from voltage ramps introduced at the peak of muscimol event (black) and the baseline period (red). Estimated E_{GABA} is the voltage point where the two I-V curves intercept.

2.6 Cortical expression of optogenetic proteins

All animal handling and experimentation were done according to UK Home Office guidelines. Optogenetic proteins were expressed by doing injection of the relevant viral vectors or by using genetically engineered transgenic mice. To achieve pyramidal expression of Halorhodopsin (HR), AAV-CamkII-cre-GFP (UNC viral vector core) was injected into homozygous floxed-HR mice (Ai39; B6; 129S-Gt(ROSA)26Sor^{tm39(CAGHOP/EYFP)Hze}/J; Jackson Laboratory, stock number 014539). For general neuronal expression of HR, pAAV-hSyn-eNpHR3.0-mCherry virus (UNC viral vector core) was injected into wild type mice (C57BL/6J). For pyramidal expression of ArchaeorhodopsinT (ArchT), pAAV-CaMKIIa-eArchT3.0-EYFP (UNC viral vector core) was injected into wild-type C57BL/6J mice.

Injections were made either into postnatal day 0-1 pups, or into young adult mice. The pups had EMLA cream applied to the left top of their head, and were anaesthetised subsequently using isoflurane inhalation. A single injection of virus was made using a 10 μ L Hamilton syringe, with a bevelled 36 gauge needle (World Precision Instruments) approximately 1mm anterior to lambda, and 1mm lateral to the midline into the left hemisphere, at 1.7-0.8mm deep to the skin (four separate 50 nL injections, deepest first). Approximately 0.2 μ L ($\sim 10^{11}$ - 10^{12} viral particles) were injected over a 10 minute period. This reliably labelled neurons or pyramidal cells throughout the hemisphere, and at the time of recordings, at age 5 weeks – 3 months, there was no cortical scarring apparent from the injection tract. This became the preferred method for labelling, but for the early experiments, adult animal injections were also performed as follows.

Young adult mice (5-8 weeks old) were anaesthetized by ketamine-methoxamine intraperitoneal injection and placed in a stereotaxic head-holder (David Kopf Instruments). Subsequent anaesthesia was maintained using isoflurane inhalation. Injections were made at 3-4 locations in an anterior-posterior row, in a single hemisphere, 1.5-2mm lateral to the midline, and 1-0.4 mm deep to the pia (0.6 μ L, injected over 15 mins). This gave an expression across all cortical layers however it was far more restricted laterally, extending 0.2-0.5mm in coronal slices. The illumination and recordings were then targeted to the centre of this area.

Cortical HR expression was also achieved by using genetically engineered transgenic mice. Brain slices were prepared from first generation cross-breeding of the floxed-Halorhodopsin animals with CamKIIa-cre mice (B6.Cg-Tg(Camk2a-cre)T29-1Stl/J; Jackson Laboratory, stock number 5359).

2.7 Brain slices experiments

Coronal brain slices with a thickness of 400 μm were prepared from the injected or breeding animals (3-10 months), on ice-cold oxygenated (95% O_2 /5% CO_2) artificial cerebrospinal fluid (ACSF: NaCl 125mM, NaHCO_3 26mM, glucose 10mM, KCl 3.5 mM, $\text{NaH}_2\text{PO}_4^-$ 1.26 mM, MgCl_2 3mM, kynurenic acid 1.5mM, and ascorbic acid 0.3mM). After cutting, the slices were transferred to an incubation, interface chamber (room temperature) perfused with oxygenated ACSF (NaCl 125 mM, NaHCO_3 26 mM, glucose 10 mM, KCl 3.5 mM, NaH_2PO_4 1.26 mM, CaCl_2 1.2mM, MgCl_2 1mM) for at least 1 hour before transferring them to a recording interface chamber (33-36°C), perfused with this same ACSF. The concentration of divalent cations was used following Sanchez-Vives and McCormick (2000), because this allowed the reliable triggering of sustained bursts of activity, with a prominent high frequency discharge of fast-spiking interneurons (Sanchez-Vives & McCormick, 2000), by white matter stimulation (putative thalamic inputs).

Single-electrode extracellular recording were made through broken-tip borosilicate patch pipettes (Harvard Apparatus), conducted using either Multiclamp 700B (Molecular Devices, California) or Axoclamp 1D amplifiers (Molecular Devices), a 1401-3 Analog-Digital converter (Cambridge Electronic Design, Cambridge) and Spike2 software (Cambridge Electronic Design) with sampling rate of 5-10 kHz. Multichannel extracellular recordings were collected at 10 kHz, using 4-channel-probe configuration (Q1x1-tet "tetrode"; NeuroNexus; figure 1.2) connected to a ME16-FAI- μPA -system and MC_Rack software (Multichannel Systems, Reutlingen). Bipolar electrical stimulation (0.2 ms duration) was delivered via tungsten electrodes onto the white matter.

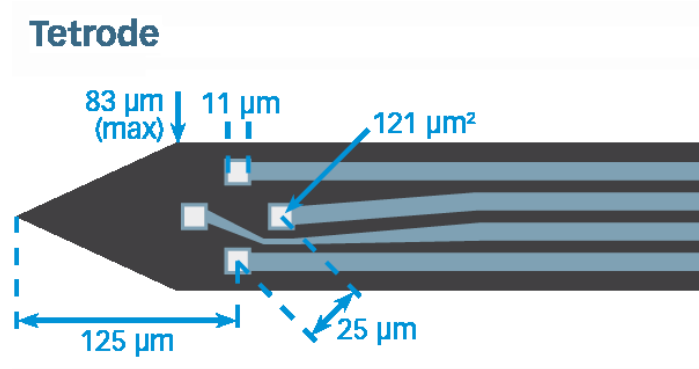


Figure 2.2 Tetrode configuration of extracellular electrodes – from Neuronexus.

2.8 Optogenetic illumination

HR and ArchT were activated by 561nm, 50mW solid-state laser (Cobolt) connected to a fiber optic with a fine cannula (400 μm core, 0.20 NA; Thorlabs). After optimizing the optic fibre coupling, the total light power at the cannula tip was measured at 15-30 mW. In order to achieve a comparable inhibitory effect by HR and ArchT, light intensity was adjusted by adding different neutral density filters (ND filters 0.2 – 0.6; Thorlabs) placed in the light patch between the laser and the optic fibre. Different filters could be used for different slices, however it was always constant at any given slice. After adding neutral density filter, laser output power ranged between 3-20 mW measured at the tip of the cannula. This gave a roughly equivalent optogenetic suppression of electrical stimulation as measured by a reduction in the line-length (cumulative voltage difference between consecutive data points) of the unfiltered signal 500 ms after the electrical artefact (Guo *et al.*, 2010). Mean reduction in line-length of evoked event: HR = $82.9 \pm 2.8\%$, n=5; ArchT = $88.5 \pm 4.4\%$, n = 5; n.s p<0.2.

Patch clamp studies showed that a more stable optogenetic current could be obtained by co-illumination of both 561 nm and 491 nm light, thought to be due to improved cis-to-trans recovery of the activated retinal by blue light (Han & Boyden, 2007). Therefore co-illumination of the brain slices was prepared using the 561 nm laser light with blue epi-fluorescence light (460 +/- 20nm excitation filter) through a 4x air objective (0.28 NA, Nikon). It was confirmed that this co-illumination strategy provided

an enhanced and sustained HR current by assessing the suppressive effect on electrical stimulation at different times during a long illumination period (figure 3.6B); contrast the intermittent breakthrough discharges as the HR current wains with just 561 nm illumination, and the consistent suppression of electrical stimulation with the combined 491 nm and 561 nm illumination.

2.9 Molecular biology

2.9.1. Enzyme digestion

All enzyme digestions were done in a 50 µl volume reaction containing 1 mg plasmid DNA, 1X bovine serum albumin (BSA), the appropriate buffers (as suggested by the company, depending on the restriction enzymes used), 0.5 – 1 µl restriction enzyme/s and nucleotide free water (Promega). Digestion reactions were incubated at 37° C incubator for 2-3 hours before agarose gel electrophoresis.

2.9.2. Electrophoresis

Generally 0.8% agarose was made by mixing 0.8 g agarose in 100 mL tris-acetate-EDTA (TAE) buffer heating it up in a microwave until all agarose was dissolved. 10 µl of ethidium bromide was added per 100 mL agarose mixed. Agarose mixed was poured onto the gel tray with the comb on and incubated in room temperature for 30 minutes or until it solidified. Plasmid DNA was diluted 1:6 in a DNA loading dye (Promega) and loaded into the wells. The hyperladder 1 was used as the DNA size indicator (Bioline). Electrophoresis was done in by applying 100 mV electric field using a horizontal electrophoresis system (Bio-rad) for 30-45 minutes.

2.9.3. Ligation

All ligations were done in a 20 µl ligation reaction containing 50 ng of the desired vector and insert with 1:3 molar ratio of vector and insert. T4 ligase and buffer were purchased from Promega. Reaction was then incubated in room temperature for overnight before proceed to bacterial transformation.

2.9.4. Bacterial transformation

All pcDNA3.1 constructs were amplified by transformation of Mach1 competent cell (Invitrogen) while all pLenti and pAAV constructs were amplified by transformation of Stbl3 competent cell (Invitrogen) to avoid homologous combination of the long terminal repeats found in lentiviral and retroviral expression vectors. For side directed mutagenesis, PCR products were transformed into XL1- gold cells (Stratagene). The same protocol was used for all competent cells. All cells were stored at -80° C and thawed in the ice just before use. 50 – 100 ng plasmid DNA was added to 100 µl cells then incubated in the ice for 30 minutes. Cells were then heat-shocked, by 40 s incubation at 42° C heat bath followed by 2 minutes incubation in the ice. 500 µl pre-warmed LB media was then added and cells then horizontally spun in 37° C room for 1 hour. LB plates containing 100µg/ml ampicillin was pre-warmed in the 37° C incubator for 30 minutes. 100-200 µl of cells were then spread on the LB plate and incubated in the 37° C incubator overnight before transferred to the cold room (4°C).

2.9.5. Plasmid prep

Single colonies of transformed bacteria with the desired plasmid were inoculated in 5 ml LB media for mini preps and 50 ml LB media for midi preps. Cells were grown overnight in a shaker with the temperature set to 37°C. Cells were collected by centrifugation at a maximum speed for 1 minute for mini prep and 5 minutes for midi prep. All plasmid preparations were done using Promega mini prep kit or QIAGEN midi prep kit.

2.9.6. Different constructs preparation

For all constructs made, enzyme digestion and sequencing were done to confirm the exact sequence of the product.

1. pcDNA3.1 - mutHR-EYFP

mutHR was created by conducting two stage site directed mutagenesis on pcDNA3.1-HR-EYFP plasmid (gift from Karl Deisseroth).

a. Forward primer: CGT-TTT-TAT-GAC-CGA-AGG-ACT-CGA-TGA-TC

Reverse primer: GAT-CAT-CGA-GTC-CTT-CGG-TCA-TAA-AAA-CG (eurogentec)

Annealing temperature: 50°C

b. Forward primer: GAC-TCG-ATG-ATC-CAG-AGG-CAC-AAC-TTA-TTG-CTG-TGT-C

Reverse primer: GAC-ACA-GCA-ATA-AGT-TGT-GCC-TCT-GGA-TCA-TCG-AGT-C (eurogentec)

Annealing temperature: 45°C

QuikChange XL Site-Directed mutagenesis Kit protocol was used. After transformation of competent cells 5 random colonies were selected, grown, and DNA was extracted using promega miniprep kit. DNA samples were sequenced to confirm the success of mutagenesis.

2. pcDNA3.1 - mutHR-IRES-EYFP

{Not1}STOP CODON-IRES{Not1} was synthesised by GeneArt – life technology. mutHR-EYFP was digested with Not1 enzyme that linearized the construct by cutting the Not1 site located between mutHR and EYFP. _{Not1}STOP CODON-IRES_{Not1} was ligated with the linearized mutHR-EYFP. Since _{Not1}STOP CODON-IRES_{Not1} could be ligated in 2 different orientations, screening had to be done by enzyme digestion before sequencing.

3. pcDNA3.1 -LepA-GFP-HR

{Kpn1}LepA{Not1}-GFP_{Not1}-HR_{Xba1} DNA was synthesised by GeneArt – life technology, and subcloned to the multiple cloning site region of pcDNA3.1 by Kpn1 and Xba1 enzyme digestion and ligation.

4. pcDNA3.1 -CD8-GFP-HR

$Kpn1$ CD8 $Not1$ DNA was synthesised by GeneArt – life technology. LepA-GFP-HR construct was partially digested with Kpn1 and Not1 to isolate GFP-HR component, and CD8 was subcloned by ligation.

5. pcDNA3.1 -CD8-EYFP

EYFP with a stop codon was isolated from the original HR-EYFP construct using Not1 and Xba1 while pcDNA3.1-CD8 DNA was obtained from CD8-GFP-HR construct by Not1 and Xba1 digestion. pcDNA3.1-CD8 and EYFP were then ligated to get CD8-EYFP construct.

6. pcDNA3.1 -CD8-HR-IRES-EYFP

CD8-HR was generated from a complete Not1 digestion of CD8- $Not1$ GFP $Not1$ -HR construct, GFP band was removed and CD8-HR was then ligated back.

7. pAAV-hSyn- ChloC-2A-tDimer and pAAV-hSyn -slowChloC-2A-tDimer

These plasmids were purchased from Addgene, plasmid #52495 for ChloC and plasmid #52494 for slowChloC.

8. pAAV-CAG –ArchT-GFP

This plasmid was purchased from Addgene, plasmid #29777.

9. pAAV -ChloC-2A-ArchT-GFP

This construct was built by removing tdDimer from the pAAV-ChloC-2A-tDimer construct by complete digestion using BamHI and HindIII. ArchT-GFP was isolated from pAAV-ArchT-GFP also by complete digestion using BamHI and HindIII. pAAV-ChloC-2A was then ligated to ArchT-GFP.

2.10 Immunofluorescence staining

Initially, dissociated neuronal culture cells attached to the coverslips were washed twice using 0.2 M phosphate buffer saline (PBS) with pH 7.2 – 7.4. Cells were then fixed using 4% paraformaldehyde (PFA) in PBS for 20 minutes at room temperature. Post fixation, cells were washed with PBS three times before adding a mixture of 0.1% gelatin and 0.1% triton in PBS, incubated at room temperature for one hour. Anti HR as the primary antibody used was purchased from Agrisera (AS12 1851) which was a rabbit polyclonal antibody. Cells were then incubated in Anti HR with 1:200 dilution in 0.1% gelatin, 0.1% triton in PBS for 30 minutes at room temperature. Solution was discarded and cells were washed three times in PBS. Secondary antibody against rabbit antibody with red fluorescence tag was used with 1:500 dilution in 0.1% gelatin, 0.1%triton in PBS. Added to the cells and incubated for 30 minutes at room temperature. Finally cells were washed again three times with PBS and mounted.

2.11 Analysis

Offline analysis was done using Igor (Wavemetrics, Oregon), Matlab and Microsoft Excel software. Boxplots were generated using online software (<http://boxplot.tyerslab.com>).

2.11.1. E_{GABA} measurement

The I_{GABA} was derived from the difference between the voltage ramp introduced at the peak of muscimol event and the voltage ramp introduced at the baseline period (figure 1.1) to allow a GABAergic I-V curve to be plotted. I-V plots were derived with and without prior HR activation, and the effect of HR activation on E_{GABA} was estimated from the shift in the x-intercept of the I-V plot (figure 2.1B). Series resistance was compensated offline.

The time course of $[Cl^-]_i$ modulation was assessed by measuring E_{GABA} with an increasing delay after a 2-3s optogenetic activation. E_{GABA} was calculated and normalized to the E_{GABA} shift produced with the shortest delay (usually the one with the biggest E_{GABA} shift) and exponentially fitted. The time constant (τ) of the curve fit was obtained as the time constant of HR or ArchT-ChloC variant $[Cl^-]_i$ modulation. The

mean time course was always calculated by averaging the individual cells' τ rather than extrapolating the pooled decay plot's τ .

2.11.2. Afterdischarge terminating oscillation

Propagation speed of ATO was measured between the time when the peak of sustained potential shift was recorded in 1 electrode to the time when it was recorded in another electrode of the same tetrode that is 50 μm apart. Recovery time of cells' activity post ATO was counted starting from the end of sustained potential shift observed in the LFP trace (1 -300 Hz) until the time when unit activity reappeared in the high pass trace (300 – 5000 Hz).

2.11.3. Assessment of GABA modulation in I_{Clamp} recording

GABA events were isolated based on the timing of the TTL pulse sent to the picospritzer to deliver muscimol puff. Amplitude of the GABA event was measured by averaging the amplitude of the current, 100 ms before and after the peak of the GABA event.

Chapter 3. Characterisation of halorhodopsin chloride pump

3.1 Introduction

Halorhodopsin is one of the most commonly used hyperpolarising optogenetic proteins, naturally found in *Natromonas pharaonis*. Upon light activation by illumination of 580 nm light, HR actively pumps chloride ion (Cl^-) into the cell, driving the membrane potential to be more hyperpolarised (Zhao *et al.*, 2008). In principle, the consequent changes induced by HR activation should affect both Cl^- ion concentration and membrane potential. However, despite its general use as a tool to modulate membrane potential, HR had not been characterized as a tool to modulate Cl^- concentration until just recently (Raimondo *et al.*, 2012).

To study the effect of Cl^- in inhibition, one should have a way of modulating Cl^- level independent of GABA and glycine, the two chloride channels that are responsible for inhibition. Previously, loading cells with Cl^- independent of GABA and glycine activity was only possible by doing whole cell patch of individual cell with the desired amount of chloride contained in the patching pipette solution. The continuity between the cytoplasm of the cell and the patching solution allows the diffusion of the patching pipette solution with the internal milieu of the cell. The technical difficulties set a limit on the number of cells that could be manipulated simultaneously. With HR optogenetic activation on the other hand, many cells could be targeted and activated at the same time without involving the naturally expressed chloride channels such as GABA and glycine. This makes HR a potential good tool as a $[\text{Cl}^-]_i$ modulator as well as its general use as a hyperpolarizing tool.

In this chapter, I will assess the usefulness of HR to load cells with Cl^- at a single cell level, answering the question of whether the light activated HR current sufficient for membrane hyperpolarization is large enough to change the internal Cl^- concentration of neurons significantly as to modulate GABA reversal potential (E_{GABA}). I will then explore the optimal way of activating HR and describe how to implement this in the network level for the next part of the project.

3.2 Results

3.2.1 Halorhodopsin activation causes a transient chloride loading effect

Mixed cortical and hippocampal dissociated neuronal culture from rats were prepared and transfected with two different constructs of HR, the original HR (NpHR-EYFP) and the newer version of HR (eNpHR3.0-EYFP). The original HR gave a relatively small current with an average current of 13.79 ± 4.73 pA, $n=6$ while the new version one had an enhanced current with mean amplitude of 163.89 ± 108.94 pA, $n=14$; note that the same illumination paradigm was used for these two measurements. The HR Cl^- loading effect was assessed by doing gramicidin perforated patch clamp recordings of the neurons that expressed HR, screened by the EYFP expression. Muscimol (GABA_A agonist) was applied locally on the cell soma and voltage ramps were introduced one at the peak of the muscimol event and one at baseline as explained in chapter 2. The current-voltage relationship (I-V curve) was derived from the two ramps to obtain the E_{GABA} .

To assess baseline stability, three muscimol events were triggered at one minute intervals, for each neuron. When holding the membrane potential at -70 mV, GABA_A activation from muscimol puff gave rise to a downward deflection (depolarizing), indicating that in these cells, E_{GABA} was more positive than -70 mV (figure 3.1Ai). The amplitude of the baseline muscimol events were relatively stable with a mean E_{GABA} shift that lay very close to zero (-0.62 ± 1.4 mV, $n=8$). Keeping the same interval, the following muscimol events were triggered with prior HR activation with increasing duration of illumination (2s-8s). Prior light activation potentiated GABA excitatory current (figure 3.1Aii), indicative of a more depolarized E_{GABA} as a consequence of raised $[\text{Cl}^-]_i$ induced by HR priming, with a mean E_{GABA} shift of 1.03 ± 0.18 mV/s, $n=6$ (E_{GABA} shift post 2s NpHR activation vs baseline, $p < 0.01$, Student's t-test) illumination by the original HR and 6.95 ± 1.5 mV/s, $n=14$ by the new HR (E_{GABA} shift post 2s eNpHR3.0 activation vs baseline, $p < 0.001$, Student's t-test). This positive shift in E_{GABA} tends to be larger the more chloride flux there was, measured as function of the integral of the HR current over the entire duration of illumination. It varied from cell to cell but it should be noted that the shift sometimes could be rather big (up to -23 mV, figure 3.1Aiii).

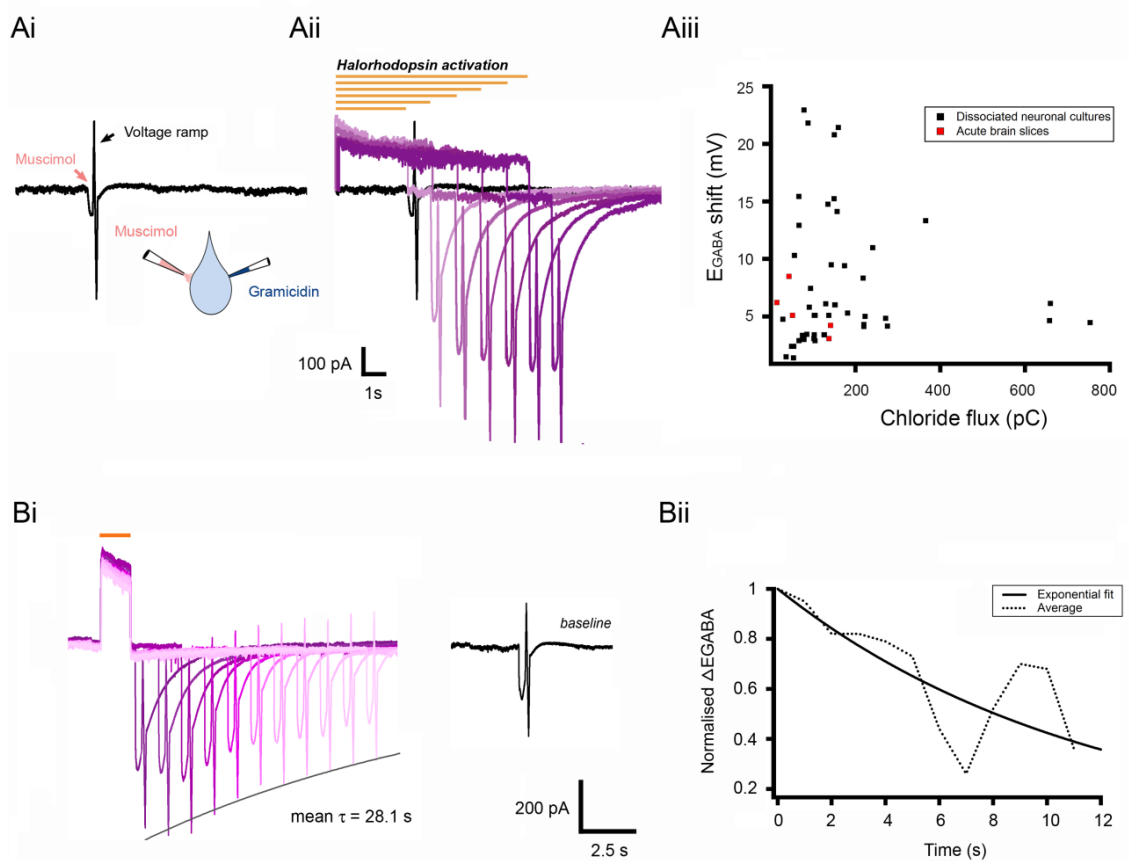


Figure 3.1 Halorhodopsin chloride loading effect. Ai. E_{GABA} was measured by doing perforated gramicidin patch recording and applying muscimol with or without prior HR activation. Aii. Example traces from a single neuron showing a progressively larger muscimol excitatory event with longer duration of HR illumination. Aiii. Scatter plot showing the shift in E_{GABA} versus the total loading charge calculated as the integral of the current over the illumination period. The plot includes multiple data points from single dissociated neurons, derived from different duration HR activations ($n=14$ cells) and 5 data points from 5 neurons (red) in adult brain slices, all from 2.5 s illumination. B. Duration of HR chloride loading was assessed by applying muscimol with increasing delay after 2s HR activation. Bi. Example measurement from a single neuron from the dissociated neuronal culture showing a progressively smaller muscimol event with a longer delay introduced between the light activation and the muscimol puff. Note that exponential fit to the minima of the ramps is simply for demonstration purpose, while the true τ was calculated from an exponential fit of the E_{GABA} shift measurements. Bii. Pooled data show the recovery of E_{GABA} following Halo activation in dissociated neuron cultures. Single exponential fits of the mean data are shown, but the time constants reported in the results section are the averages of fits made to each individual cells' E_{GABA} measurement. Mean time constant of E_{GABA} recovery post HR activation was 28.1 ± 9.2 s in dissociated neuronal cultures ($n = 14$).

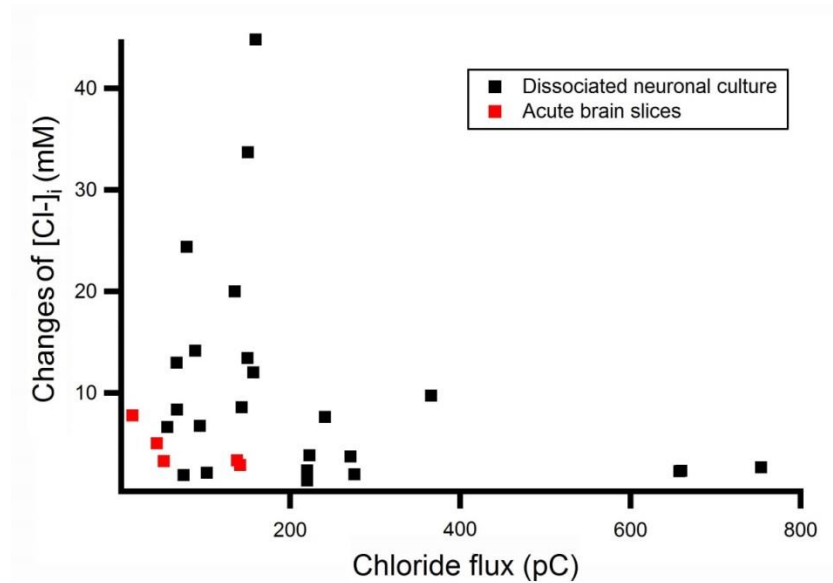


Figure 3.2 Estimation of the changes in $[Cl^-]_i$ induced by HR activation. $[Cl^-]_i$ was estimated from the E_{GABA} measurement using Nernst equation for Cl^- only. Temperature was considered to be constant ($33^\circ C$).

I then characterized the time course of this effect by activating HR for a short period and applying muscimol with an increasing delay. The biggest E_{GABA} shift could be observed in the first muscimol puff that was triggered soon after the HR illumination (100 ms delay), a smaller potentiation of GABA current was produced following a longer delay between HR illumination and the muscimol puff. E_{GABA} shift measurements with the different delays were exponentially fitted to derive the time constant of the E_{GABA} recovery. Indeed this effect decayed over time with a mean time constant of $28.12s \pm 9.26 s$ (mean \pm s.e.m; $n=14$; figure 3.1B) for dissociated neuronal culture cells.

The same characterization was also done in acute brain slices taken from 5 months old mice, expressing HR under CamKII promoter. Putative pyramidal cells from layer 2-5 of neocortex were selected, based on differential interference contrast (DIC) visualization (cells not filled). In these cells, E_{GABA} recovered more rapidly post HR activation with a mean time constant of $8.01 \pm 2.85 s$ (mean \pm sem, $n=5$; figure 3.2) although this is not significantly different from the time constant calculated for culture neurons (acute brain slices vs cultures: not significant, $p>0.05$, Student's t-test).

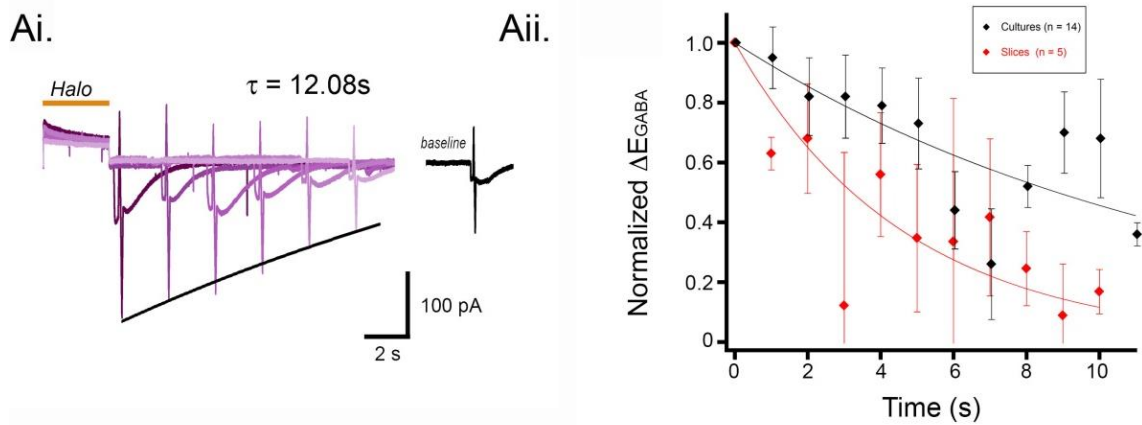


Figure 3.3 HR Cl⁻ loading effect in acute brain slices taken from adult mice. The same protocol assessing the time constant of E_{GABA} recovery post HR activation was done on acute brain slices taken from 5 months old mice. Ai. Example traces from a single neuron recording in which muscimol was applied with an increasing delay post a 2.5 s HR illumination. Note that exponential fit to the minima of the ramps is simply for illustration purpose, while the true τ was calculated from the E_{GABA} measurements. Aii. Pooled data of the recovering E_{GABA} was shown for data collected from dissociated neuronal culture (black, same data from figure 3.1B) and from acute brain slices (red). E_{GABA} recovered more rapidly in the acute brain slices (mean \pm sem : 8.01 ± 2.85 s, $n=5$) than in cultures (mean \pm sem : 28.1 ± 9.2 s, $n=14$).

This decay should mainly depend on the neuronal chloride clearance mechanism and the well-established one is KCC2 co-transporter as explained in chapter 1. Based on this, I then performed the same experiment while blocking KCC2 using 100 μ M furosemide. Due to the difficulty of maintaining gramicidin patch over a long period of time, continuous recording of baseline (ACSF), furosemide application, and washing out of the furosemide were only made from 3 cells. The rest of the data points were population based sampling. E_{GABA} shift data points with the different delay were normalised to the E_{GABA} shift produced with the shortest delay (100 ms). Data were pooled and plotted against the time post-HR illumination and fitted with a single exponential decay to compare how long the HR Cl⁻ loading effect last with and without furosemide. With furosemide in the bath, the chloride loading effect from 2s illumination lasted almost 3 times longer than control (Pooled decay plot shows $\tau_{control}$: 14.08 s and $\tau_{furosemide}$: 40 s; figure 3.3Biii). This confirms that indeed the time course of HR Cl⁻ loading effect was significantly longer when Cl⁻ extrusion mechanism is compromised.

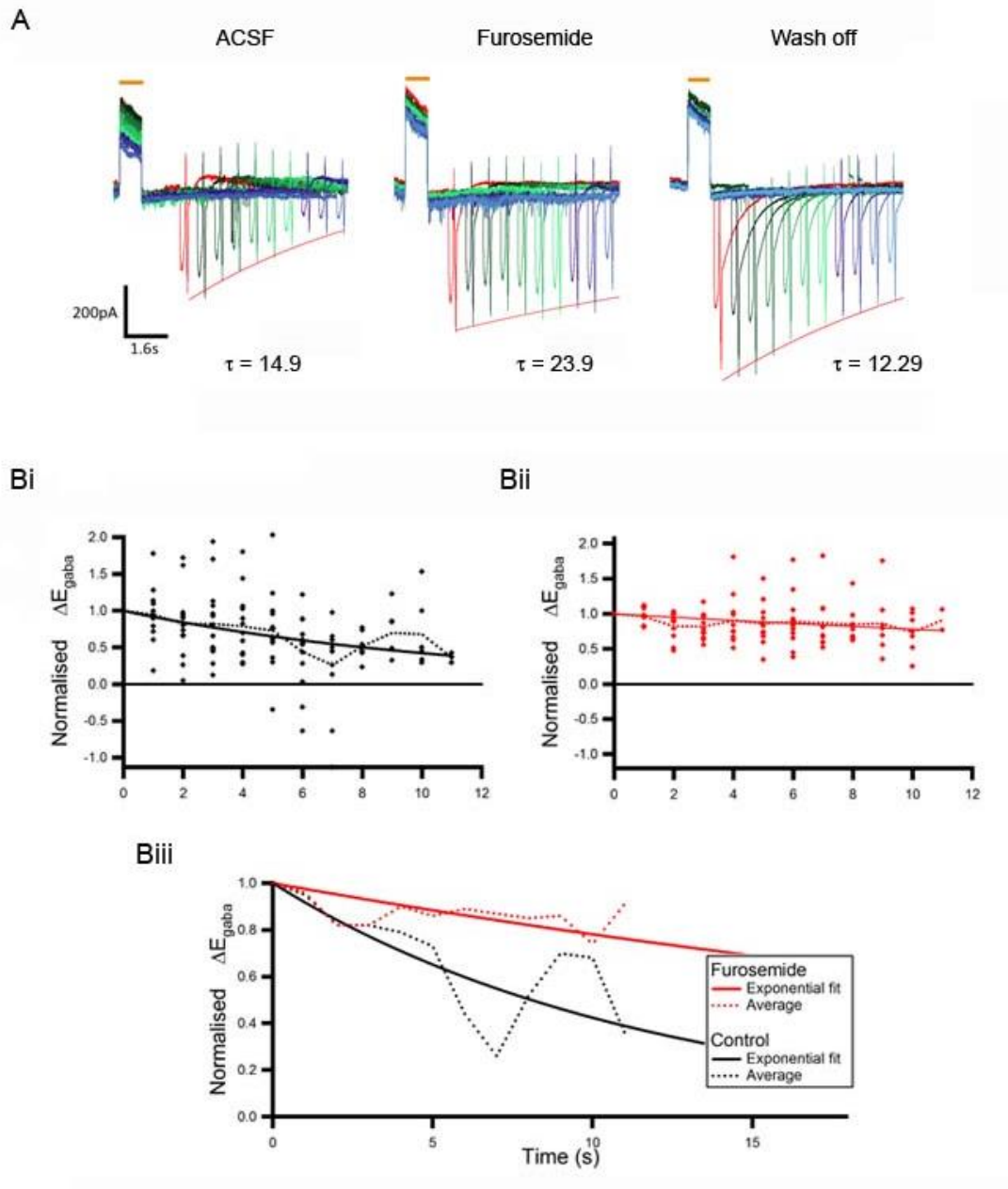


Figure 3.4 Furosemide prolonged the decay of HR chloride loading effect. Time course of Cl⁻ clearance post HR activation was assessed when KCC2 was blocked by bath application of 100 μ M of furosemide. A. Example of traces recorded from a single neuron of the dissociated neuronal culture with and without KCC2 blocker, furosemide (all from the same neuron). Time constant was longer in the presence of furosemide. Note that exponential fit to the minima of the ramps is simply for illustration purpose, while the true τ was calculated from the E_{GABA} measurements. B. Pooled data shows a slower decay of HR effect on the E_{GABA} shift in the presence of furosemide. Normalised E_{GABA} shift data points were pooled and plotted against time post HR illumination for (Bi) control with ACSF only and (Bii) with furosemide on the bath. Biii. Pooled decay plot gave a mean τ of 14.08 s for control (black) and 40 s for furosemide (red).

3.2.2 Blue light stabilizes halorhodopsin current

To make use of HR as a tool to modulate $[Cl^-]_i$ concentration, it is essential to investigate how to maximize the HR current, and so its consequent Cl^- loading effect on cells. This should be mainly dependent on the size of the HR current and the duration of illumination. In terms of the size of HR current, this is largely affected by the level of expression of the protein. Gradinaru et al (2008) has brilliantly optimized this in their eNpHR3.0 construct (also used in most of my experiments) by adding extra signal peptide into the DNA construct that assists the membrane targeting of HR from the endoplasmic reticulum (ER) (Gradinaru *et al.*, 2008). This signal was originally found in inward-rectifier potassium channel 2.1 (Kir 2.1) and it has been shown that when this signal was omitted, Kir2.1 protein aggregated in the ER. This highlights the importance of this signal in sending a protein out of the ER and into the membrane. The addition of this signal peptide to the HR construct significantly improved the level of membrane expression and light activated current of HR (Gradinaru *et al.*, 2008).

Another way of loading more Cl^- into the cell is by increasing the duration of illumination. When doing this however there was an issue of the decaying current over a longer period of light activation. This compromises the chloride loading effect as less Cl^- per second is being pumped into the cell when longer illumination was applied (figure 3.4Ai & 3.5 orange). The decaying current could be explained by a lower amount of readily activated retinal chromophore over time that is needed for the conversion of light into the energy needed for the Cl^- pump. Retinal chromophore exists in two forms of isomer, trans and cis configuration. Readily activated retinal is in the trans configuration. Once activated by light, this is converted into cis configuration that provides energy for the passage of a Cl^- . Until retinal is reconverted back into trans configuration, the protein remains inactive.

Han and Boyden used blue light, which is known to assist the reversion of cis-retinal back to trans-retinal, by delivering a short pulse of blue light illumination before a long orange light illumination for HR activation (Han & Boyden, 2007). Applying this, I compared the E_{GABA} shift after HR activation by orange light only in comparison to intermittent orange-blue illumination and indeed a marginal increase in E_{GABA} shift was observed by about 2 mV (figure 3.4).

To improve this further, instead of using an epifluorescence bulb with different filter sets in which two colours illumination is impossible, I then tried using 491 nm and 561 nm lasers, which allows simultaneous orange and blue light illumination for HR activation. This strategy stabilized the HR current as shown by a linear relationship between duration of illumination and Cl flux (current x duration of illumination) figure 3.5.

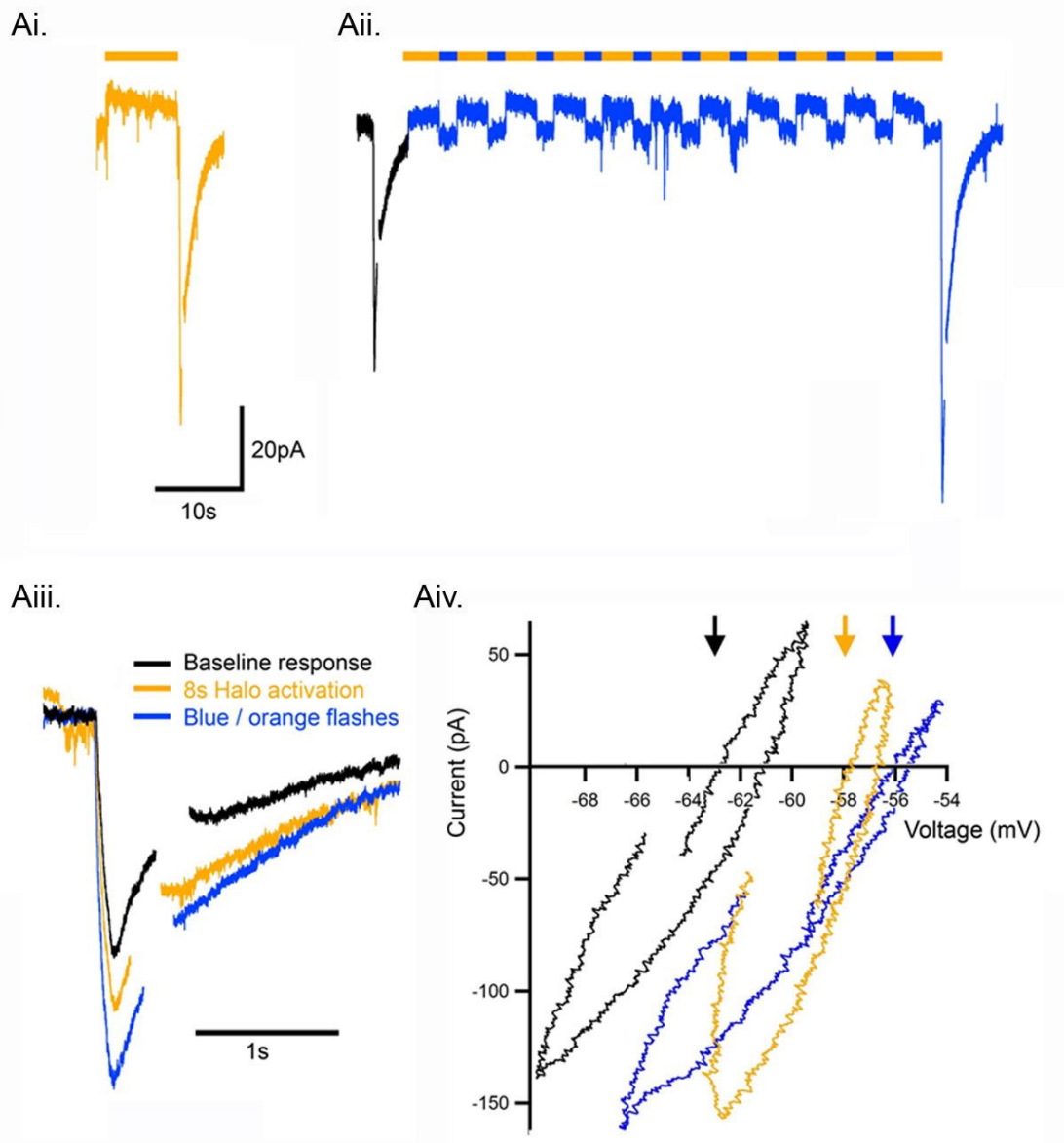


Figure 3.5 Intermittent illumination of blue and orange light optimizes HR Cl^- loading effect. Example traces from a single neuron expressing old HR to assess the usefulness of blue light in optimizing HR Cl^- loading effect. Ai. Conventional 8 s orange light illumination positively modulated muscimol event. However, at the end of the illumination HR current diminished to almost zero. Aii. Intermittent blue and orange light illumination allowed repeated HR activation with sustained amplitude of HR current. Aiii. It resulted in a bigger amplitude of GABA excitatory event (blue in comparison to black) indicative of a bigger positive shift in E_{GABA} (ramps are clipped). Aiv. This is also shown by the I-V curved derived from the ramps.

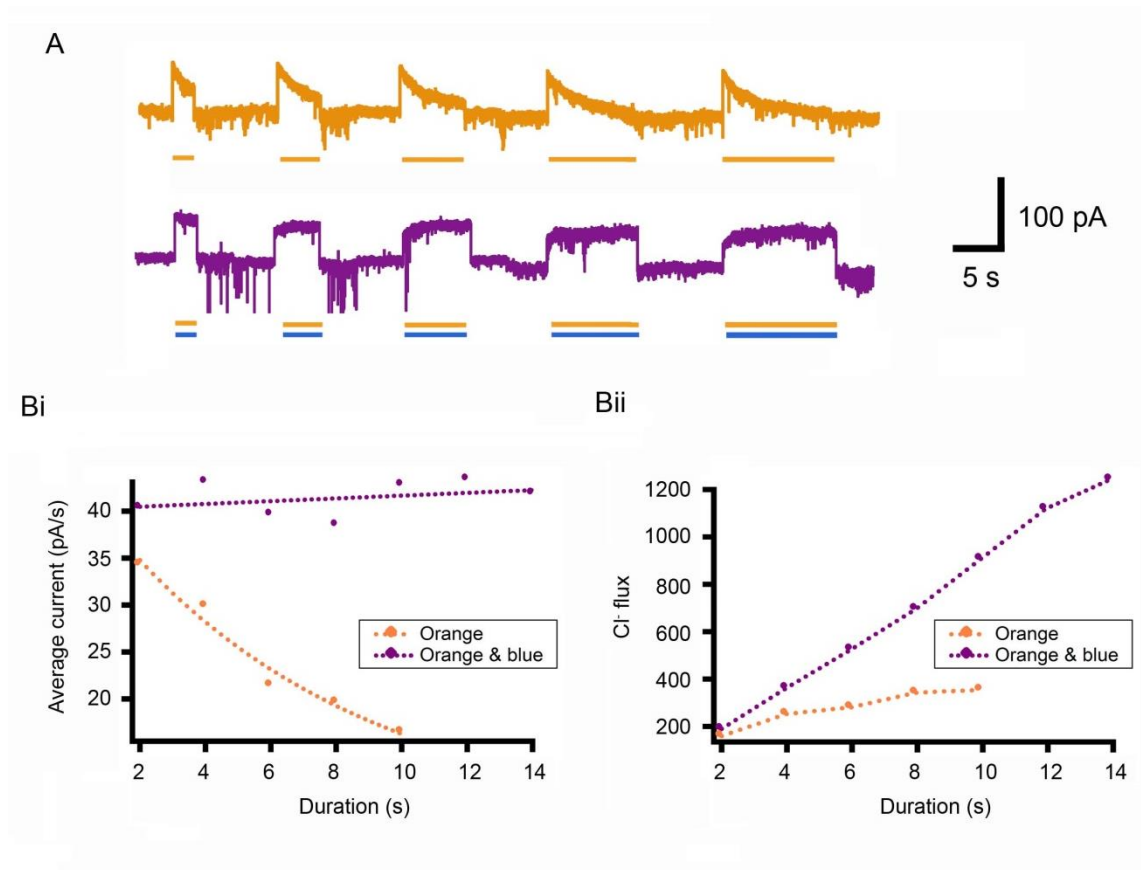


Figure 3.6 Co-illumination of both 561 nm and 491 nm light optimizes halorhodopsin current. A. Voltage clamp recording of a neuron from dissociated neuronal culture expressing new HR: 561 nm light illumination showed a decaying HR current overtime (top, orange trace) whereas co-illumination of 561 nm and 491 nm light give rise to a more stable HR current (bottom, purple trace). Bi. HR current per second was constant with double illumination as opposed to the drastically decaying current with single 561 nm illumination. Bii. Linear relationship between the duration of illumination and the Cl⁻ flux using the double illumination paradigm confirms the effect of co-illumination using both 561 nm and 491 nm light in stabilizing the HR current.

3.2.3 Designing HR illumination system for field recording in the interface chamber

So far all the collected data have confirmed that HR current necessary to hyperpolarise the neurons is sufficient to create an appreciable rise in the intraneuronal Cl^- level. Moving forward from this, I wanted to make use of HR as a tool to artificially load subset of cells with Cl^- . To do this, a way of illuminating multiple cells and assessing HR activity in a network level that will be done in an interface chamber rig has to be set up. When working with local field potential (LFP) recording and light stimulation, an important issue to be noted is the light induced artifacts that appear as a large voltage swing seen during light activation or inactivation. This sometime could be mistaken as the optogenetic current (Cardin *et al.*, 2010). It is due to a phenomenon also known as the Becquerel effect when there is unequal illumination of an electrode in the presence of electrolyte (Cardin *et al.*, 2010). Designing a test of HR current becomes absolutely necessary to confirm that the optogenetic current exist, since LFP deflection during light illumination could be a mere artifact.

Coronal brain slices from HR expressing animals were prepared and recording was done in an interface chamber perfused with oxygenated ACSF. On top of the interface chamber, an epifluorescence microscope was mounted with a 4X air objective (Olympus, NA0.28; figure 3.6C). Initially, 4X air objective was used to deliver the 580 nm light for HR activation. The HR current was tested by delivering electrical stimulation on the white matter and recording from the layer 5 of coronal slices, with and without HR illumination. Apart from a marked deflection during light-on and light-off period, there was no substantial reduction in the electrically evoked event recorded during light illumination, suggestive of no hyperpolarising HR current induced in this set up. Failure to activate HR using 4X air objective could be explained by the fact that in this set up, light is scattered around the entire slice that consequently reduces the light intensity per surface area. I then changed the illumination system by using a 561 nm laser, connected to a fibre optic that feeds into a thin cannula to be placed very close to the surface of the slice by a micromanipulator (figure 3.6C). This way, light could be delivered more focally hence maximizing the light intensity per surface area. When repeating the same test, light illumination suppressed the electrically evoked event substantially confirming that this illuminating system works in activating HR current (figure 3.7A).

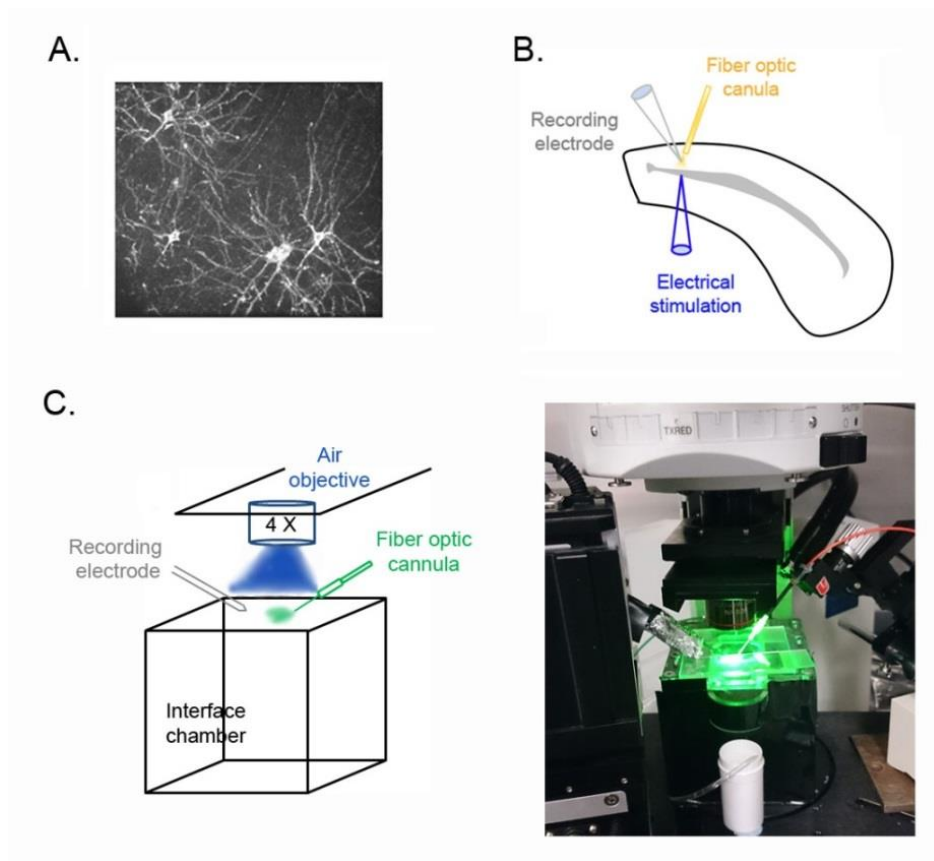


Figure 3.7 Network activity recording arrangement. A. Confocal image showing sparse expression of HR-EYFP in pyramidal cells when expressed under CamKII promoter. B. Schematic showing the locations of the recording electrode in layer 5 (grey), stimulating electrode (blue) in the underlying white matter, and a fibre optic delivering 561 nm wavelength light. C. Schematic (left) and photograph (right) of the illumination system: 561 nm light was delivered by laser connected to a fibre optic cannula that was controlled by a manipulator to direct it to the surface of the slice, while 491 nm light was delivered through 4X air objective, to stabilize the HR current.

The effect of blue light (491 nm) in stabilizing the HR current was also assessed on the LFP by doing repetitive electrical stimulation with 30s interval and activating HR using 561 nm light only or with co-illumination by 561 nm and 491 nm light. 561 nm laser was delivered via the cannula as mentioned earlier, while the 491 nm was delivered via the 4X air objective lens (figure 3.6C). As shown in figure 3.7B, electrical stimulation at 0.25 Hz evoked a relatively stable amplitude of network event (figure 3.7B, black). These electrically evoked events show a 'threshold effect' where just a small reduction in the power of the electrical stimulation will abolish these events altogether. When activating HR with 561 nm alone, this electrically-evoked events were suppressed but rather variably with some breakthrough activity recorded (figure 3.7B, orange). This suggests that there is a decaying effect of the HR current. In contrast, 491 nm and 561 nm co-illumination consistently suppress these events throughout a long period of illumination (up to 40 s; figure 3.7B, purple), suggesting of a more stable HR current.

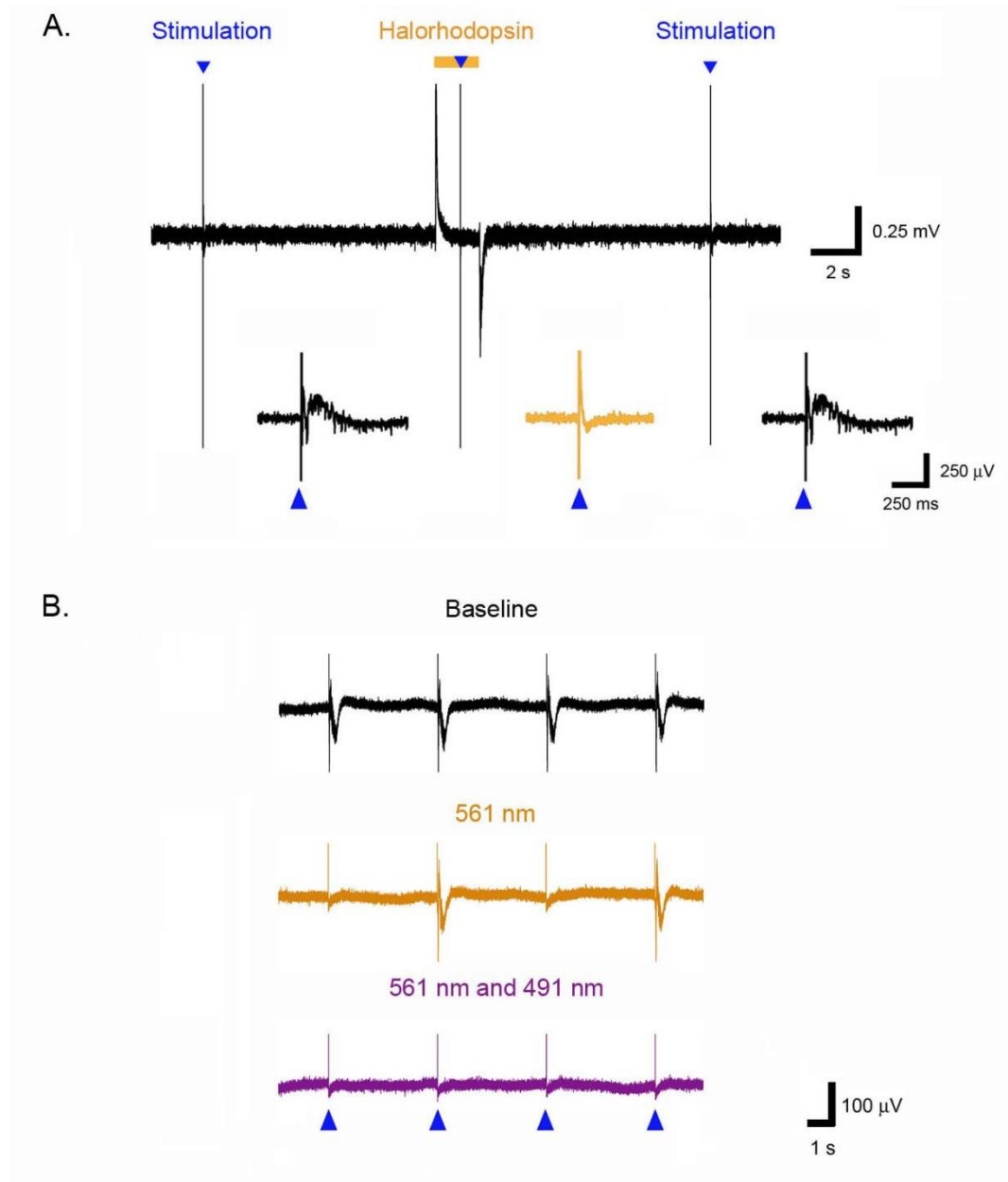


Figure 3.8 Halorhodopsin current suppresses electrically evoked event. A. Example from 1 brain slice showing that 560 nm illumination greatly suppresses the electrically evoked neural activity, thereby demonstrating the existence of a prominent HR current. Blue triangles mark the onset of the electrical stimulation. Orange bar shows the onset of the light activation. Upward and downward deflection could be observed on the LFP trace at the start and the end of light activation respectively. B. Evidence of sustained HR current by 561 nm and 491 nm light in the extracellular recording. Electrical stimulation was applied every 4s. Steady baseline was recorded without light stimulation, showing a stable response. When HR was activated continuously with 561 nm, the suppression was initially strong, but breakthrough bursts often recorded. With persistent 561 nm-491 nm light illumination, the suppression of activity was maintained throughout the illumination period, indicating that with this form of illumination, the HR current remains large, as was shown in the single cell assays (figure 3.5). This effect was maintained for illumination periods of up to 40s.

3.3 Discussion

For a long time, people have been focusing mainly on the hyperpolarizing effect of HR while discounting its effect on the $[Cl^-]_i$ modulation. One of the reason is due to the uncertainty of whether the light activated current that is enough to hyperpolarize the membrane potential could also provide a substantial change in the $[Cl^-]_i$. Earlier study by Tonnesen et al (2009) claimed that this is not the case as they did not see a significant shift in E_{GABA} during HR activation compared to no activation (Tønnesen *et al.*, 2009). The failure to see the shift in this study could be explained by the fact that they performed the E_{GABA} measurement after only a very brief light activation (200 ms) compared to a much longer activation (in seconds duration) that they and many others introduced when using HR as a hyperpolarizing tool. In addition, they were using the original version of HR that has a relatively small current.

In this chapter, I have demonstrated clearly that it is indeed possible to load cells non-invasively and non-synaptically with Cl^- simply by activating HR optogenetically. This is based on the fact that HR activation significantly alters E_{GABA} into a more depolarized level indicative of a higher $[Cl^-]_i$. This effect does rely on the size of the current and the duration of illumination, however in our hand a positive shift in E_{GABA} was readily induced when cells were primed with HR activation even with 2 s illuminations only, both with the original HR or the new one eNpHR3.0, depending on the cells but the shift could be really big (up to 23 mV). The same result has been shown also by Raimondo et al in hippocampal pyramidal neurons from organotypic culture and acute brain slices (Raimondo *et al.*, 2012).

HR effect on E_{GABA} or $[Cl^-]_i$ is transient, as demonstrated by the progressively smaller E_{GABA} shift with an increasing delay between HR activation and muscimol puff. The time constant of this decay reflects the efficiency of Cl^- clearance mechanism of the cell, as shown by the prolonged decay when KCC2 was blocked (figure 3.3). Hence this experimental protocol could also be useful as an assay to measure a cell's ability to clear Cl^- . The time constant of Cl^- clearance post HR illumination was also measured in acute brain slices taken from 5 months old mice, to give an insight in designing the illumination paradigm for the next chapter, in which HR will be used as a $[Cl^-]_i$ modulation tool. Knowing that in these slices, E_{GABA} recovered with a time constant of

8.01 ± 2.85 s post HR illumination, any future observation about high $[Cl^-]_i$ effect should only be made within this time period.

HR Cl^- loading effect could explain the commonly observed rebound burst of action potentials after HR activation in many different set up of experiments (Tønnesen *et al.*, 2009; Madisen *et al.*, 2012). However, rebound firing could also be explained by the activation of the hyperpolarization-activated cyclic nucleotide-gated (HCN) channel that is activated by hyperpolarization and gives rise to a depolarizing current (I_H) towards the threshold of action potential. This is supported by the same rebound firing observation when Arch, the outward proton pump that hyperpolarizes the cell without changing Cl^- concentration, was used (Madisen *et al.*, 2012). Evidently, this is likely to be weaker than the effect of HR Cl^- loading as shown by Raimondo *et al.* (2012). HR activation consistently increases the spike probability in a single cell level, whereas Arch activation that should still activate I_H but without Cl^- loading effect showed a variable and insignificant increased in spike probability post hyperpolarization (Raimondo *et al.*, 2012). This could be due to the fact that cells vary in their I_H levels.

This is an important insight for further use of optogenetics as it is essentially an artificial way of altering certain ion level intracellularly. Inevitably, there could be some consequences on the neuronal system that naturally regulated by a certain balance state of the manipulated ion. For instance with HR, its Cl^- inward pump results in the transient alteration of Cl^- balance that results in the modulation of E_{GABA} . As presumably for ArchT, the outward H^+ pump might affect the H^+ concentration within the cell and potentially the pH level, although this might be rapidly equilibrated by the buffering mechanism.

To use HR as a hyperpolarising tool, one should be fully aware that the HR hyperpolarizing effect always comes with the Cl^- loading effect and vice versa, hence careful thought in designing the experiment is important. For instance, many groups have tried to use HR as a tool to control epileptic seizures (Tønnesen *et al.*, 2009; Krook-Magnuson E *et al.*, 2012; Paz *et al.*, 2012; Wykes *et al.*, 2012; Sukhotinsky *et al.*, 2013) and in this situation HR Cl^- loading effect could potentially contribute further to the hyper-excitability and promote seizure initiation. Furthermore, it has been shown before that in human epileptic tissue there appears to be a reduction in the KCC2 level

of expression (Huberfeld *et al.*, 2007b) that based on my experimental data will extend the HR Cl⁻ loading effect on cells to almost three times longer than when Cl⁻ clearance mechanism is intact (figure 3.3). This is not to close the possibility of using HR in epilepsy as Cl⁻ loading effect of HR is only transient and naturally HR current decays overtime. However this is an important consideration to be primed about. This will be further discussed in chapter 6.

The same concern applies when intending to use HR Cl⁻ loading effect as a tool to artificially load cells with Cl⁻. It should be noted that the effect is inseparable from the hyperpolarizing effect and hence a proper control for the hyperpolarizing effect is needed to isolate the Cl⁻ dependent effect of the result such as the use of Arch by Raimondo et al (Raimondo *et al.*, 2012).

Illumination paradigms could be tailored accordingly to the ultimate goal of HR use. For example, when hyperpolarizing effect is desired without causing a rebound firing that might contribute to hyper-excitability, the naturally decaying HR current might be suitable however decaying the current further could also be helpful. This is possible by ramping down the light at the end of an illumination. This is particularly helpful for the new version of HR that has a large current compared to the old one. Ramping down the light has been shown to successfully reduced rebound firing induced by the new version of HR by 60% (Chuong *et al.*, 2014). When a strong Cl⁻ loading effect is needed as for what this thesis is aiming for, simultaneous orange and blue light illumination is favorable to stabilize the HR current hence the Cl⁻ loading effect as shown in figure 3.5 & 3.7.

3.4 Summary

I have shown that HR activation modulates intraneuronal Cl^- level significantly and hence could be used as a tool to artificially load cells with Cl^- . The effect is transient with a mean time constant of $28.1 \pm 9.2\text{s}$ in dissociated neuronal cultures and of $8.01 \pm 2.85\text{ s}$ in adult acute brain slices, which is the window of opportunity to observe the network activity when cells are loaded with Cl^- before it returns back to baseline. For this purpose, co-illumination of orange and blue light is beneficial to stabilize the inward Cl^- drive. I also have provided the best strategy for applying this to the network level to move forward to the second aim of this thesis that is to study how high $[\text{Cl}^-]_i$ modulate network activity and how it relates to epilepsy.

Chapter 4. Characteristics of epileptic network activity arising from raised intraneuronal chloride

4.1. Introduction

It has been reported before that seizures are commonly associated with a marked increase of intraneuronal Cl^- ($[\text{Cl}^-]_i$) in different in vitro models of epilepsy (Fujiwara-Tsakamoto *et al.*, 2006; Huberfeld *et al.*, 2007c; Dzhala *et al.*; Lillis *et al.*, 2012; Ellender *et al.*, 2014; Pallud *et al.*, 2014). It is well established that when Cl^- accumulates intracellularly, the driving force for hyperpolarizing GABA is reduced and eventually becomes depolarising (Thompson & Gahwiler, 1989a; Staley *et al.*, 1995; Ben-Ari, 2002). However, to what extent high $[\text{Cl}^-]_i$ state is really involved in the generation of the epileptic network activities, and whether it is by itself sufficient to trigger seizure, is still unclear.

Using the HR Cl^- loading effect, that has been characterised in the previous chapter, as a mean to load subsets of cells with Cl^- at the same time, I explore how high $[\text{Cl}^-]_i$ modulates the network activity and investigate the role of high $[\text{Cl}^-]_i$ in the generation of certain patterns of epileptic network activities, also answering the question of whether high $[\text{Cl}^-]_i$ by itself could lead to seizure initiation.

4.1.1. High frequency activity in epileptic networks

One clinically relevant network activity, which has been associated with epilepsy, is the generation of high frequency oscillations (HFOs) that range from 150 to 600Hz (Engel Jr *et al.*, 2009; Alvarado-Rojas *et al.*, 2014). HFOs have been recorded in vitro or even on EEG recording from patients with epilepsy. This pattern of activity has been linked clinically as a hallmark of epileptic focus zone (Bragin *et al.*, 2002a; Bragin *et al.*, 2002b; Staba *et al.*, 2002; Jiruska *et al.*, 2010).

However, not all HFOs are considered pathological as HFOs are also commonly recorded in healthy rodents (Buzsaki *et al.*, 1992), monkeys (Skaggs *et al.*, 2007), and humans (Le Van Quyen *et al.*, 2008) during quiet wakefulness and slow-wave sleep. This physiologic HFO is suggested to play a role in memory consolidation during sleep

(Wilson & McNaughton, 1994). As HFO could reflect both physiological and pathological network activity, it is therefore important to be able to differentiate them by recognizing the different characteristics of those patterns of activity.

Recent study, in which simultaneous intracellular and extracellular recording were performed during HFO, indicated that it is difficult to classify HFO that is <250 Hz as epileptic or physiologic, judging only from the extracellular recording (Alvarado-Rojas *et al.*, 2014). This is because there are multiple underlying cellular and synaptic mechanisms that could give rise to this pattern of activity, including the physiological and the pathological ones (Alvarado-Rojas *et al.*, 2014). In contrast, activity that is >250 Hz, also known as fast ripple, is better associated with epilepsy, as this is only generated in situations where there is an enhanced excitability and a failure of GABAergic signalling (Huberfeld *et al.*, 2011; Alvarado-Rojas *et al.*, 2014). Furthermore, this feature has also never been recorded in healthy territories (Alvarado-Rojas *et al.*, 2014).

Additionally, it has been reported before that a highly characteristic pattern of epileptic fast ripples in rats (Foffani *et al.*, 2007b; Ibarz *et al.*, 2010a) is the notable harmonic feature of a prominent frequency band at 150-300Hz and another at approximately double the frequency, which they suggested may arise from subpopulations of neurons firing out of phase of each other. However, how these subpopulations of neurons arise is still unknown and further understanding is needed as these issues can impact directly on clinical practice, regarding the use of HFO as a hallmark of epileptic foci. Furthermore, a proper explanation of these pathological activity patterns may also suggest novel therapeutic avenues as manipulation that reduces HFO also has been shown to reduce seizure propensity at the same time (Grenier *et al.*, 2003).

4.1.2. Seizure termination

Most of the time, epileptic network activities including seizures are transient and self-terminating. However, the mechanism of how seizures terminate is still poorly understood. Typically, seizures are followed by post ictal depression that clinically manifests as extreme exhaustion (Löscher & Köhling, 2010). During this refractoriness, seizure threshold is increased (Löscher & Köhling, 2010). Several different mechanisms

have been suggested as possible explanations of how this might happen and all could be true for the different cases of seizures or epilepsy models.

First, it has been suggested that post-ictal hyperpolarization might be responsible for post-ictal depression state, as commonly observed from the intracellular recordings (Somjen, 2004; Ilie *et al.*, 2012). This prolonged hyperpolarization could last for several minutes and is mainly imposed by K^+ current, which is facilitated by G-protein coupled receptors such as $GABA_B$ and adenosine receptors (Löscher & Köhling, 2010; Ilie *et al.*, 2012). Additionally, activity of voltage-gated and calcium-activated K^+ channels could also contribute further to this hyperpolarization (Somjen, 2004).

A second mechanism proposed is by the metabolic processes such as the depletion of energy and neurotransmitters pool, which limits the sustenance of further neuronal activity (Somjen, 2004; Löscher & Köhling, 2010). In addition, pH alteration following intense neuronal activity could also contribute to the post-ictal depression state. Lactic acid accumulation and hence acidification in the extracellular matrix could be observed post seizure and this has been shown to reduce neuronal excitability (Somjen, 2004; Löscher & Köhling, 2010).

Lastly, spreading-depression like event due to depolarization block also has been suggested as a mechanism underlying the post-ictal depression phenomena at the end of a seizure (Somjen, 2004). Depolarization block is a situation of an extreme depolarization of the membrane potential due to extracellular K^+ accumulation, which deactivates voltage-gated sodium channels, leaving the cells incapable of generating action potentials (Somjen, 2004). In spreading depression, the depolarization

propagates slowly and so does the depression state it induces (Bragin *et al.*, 1997). Post-tetanic stimulation seizures are often followed by spreading-depression like events that could also contribute to its termination (Somjen *et al.*, 1985; Bragin *et al.*, 1997). However this might not be applicable to all seizures as mentioned earlier, since most intracellular recordings from a seizure show a post-ictal hyperpolarization rather than depolarization (Somjen, 2004).

It has been shown that spreading depression happens when K^+ outside surpasses the limit of 8-12 mM (Somjen, 2004). However it still poorly understood how K^+ could accumulate to that extent during spreading depression and how it propagates. Further understanding could give an explanation of why some seizures are terminated with spreading-depression like event while others not.

4.2. Methods

4.2.1. High frequency oscillation analysis

Frequency band analyses were done on the raw data, whereas for multi-unit analyses, a band pass filter of 300-5000 Hz was applied and spikes were detected by a simple thresholding algorithm. Spike analyses were only performed for periods when the tissue was not illuminated (that is to say, not during the periods of optogenetic activation). Hilbert transform analysis was performed on the dominant oscillation signal (75-300 Hz band-pass filtered), which allows this signal to be plotted as a continuous circular trajectory. To analyse spike timing according to the dominant oscillation, detected spikes were plotted on the Hilbert transform of the corresponding dominant oscillation. Angle and linear histograms were derived from the Hilbert plot. Baseline data was centralised and fitted to a Gaussian curve to obtain the baseline half-width. In order to assess the action potential jitter and out-of-phase firing across multiple experiments, we derived a “half-width index”, which was calculated using the following formula:

$$\text{Half width index} = \frac{\sum(\text{spikes outside baseline HW})}{\sum(\text{spikes within baseline HW})}$$

Where HW is the half-width measured on the baseline period. Note that the baseline HW is used for all analyses for a single experiment, including for the optogenetically-primed data sets which have a different width modal histogram peak.

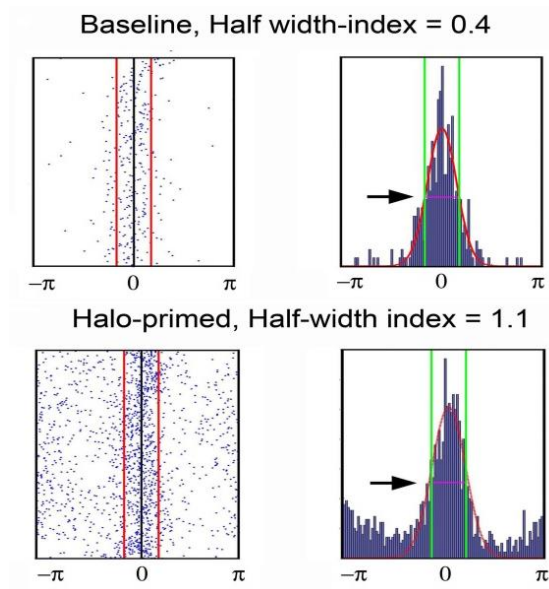


Figure 4.1 Measurement of half-width indices to quantify the increased jitter and out-of-phase firing. Half-width index measures the ratio between the numbers of out-of-phase spikes to the in-phase spikes, which were taken to be the spikes within bounds set by the half-width of a Gaussian fit to the main spike peak in the histograms. Example from a single recording during baseline period and HR primed period: left panels show the centralised raster plots for baseline (top) and HR primed tissue (bottom), and the right panels show the centralised histograms of the spike times.

4.2.2. Control analysis for spectral leak

An important consideration when analysing spike phase relationships, especially when relating units and field recordings made in the same electrode, is spectral leak, which is where a very high frequency event will create a small ripple also in lower band pass filtered traces. Note however, that the ripple is very small relative to the original signal (<1%), but because it arises from that sharp signal, it will always have a fixed phase relationship to it. For this reason, it was important to assess whether, despite its small amplitude, the pooling of many units might produce a distribution which is unduly influenced by this fixed phase artefact.



Figure 4.2 Spectral leak from a delta-function. The plot illustrates the problem of spectral leak, with a δ function in lieu of an action potential spike. A 75-300Hz bandpass filter was performed on the “raw trace” (black), which is a 10 kHz sampled flat data set with a single data point of unit amplitude. The filtered version of this has a single cycle oscillation with approximately 0.8% peak-to-peak amplitude. Action potentials will thus also create an additional oscillation in the lower frequency bandwidths, but as this illustrates, this effect is very small.

In order to separate out the spectral leak from the spike-independent field oscillation, I reanalysed the spike-phase data in two ways: first, by amputating the spikes from the data; and second, by analysing the phase of oscillation at a time point 1-2 ms ahead of the spikes, with and without spike amputation (figures 4.8A). The reasoning was that if the spikes were indeed embedded within genuine oscillations, then these oscillations would extend sufficiently far in front and after the spike that the relationship would still exist for time-shifted points. A forward time-shift was chosen to avoid any postsynaptic influences. With 1-2 ms ahead, there was no significant difference between the spike time distributions for the original or amputated versions, which indicates that the oscillation in this time point is not influenced by the spectral leak from the spike.

4.3. Results

4.3.1. Raised intraneuronal chloride induces high frequency oscillation

Coronal brain slices were prepared from the animals that express halorhodopsin (HR) or archaerhodopsinT (ArchT) under a pyramidal cell specific promoter, CamkII (figure3.6Ai). Recording was done in layer 5 of somatosensory cortex and electrical stimulation was applied onto the white matter (figure3.6Aii). HR and ArchT current were assessed by applying electrical stimulation during optogenetic illumination and observed that this was suppressed markedly compared to baseline (chapter 3.3, figure 3.6Bi). Only slices that showed this optogenetic suppression of electrically evoked events were included in the experiment.

Generally, experiment was started with a baseline cycle that comprised of 10 repeats of electrical stimulations delivered every 30 s without any optogenetic activation. This was then followed by optogenetic priming cycle that comprised of 20 repeats of both electrical stimulations and optogenetic activation. Electrical stimulations were timed to be at 4.5 s before and 0.5 s after the optogenetic illumination that each lasted for 25 s (figure 4.3Ai). This allows a comparison of the electrically evoked network event before and post HR-priming period. Typically, a second baseline cycle and optogenetic priming cycle were also done at the end (figure 4.3Aii).

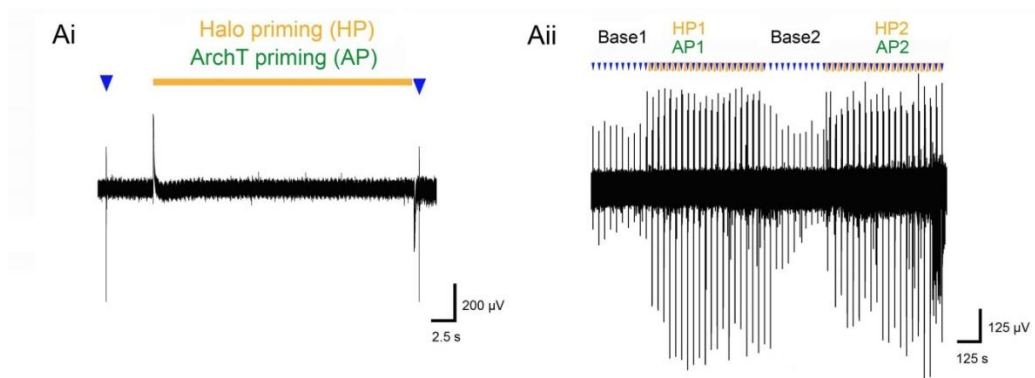


Figure 4.3 Experimental protocols for HR priming and ArchT priming. A. Chloride loading was achieved by interspersing 25s periods of 561 nm illumination to activate HR (“Halo priming”) while the control for hyperpolarization was conducted by replacing HR priming with ArchT priming. Electrical stimulations were applied during the dark periods (5s). One was applied 0.5s after, and one was 4.5s before the illumination. The interval between stimuli was always 30s. Baseline periods had the same electrical stimulation frequency, but without any illumination. Aii. Two baseline cycles and 2 optogenetic priming cycles were recorded one after another.

Baseline electrical stimulation on the white matter evoked a network activity that peaked at <150 Hz (figure 4.4A). Tissues that have been primed by HR illumination showed a potentiation of this event especially in the high frequency oscillation (HFO) range (300-600 Hz; figure4.4A&C). As a control for the hyperpolarisation effect of HR priming in the modulation of the network activity, the same experiment was done using ArchT, which is another hyperpolarising optogenetic tool that pumps protons out (Han *et al.*, 2011) and is therefore Cl⁻ independent (Raimondo *et al.*, 2012). In contrast, when tissues were primed with ArchT there was no change in the HFO range confirming that the HR-primed induced HFO was Cl⁻ dependent and not merely due to rebound firing subsequent to synchronized hyperpolarisation of pyramidal cells (Figure4.4B&D).

Power analysis of different frequency bands were done comparing 75-150 Hz, 150-300 Hz, 300-600 Hz, and 600-1200 Hz components for HR and ArchT primed events. HR priming showed stronger potentiation across all frequency bands compared with ArchT, but only at 300-600Hz was HR modulation significantly different from ArchT (n=11 for both HR and ArchT, Student'S t-test p<0.01; figure 4.5). The 600-1200 Hz power for both HR and ArchT showed a very little deviation from baseline (figure 4.5A). This suggests that the modulation between 300-600 Hz was not due to a simple harmonic phenomenon of the lower frequency bands. Rather it was a genuine biological modulation due to Cl⁻ loading, as harmonic will increase the higher frequency band (600 -1200 Hz) as well.

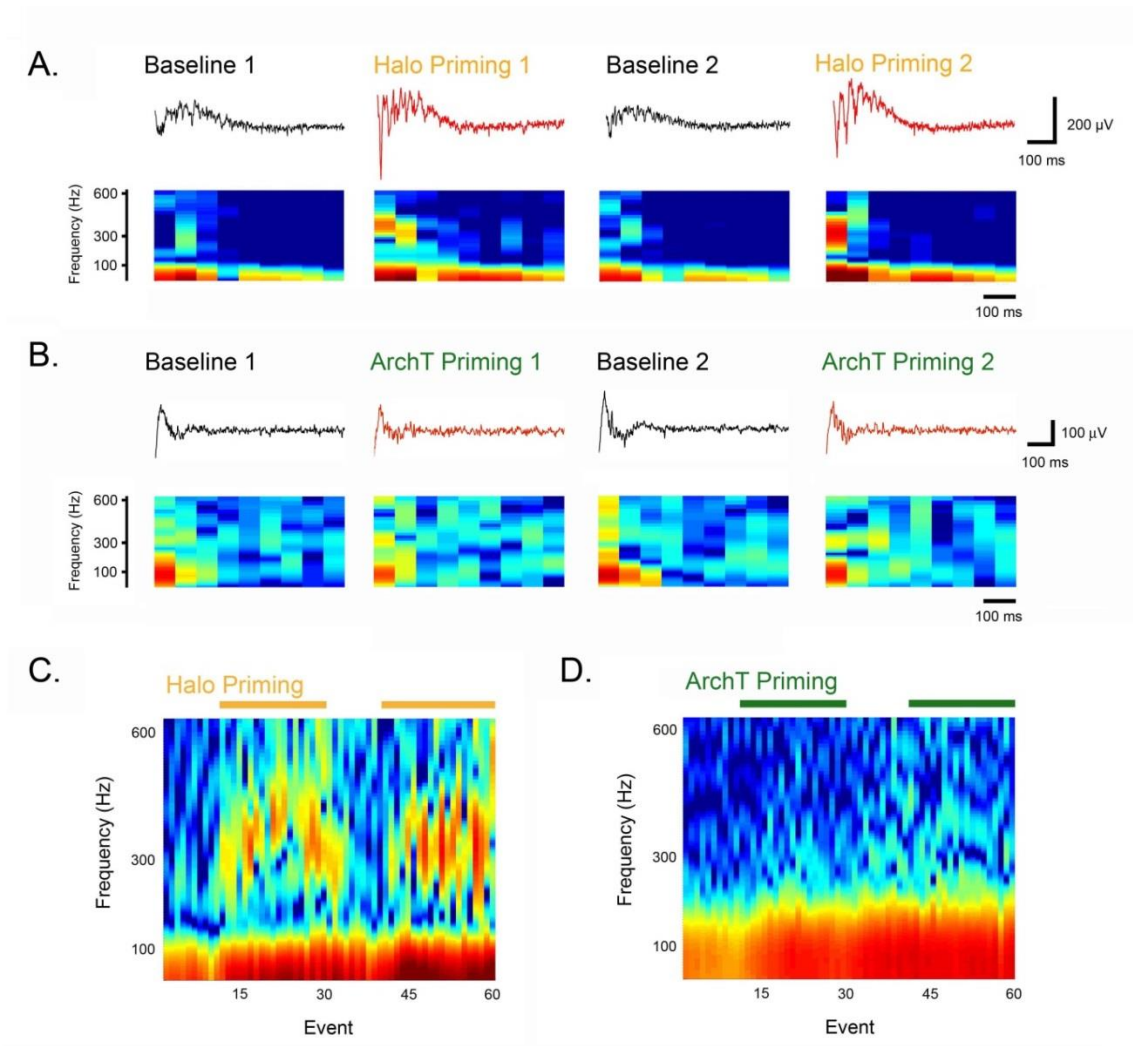


Figure 4.4 Halorhodopsin chloride loading induced high frequency oscillations. A. Representative traces and spectrograms from a single brain slice taken during two periods of electrical stimulation without HR illumination (baseline 1 and 2), and two periods with illumination (HP1 and 2). Note the large increase in power at 300-600 Hz during the halo-priming periods, which reversed rapidly without illumination (baseline 2 and C). B. Representative traces and spectrograms from a single brain slice expressing ArchT, during baseline 1 and 2 (black traces) and during ArchT priming 1 and 2 (red traces). In contrast to HR priming traces, no increase in power could be seen at 300-600 Hz with ArchT priming. C. Composites of sequential spectrograms from the same brain slice in A to show the changes during the entire experiment, showing the rise in high frequency power (200-500 Hz) induced by halo priming and the reversion to baseline without illumination. D. Composites of sequential spectrograms from the same brain slice in B with ArchT induced a small increase in amplitude of the network event, but without any change in the high frequency activity.

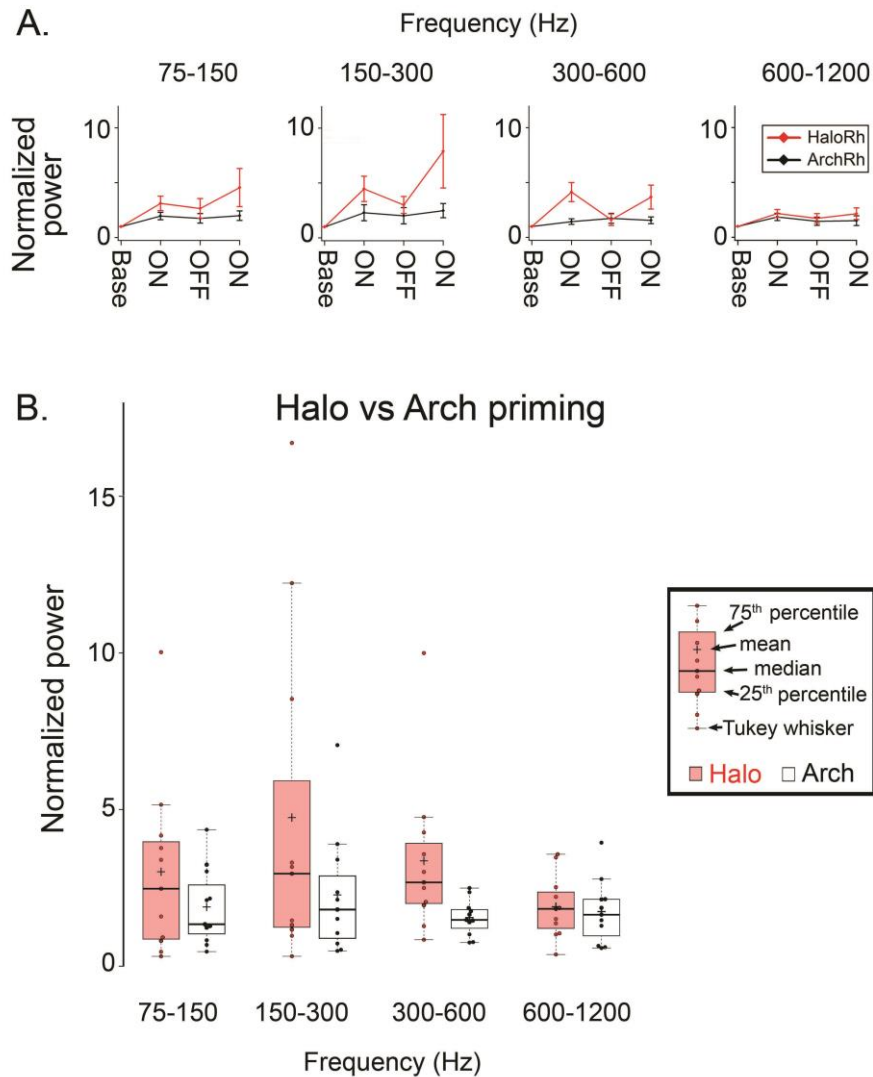


Figure 4.5 Frequency analysis of HR-priming versus ArchT-priming experiments. A. Power spectrum of different frequency bands for HR-primed (red) and ArchT-primed (black). B. Boxplot of the averaged ON-periods power during HR-priming and ArchT-priming for different frequency bands. HR activation positively modulated activity across all frequency bands, but only differed significantly from ArchT activation on 300-600 Hz component ($n = 11$ for HR and ArchT, $p < 0.01$ Student's t-test).

Additional to this, the same experiment was repeated but with HR being expressed under the synapsin promoter that affects both pyramidal cells and interneurons. In contrast to CamKII HR expression system, when HR was expressed under synapsin promoter HR priming did not induce any significant modulation of the evoked activity across all frequency band. (HR-primed versus baseline not-significant for 75-150 Hz, 150-300 Hz, and 300-600 Hz with $p > 0.05$, Student's t-test, $n=10$; figure 4.6C).

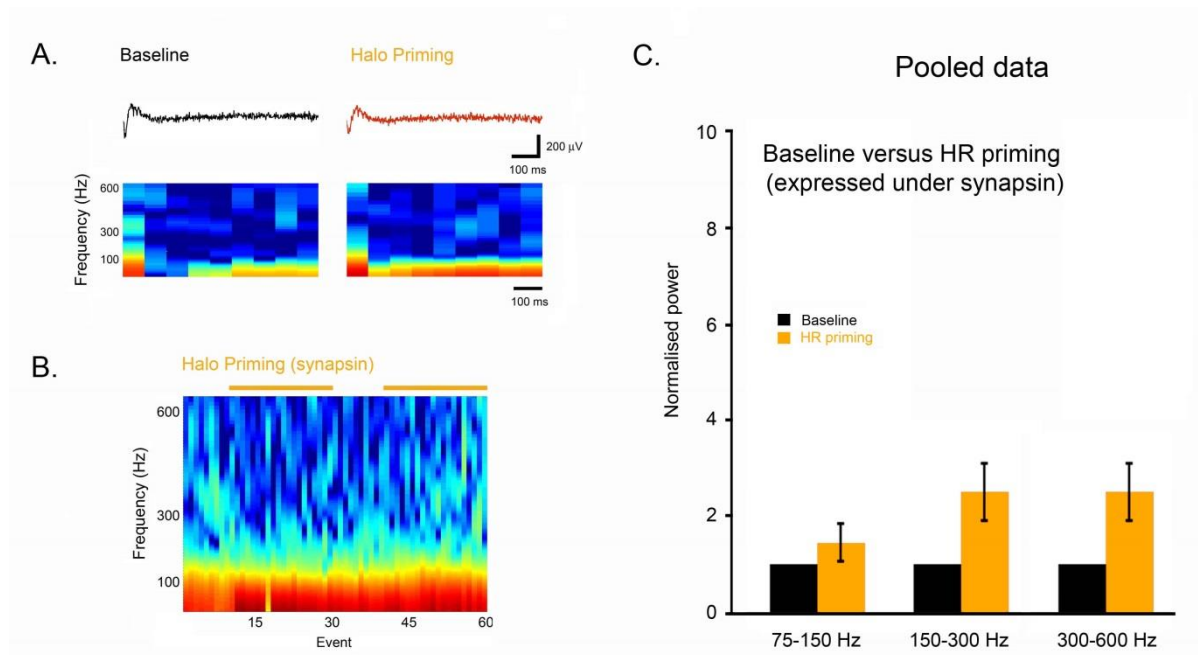


Figure 4.6 When expressed under synapsin promoter, HR priming failed to induce high frequency oscillation. The same experiment was conducted by expressing HR on both pyramidal cells and interneurons under synapsin promoter. A. Representative traces and spectrograms from a single brain slice expressing HR under synapsin from the baseline period (left) and from the HR priming period (right). No modulation in HFO range could be observed when HR was expressed under synapsin promoter. B. Representative composite of sequential spectrograms from the same brain slice in A showed no modulation of the HFO range throughout the entire experiment. C. No significant modulations were induced by HR priming across all frequency range ($n=10$, $p > 0.05$, Student's t-test).

Based on a result from the previous chapter describing how blocking KCC2 with 100 μM furosemide extends the period of high $[\text{Cl}^-]_i$ state post HR illumination, I also tried to repeat the same experiment by supplementing 100 μM furosemide in the ACSF. In this situation, HR priming also did not result in any significant activity modulation across all frequency bands. (HR-primed versus baseline not significant for 75-150 Hz, 150-300 Hz, and 300-600 Hz with $p > 0.05$, Student's t-test, $n=6$; figure 4.7).

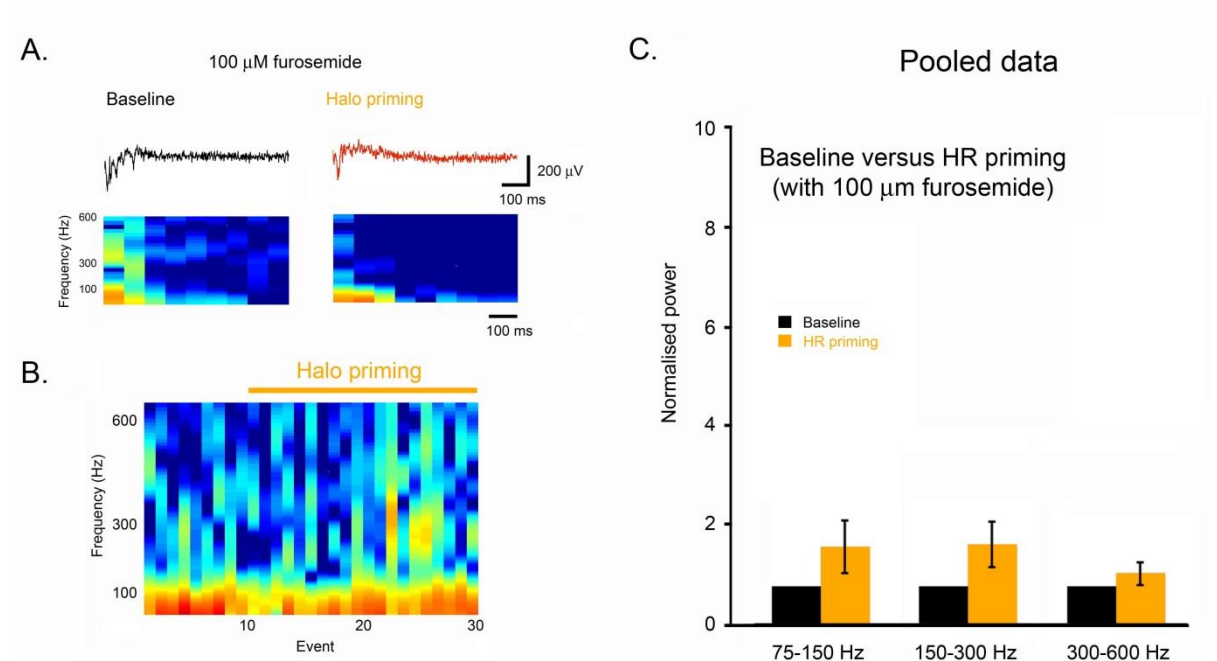


Figure 4.7 HR priming failed to induce high frequency oscillation in the presence of 100 μM furosemide. The same experiment was conducted on slices expressing HR under CamKII (pyramidal cells) with 100 μM furosemide in the ACSF to block KCC2. A. Representative traces and spectrograms from a single brain slice taken from the baseline period (left) and halo priming period (right) showed no modulation in HFO range by HR priming when ACSF was supplemented with furosemide. B. Representative composite of sequential spectrograms from the same brain slice in A showed no modulation in the HFO range throughout the entire experiment. C. No significant modulations were induced by HR priming across all frequency range ($n=6$, $p > 0.05$, Student's t-test)

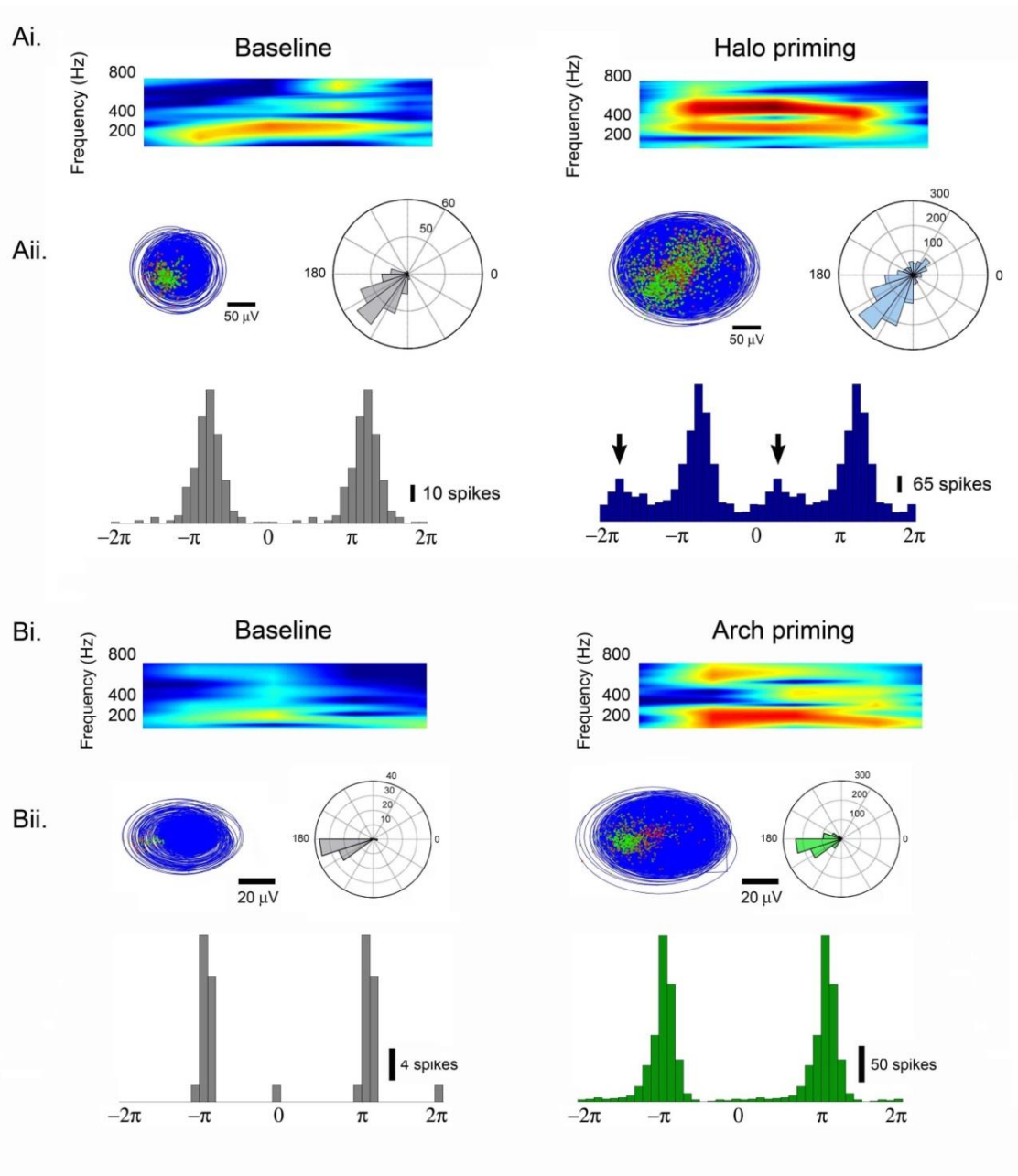


Figure 4.8 Neuronal Cl^- loading triggered out-of-phase firing during spontaneous bursts of activity. Ai. Representative spectrograms of spontaneous bursts of activity recorded extracellularly in baseline (left) and Halo-primed (Cl^- -loaded) tissue from a single brain slice. Note the prominent “double-frequency” signal in the HR primed tissue. Aii. Detected spikes (dots, red to green shows a progression of time) were plotted on the Hilbert transform of the dominant oscillation (75-300Hz; blue circular trace), and the rose-plots represent the numbers of action potentials occurring at different phases of the oscillation. Note the out-of-phase spiking in the HR primed data set, also apparent as a second minor peak (arrowed) in the conventional histogram (duplicated data beyond $-\pi$ and π). B. In contrast, periods of hyperpolarisation using ArchT caused a rebound increase in spiking (contrast the calibration bars for the histograms), but no change in the phase distribution of spikes.

From the pyramidal cells Cl^- loaded data (CamKII expression of HR), I next explored how raised $[\text{Cl}^-]_i$ affects the number of spikes and the spike time reliability with respect to the dominant oscillation by analysing multiunit activity recorded from the extracellular recording. Following HR-priming, there was a significant increase in the multiunit firing rate (note the different scale bars in Figure 4.8; baseline multiunit rate = 6.7 ± 2.5 spikes/s; HR-primed = 38.3 ± 6.6 spikes/s; $n = 8$; $p < 0.001$; HR-priming increase, normalised to baseline = 12.7 ± 4.8). In contrast, ArchT-priming produced only a small, but non-significant, trend towards increased firing over baseline (ArchT baseline multiunit rate = 6.5 ± 1.9 spikes/s; Arch-primed = 10.2 ± 2.6 spikes/s; $n = 6$; n.s.; ArchT-priming increase = 2.2 ± 0.7).

To assess the spike timing with respect to the dominant oscillation, the 75-300 Hz range was selected as the dominant oscillation based on the speculation that the dominant oscillation may be dictated by bursts of fast-spiking interneurons that entrain pyramidal cells firing, which are known to fire in this frequency range (Grenier *et al.*, 2003). Also, this was the frequency range whereby HR and ArchT priming did not show any significant difference (figure 4.5). A Hilbert transform was done on the 75-300 Hz band, which allows the oscillating signal to be plotted as a continuous circular trajectory, and then plotting histograms of the spike times with respect to this cycle (Figure 4.8Aii,Bii). Both baseline period and ArchT-primed experiments showed phase-locked spike timings confined to the lower left quadrant of the cycle representing the trough of the oscillation (figure 4.8A-left,B).

Notably, in the majority of HR primed experiments (5 out of 8 slices), spike time distribution were broadened, which indicates that there is an increased jitter in spike time reliability, reflecting a situation where pyramidal cells' activity are less strongly dictated by the dominant oscillation (figure 4.9). Distinctively, in the remaining HR-primed experiments (3 out of 8 slices), a bimodal spike time distribution was observed, with a dominant peak confined to the lower left quadrant and another one to the upper right quadrant (figure 4.8A-right). This is equivalent to a bimodal distribution of spikes that happen at the trough and also at the peak of the oscillation (HR-expressing tissue, mean phase angle = 3.34 ± 0.15 Rad, $n = 6$; ArchT-expressing tissue, mean phase angle = 3.42 ± 0.09 Rad, $n = 5$).

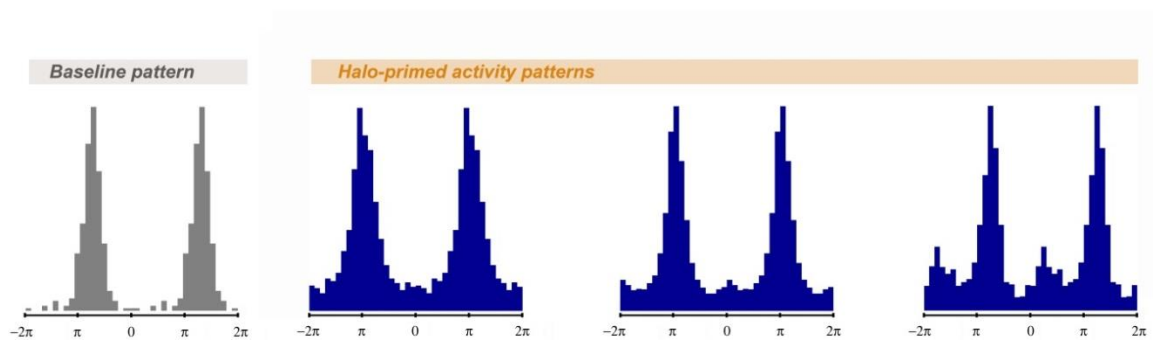


Figure 4.9 Different spike time distributions of HR priming data sets. Left: an example baseline spike time histogram taken from a single brain slice (grey) shows a single peak distribution. Note that two cycles were plotted in the histogram. Right: spike time distributions taken from 3 different slices showing that HR priming (blue) induced a broadening of the spike time distributions that sometimes result in a bimodal distribution.

To quantify the changing of spike time distributions induced by HR priming, half-width indices were calculated for baseline, HR primed, and ArchT primed recordings as explained in the method section. The mean half-width index of HR-primed spike distributions was higher compared to baseline and ArchT-primed spike distributions indicative of a significant increase of jitter in spike timing and out-of-phase firing due to Cl⁻ loading (figure4.10). Pooled data show that the difference between HR-primed and baseline spike time distributions and also between HR-primed and ArchT primed spike time distributions are statistically significant, while ArchT-priming did not show any significant difference from its baseline. (n=5 for HR primed and n= 6 for ArchT primed; HR primed versus baseline: $p<0.001$; HR primed versus ArchT primed: $p<0.02$; Student's t-test).

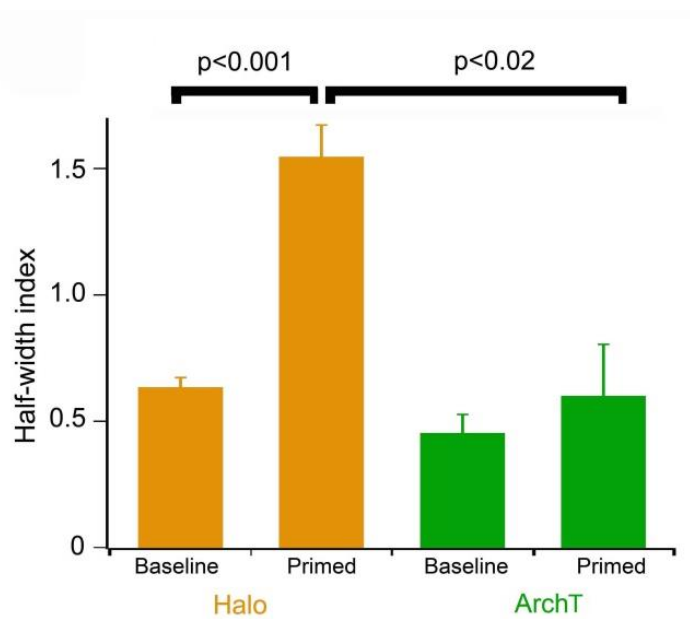


Figure 4.10 Half-width indices from baseline, HR primed, and ArchT primed periods. Mean half-width indices from baseline periods versus HR primed periods and baseline periods versus ArchT primed periods. HR primed gave a significantly higher half-width indices compared to baseline (n =5, $p<0.001$, Student's t-test). In contrast, there was no significant difference between baseline and ArchT primed periods. Furthermore, half-width indices from HR primed slices were also significantly different from ArchT-primed tissue (n=5 for HR and n=6 for ArchT, $p<0.02$, Student's t-test).

To assess whether spectral leak effect could account for the different spike-phase relationship observed in the HR primed tissues, spike amputation and time-shift analyses were performed as explained in the method section. The spike amputation had a small reduction in the amplitude of the oscillation (figure 4.11B, black versus blue traces) and the rose plots were slightly broader (figure 4.11, red versus yellow), indicating that there was indeed a small contribution from spectral leak. Importantly, though, the spike-phase distributions were still markedly skewed and centred at the same phase as for non-amputated data (figure 4.8 yellow versus red). Similarly, when spikes were plotted according to the dominant oscillation 1-2 ms ahead of the spike where it is not influenced by the spectral leak, spike distribution was broader however it was still skewed (figure 4.11C). Note that the shifted phase of the peak was introduced by the time shift analysis (figure 4.11C).

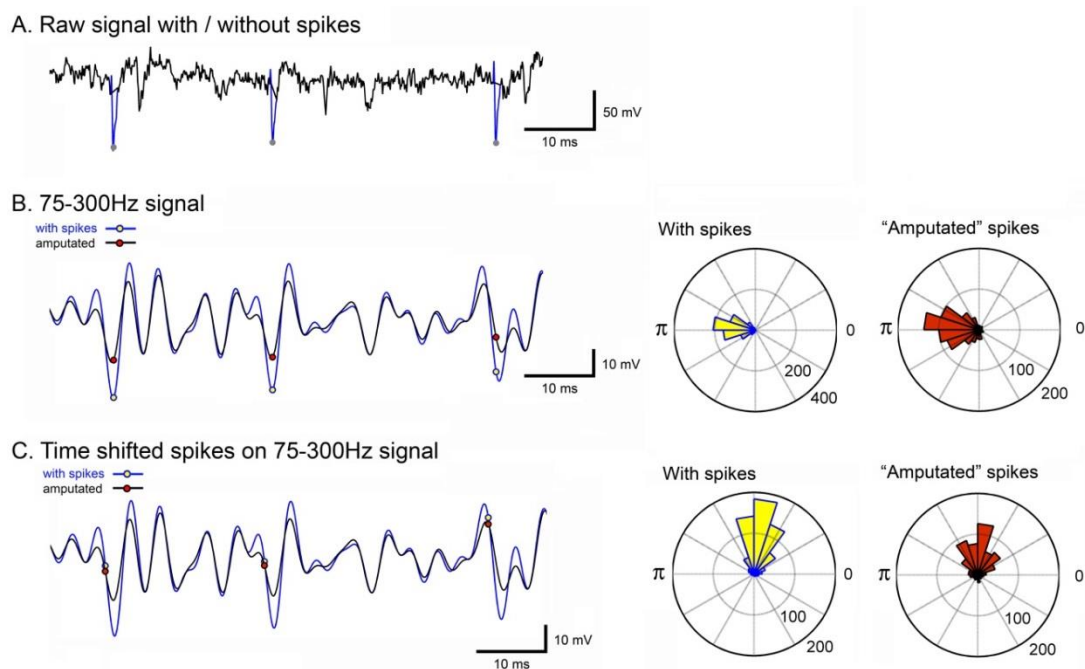


Figure 4.11 Control analyses for spectral leak: spike amputation and time shifted. A. An example trace that shows the raw data, with the spikes (blue) and the amputated version (black). B. Left: the raw signal from A was band-pass filtered for 75-300 Hz both with spikes (blue) and the amputated version (black). When spikes were amputated (blue), the 75-300 Hz signal showed reduced amplitude peaks, but no phase shift. Right: The spike-phase plots were still heavily skewed albeit with a broader main peak. The yellow and red dots represent the detected spike times. C. Left: the same 75-300 Hz signal from B but with spike times indicated 2 ms ahead of the real spike times, compare the locations of the time-shifted spikes with the same plots in panel B. Right:

heavily skewed spike-phase relationships, albeit with a shifted phase, were also found at time points ahead of the spikes

Half-width indices were re-derived for all control analyses (spike-amputated; time-shifted; and both amputated and time-shifted). There remained highly significant differences, for all analyses, between the HR primed and baseline periods, and also between the HR-primed and ArchT-primed data (figure 4.12B). In slices where HR priming gave bimodal distributions of spike times, after all analyses, baseline spike-phase distribution still showed single peaks (figure 4.12A, grey), while the HR primed data sets consistently showed double peaks (figure 4.12A, orange). This confirmed that the spectral leak issue is not the reason for the different spike-phase relationship observed between HR priming versus baseline and ArchT priming.

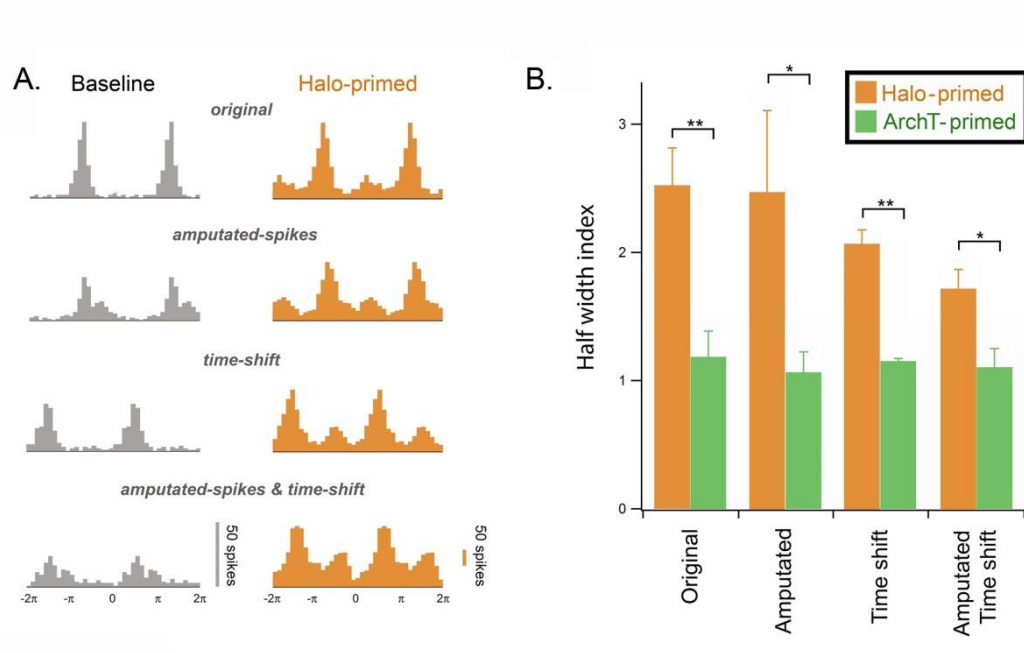


Figure 4.12 Spike time histograms and half-width indices derived after control analyses. A. Example histograms derived from a single brain slice in which HR priming gave a bimodal distribution of spike time. Baseline spike-phase plots (grey) all had single peaks, while the distributions for all HR primed analyses showed double peaks (orange). B. There were highly significant differences between the HR-primed and ArchT-primed matched analyses. (* $p < 0.05$; ** $p < 0.01$; *** $p < 0.001$).

I have shown here that artificially loading neurons with Cl^- by HR priming consistently induced modulation of network activity especially in the high frequency range (300-600 Hz). It was initially expected that spontaneous epileptiform events would ensue when cells are intensely loaded by Cl^- as was done during these experiments. Interestingly, despite evidence for a clear increase in excitability, and even with repeated electrical stimulation delivered to the underlying white matter, no single epileptiform discharge was recorded in any experiment. This implies that while Cl^- loading may contribute to a certain epileptic state, for these network to progress into a full ictal event, either the pathological loading must be far more widely experienced than provided by the spot-illumination, or that other pathological factors are also required.

4.3.2. In a pro-epileptic state focal raised intraneuronal chloride initiates ictal activity

I then followed this up by altering the basal excitability of the slices by applying a low concentration of 4-AP (20 μM), much lower than what is normally used to induce ictal activity (50-100 μM). The main idea of using 4-AP is because this drug is known to block potassium channels, especially those expressed in fast-spiking interneurons, triggering high frequency burst of these cells (Bouchard & Fedida, 1995; Cammarota *et al.*, 2013). A similar illumination paradigm was used where HR was activated as repeated cycles of 25s-ON and 5s-OFF but without applying any electrical stimulation this time. Baseline was recorded for 10-20 min before starting the optogenetic illumination. Indeed, in comparison to the epileptic concentration, the slices were much less excitable with no spontaneous full ictal discharges recorded during baseline period. Some variability was observed for the 20 μM 4-AP baseline with the majority of slices (60%, 12/20 slices) showed a stable quiescent baseline (figure 4.13A black trace), 20% occasionally showed a brief spontaneous epileptiform discharge that was short lasting and smaller in amplitude (figure 4.13A, dark grey trace) compared to a 100 μM full blown ictal discharge (figure 4.13A, red trace), and the remaining 20% showed very regular non-stop epileptiform discharges since an early stage (figure 4.13A light grey trace).

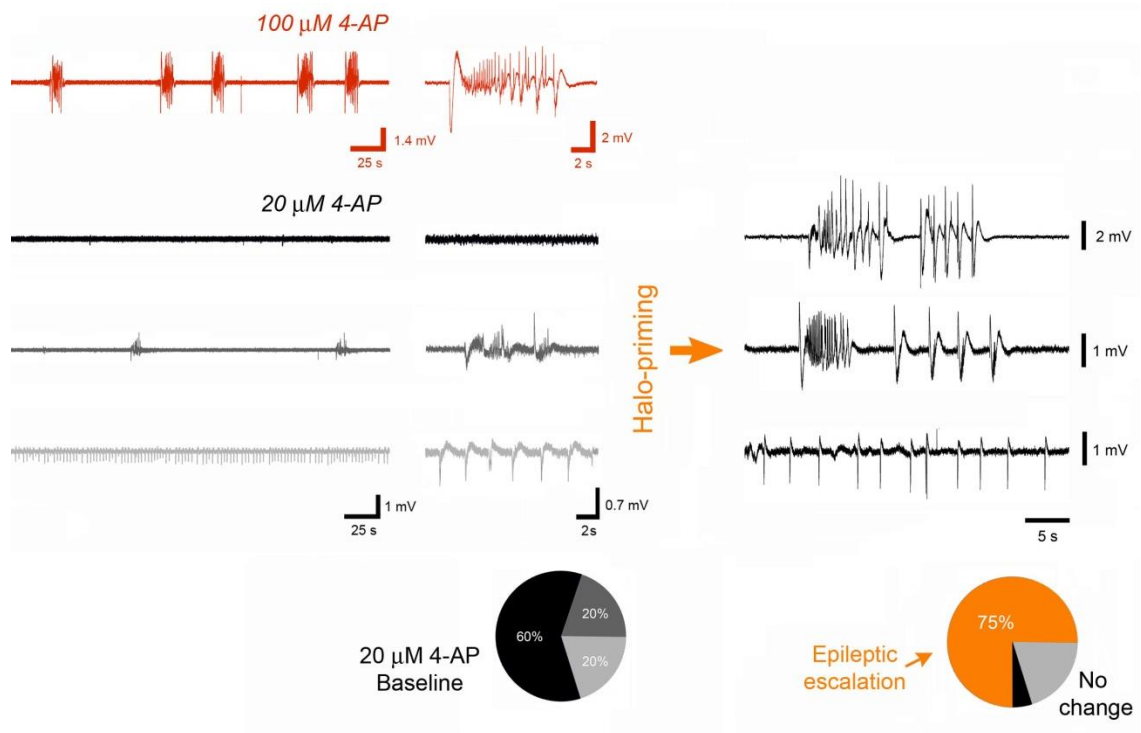


Figure 4.13 Epileptic escalation by HR priming in the presence of 20 μM 4-AP. Left: LFP traces (1-300 Hz) of different baseline activity prior to HR priming: Red trace shows an example baseline activity with 100 μM 4-AP showing that within the 5 min multiple ictal discharges were recorded spontaneously. Baseline with 20 μM 4-AP: Black trace is a representative stable quiescent baseline that accounted for 60% of the slices. Dark grey trace shows an example baseline where some rare short discharges were recorded (20%). Light grey trace represents the remaining 20% of the slices that showed regular bursts since the early stage. Right: Representative LFP traces showing the outcome of HR priming of the corresponding baseline activity. Most of the slices with quiescent baseline and rare short discharges developed ictal events after periods of HR priming, while slices with regular burst did not.

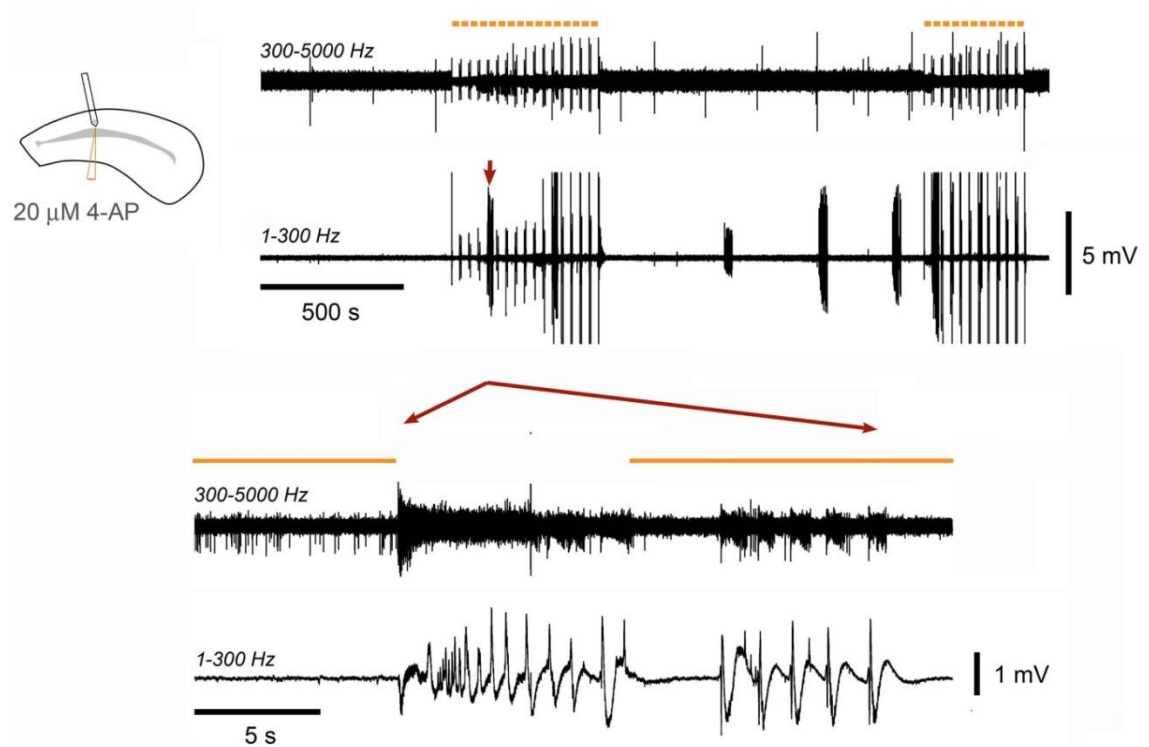


Figure 4.14 Rapid ictal event induction by HR priming in conjunction with 20 μ M 4-AP. Representative traces recorded from a single brain slice that showed a quiescent stable baseline. Units trace (300 – 5000 Hz, top trace) and LFP (1-300 Hz, bottom trace) of the entire length of the experiment showing a full ictal event recorded after 4 cycles of HR priming (25s ON/ 5s OFF), which resembled spontaneous ictal events commonly induced by 100 μ M 4-AP application.

In the majority of the slices (15 out of 20), HR priming successfully triggered ictal discharges within 4.47 ± 1.56 minutes ($n=15$) from when the 25s-ON/5s-OFF HR activation paradigm was initiated, equivalent to 9 cycles of HR priming (25s ON/5s OFF). Events are categorized as ictal discharges when it lasts longer than 5s, and showing a pattern of activity that consists of initial tonic discharges followed by rhythmical after-discharges. These discharges very much resembled the full ictal discharges commonly induced by application of 100 μ M 4-AP (figure 4.13&4.14). Full ictal discharges were not always triggered by HR priming when a long series of HR priming cycles were done. It was very common for the slices to later generate some spontaneous seizures without HR priming once an ictal discharge had been successfully triggered by HR activation (figure 4.14). As a control, long baseline recordings with 20 μ M 4-AP (45 to

60 minutes, n=4) were done to assess whether this concentration of 4-AP alone is enough to develop spontaneous ictal discharges over the duration of 1 full experiment, and evidently without any HR activation, none of them developed spontaneous full ictal discharges.

4.3.3. Characteristic seizure terminating pattern

An incidental observation coming from these experiments was that in 4 out of 15 slices in which HR successfully triggered ictal discharges, there was a distinctive pattern of activity recorded at the end of HR priming period. This pattern of activity has been documented before and named as afterdischarge terminating oscillation (ATO), which was a spreading-depression like event that seemed to mark the termination of in vivo post-tetanic stimulation seizures (figure 4.15; Bragin et al, 1997). In these 4 slices, illumination cannula was placed side by side from the tetrode recording instead of on top of the tetrode recording. The terminating event is characterised by an onset of a short-lasting low amplitude oscillation (40-90Hz) followed by a slow sustained potential shift that results in a post-ictal depression state (Bragin *et al.*, 1997).

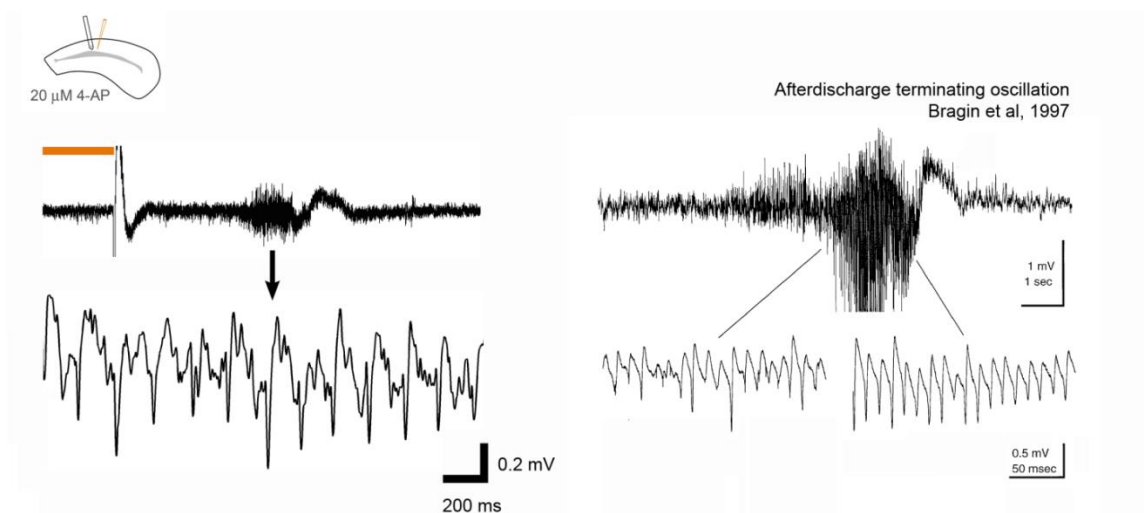


Figure 4.15 Afterdischarge terminating oscillation (ATO). Left: An example of ATO recorded from the HR priming experiment in conjunction with 20 μM 4-AP where illumination cannula was placed at a distance from the recording electrode. ATO was recorded at the end of long repeats of HR priming. Right: This resembled what Bragin et al (1997) described as an ATO that they proposed as a spreading-depression like event that terminates seizures activity (Bragin et al, 1997).

To look further into this, the same experiment was repeated only this time recording was done using two tetrodes separated by approximately 1 mm. In this set up, more ATOs were successfully recorded, suggesting that the failure to observe more ATOs in the previous experimental set up was because ATOs were less likely to be captured while using only a single recording tetrode.

ATOs were recorded after repeats of HR priming for 9.48 ± 1.65 minutes (mean \pm sem, $n = 9$) or equivalent to 19 cycles of HR priming (25s ON/5s OFF). Note that this is double the time needed to induce an ictal discharge and usually it only happened after multiple ictal discharges had been induced. ATO was generated in 9 slices in which 8 of them HR priming successfully triggered seizures and 1 of them had very regular discharges since the early stage (figure 4.13A, light grey). In these 9 slices, ATO was always followed by a period of depression that resembles a post-ictal depression before activities reappeared in both LFP and multiunit activity trace with a mean recovery time of 84.4 ± 10.68 s (mean \pm sem, $n=9$; figure 4.16). Note that recovery time was measured between the times at the end of the ATO event observed from the LFP trace until the appearance of the first unit activity. Illumination was shifted between the two recording tetrodes and it was found that ATOs appeared to be initiated from the illuminated area that then invaded the less illuminated area (figure 4.17). When illumination was shifted to the other tetrode, the ATO initiation focus also changed following the spot of illumination (figure 4.17). It was confirmed that ATOs were initiated from the Cl^- loaded area (illuminated) that propagates to the less Cl^- loaded area (less illuminated).

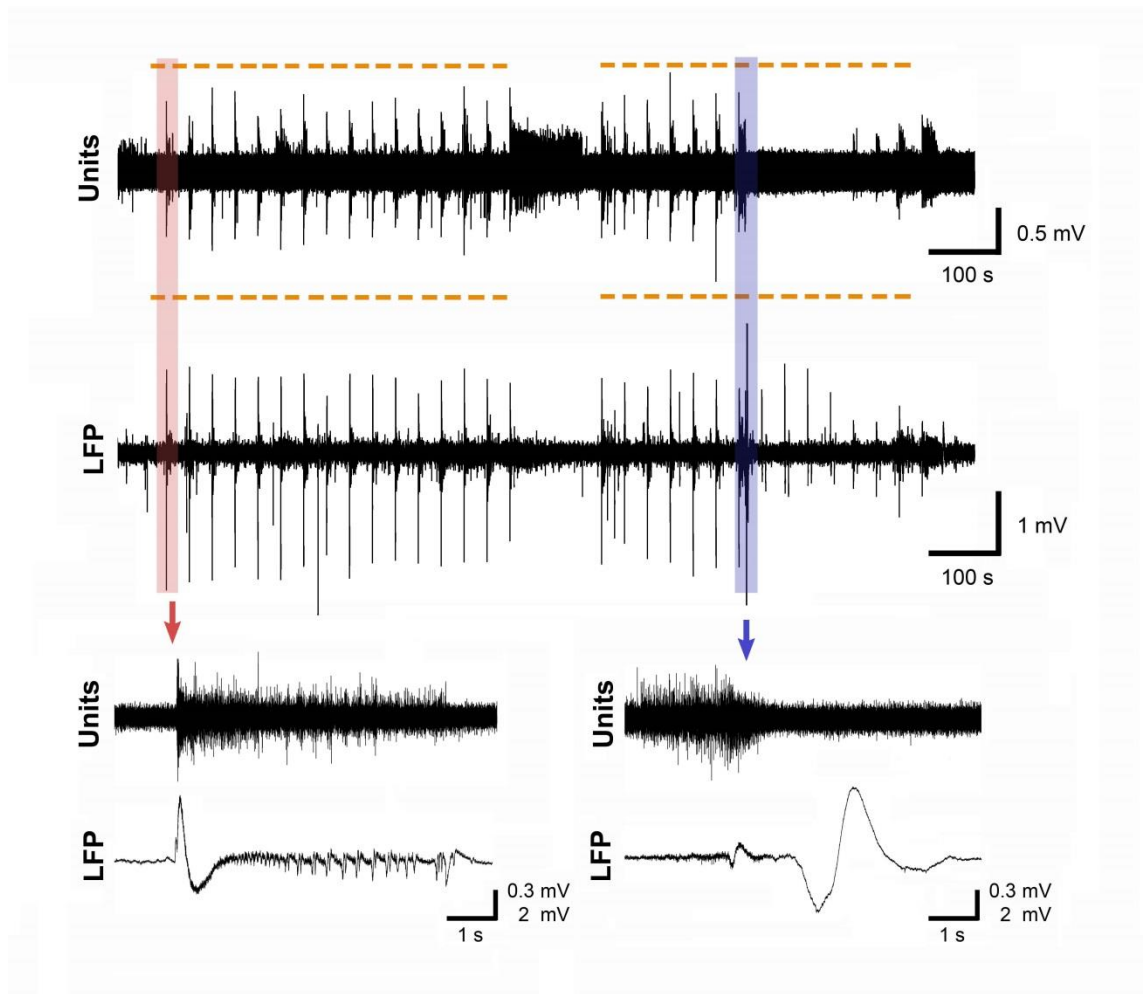


Figure 4.16 ATO was recorded following a long series of repeated HR priming, and is associated with a subsequent period of neuronal suppression. Representative traces recorded from a single brain slice with 20 μ M 4-AP supplemented in the ACSF. Top trace was band pass filtered between 300-5000 Hz for multiunit activity and the bottom trace was filtered between 1-300 Hz for LFP. HR priming successfully induced ictal discharges (red bar: example ictal discharge) as shown by the epileptiform discharges on the LFP (bottom trace) accompanied by intense firing of cells shown in multiunit activity trace (top trace). ATO (blue bar) was recorded after 21 cycles of HR priming (25s ON/5s OFF), which was followed by a slow sustained potential shift that silenced the network depicted by the absence of any unit activity (top trace) that only recovered 141.6 s later. Representative high magnification of ictal discharge (red arrow) and ATO (blue arrow) were shown on the bottom.

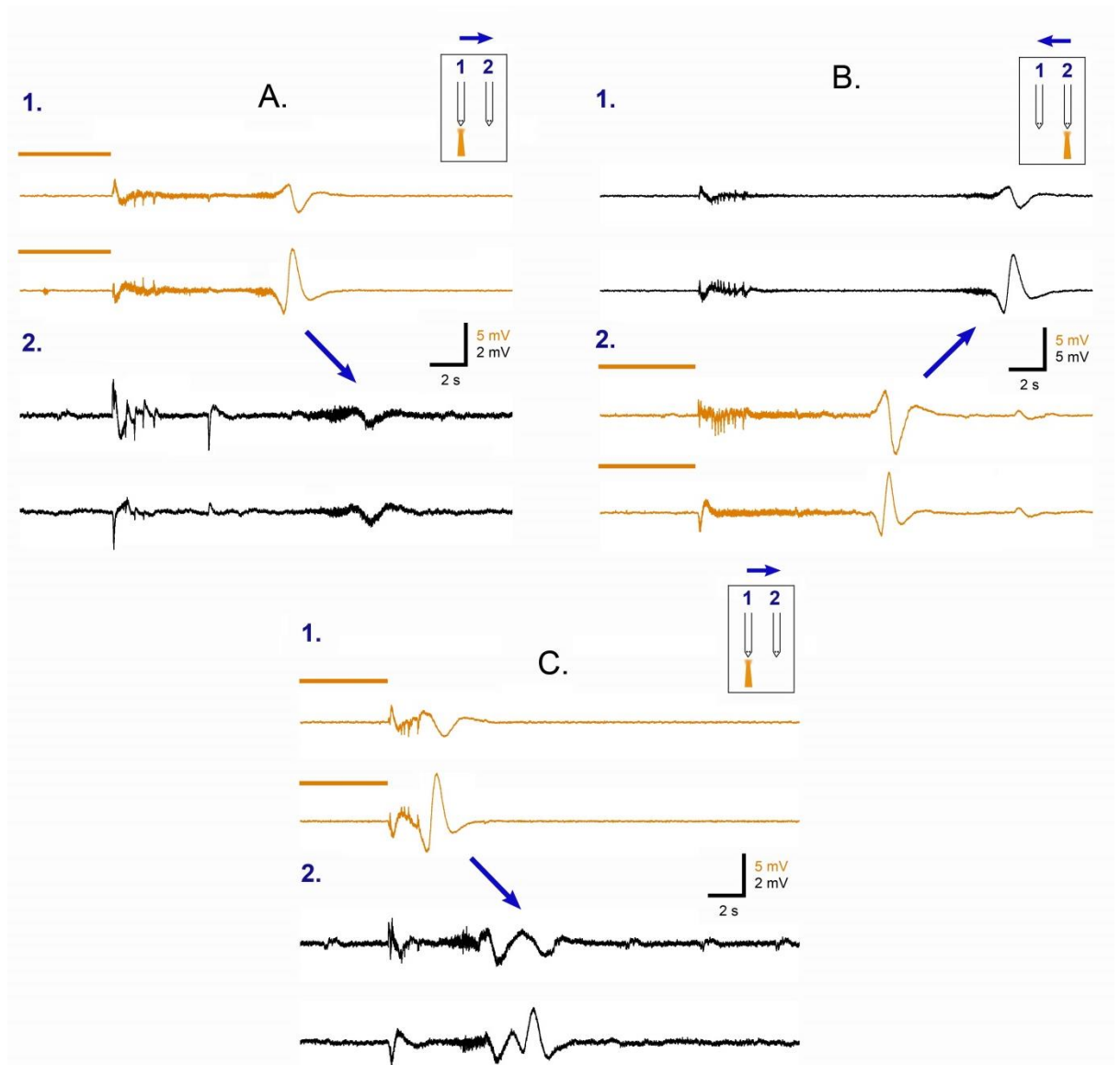


Figure 4.17 ATO was initiated in the Cl^- loaded area. Representative traces recorded by two tetrodes separated by a distance, from a single brain slice, with $20 \mu\text{M}$ 4-AP supplementation in the ACSF. Two traces were shown from each tetrode, recorded by two electrodes of the tetrode that were $50 \mu\text{m}$ apart. Orange traces were from the tetrode in which illumination was focussed on. HR priming successfully triggered ictal discharges and ATOs were recorded. A. ATO was initially observed in tetraode 1 before tetraode 2 when illumination was focussed on tetraode 1. B. When spot illumination was shifted to tetraode 2, ATO was then initiated in tetraode 2 consistent with where Cl^- loading was introduced. C. ATO was then back generated in tetraode 1 before captured by tetraode 2 when illumination was shifted back onto tetraode 1 confirming that the ATO is first initiated in the Cl^- loaded area.

ATO seemed to propagate slowly as shown from the dual tetrodes recording (figure 4.17 and figure 4.18). The propagation speed of ATO was calculated by measuring the time difference between the peak of the potential shift in 1 electrode to the peak recorded by the other electrode from the same tetraode that is known to be 50 μm apart. The mean propagation speed of the ATO was 0.19 ± 0.02 mm/s (mean \pm sem, n=7). Contrast the almost instantaneous event affecting the 2 tetraodes when ictal discharges were recorded compared to the slowly propagating ATOs (figure 4.18).

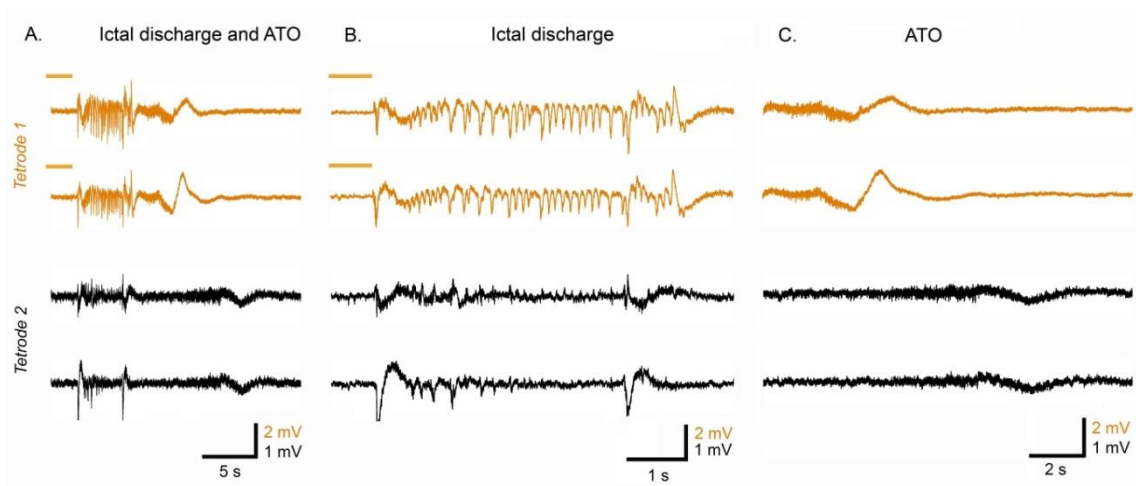


Figure 4.18 Propagation of HR priming induced ictal discharge and the associated ATO. Representative traces from a single brain slice from HR priming experiment with 20 μM 4-AP in the ACSF, with the same recording set up from the previous figure. A. An ictal discharge was initiated post HR activation that was terminated by an ATO. B. Ictal discharge was recorded almost simultaneously in all electrodes. C. In contrast, ATO was slowly propagating from 1 tetraode to another with a speed of 0.15 mm/s in this particular trace.

4.4. Discussion

4.4.1. HR chloride loading as a model for high $[Cl^-]_i$

Raised $[Cl^-]_i$ and hence depolarising GABA has been long associated with epilepsy. However how far thus this contributes to ictogenesis was not clear. The 3 main ideas of how Cl^- accumulates intracellularly during seizure are

1. Due to a deficiency of Cl^- clearance mechanism as shown by Huberfeld et al (2007) that resected human epileptic tissues show a reduced expression of KCC2 (Huberfeld *et al.*, 2007c).
2. Via NKCC1 activity that is enhanced after repetitive seizures that drive Cl^- into the cell (Dzhala *et al.*, 2010b)
3. Through intense GABA activation (Lillis *et al.*, 2012) as part of the inhibitory restraint mechanism during the recruitment of new territory into a seizure.

A combination of all 3 could potentially contribute to a high $[Cl^-]_i$ state found in epilepsy and the level of contribution from each path might be different one case from another, one seizure model from another.

In this chapter, HR Cl^- loading effect was used as a model of intracellular Cl^- accumulation to study the consequence of it in regards to the epileptic network activity. The way HR activation loads cells with Cl^- is by imposing an instantaneous hyperpolarising current that is a Cl^- inward current, which consequently causes an abrupt change in the membrane potential. This may be different from Cl^- accumulation brought about by co-transporters dysregulation (low KCC2 or high NKCC1) that is electro-neutral and hence does not result in instantaneous change of the membrane potential. It should be noted that inevitably the instantaneous hyperpolarisation of HR could also activate voltage gated channels that are activated by membrane hyperpolarisation. For instance, HCN channel is known to open when E_m is

hyperpolarised giving rise to the depolarising I_H ; Also CLC_2 channels, which are inwardly rectifying Cl^- channels that are activated by hyperpolarisation, induce an outward Cl^- current. I_H depolarising current could bias the internal Cl^- accumulation effect in promoting network excitability whereas CLC_2 mediated Cl^- efflux might attenuate the effect of HR Cl^- loading on the network excitability. As a control for the I_H imposed by HR hyperpolarisation, ArchT was used. This however still leaves an open question of how ictogenic high $[Cl^-]_i$ is when CLC_2 is not activated by hyperpolarization such as those imposed by co-transporter dysregulation. This could be answered by repeating the same experiment with the use of CLC_2 specific blocker GaTx2, or knock-out animals.

4.4.2. Heterogeneity of $[Cl^-]_i$ explains the out-of-phase firing in the HFO

To further explore the nature of the spiking patterns recorded during the HR priming period, Dr. Andrew J. Trevelyan conducted a computer simulation showing how this activity patterns could be explained by heterogeneity within the Cl^- loaded pyramidal population using a compartmental modelling approach (Hines & Carnevale, 2001). This is to investigate how a fast-spiking interneuron might influence its postsynaptic pyramidal targets when there is also a concurrent intense glutamatergic barrage. Pyramidal cells were simulated to receive an intense, desynchronized glutamatergic drive, on to which was imposed a high frequency barrage of IPSCs on to the soma and proximal dendrites; figure 4.19A shows repeated simulations of postsynaptic spiking for a cell with a relatively hyperpolarising E_{GABA} (-75mV), which are collated into spiking phase-histograms based on the cycle of IPSCs. He next simulated how the effect of this same inhibitory barrage changed with E_{GABA} shifting towards more positive levels (Figure 4.19B), to show that the window of opportunity for pyramidal spiking broadens, as the effective inhibition diminishes (E_{GABA} shifting from -75, to -65, to -55mV). Eventually, when E_{GABA} exceeds the action potential threshold, there is a sudden 180° (π) phase shift in the spiking (figure 4.19B, left).

Previous studies have shown that the output of fast-spiking interneurons is precisely synchronised onto the multiple postsynaptic pyramidal cells (Miles *et al.*, 1996; Trevelyan, 2009). Considering that this postsynaptic population has a distribution of E_{GABA} values, as measured by Huberfeld *et al.* (Huberfeld *et al.*, 2007a), and also shown using Cl^- imaging (Dzhala *et al.*, 2010a), he then simulated the multiunit spiking patterns in this heterogeneous population. The distribution of E_{GABA} values described in Huberfeld *et al.* (Huberfeld *et al.*, 2007a), a negatively shifted one as the physiological distribution, and a positively shifted one as an extremely depolarised E_{GABA} distribution were used. The physiologically shifted distribution (mean $E_{GABA} = -68.5mV$; Figure 4.19B, top right) showed a unimodal spiking distribution with respect to the rhythm imposed by the basket cells. In contrast, only a small positive shift in E_{GABA} (mean $E_{GABA} = -60.8mV$; Figure 4.19B, middle right) allowed a marked increase in spiking due to the broadening of the main peak, but also the appearance of an out of phase peak that was shown even more prominently when the E_{GABA} was further shifted to a more depolarized level (figure 4.19B, bottom right). These distributions were reproduced very well by the histograms drawn from different HR-primed brain slices as shown earlier (Figure 4.9).

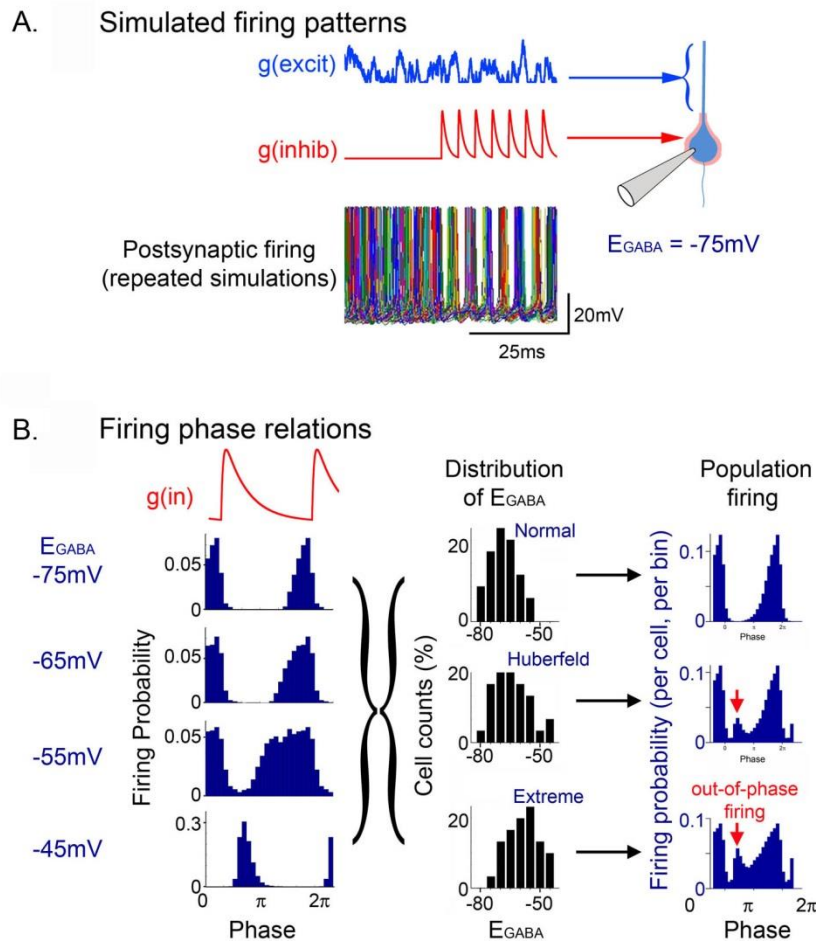


Figure 4.19 Heterogeneity in levels of intracellular Cl^- can explain the appearance of out-of-phase population firing. A. Simulation using NEURON, of how a train of high frequency IPSCs from a fast-spiking interneuron superimposed onto a noisy, desynchronised glutamatergic drive, creates a patterned firing in the pyramidal cell. Action potential threshold was about $-48mV$. (courtesy of Dr. Andrew J. Trevelyan) B. Simulations in the same model, at four different GABAergic reversal potentials. The firing probability is plotted with respect to the field oscillation, which is approximately $\pi/4$ phase shifted from the start of the IPSC, as judged by comparisons with the timing of fast-spiking interneuron action potentials (Hasenstaub *et al.*, 2005). When these different probability histograms are convolved with estimates of the distribution of E_{GABA} in the pyramidal population, one can derive population firing probabilities with respect to the cycle imposed by the fast-spiking interneuron. (courtesy of Dr. Andrew J. Trevelyan)

4.4.3. HR Cl⁻ loading and how ictogenic it is

From the first experiment of this chapter, it was clear that Cl⁻ loading by itself did not trigger a full seizure in brain slices, even when electrical stimulation was applied to the network as a putative thalamic input onto the cortex. Note that both KCC2 and CLC₂ are intact. However, in these healthy brain slices (when bathed in normal ACSF), loading cells with Cl⁻ and applying electrical stimulation on the white matter give rise to HFO with doubling of frequency characteristic. Spike time distributions post HR priming showed an increased jitter by the broadening of the window of opportunity for cells firing. Notably, in some slices this resulted in a marked appearance of a second peak that was out-of-phase of the dominant peak.

HFO with doubling of frequency characteristic has been associated with epilepsy before (Foffani *et al.*, 2007a). Activity in this range could not be generated by a single population of pyramidal cells as this exceeds the general limit of single cell firing rate. Previous study then suggested that this pattern of activity comes about due to an out of phase firing of different populations of cells that gives the characteristic doubling of frequencies (Foffani *et al.*, 2007a; Ibarz *et al.*, 2010b). The experimental data from this chapter and the modelling by Dr. Andrew Trevelyan together provide a detailed explanation that these populations that fire out of phase of each other during HFO could be different in terms of their [Cl⁻]_i. Hence our results show a clear link between two important concepts in epileptology: namely, raised intraneuronal chloride and high frequency oscillations.

Furthermore, the multiunit analysis from the HR priming data has shown how raised [Cl⁻]_i alters the spike timing of cells with respect to the dominant oscillation, increasing jitter in spike time reliability and eventually the likelihood of an out of phase firing as shown by the appearance of the second peak in the spike histogram. The modelling then explained how this could arise due to a heterogeneity of [Cl⁻]_i dictating cells that have [Cl⁻]_i above certain threshold to fire out-of-phase of the cells that have a relatively lower [Cl⁻]_i explaining the second peak in spike histograms. This certain threshold is when [Cl⁻]_i is high enough to give an E_{GABA} that surpasses the threshold for action potential that was around -48 mV. Unfortunately, in our experimental set up it is not

possible to monitor $[Cl^-]_i$ of multiple neurons such as enabled by for example Cl^- imaging, and so this could not be proven experimentally.

Reaching -48 mV E_{GABA} may seem like a high target for HR Cl^- loading effect to achieve, however this is made possible by the fact that pyramidal cells naturally have a broad range of baseline E_{GABA} (-80 mV to -50 mV with a mean E_{GABA} of -68.5 mV). Hence in some cells that originally have quite high $[Cl^-]_i$ for instance with an E_{GABA} of -50 mV, a 5 mV shift in E_{GABA} is enough to push it towards the threshold for action potential. It should be highlighted that the computer modelling has shown that this extreme E_{GABA} only has to affect a small percentage of the cell population to give rise to HFO as out-of-phase firing probability is significantly higher when E_{GABA} reach the threshold for action potential.

The next question I was asking is what happens if the interneurons also experience the state of high $[Cl^-]_i$ together with the pyramidal cells. I then repeated the same experiment using slices that express HR both in interneurons and pyramidal cells under synapsin promoter, hoping this will induce hyperexcitability in both classes of cells. Unfortunately, HFO cannot be triggered when Cl^- loading was imposed onto both the pyramidal cells and interneurons by expressing HR under the synapsin promoter. This could simply be due to a lower level of HR expression under the synapsin promoter compared to CamKII, which is recognized as a strong promoter that drives high level of protein expression (Wang *et al.*, 2013), hence insufficient Cl^- loading effect to trigger HFO. Another possibility is because of an imbalance expression by the synapsin promoter with more HR expressed in interneurons than in pyramidal cells that results in Cl^- loaded and hence more excitable interneurons that presumably increases GABA release but still have a hyperpolarising effect on the less Cl^- loaded post-synaptic neurons, the pyramidal cells. This open an interesting future experiments to assess what happens when only interneuron or both interneurons and pyramidal cells are loaded with Cl^- .

The fact that Cl^- loading by itself did not trigger any seizure, led to the idea of testing whether together with blocking KCC2, the Cl^- clearance mechanism of the neurons, will lead to an exacerbation of the HFO that eventually leads to seizure initiation. This condition theoretically should mimic a sudden influx of Cl^- via GABAergic synapses into

the cells (by HR Cl⁻ loading) that hypothetically already have a higher basal Cl⁻ level due to a reduced functional KCC2 (by KCC2 blocker). However, when supplementing the ACSF with 100 μM furosemide to block KCC2, even HFO was failed to be induced by HR priming. When adding furosemide after a baseline recording without any HR activation, furosemide attenuated the baseline before HR paradigm was even started. This could be due to the non-specificity of furosemide that is known to also block NKCC1 in this concentration, the co-transporter responsible for Cl⁻ import into the cell (Löscher *et al.*, 2013). Furosemide might also affect other receptors that are essential in the generation of the baseline network event and consequently the HFO. It remains an open question then how ictogenic the intraneuronal Cl⁻ accumulation is when Cl⁻ clearance is not intact. A future experiment that could be done to answer this question would be by repeating the same experiment using more specific blockers of KCC2 such as VU0240551 or the use of a knock out animal.

The following experiment was trying to combine Cl⁻ loading with other pathological state; in this case by application of 20 μM 4-AP. 4-AP is a potassium channel blocker that affects mainly fast-spiking interneurons but also pyramidal cells (Cammarota *et al.*, 2013), inducing hyper-activation of the network. In this situation, Cl⁻ loading rapidly induces ictal activity in less than 5 minutes or 9 cycles of HR priming (25s ON/5s OFF), highlighting the adjunctive role of high [Cl⁻]_i in tipping over the balance of the network activity into ictal activity. This cumulative effect of HR Cl⁻ loading in seizure initiation could be explained by the fact that in these slices taken from adult mice, a shorter time constant of HR Cl⁻ loading effect was observed compared to the dissociated neuronal culture (mean ± sem τ: 8.01 ± 2.84 s for old brain slices vs 28.1 ± 9.2 s for dissociated neuronal culture; chapter 3). This means that these slices clear Cl⁻ more effectively explaining the need of accumulative HR Cl⁻ loading effect over time to reach a certain threshold for seizure initiation. This could also suggest that seizure initiation was not due to rebound firing by I_H, as I_H is less likely to have a cumulative effect over a long period of time.

As this provide a proof of principle that Cl⁻ loading has the adjunctive role towards ictogenesis when combined with other pathological state, other scientifically and clinically relevant models of other pathological state will be worth exploring to start teasing out possible sets of circumstances that could result in seizure initiation. For

instance, maybe a focally delivered agent could give a better idea of how focal seizure could progress into generalised one. One possibility to assess this is by expressing and activating ChR2 on interneurons and HR on pyramidal cells locally. It is also interesting to explore the effect of Cl⁻ in different epileptic model such as maybe brain slices taken from chronic model of epilepsy.

Additionally, the fact that Cl⁻ loading only has an adjunctive role in vitro does not close the possibility that Cl⁻ could play a bigger role in seizure initiation in vivo since brain slices are known to be less excitable compared to an intact whole brain that presumably have more inputs coming from the long connections that are cut in brain slices preparation.

4.4.4. Afterdischarge terminating oscillation

Initially, ATO was incidentally recorded during the 20 μM 4-AP and HR priming experiments after multiple ictal discharges were induced. This event has been reported before in vivo to be associated with seizure termination (Bragin *et al.*, 1997). In their study Bragin et al induced seizures in vivo by applying electrical stimulation onto the perforant or commissural path and did recording in the CA1 and CA3 part of the hippocampus. They only observed ATO when the induced seizures were long lasting (over 15 s); while when seizures were short lived they terminated abruptly. Our experiments also show a similar phenomenon in which ATO was only recorded after a long HR priming that was after multiple ictal discharges were successfully recorded. This was after a mean duration of 9.48 ± 1.65 minute of HR priming; note that it only took a mean duration of 4.47 ± 1.56 minute of HR priming to induce a single ictal discharge.

Bragin et al has shown that ATO happens when V_m is really positive (> -30 mV) that the sodium channels are deactivated leaving the neurons incapable of firing. They also showed that they could mimic this by injecting potassium chloride (KCl) extracellularly (Somjen & Giacchino, 1985; Bragin *et al.*, 1997). In our result ATO appeared to be triggered locally where the HR priming was applied, suggesting that this is related with the Cl⁻ loading effect of HR. One possible mechanism that links the 2 mechanisms is due to the fact that HR accumulates Cl⁻ inside the cell that eventually has to be cleared

out. One way is through KCC2 that will extrude Cl^- together with K^+ . Additionally, seizure activity is known to be associated with increased extracellular K^+ due to high neuronal activity (Somjen *et al.*, 1985; Somjen & Giacchino, 1985). Note that due to the relatively narrow extracellular space, even small compartmental movement of K^+ could change the concentration significantly. Together this could lead to a significant accumulation of K^+ outside that is enough to cause a depolarization block of the network. To what extent KCC2 is involved in this could be further explored by repeating the same experiment with the KCC2 blocker.

Lastly, both Bragin et al and our data have shown how ATOs seem to propagate in a slow speed (0.1-0.2 mm/s in Bragin et al and 0.19 ± 0.02 mm/s in our experiment). Contrast this with epileptiform discharges that tend to propagate rapidly (20-100 mm/s when inhibition is compromised) (Trevelyan *et al.*, 2007b). This suggests a different mechanism possibly non-neuronal in the spreading of ATO. Note that a similar speed of propagation also has been recorded for cortical spreading depression (Leao, 1944; Bragin *et al.*, 1997). Bragin et al hypothesized that astrocytes might be involved as ATO propagation speed is comparable to the speed of calcium wave propagating between astrocytes. However this was still only a hypothesis that should be further explored. As my recordings showed rare instances where in vitro model of seizures are terminated by spreading-depression like event, this model could provide a more accessible preparation to test such a hypothesis that would be otherwise difficult to be done in vivo.

It has been reported before that in several models of epilepsy, seizures are terminated by a spreading-depression like event that has a similar underlying mechanism with ATO, which is depolarization block (Somjen *et al.*, 1985; Bragin *et al.*, 1997). However what ATO involvement in seizure termination is still questionable. Especially that this is not regularly observed in the commonly used epilepsy models such as 0 Mg^{2+} or 4-AP also the chronic models of epilepsy such as kainic acid, picrotoxin or tetanus toxin model of epilepsy. This suggests that probably this is not the general terminating mechanism that is applicable to all seizures. However this could potentially act as a secondary terminating mechanism when seizure is really long or when the convulsant persists as a defence mechanism to prevent long seizure to turn into status epilepticus.

Chapter 5. Designing a new optogenetic tool to correct raised intraneuronal chloride in epilepsy

5.1. Introduction

This chapter focuses on addressing the secondary aim of this project which was to develop an optogenetic tool to be used to extrude chloride from neurons. This would be particularly valuable as a tool for chloride research and potentially an ideal strategy to halt seizures, as extruding chloride would restore the natural GABA inhibition.

To date, Cl⁻ flow conducting optogenetic proteins are available in forms of light activated electrogenic pumps that are halorhodopsin (HR) and the red shifted cruxhalorhodopsin known as jaws (Gradinaru *et al.*, 2008; Chuong *et al.*, 2014), or light activated Cl⁻ channel consisting of iC1C2 family and ChloC family (Berndt *et al.*, 2014; Wietek *et al.*, 2014). Some of these proteins are the basic optogenetic proteins being explored in this chapter to be modified as novel Cl⁻ extrusion tools.

5.1.1. Reversal of light activated Cl⁻ pump - Halorhodopsin

Unlike the excitatory optogenetic protein channelrhodopsin, a cation channel in which ion flows is determined by the ion's reversal potential and the membrane potential (E_m) (Nagel *et al.*, 2003), HR is an electrogenic inward chloride pump that uses energy from light to transfer chloride ions into the cell (Deisseroth *et al.*, 2006). Consequently, HR has a one way Cl⁻ flow that is inward, bringing Cl⁻ from the extracellular space into the cell. We speculated that reversing the orientation of HR on the membrane would reverse the direction of chloride pump during its activation.

One important consideration before starting any attempt in reversing HR orientation is whether HR would still be capable of pumping Cl^- in the reversed orientation. The main concern comes from the fact that Cl^- concentration is different inside and outside the cells. As extracellular Cl^- is generally an order of magnitude higher than the intracellular Cl^- , wild-type HR effectively works in the same direction with the concentration gradient of Cl^- . If HR is reversed, it then has to work against the concentration gradient, which might compromise the HR Cl^- pump. It is then necessary to start with simulating the effect of going against the Cl^- concentration gradient on the wild-type HR current to assess whether it would still be capable of pumping Cl^- .

The next step then was to design the strategy to reverse the orientation of HR. Two strategies were used as an attempt to reverse HR orientation: altering the distribution of charged residues and protein anchoring.

Altering the distribution of charged residues

The first involved changing the transmembrane distribution of positive and negative charged amino acid residues of HR. This is based on the hypothesis that membrane proteins including HR are oriented post-translationally inside the translocon protein, where membrane proteins are oriented following a positive inside rule, and once it achieves its permanent orientation, it is released to the membrane (von Heijne, 1992)(figure 5.1A). The positive inside rule indicates that on transmembrane helices, positive charges tend to be distributed on the cytoplasmic side while the negative charges are on the extra cellular side and it has been suggested that this signature of charges distribution dictates the membrane protein orientation (von Heijne, 1992).

Supporting evidence comes from the naturally dual-oriented protein EmrE, a small multidrug resistant protein that is naturally expressed in 2 different orientations (Rapp *et al.*, 2007). The two variants have different distributions of the positively charged residues that are consistent with the positive inside rule, and these orientations could be reversed by swapping the distribution of the positive and negative charges using site-directed mutagenesis (Rapp *et al.*, 2007).

The same principle has also been shown in a eukaryotic system, where certain membrane proteins' orientations could be reversed by changing the distribution of positive and negative residues when expressed in human cervical cancer cells, HeLa cells (Sommer *et al.*, 2013). This phenomenon could be explained by the natural tendency of the protein to forfeit its orientation to maintain the topology when the charge distribution is altered (Tate, 2010). Membrane protein orientation however is also affected by additional factors other than the distribution of positive and negative charges, such as the size and the folding of the N-terminal domain, and also the length and the hydrophobicity of the transmembrane domains (Sommer *et al.*, 2013).

Based on the success of these previous works (Rapp *et al.*, 2007; Sommer *et al.*, 2013), in which reversal of different membrane proteins orientation was achieved by altering the distribution of positively and negatively charged amino acid residues located in the inner and outer membrane, I hypothesised that by doing the same with HR I could potentially reverse the orientation of HR in the membrane and the direction of the Cl⁻ flow (figure 5.1B).

Different combinations of mutations targeting the positive and negative charged residues were introduced. To visualise the cells, enhanced yellow fluorescent protein (EYFP) was co-expressed together with the mutant HR, using several different strategies. First EYFP was fused to the C-terminal of the HR mutant that allows the mutant protein and EYFP to be produced as a single protein in all transfected cells. Second, to avoid any potential interference of the EYFP fusion with the HR mutant orientation, an extra construct was made that utilised the internal ribosomal entry sites (IRES) system to label the transfected cells with fluorescent marker. IRES is commonly used for co-expression of two proteins as this viral origin nucleotide sequence enables a second protein translation initiation in the middle of mRNA (Douin *et al.*, 2004) allowing two proteins to be synthesized under a single promoter. The IRES system would allow the expression of both mutant HR and EYFP as two separate proteins, hence avoiding any interaction between the two proteins.

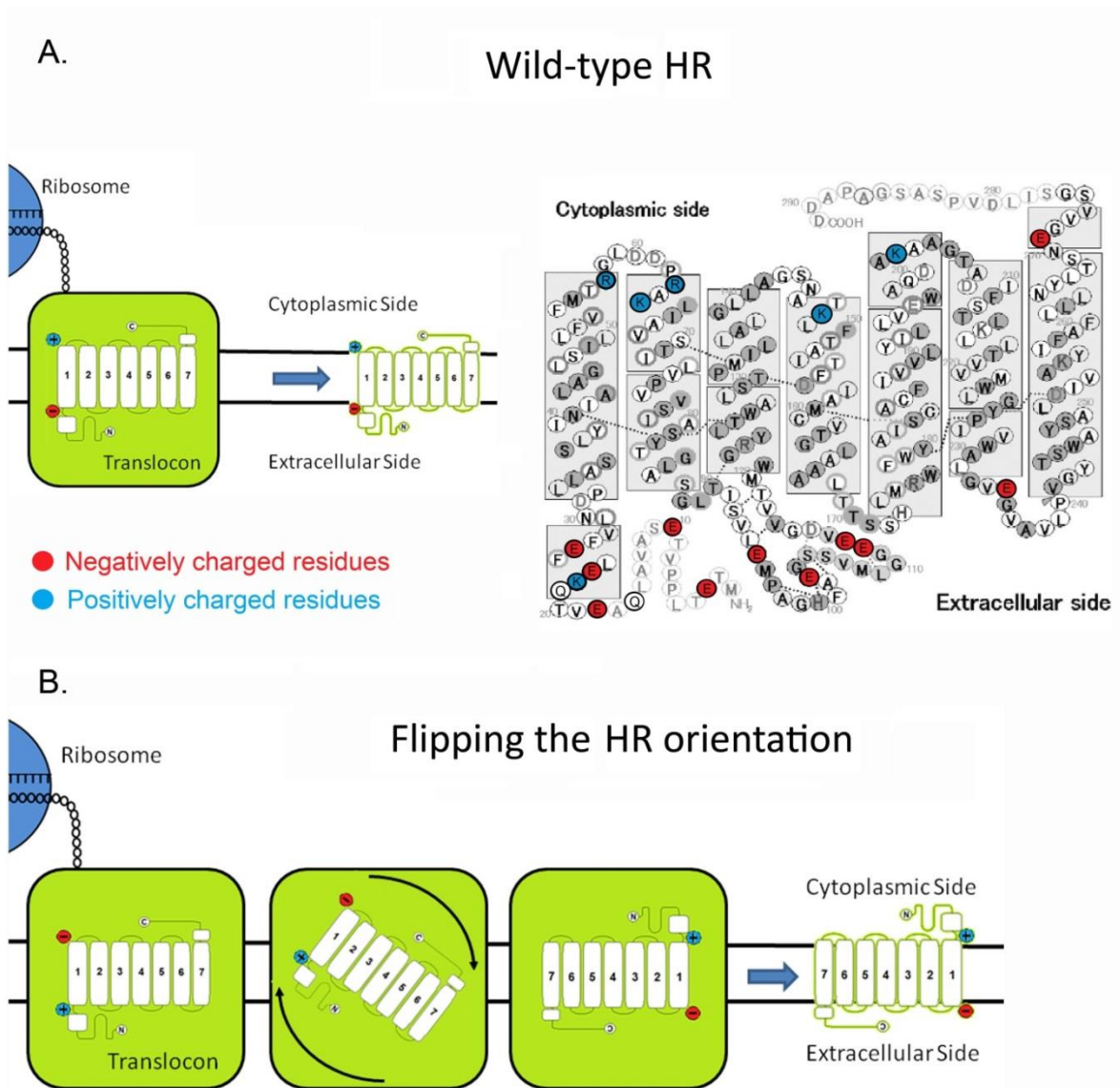


Figure 5.1 Altering the distribution of charged residues strategy. A. Left: After translation from the ribosome, membrane protein would be folded and oriented on the membrane within the translocon protein according to the positive inside rule. The side with more positively charged residues (blue) will be positioned in the cytoplasmic side while the side that has more negatively charged amino acids (red) will be located in the extracellular side. Right: Accordingly, wild-type HR shows a pattern of charged residues distribution that follows the positive inside rule with more positively charged (blue) amino acids arginine (R) and lysine (K) found in the cytoplasmic side, while more negatively charged (red) amino acids, glutamic acid (E) is found in the extracellular side, adapted from (Kouyama *et al.*, 2010). B. It is hypothesised that changing the distribution of positive and negative residues could potentially reverse HR orientation across the membrane.

Protein anchoring

The second strategy to reverse the orientation of HR is by protein-anchoring. Protein translation is started from the N-terminus where it has a start codon for methionine. The next amino acids are then added to the C-terminus until it reaches the stop codon. Accordingly, HR production is started from the N-terminus that happens to be located on the extracellular side and finished with its C-terminus on the cytoplasmic side ($N_{out}-C_{in}$) (figure 5.2A). Based on this, we speculated that by fusing a single pass membrane protein up stream of the HR, it would anchor the HR N-terminus to the cytoplasmic side, forcing the rest of the protein to be translated in a $N_{in}-C_{out}$ manner; hence reversing the orientation of the HR (figure 5.2B-D).

The anchoring protein should be a single pass membrane protein of the right length to anchor the N-terminal of HR to the cytoplasmic site. Additionally, it also has to be correctly targeted and expressed at the membrane. LepA (leader peptidase A) and CD8 were selected as potential anchors. LepA, of bacterial origin, is a 7.4 kDA single pass transmembrane protein. It is a nonessential protein that separates the leader peptidase from its promoter. A LepA deleted mutant does not appear to have any defect on leader peptidase function showing its nonessential role (Dibb & Wolfe, 1986). LepA was chosen based on its relatively simple structure and its nonessential role. However the success and the stability of LepA anchoring when fused with a bigger protein such as HR (37 kDA) is highly speculative. Additionally, LepA is a bacterial origin protein, and so the success of its membrane targeting in eukaryotic systems is not assured.

The second candidate anchor protein was CD8. CD8 is a 13.5 kDA membrane protein that functions as a co-receptor of immune T-cells (Pascale *et al.*, 1992). This well characterised protein is naturally expressed in mammalian systems making it a good candidate for neuronal expression. Furthermore, CD8 is equipped with a signal peptide that might assist membrane targeting of potentially reversed HR (Pascale *et al.*, 1992). A previous study has successfully expressed CD8 in a neuronal system as a CD8-GFP-HCN1₇₇₆₋₉₁₀ construct, although for a different purpose (Santoro *et al.*, 2011). In their study, Santoro et al fused CD8 to the N-terminal of progressively shorter and shorter hyperpolarization-activated cyclic nucleotide-gated (HCN) channel components whilst still ensuring that they were still anchored to the membrane. Here, we tried to adapt the use of CD8 to not only anchor the protein to the membrane but also to alter the orientation of the downstream fused protein, namely HR.

For visualisation purposes, fluorescent marker expression is required. Green fluorescent protein (GFP) was fused between the anchor protein and HR (figure 5.2B-C) or at the N-terminus of HR. This is because GFP may not fold properly outside the cell (or preteolytically removed), and so might not be fluorescent if fused to the externally located C-terminus of HR. Finally I also considered whether the presence of GFP, could also provide an extra anchoring effect on HR in addition to its visualisation role. As a water soluble protein, GFP will be folded in the cytoplasm, thereby anchoring the HR N-terminus to the cytoplasmic side (figure 5.2B-C).

We hypothesized that combining lepA or CD8 and GFP, with HR might physically reverse its membrane orientation, and thus the direction of the chloride pump of HR. LepA-GFP-HR and CD8-GFP-HR constructs were generated. On the other hand, it is possible that placing GFP, a soluble protein, between two membrane proteins, may actually cause a misfolding of the protein. Consequently, CD8-HR-IRES-GFP construct was also generated to separate CD8-HR from the GFP while still enabling cell visualisation (figure 5.2D).

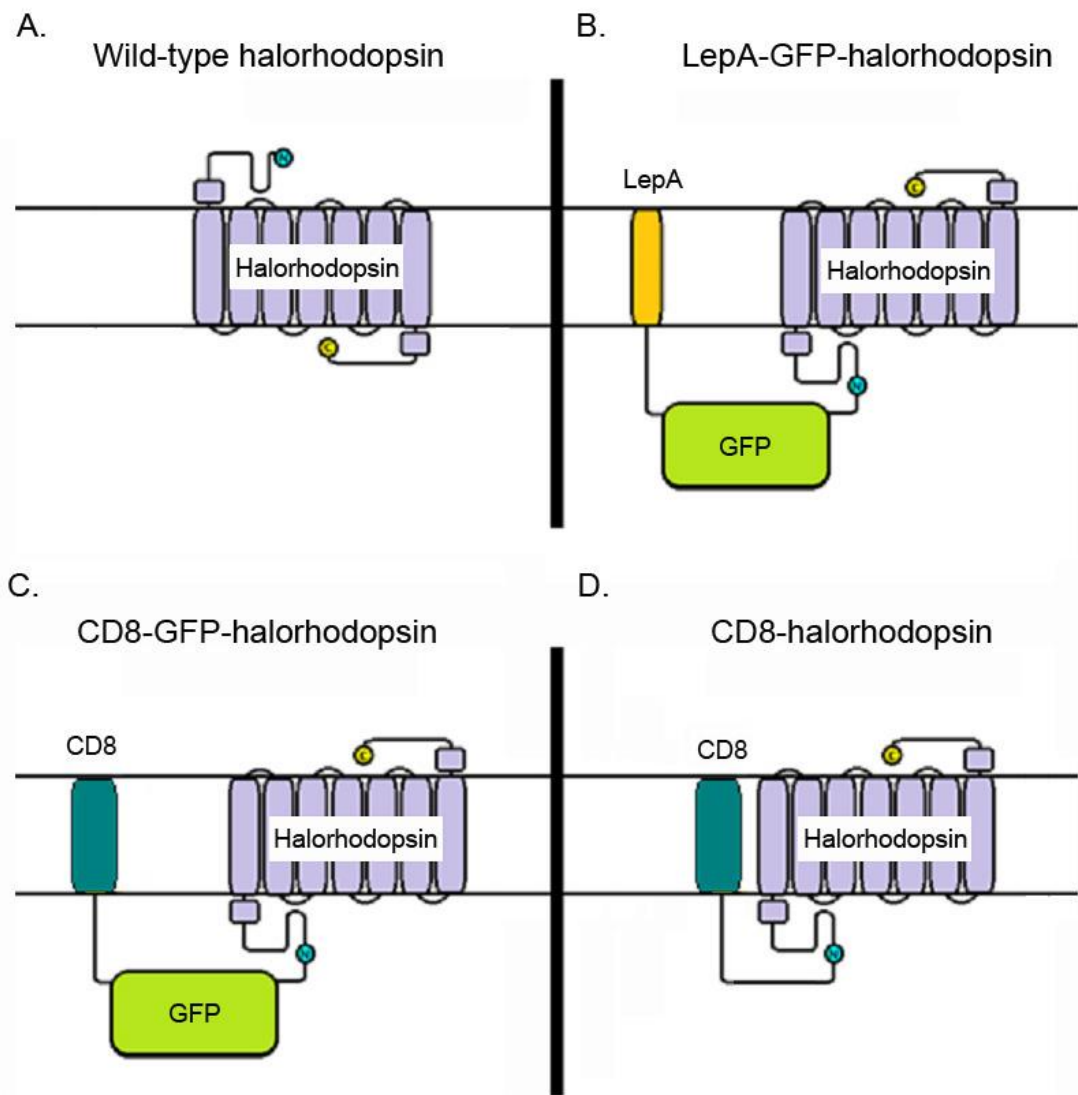


Figure 5.2 Protein anchoring strategy. A. Wild type HR is naturally expressed in a $N_{out}-C_{in}$ manner. B-C. By fusing *lepA* or CD8 (a single pass membrane protein) and GFP upstream to the HR, the anchor proteins are intended to anchor the N-terminal of HR to the cytoplasmic side, forcing its expression to be in a reversed orientation ($N_{in}-C_{out}$). D. As another alternative, CD8 only is used as an anchor without GFP. However to assist the visualisation of the cells, a fluorescence marker is still needed and so this was achieved by utilizing an IRES within the CD8-HR-IRES-GFP construct to allow GFP to be expressed separately from CD8-HR.

5.1.2. Light activated Cl⁻ channel: iC1C2 and ChloC

The development of optogenetic tools continue to progress in many different labs. New proteins are being discovered, generated and enhanced by modification of the available ones. One recent success is the mutagenesis of the originally excitatory channelrhodopsin into light activated chloride channels namely iC1C2 and its slow kinetics version SwiChR_{CT}, also ChloCs and its slow kinetic version slow-ChloC (Berndt *et al.*, 2014; Wietek *et al.*, 2014). The slow kinetic version is a variant of the corresponding channel, modified to stay open for longer than the duration of illumination, allowing the light induced current to outlast the illumination with a time constant of 7.5 s for SwiChR_{CT} and 10.5 s for slowChloC (Berndt *et al.*, 2014; Wietek *et al.*, 2014). All these channels are activated by blue light and are mainly permeable to Cl⁻.

In contrast to HR that has a fixed direction of chloride flow (inward), in principle the activity of these light activated Cl⁻ channel should be comparable to GABA_A receptor in which the direction and the driving force of the chloride flow is determined by the chloride reversal potential (E_{Cl^-}) and the membrane potential. When the membrane potential (E_m) is more positive than E_{Cl^-} , Cl⁻ will enter the cell; while when E_m is more negative than E_{Cl^-} , Cl⁻ will leave the cell. This suggests that if we could modulate E_m sufficiently to stay more negative than E_{Cl^-} while opening a light activated Cl⁻ channel, Cl⁻ would be extruded.

Following this logic, I therefore considered a novel approach to extrude chloride by co-expressing a light activated chloride channel together with a hyperpolarising optogenetic outward proton-pump. I hypothesized that co-expression of these 2 types of optogenetic tools will enable hyperpolarisation of the membrane potential to be more negative than E_{Cl^-} , resulting in the extrusion of the chloride from the cell.

The widely available Cl⁻ independent-hyperpolarising opsins are Archaeorhodopsin (Arch) originally found in *Halorubrum sodomense* and Archaeorhodopsin-T from *Halorubrum* strain TP009 (Chow *et al.*, 2010; Han *et al.*, 2011). Both work as light activated outward H⁺ pumps. ArchT was selected as this strain has a higher light sensitivity compared to Arch. Both iC1C2 and ChloC variants are possible candidates to be explored as the light activated Cl⁻ channel to be used for this purpose.

Finally, I considered ways to reliably co-express two optogenetic proteins under the same promoter. This is to avoid a single expression of either ArchT or Cl⁻ channel alone that theoretically might give different effect on cells in regards to [Cl⁻]_i modulation.

Several techniques have been developed before for this purpose namely by protein fusion (Kleinlogel *et al.*, 2011b), by the use of bi-cistronic expression system such as IRES peptide, or by using 2A peptides (Douin *et al.*, 2004; Tang *et al.*, 2009). Fusion protein has been used widely especially for co-expression of a certain target protein with a fluorescent marker that is a water soluble protein. This technique guarantees a stoichiometric expression of the multiple proteins as they are basically produced as a single protein. This however is not easily translated for co-expression of two membrane proteins such as optogenetic proteins, as this might affect the orientation of the downstream protein and hence its function (Kleinlogel *et al.*, 2011b). This is less of an issue for other expression systems such as IRES and 2A peptides, as these techniques allow for multiple proteins to be expressed as separate proteins rather than fused. The disadvantage of this technique however is that they tend to give an unbalanced level of expression for the different proteins (Chan *et al.*, 2011).

As explained earlier in this chapter, IRES sequences work by enabling initiation of a second protein translation under a single promoter. On the other hand, 2A peptides that consist of 18-22 amino acids, work by initiating cleavages of the encoded proteins into multiple components on translation (Chan *et al.*, 2011). This allows separation of the encoded multiple proteins into different individual proteins. In contrast to an IRES that tends to give a much higher level of expression of the upstream protein compared to the downstream protein (Hennecke *et al.*, 2001), 2A peptide has been known to give a more equal level of expression between the 2 proteins.

Most commonly used 2A peptides for multiple proteins expression are from foot-and-mouth disease virus (F2A peptide), *Thosea asigna* virus (T2A peptide), Porcine teschovirus-1 (P2A peptide), and equine Rhinitis A virus (E2A peptide) (Zhang, 2013). Efficiency of 2A peptides depends more on the different turnover rate of the target proteins to be expressed rather than the different types of 2A peptides itself (Zhang, 2013). Here, I utilized the T2A peptide to be used for the co-expression of ArchT and

light activated Cl^- channel based on the previous success of this 2A peptide for the co-expression of two optogenetic proteins before namely ChR2 and HR (Tang *et al.*, 2009).

5.2. Results

5.2.1. The effect of Cl^- concentration gradient on HR current

Initially, I assessed the effect of Cl^- concentration gradient on wild-type HR Cl^- pump. This is to simulate the condition which potentially reversed HR will have to face if successfully made, namely that it has to pump Cl^- against the Cl^- concentration gradient from inside the cell to the extracellular space. Note that $[\text{Cl}^-]_i$ is always kept lower than outside in the neurons (Chapter 1). Cl^- substitution experiments with the wild type HR current was done by doing a whole cell patch recording of the cells expressing HR using a high internal Cl^- solution ($\text{Cl}^- = 135 \text{ mM}$) in the patching pipette. Continuity between pipette and the cells achieved by whole cell patch allows high Cl^- in the internal to diffuse into the neuron. From each cell, HR current was then measured in the presence of normal ($\text{Cl}^- = 131.5 \text{ mM}$) and low level of chloride ($\text{Cl}^- = 9.5 \text{ mM}$) in the ACSF. The mean HR current was reduced from $97.95 \pm 27.07 \text{ pA}$ to $30.64 \pm 6.03 \text{ pA}$ when washing in low Cl^- ACSF ($p < 0.05$, paired t-test, $n = 3$; figure 5.3), indicating that the amplitude of HR current was markedly affected by the chloride level in the ACSF. However, it did not abolish the current completely, indicating that it is still capable of pumping Cl^- against the Cl^- concentration gradient that was from 9.5 mM Cl^- outside to 135 mM Cl^- inside.

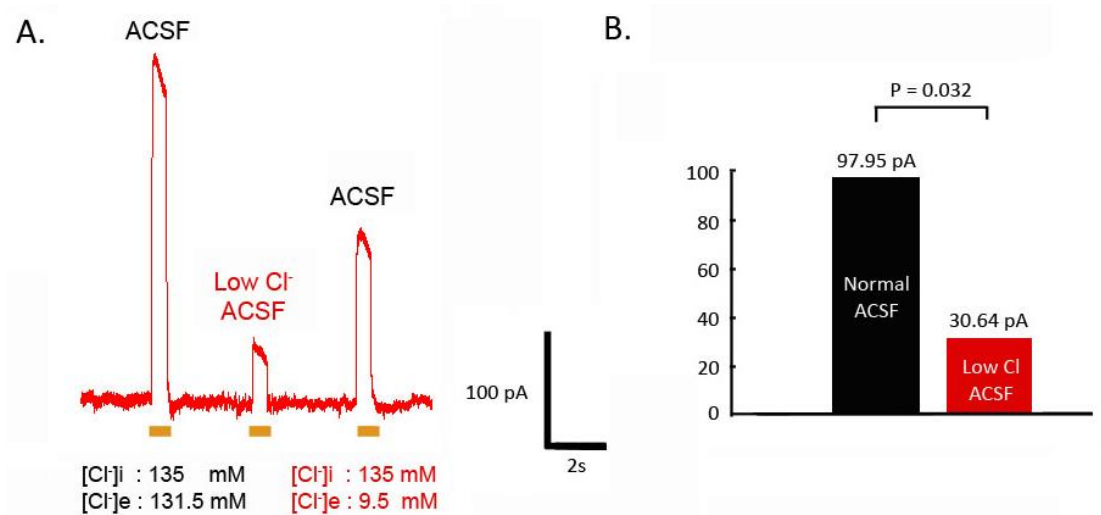


Figure 5.3 The size of HR current is affected by chloride concentration. A. Example trace recorded from a neuron patched with high Cl⁻ internal (135 mM). Orange light illumination induced smaller HR current when washing in low Cl⁻ ACSF (Cl: 9.5 mM) compared to normal ACSF (Cl: 131.5 Mm) and this was recovered during the wash out period. B. Pooled data gives a mean HR current of 97.95 pA when high level of chloride presented outside while the average current of HR was significantly reduced to 30.64 pA when only low amount of chloride presented outside (P<0.05, n=6, paired t-test).

5.2.2. The reversal of HR by altering the distribution of charged residues

The strategy of changing the distribution of positive and negative charged residues of HR was then done by conducting amino acid substitutions which are located on the inner and outer part of the helix/helices. 4 different mutants with different combinations of residue mutations were generated (figure 5.4, table 5.1, designed by Prof. Jeremy H. Lakey). The basic principles of the mutant design is first to alter the distribution of positive-negative residues that is thought to be influential in protein orientation on the membrane, favouring the reversed orientation, and second to avoid residues that are known to be essential for protein folding and chloride pumping so as to preserve its function as a light-activated chloride pump.

The following mutants were generated:

1. Mutant 1 had most of the positive and negative residues in the inner and outer part of helices interchanged (figure 5.4A).
2. Mutant 2 had the positive charges on the inner part of the first helix changed into negative ones (figure 5.4B).
3. Mutant 3 had the negative residues on the outer part of the first helix substituted into positive ones (figure 5.4C).
4. Mutant 4 had its positive and negative residues on the first helix interchanged or combination of mutant 2 and 3 (figure 5.4D).

The three main charged amino acids involved in the design of the mutants are the arginine (R) that is positively charged, glutamic acid (E) that is negatively charged, and glutamine (Q) that is neutral (table 5.1). Mutants 2-4 focus on charged residues of the first helix only as this is the helix that first enters the membrane and thus theoretically is the most influential orientation signal (Rapp *et al.*, 2007; Seppala *et al.*, 2010).

Previously, these 4 different mutants had been expressed in *E.Coli* AI strain system to screen for their ability to fold and bind to the retinal properly. Mutant 3 and mutant 4 were both successfully expressed and purified, but only mutant 3 bound to the retinal, the chromophore that allows the use of light as the energy source of HR (My Master of Research project). Without retinal binding, the protein loses the light sensitivity and so only mutant 3 was taken further to subsequent experiments.

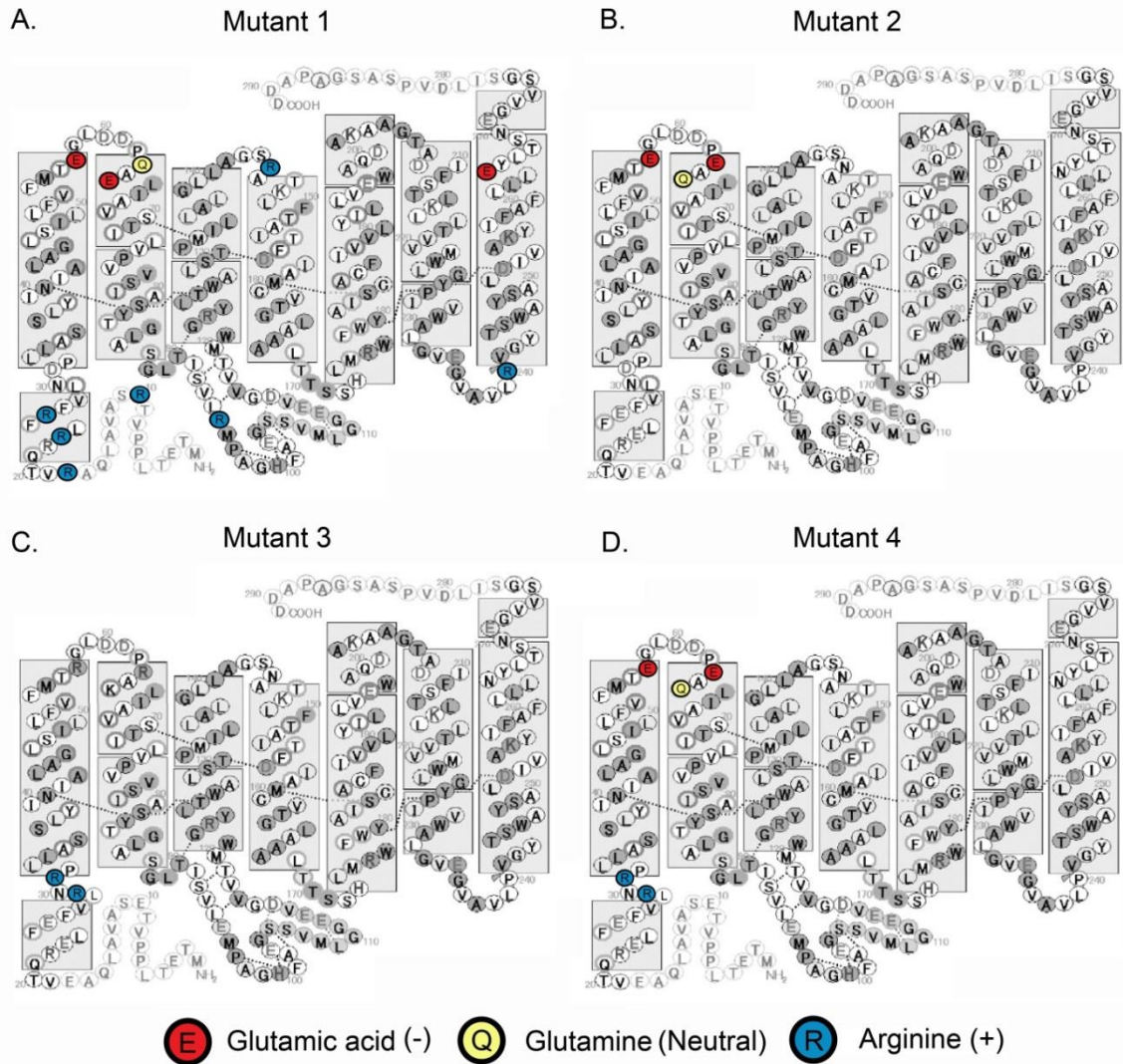
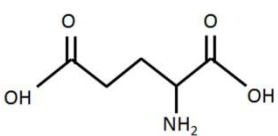
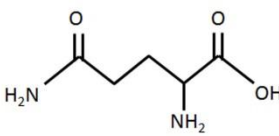
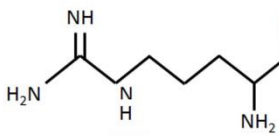


Figure 5.4 Charged amino acid substitutions of HR to reverse its orientation. A. Mutant 1 has most of its positive and negative charges on the edge of the transmembrane helices completely swapped. B. Mutant 2 has the positive charges on the inner part of the first helix changed into negative charges. C. Mutant 3 has the negative charges located on the outer part of the first helix substituted with positive charges. D. Mutant 4 has its charges swapped on the first helix only (combination of mutant 2 and 3). *Figures adapted from (Kouyama et al., 2010).*

Table 5-1 Amino acids sequence of wild-type HR and 4 different mutants HR. Amino acid substitutions and insertions introduced by site-directed mutagenesis are shown in red.

<u>Halorhodopsin (Natronomonas pharaonis)</u>		
<u>Wild-type</u>		
Halorhodopsin Wild Type with 6-His tag		
MTETLPPVTESAVALQAEVTQRELFEFVLNDPLLASSLYINIALAGLSILLFVFMTRGLD DPRAKLIAVSTILVPVVSIA SYTGLASGLTISVLEMPAGHFAEGSSVMLGGEEVDGVVTM WGRYLTWALSTPMILLALGLLAGSNATKLFTAITFDIAMCVTGLAAALTTSSHLMRWFY AISCACFLVVLYILLVEWAQDAKAAGTADMFTLKLTTVVMWLGYPVWALGVEGIAVLP VGVTSWGY SFLDIVAKYIFAFLLNLYLTSNESVSVSGSILDVPSASGTPADDs shhhhhh		
<u>Mutants</u>		
Halorhodopsin Mutant 1 with 6-His tag		
MTETLPPVTRSAVALQARVTRQLRFVFLNDPLLASSLYINIALAGLSILLFVFMTEGLD DPQAE ^E LI ^A AVSTILVPVVSIA SYTGLASGLTISVLR ^R MPAGHFAEGSSVMLGGEEVDGVVTM WGRYLTWALSTPMILLALGLLAGSNATKLFTAITFDIAMCVTGLAAALTTSSHLMRWFY AISCACFLVVLYILLVEWAQDAKAAGTADMFTLKLTTVVMWLGYPVWALGVEGIAVLR ^R VGVTSWGY SFLDIVAKYIFAFLL ^E YLT ^E SNESVSVSGSILDVPSASGTPADDs shhhhhh		
Halorhodopsin Mutant 2 with 6-His tag		
MTETLPPVTESAVALQAEVTQRELFEFVLNDPLLASSLYINIALAGLSILLFVFMTEGLD DPEA ^Q LI ^A AVSTILVPVVSIA SYTGLASGLTISVLEMPAGHFAEGSSVMLGGEEVDGVVTM WGRYLTWALSTPMILLALGLLAGSNATKLFTAITFDIAMCVTGLAAALTTSSHLMRWFY AISCACFLVVLYILLVEWAQDAKAAGTADMFTLKLTTVVMWLGYPVWALGVEGIAVLP VGVTSWGY SFLDIVAKYIFAFLLNLYLTSNESVSVSGSILDVPSASGTPADDs shhhhhh		
Halorhodopsin Mutant 3 with 6-His tag		
MTETLPPVTESAVALQAEVTQRELFEFVL ^{RNR} PLLASSLYINIALAGLSILLFVFMTRGLD DPRAKLIAVSTILVPVVSIA SYTGLASGLTISVLEMPAGHFAEGSSVMLGGEEVDGVVTM WGRYLTWALSTPMILLALGLLAGSNATKLFTAITFDIAMCVTGLAAALTTSSHLMRWFY AISCACFLVVLYILLVEWAQDAKAAGTADMFTLKLTTVVMWLGYPVWALGVEGIAVLP VGVTSWGY SFLDIVAKYIFAFLLNLYLTSNESVSVSGSILDVPSASGTPADDs shhhhhh		
Halorhodopsin Mutant 4 with 6-His tag		
MTETLPPVTESAVALQAEVTQRELFEFVL ^{RNR} PLLASSLYINIALAGLSILLFVFMTEGLD DPEA ^Q LI ^A AVSTILVPVVSIA SYTGLASGLTISVLEMPAGHFAEGSSVMLGGEEVDGVVTM WGRYLTWALSTPMILLALGLLAGSNATKLFTAITFDIAMCVTGLAAALTTSSHLMRWFY AISCACFLVVLYILLVEWAQDAKAAGTADMFTLKLTTVVMWLGYPVWALGVEGIAVLP VGVTSWGY SFLDIVAKYIFAFLLNLYLTSNESVSVSGSILDVPSASGTPADDs shhhhhh		
E: Glutamic acid (-)	Q: Glutamine (Neutral)	R: Arginine (+)
		

Mutant 3 HR (mutHR) was subcloned into a pcDNA3.1 vector and fused with EYFP (mutHR-EYFP) for mammalian expression and electroporated into the dissociated neuronal cultures. MutHR-EYFP expressing neurons (figure 5.5Ai) were patched in a whole cell mode using high chloride internal ($\text{Cl}^- = 135 \text{ mM}$) to facilitate an optimal mutHR current. Three repeats of electroporation of mutHR-EYFP were done each time with wild-type protein as a control for the electroporation process. A total number of 20 cells were patched, 5 to 10 cells per electroporation. Two out of 20 cells (10%) expressing the mutHR-EYFP protein gave an upward deflection ($n=2$, figure 5.5Aii) during orange light illumination indicative of an inward chloride movement as observed in wild type HR. The remainder of the cells (90%) gave no response at all during illumination ($n=18$, figure 5.5Aii). No obvious differences could be observed from the morphology and EYFP expression between these 2 differently responding cells. This suggests that the chloride pump of mutHR-EYFP was not successfully reversed in these cells.

If HR orientation is successfully reversed, it would have its N-terminal located inside and C-terminal outside. We therefore considered the possibility that fusing EYFP a water soluble protein to the C-terminal of mutHR might interfere with the reversion of mutHR orientation by anchoring the C-terminal to the cytoplasm. To test whether the failure of mutHR-EYFP construct reversion is not due to the fusion of EYFP to the C-terminal, mutHR-IRES-EYFP construct was generated. Here mutHR and EYFP were produced separately as 2 different proteins that one should not interfere with the other. When this was expressed in the neuronal culture (4 electroporations), all the recorded fluorescent cells showed no response to light activation (n =24, figure 5.5B).

There are several possible explanations for the absence of light activated current of mutHR-IRES-EYFP construct.

- i. mutHR was not being produced by the cell machinery
- ii. mutHR was produced but not targeted to the membrane
- iii. mutHR was in the membrane but dysfunctional

To answer this, post-hoc immunofluorescence labeling against HR in cells transfected with mutHR-IRES-EYFP was done (the HR antibody should also bind to mutHR as this construct only has 3 point mutations from the wild type HR). Staining result showed aggregates in the organelles that are likely to be the endoplasmic reticulum (figure 5.5Biii). This suggests that the cells indeed produced mutHR but it was not targeted properly to the membrane. This tells us that the absence of light activated current of mutHR construct is due to the lack expression of the protein at the plasma membrane of the cell surface.

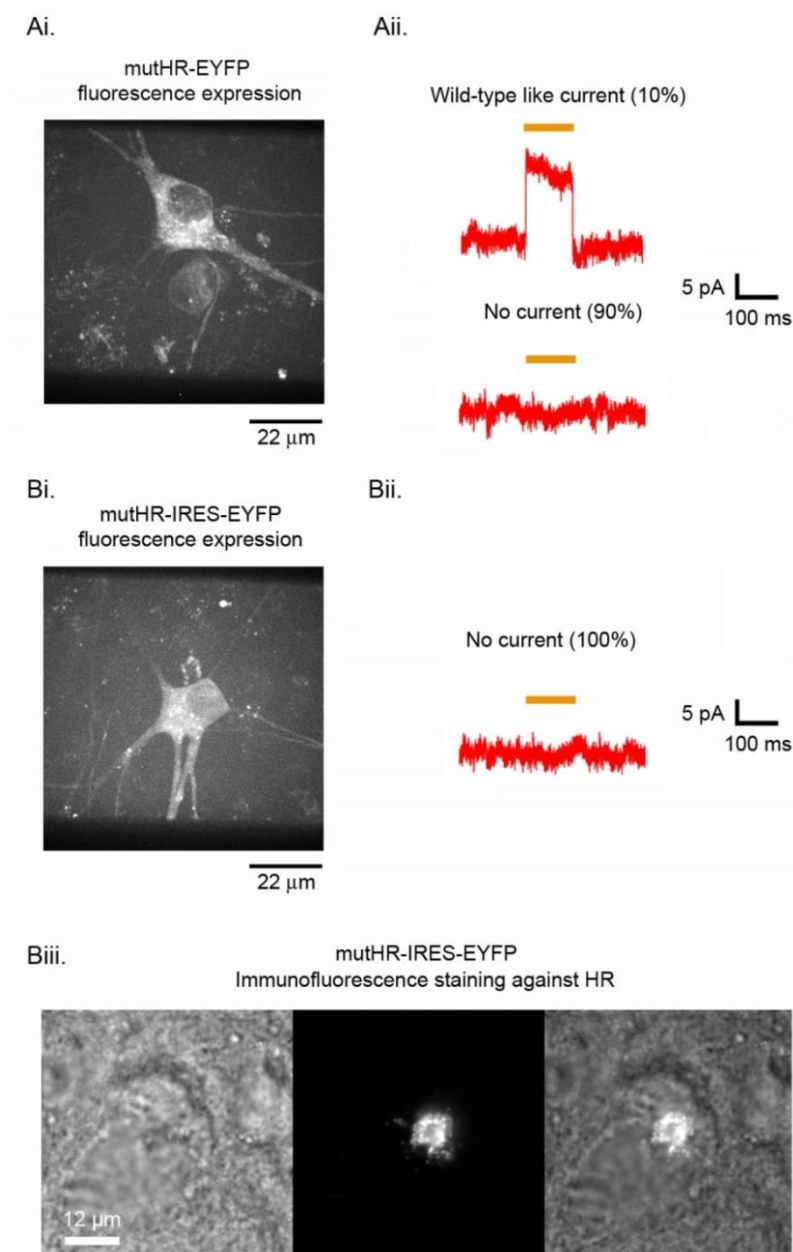


Figure 5.5 mutHR-EYFP and mutHR-IRES-EYFP expression and electrophysiology recording. Ai. Representative neuron expressing mutHR-EYFP imaged under fluorescence microscope for EYFP using 100x objective. Aii. A very small proportion of cells (10%; n= 2 out of 20) showed a wild-type like current (inward movement of Cl⁻) with a relatively smaller amplitude (representative trace from 1 neuron). Aiii. 90% of the cells (n=18) showed no light activated current with orange light (representative trace from 1 neuron). Bi. Cells transfected using mutHR-IRES-EYFP plasmid imaged under fluorescence microscope for EYFP using 100x objective. Bii. All cells patched (n=24) did not show any light activated current with orange light (representative trace from 1 neuron). Biii. Immunofluorescent staining against HR on cell expressing mutHR-IRES-EYFP. Left panel shows the brightfield view of the cell, middle panel shows mutHR labelling, and right panel shows the overlay of the two showing that mutHR was aggregating surrounding the nucleus.

5.2.3. Reversion of HR by protein anchoring

LepA-GFP-HR construct had also been previously expressed and purified in *the E.Coli* system to test that this fusion protein could fold and bind to retinal (done by Scott Mitchell, Master of Research project co-supervised by me). The LepA-GFP-HR expressing cDNA was then subcloned into pcDNA3.1 vector for mammalian cells expression that was then expressed in the dissociated neuronal culture by electroporation. Fluorescence imaging of these cells showed that the GFP labeling was not well diffused throughout the cell and its processes; instead it clumped within the cell body (figure 5.6, left). No current could be recorded during orange light illumination when patched with high Cl⁻ internal. Scott Mitchell then expressed this construct in HeLa cells for imaging purpose and took high magnification images of the cells. It was clearly visible how most of the GFP appeared to aggregate within the cytoplasm (figure 5.6, right).

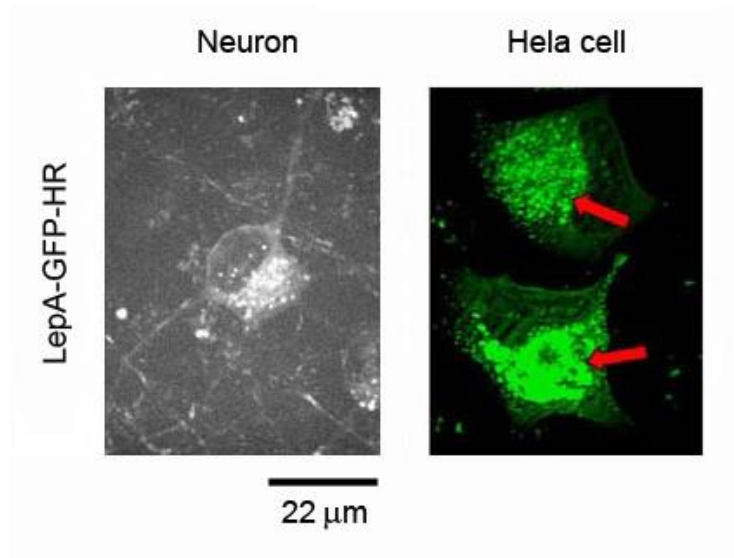


Figure 5.6 Expression of lepA-GFP-HR construct. Left: An example neuron that expressed lepA-GFP-HR imaged under confocal microscope for GFP expression using a 100X objective. Right: Example HeLa cells expressing LepA-GFP-HR imaged under confocal microscope for GFP expression using a 100X objective (S. Mitchell).

Several different factors could lead to the failure of membrane localization of lepA-GFP-HR protein when expressed in primary neuronal culture. Firstly, this might be due to the incompatibility of lepA protein as an anchor protein in neuronal system. To answer this, CD8-GFP-HR construct was generated replacing lepA with CD8, a native mammalian protein that had been successfully expressed in neuronal systems in another study (Santoro *et al.*, 2011). Additionally, CD8-GFP was also generated as a control to further confirm that CD8 could be expressed properly in the neurons. Evidently the same problem remained even after replacing LepA with CD8 in the CD8-GFP-HR construct, GFP labeling still looked spotty around the cell soma and no light activated current could be recorded ($n = 15$, from 3 different electroporations; figure 5.7, middle). In contrast, CD8-GFP alone was expressed in the neurons throughout the cell body and the processes (figure 5.7, left). This suggests that the expression problem was not caused by CD8 as the anchor protein or by the GFP marker.

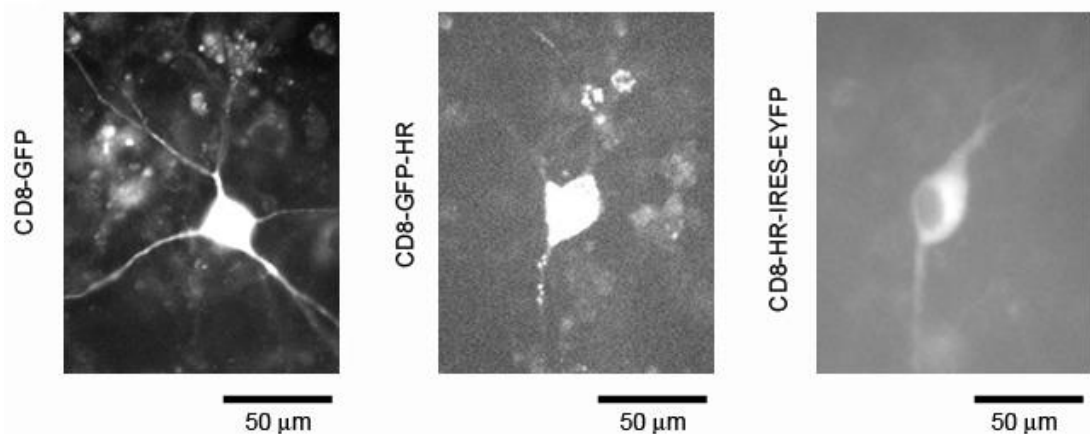


Figure 5.7 Neuronal expression of CD8-GFP, CD8-GFP-HR, and CD8-HR-IRES-EYFP. Representative neurons imaged under a confocal microscope for GFP or EYFP expression. CD8-GFP was expressed as a control (left).

Secondly, it could be due to a misfolding of the protein caused by the fusion of the GFP, a water soluble protein between two different membrane proteins. To address this, GFP was separated out from the fusion protein leaving the CD8 alone as the anchoring protein upstream of HR. To allow cell visualisation, GFP was also expressed but using the IRES system as CD8-HR-IRES-GFP construct in which CD8-HR and GFP were expressed as 2 separate proteins by the transfected cells. Cells transfected by CD8-HR-IRES-EYFP construct however still did not show a healthy expression of the protein and no light activated current could be recorded with orange light (n =15, from 3 electroporations; figure 5.7, right). To confirm that HR was being produced, a post hoc immunofluorescence labeling against HR was done on cells expressing these constructs. Similarly with mutHR protein, staining showed aggregation in the cytoplasm indicating that HR was produced by the cells but was not successfully passaged through the trans golgi network to the membrane (figure 5.8). Collectively, this data suggests that the HR alteration by protein anchoring led to protein aggregation and so fail to reverse the HR orientation.

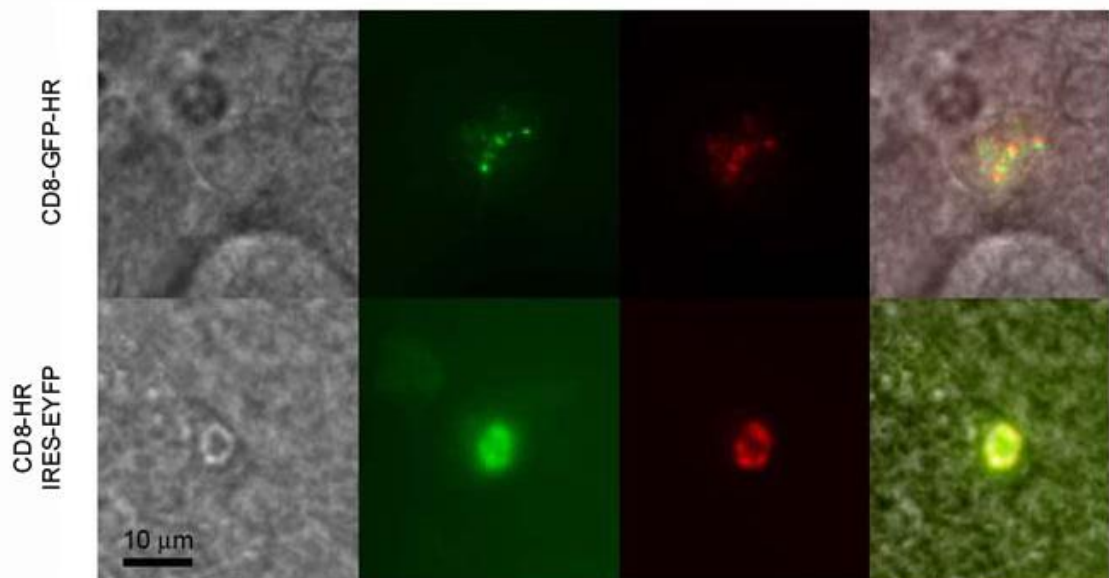


Figure 5.8 Immunofluorescence staining against HR in CD8-GFP-HR and CD8-HR-IRES-GFP construct. Representative cells imaged under brightfield, GFP filter (green), red fluorescence filter for HR labelling, and overlay of all from neurons transfected with CD8-GFP-HR construct (top) and CD8-HR-IRES-EYFP construct (bottom).

5.2.4. Co-expression of light activated Cl⁻ channel and ArchT to extrude Cl⁻

iC1C2 vs slow-ChloC light activated current

Dissociated neuronal cultures were electroporated with either pAAV-CamKII-iC1C2-EYFP or pAAV-hSyn-slowChloC-tDimer plasmid. As an initial investigation to compare the light activated current of both channels, whole cell patch recordings were done on cells 7 days post transfection. Patching pipette contained 6 mM Cl⁻ that gives an E_{Cl⁻} of -81 mV. Both iC1C2 and ChloC light activated current were depolarizing from -85 mV. Assuming that these channels are mainly permeable to Cl⁻, these depolarizing current should be generated by an outward flow of Cl⁻.

From this initial experiment, only 2 out of 8 cells expressing iC1C2-EYFP, screened by EYFP expression, showed a light activated current even when changing V_{Hold} between -90 to -30 mV. In both cells, the iC1C2 current was smaller than the slow-ChloC current (n=5 cells; figure 5.9). Based on this initial assessment that slow-ChloC gave a more reliable light activated current, all subsequent experiments were done using ChloC variants that were either the ChloC or the slow-ChloC (slow kinetic version of ChloC).

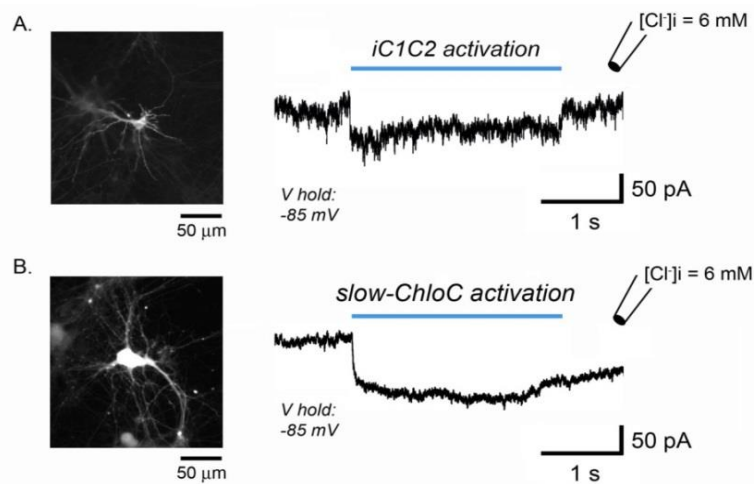


Figure 5.9 Whole cell recording of iC1C2 and slow-ChloC light activated current. Whole cell patch was done using an internal containing 6 mM Cl⁻ in a voltage clamp mode from cells expressing iC1C2 and slow-ChloC. A. A neuron expressing iC1C2 was patched with a V_{Hold} of -85 mV. Blue light illumination induced a downward deflection (EPSC) that in theory should reflect the Cl⁻ outward flow from inside the cell. B. A neuron expressing slow-ChloC also showed an EPSC during blue light illumination when patched with a V_{Hold} of -85 mV. Slow-ChloC tends to give a bigger current compared to iC1C2 (traces are example from 1 neuron each).

Co-activation of ArchT and ChloC variants induces a negative shift in E_{GABA}

Co-expression was done by electroporation of the dissociated neuronal culture with pAAV-CAG-ArchT-GFP and pAAV-hSyn-ChloC-tDimer or pAAV-hSyn-slow-ChloC-tDimer. Cells that expressed both fluorescence proteins tDimer (red) and GFP (green) were selected for the experiment (figure 5.9 & 5.13). The same experimental protocol used to characterise HR Cl^- loading effect (chapter 3) was used for the characterisation of ArchT-ChloC variants effect on $[Cl^-]_i$. Gramicidin perforated patch was performed, and E_{GABA} was measured, with or without optogenetic activation, by introducing a voltage ramp during the local application of muscimol ($GABA_A$ agonist), and another one during the baseline.

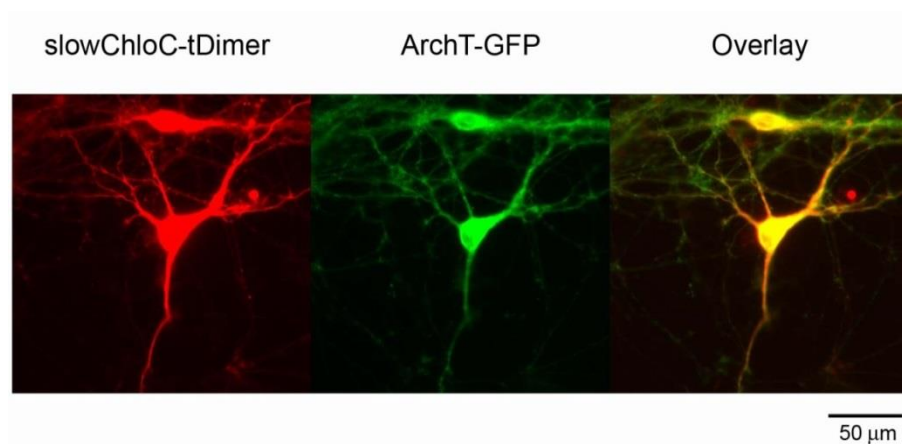


Figure 5.10 Co-expression of slowChloC and ArchT on dissociated neuronal culture. Left: A neuron expressing slowChloC that was tagged with red fluorescence protein tDimer. Middle: The same neuron also expressed ArchT that was fused with GFP (green). Right: Overlay of both red and green resulted in yellow colour confirmed the co-expression of the 2 optogenetic proteins by the same neuron.

The first set of experiments was conducted on cells expressing ArchT and slow-ChloC screened by the expression of both red and green fluorescence (figure 5.9). Simultaneous activation of both ArchT and slow-ChloC by co-illumination using light with 491 nm and 561 nm wavelength readily induced a negative shift in E_{GABA} to a more hyperpolarised level with a mean shift of -2.67 ± 0.47 mV ($p < 0.02$, $n = 5$, paired t-test; figure 5.10D), indicative of a lower $[Cl^-]_i$ post illumination. The light associated negative shift in E_{GABA} was consistent regardless of the initial $[Cl^-]_i$ as indicated by the baseline GABA response of individual cells. Optogenetic activation of both ArchT and slow-ChloC consistently drove the Cl^- out when baseline E_{GABA} was depolarizing (downward deflection), roughly equivalent to E_m (no GABAergic deflection), or hyperpolarizing (upward deflection) when doing a voltage clamp (V_{Clamp}) recording with a holding potential (V_{Hold}) of -70 mV (figure 5.10A-C).

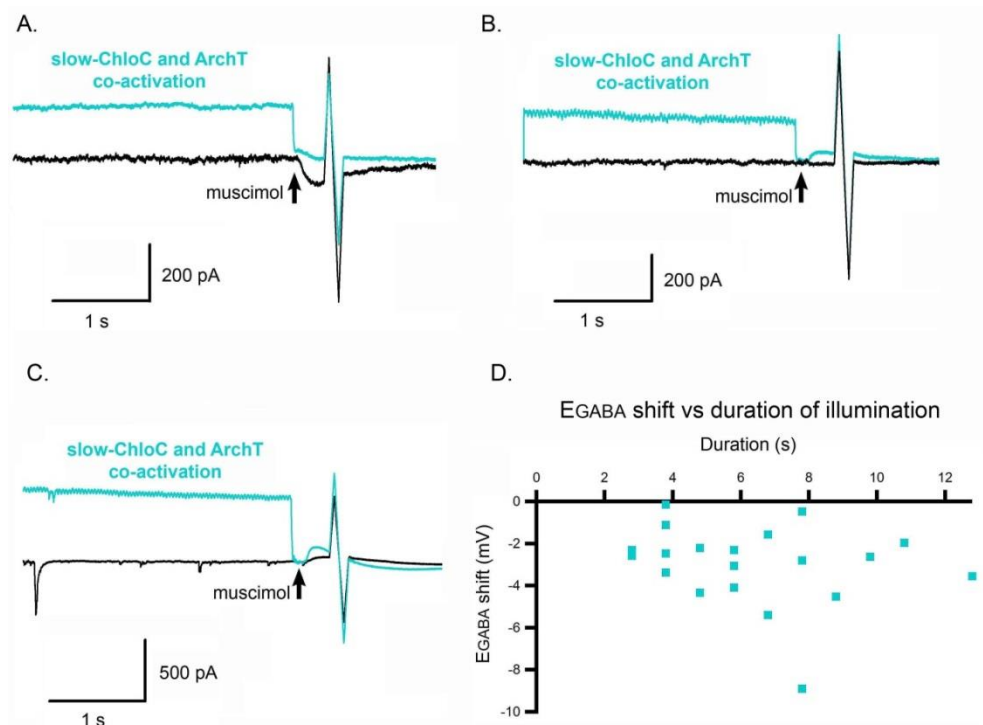


Figure 5.11 Co-activation of slowChloC and ArchT induced a negative shift in E_{GABA} . Co-activation of the 2 optogenetic proteins consistently induced a negative shift in the E_{GABA} of 3 different representative cells regardless of their initial GABA response. A. Representative trace from the cell that initially had a depolarizing GABA response. B. The representative trace from the cell that had an initial shunting (flat) GABA response. C. The representative trace from the cell that had an initial hyperpolarizing GABA response (upward deflection). D. Pooled data of the E_{GABA} shift induced by ArchT-slowChloC co-activation plotted relative to different duration of illumination.

The decay of the Cl⁻ extrusion effect was assessed by briefly co-activating the pair of optogenetic proteins, either ArchT and slow-ChloC (n =2) or ArchT and ChloC (n=3), and applying muscimol in an increasing delay (figure 5.11). A negative shift was again induced by the light activation reversing the initially depolarising baseline GABA (figure 5.11A, black) into hyperpolarising IPSC (figure 5.11A1) in this representative cell. This was indicative of a Cl⁻ clearing effect when muscimol was applied immediately (100 ms delay) after the optogenetic activation (figure 5.11A1). The amplitude of the IPSC was progressively reduced with a longer delay between light activation and the muscimol puff, and eventually collapsed back to a baseline-like GABA event (figure 5.11A-B). E_{GABA} shift produced by different delays were normalised to the E_{GABA} shift induced with the shortest delay. Data points were exponentially fitted to calculate the decaying time constant of the Cl⁻ clearing effect. Pooled data decay plot was shown in figure 5.12A with a mean time constant of 10.6 ± 2.2 s (mean ± sem, n=5), note that the mean time constant was calculated by averaging the τ of individual cells rather than extrapolating from the pooled decay plot.

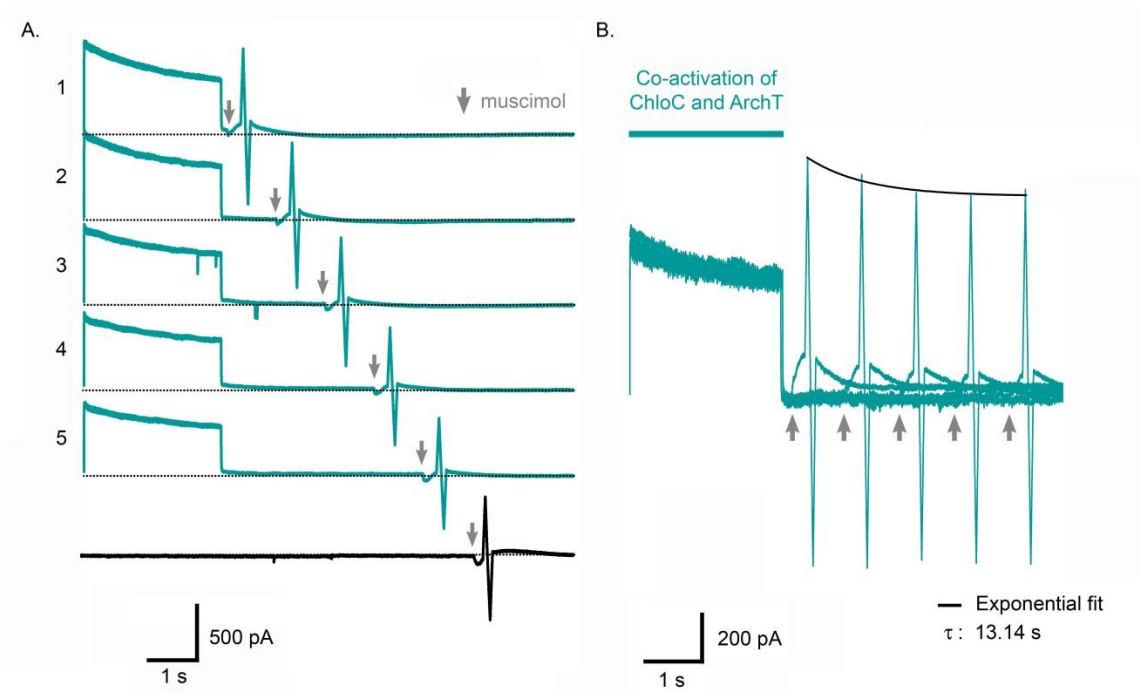


Figure 5.12 Transient effect of ArchT-ChloC co-activation in extruding Cl^- . A. Example traces from 1 neuron in which muscimol puff was applied with an increasing 1s delay after a brief co-activation of ArchT-ChloC (trace 1-5). When muscimol puff applied 100 ms post illumination, E_{GABA} was negatively modulated resulted in an IPSC (trace 1) instead of an EPSC triggered without optogenetic activation (black). This modulation were smaller the longer the delay being introduced between the light activation and the muscimol puff. B. The same traces overlapped together depicted the progressively smaller IPSC amplitude with the longer delay with a time constant of 13.14 s in this particular cell. Exponential fit to the maxima of the ramps highlights the progressively smaller hyperpolarizing event by GABA the longer delay introduced.

The negative shift however was relatively small. One explanation could be due to the fact that there was not much extra Cl^- inside available to be extruded. This is supported by the fact that the size of the shift was well correlated with the basal $[\text{Cl}^-]_i$, with a bigger negative shift is achieved by the cell that had a more depolarised baseline E_{GABA} (R^2 : -0.72, p :0.01, n =11, linear regression; figure 5.12B). Furthermore, unlike HR Cl^- loading effect (chapter 3), ArchT-slow-ChloC Cl^- clearance effect does not correlate with the duration of illumination (R^2 :-0.16, p <0.5, linear regression; figure 5.10D).

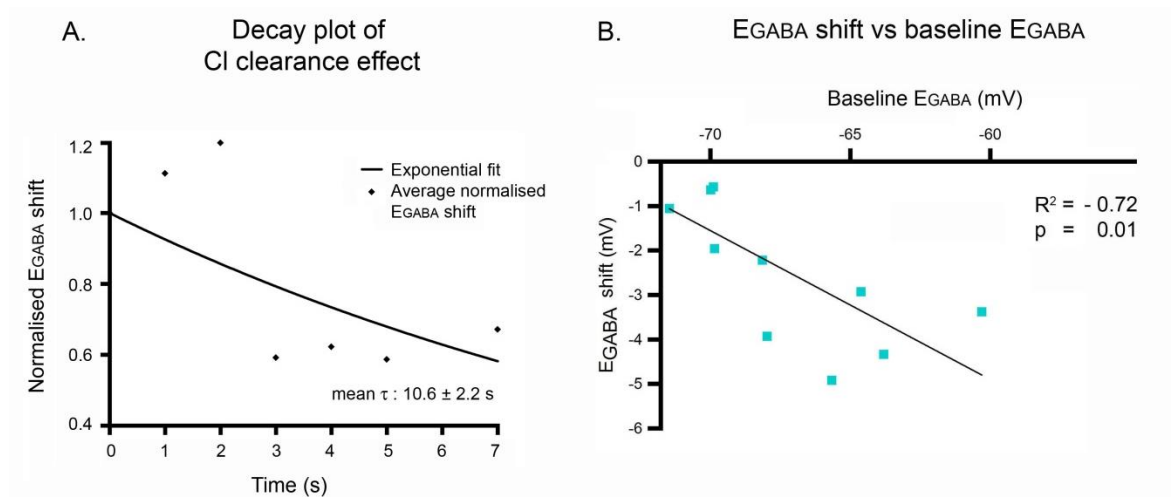


Figure 5.13 Pooled data of E_{GABA} shift introduced by co-activation of ArchT-ChloC. A. E_{GABA} shift was normalised to the E_{GABA} shift from the measurement when the shortest delay was introduced. The average from all 5 cells was plotted and exponentially fitted, with the mean time constant of 10.6 ± 2.2 s (mean \pm sem, n =5). Note however that mean τ was calculated by averaging 5 individuals τ . B. The negative shift was well correlated with the baseline E_{GABA} that represents the initial $[\text{Cl}^-]_i$ (R^2 : -0.72, p : 0.01, n =11, linear regression).

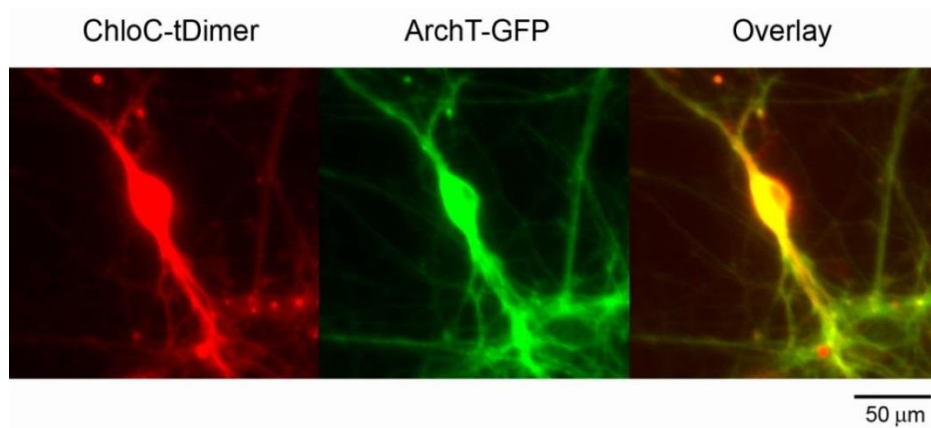


Figure 5.14 Co-expression of ChloC and ArchT on dissociated neuronal culture. Left: Example of a neuron expressing ChloC that was tagged with red fluorescence protein tDimer. Middle: The same neuron also expressed ArchT that was fused with GFP (green). Right: Overlay of both red and green resulted in yellow colour confirmed the co-expression of the 2 optogenetic proteins.

To investigate whether a bigger negative shift could be achieved when cells contain more Cl^- internally, I attempted to load cells with Cl^- by repetitive GABA_A activation prior to the optogenetic activation. Firstly, a single GABA event was recorded at the start of the experiment as a baseline (figure 5.14, black). Secondly, 10 muscimol puffs (1 Hz, 10 s) were delivered followed by a single puff as the GABA test, following repeated GABA_A activation, with a 4s delay, to measure how intense GABA_A activation alters the E_{GABA} of the cell (figure 5.14, purple). Lastly, the same paradigm was then repeated with 2 s optogenetic activation during the 4s delay just before the GABA test (figure 5.14, turquoise). Illumination of ChloC and ArchT induced hyperpolarizing current with a mean amplitude of 385.59 ± 90.57 pA (mean \pm sem, n=7).

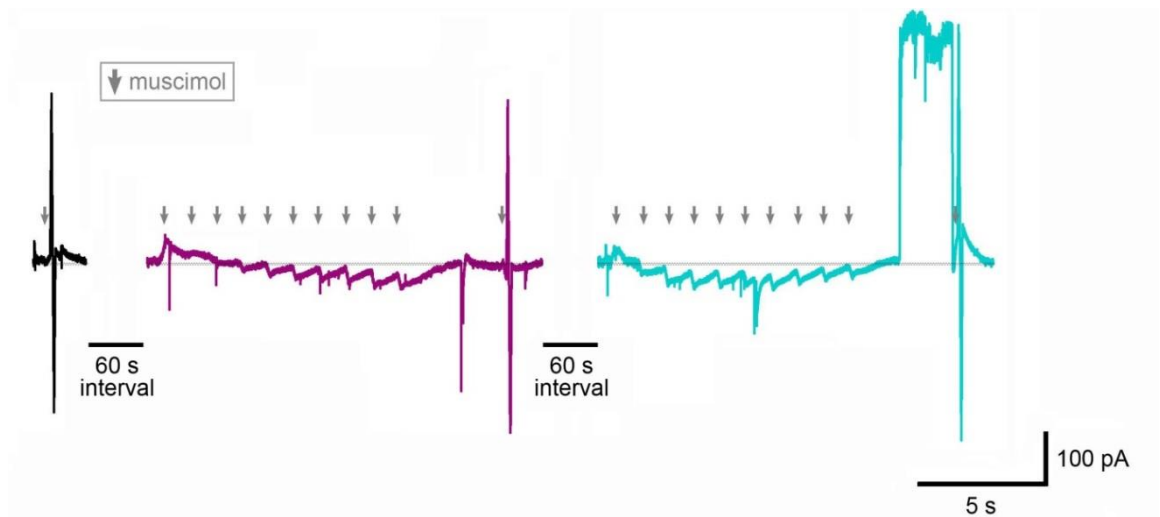


Figure 5.15 Protocol to assess the Cl⁻ clearance effect of ChloC-ArchT Cl⁻ when cells were Cl⁻ loaded prior to the optogenetic activation. Baseline E_{GABA} was recorded (black), followed by multiple muscimol puffs to load cell with Cl⁻ and a GABA test (purple), the same protocol was then repeated but with 2s light activation just before the GABA test (turquoise).

In the majority of the cells (71%: 5 out of 7 cells), single activation of GABA_A by muscimol triggered an IPSC shown as an upward deflection in a V_{Clamp} recording with a V_{Hold} of -70 mV (figure 5.15A, black). In these cells, intense activation of GABA_A by a train of muscimol puffs induced a positive shift in E_{GABA} ; as shown during the GABA test, muscimol puff triggered a reversed polarity of the initially hyperpolarizing event into a depolarizing one (figure 5.15, purple) with a mean shift of 7.1 ± 1.69 mV (mean \pm sem, n=5). This indicates that there was a $[Cl^-]_i$ accumulation through the intense GABA_A activation.

In contrast, single GABA_A activation triggered an EPSC in the remaining 2 cells (29%) that was a downward deflected event on a V_{Hold} of -70 mV recording (figure 5.15B, black). In this situation, the repetitive GABA_A activation actually induced a hyperpolarizing shift in E_{GABA} with a mean shift of -6.35 ± 6.2 mV (mean \pm sem, n=2). This was shown by a marked reduction of the muscimol-triggered EPSC amplitude (figure 5.15B, purple).

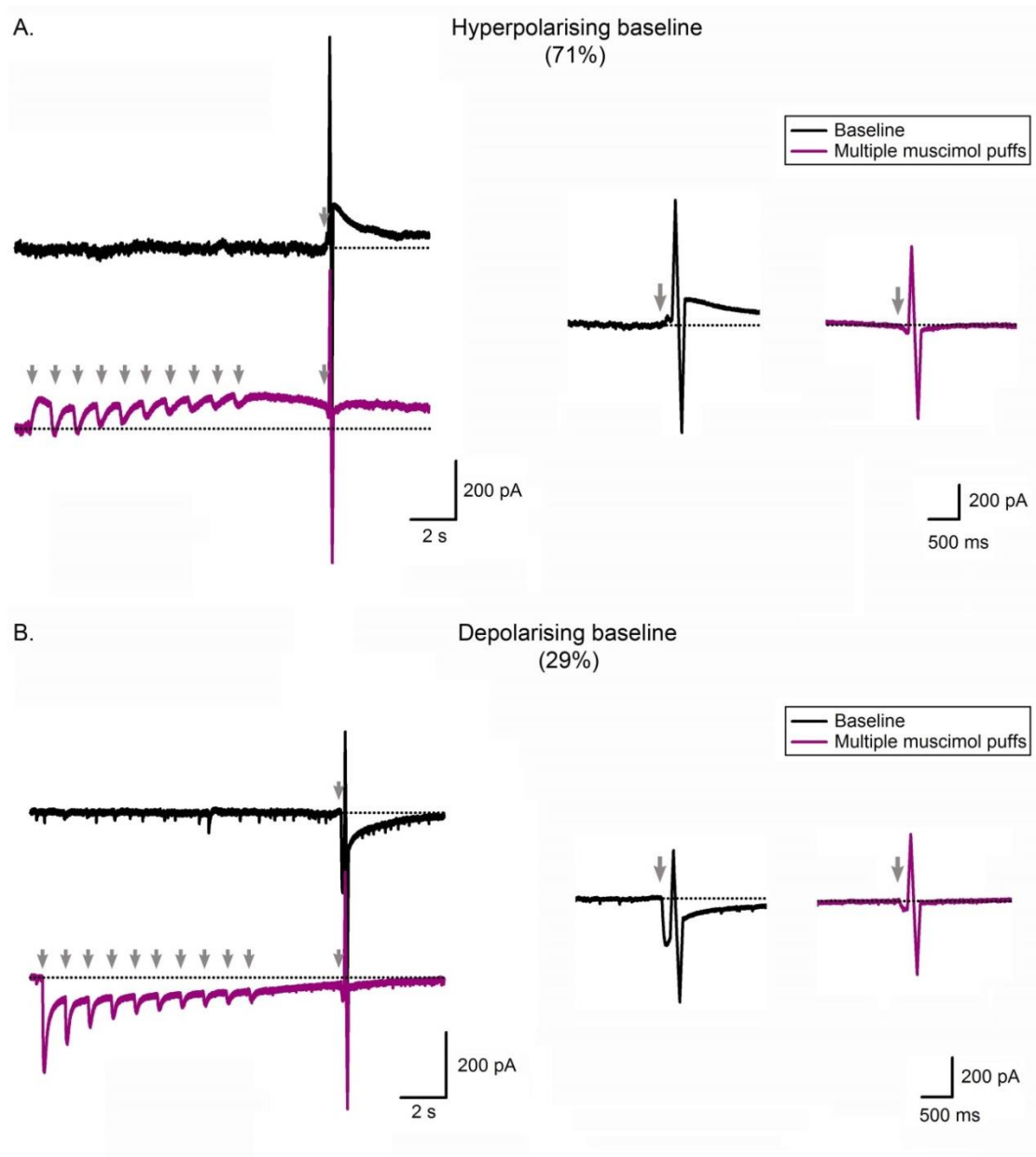


Figure 5.16 Hyperpolarizing and depolarizing initial E_{GABA} gave a different effect on the successive E_{GABA} during repetitive activation of $GABA_A$ receptor. A. Example traces from a cell that showed a hyperpolarizing GABA baseline. When initial GABA event was hyperpolarizing (black trace), trains of muscimol puffs caused a depolarizing shift in the E_{GABA} shown by the reversed of the GABA test event from upward to downward deflection (purple trace, right). B. Representative traces from a cell that showed a depolarizing GABA baseline (black trace). In this situation, repetitive $GABA_A$ activation actually had the opposite effect that was inducing a hyperpolarizing shift in the E_{GABA} as shown by a marked reduction in the amplitude of the depolarizing GABA event (purple trace, right).

A brief optogenetic activation of cells expressing ChloC-tDimer and ArchT-GFP consistently induced a positive shift in the E_{GABA} on the GABA test (figure 5.17, 5.18A-B), regardless of the initial baseline GABA event and the consequently different effect of repetitive GABA_A activation on the successive GABA event. This suggests that in all recorded cells, $[\text{Cl}^-]_i$ was lowered post light activation. Figure 5.17 shows a representative trace in which 2 s activation of ArchT-ChloC rescued the depolarizing shift in E_{GABA} introduced by intense GABA_A activation back to become hyperpolarizing again and often to an even more hyperpolarized level than the baseline E_{GABA} .

The pooled data shown in figure 5.18 demonstrated how ArchT-ChloC co-activation reliably shifted E_{GABA} to a more hyperpolarizing level, indicating a consistent Cl^- clearing effect induced by light activation ($p < 0.0002$, $n = 6$, paired t-test). This was the case for both when initial GABA was depolarizing or hyperpolarizing. In this experimental paradigm, where the cells were primed with repetitive GABA_A activation beforehand to raise $[\text{Cl}^-]_i$, a bigger hyperpolarizing shift was achieved (mean \pm sem: -9.34 ± 1.05 mV, $n = 6$; figure 5.18C, black) compared to the hyperpolarizing shift introduced by light without prior train of muscimol puffs (mean \pm sem : -2.67 ± 0.48 mV, $n = 5$; figure 5.18C, grey). Note however that experiments with a prior train of muscimol puffs were done on ChloC-ArchT expressing cells whereas the one without was conducted on slowChloC-ArchT expressing cells. This suggests that ArchT-ChloC co-activations is capable of extruding more Cl^- when there is more Cl^- inside. Nevertheless even with a low baseline $[\text{Cl}^-]_i$, the combination of ArchT and ChloC activity is still capable of driving Cl^- out.

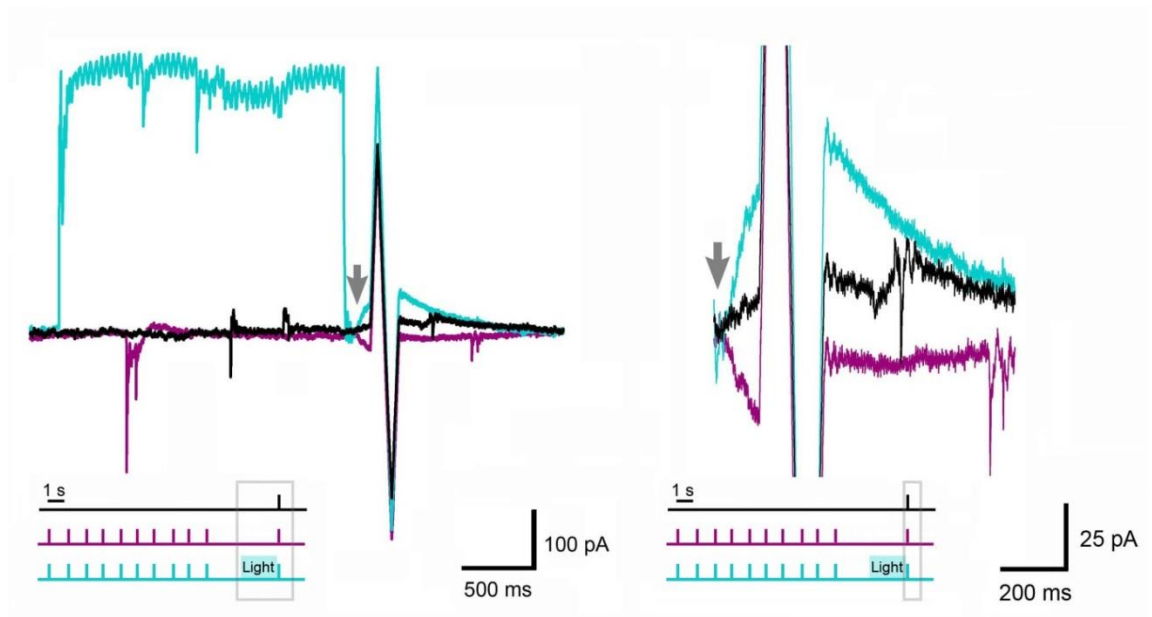


Figure 5.17 Co-activation of ChloC and ArchT rescued the E_{GABA} to a more hyperpolarised level post repetitive GABA activation. In this cell, repetitive GABA_A activation accumulated Cl⁻ intracellularly shown by a more depolarised E_{GABA} that appeared as a downward deflection during the GABA test instead of upward deflection like the initial GABA (purple vs black). This was readily rescued by short light activation that reversed back the polarity of GABA shown by the upward deflection of the last GABA test.

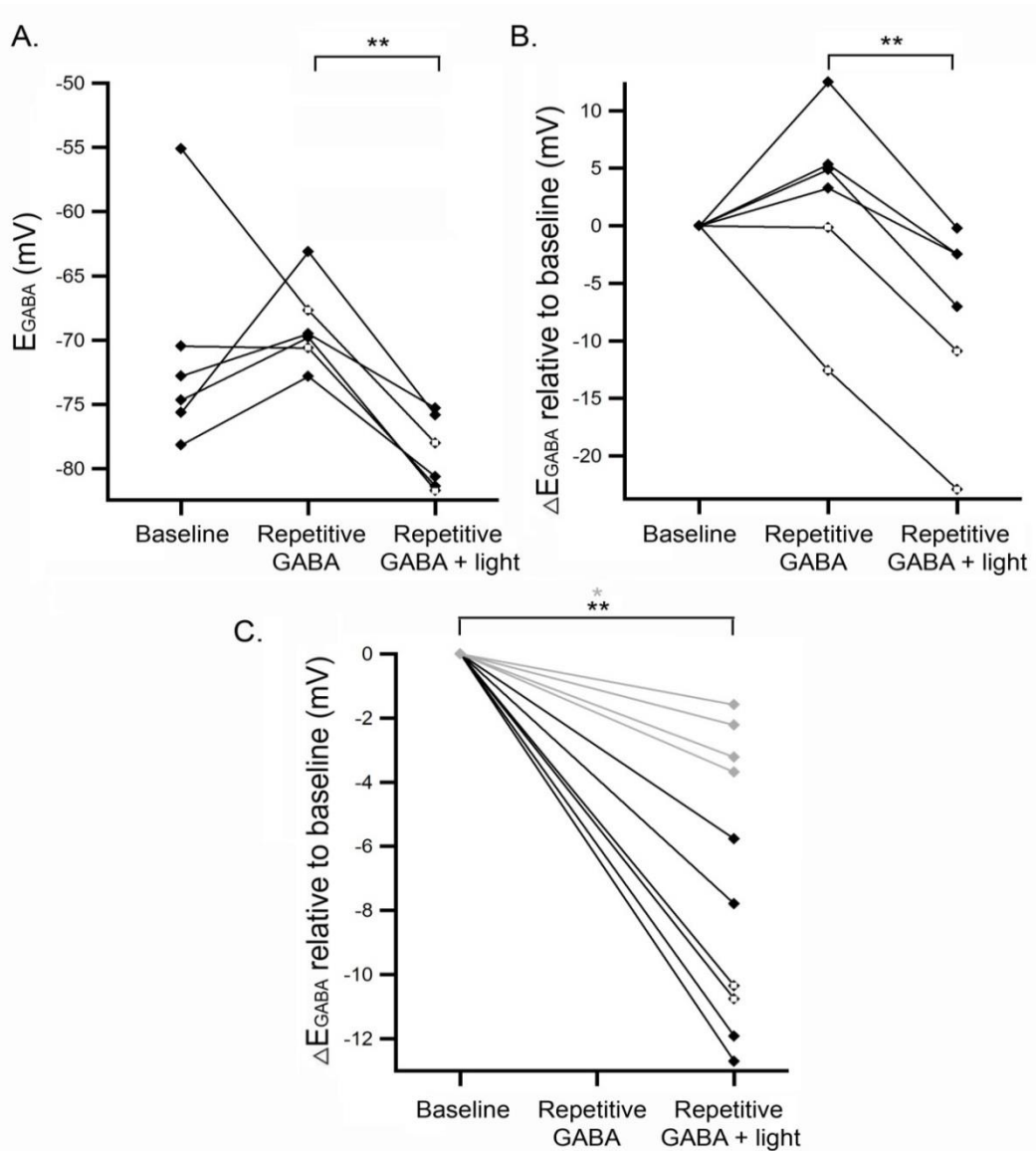


Figure 5.18 E_{GABA} measurements for baseline, post repetitive GABA activation, and with optogenetic activation of ArchT and ChloC. A. E_{GABA} measurement for baseline GABA event, post repetitive $GABA_A$ activation by train of muscimol puffs without and with ArchT-ChloC activation (**: $p < 0.0002$, paired t-test, $n = 6$). B. E_{GABA} relative to the baseline (**: $p < 0.0002$, paired t-test, $n = 6$). C. E_{GABA} relative to the baseline, this was without prior train of muscimol puffs for grey dots and with for the black dots. (grey: single activation of $GABA_A$ – results from figure 5.8 (*: $p < 0.02$, paired t-test, $n = 4$), black: hyperpolarizing baseline - multiple activation of $GABA_A$, black-white: depolarizing baseline - multiple activation of $GABA_A$).

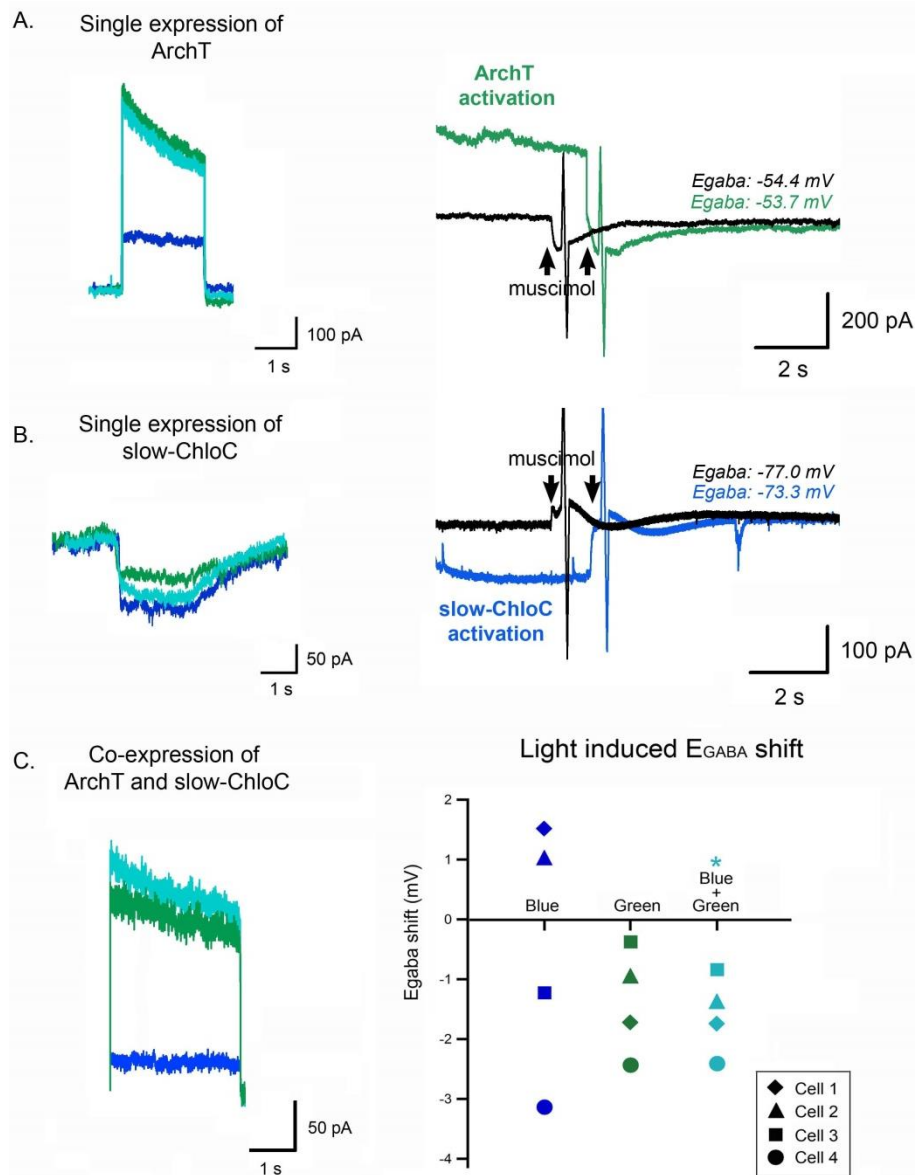


Figure 5.19 Activation of ArchT or ChloC alone does not induce a negative shift in E_{GABA} in a mature neuron. A. Single expression of ArchT showed different amplitude of light-activated current with 461 nm, 591 nm, and combined (left). ArchT was optimally activated by 591 nm light and this did not cause a negative shift in E_{GABA} (right). B. Single expression of slow-ChloC showed different amplitude of light-activated current with 461 nm, 591 nm, and both wavelengths combined, that peaked when activated by 461 nm (left). In this cell, light activation induced a small positive shift in E_{GABA} indicative of a Cl^- loading effect (right). C. Co-expression of ArchT and ChloC: when co-expressed on the same cell either 461 nm, 591 nm or combined always gave rise to a hyperpolarizing current (left). Only green or combined green-blue light (*: $p < 0.02$, paired t-test, $n=4$) consistently induced a negative shift in E_{GABA} . Together it suggests that any negative shift in E_{GABA} is the consequence of co-activation of both opsins rather than the individual opsin.

When a perforated gramicidin patch clamp was performed on cells that expressed only ArchT, a large amplitude hyperpolarizing current was recorded during illumination but this did not negatively modulate the E_{GABA} post light activation (figure 5.18A, n=1). This indicated that ArchT alone did not cause a Cl^- extrusion effect on the neuron.

On cells that expressed only slow-ChloC, illumination triggered a depolarising current although GABA events on these cells were hyperpolarising. However slow-ChloC activation by blue light illumination in these cells induced a depolarising shift in the E_{GABA} indicative of a small Cl^- loading effect by slow-ChloC (figure 5.18B, n=2). Although this is only a result from a low number of samples, this suggests the individual opsin activity is not enough to induce a hyperpolarising shift in E_{GABA} or a Cl^- clearing effect on the cell.

An extra experiment was done comparing the ArchT and slow-ChloC light current using different wavelength of light using cells that expressed only ArchT or only slow-ChloC. Both ArchT and ChloC variants showed light current with both 461 nm (blue) and 591 nm (green) light. ArchT was more optimally activated by 591 nm, with only 29% from its maximum current was generated when illuminated by 461 nm and 88% was generated using combined 591 nm and 461 nm (n=3). Slow-ChloC on the other hand showed a bigger current with 461 nm (figure 5.18A&B), while 591 nm only produces 17%, and the combination 461 nm and 591 nm produces 62% of the current generated by 461 nm light (n =3).

From cells that co-expressed both opsins, both 461 nm and 591 nm, or combined illumination always gave rise to a hyperpolarising current (figure 5.18C, left). However, only green or combination of green and blue appeared to consistently provide a Cl^- extrusion effect on the cell, with combination of blue and green giving a statistically significant shift and marginally bigger shift (mean \pm sem: -1.59 ± 0.33 mV; s: $p < 0.02$, paired t-test, n =4) compared to green (mean \pm sem: -1.37 ± 0.45 mV; ns: $p < 0.06$, paired t-test, n=4) whereas blue light gave a variable effect on the direction of the Cl^- flow (mean shift \pm sem: -0.45 ± 1.07 mV; ns: $p < 0.8$, paired t-test, n=4 (figure 5.18C).

Co-expression of ArchT and ChloC using the 2A system

Since the Cl^- clearance effect required both opsins within a single cell, I next considered strategies to ensure co-expression of ChloC and ArchT. The use of 2 plasmids transfection as done in previous experiments does not guarantee 100% co-expression level in all transfected cells, with some cells expressed only ArchT or ChloC. Since Cl^- clearance effect rely on the activation of both proteins, a strategy to reliably co-express both proteins in the same cells is absolutely needed for the network level experiments.

The T2A peptide was used for this purpose by building a ChloC-T2A-ArchT_GFP construct. In principle, this should allow an expression of the multiple proteins under a single promoter but produce ChloC and the fused ArchT_GFP as two separate proteins. The construct was electroporated into dissociated neuronal cultures; all cells were used for experiments at least 2 weeks post-transfection.

Fluorescence imaging of the cells showed GFP expression across soma and processes (figure 5.19A). Blue and green illumination gave rise to hyperpolarizing current with relatively smaller amplitude compared to the dual plasmid transfection (mean \pm sem, T2A expression: 57.74 ± 9.99 pA, n=5; dual plasmid: 385.59 ± 90.57 pA, n=7; significant, $p < 0.02$). Nevertheless, co-activation of ChloC and ArchT of these cells also showed a hyperpolarizing shift in E_{GABA} suggesting the successful co-expression of the two proteins (figure 5.19 & 5.20). Pooled data from 5 different cells showed a consistent trend of a negative shift in E_{GABA} post light activation for ChloC and ArchT with a mean shift of -6.38 ± 1.99 mV (mean \pm sem, n=5; *: $p < 0.04$ paired t-test; figure 5.20). This confirms that the T2A technique could be used to co-express ChloC and ArchT under a single promoter and was therefore potentially useful for further application of ChloC-ArchT as a tool to extrude Cl^- in network level.

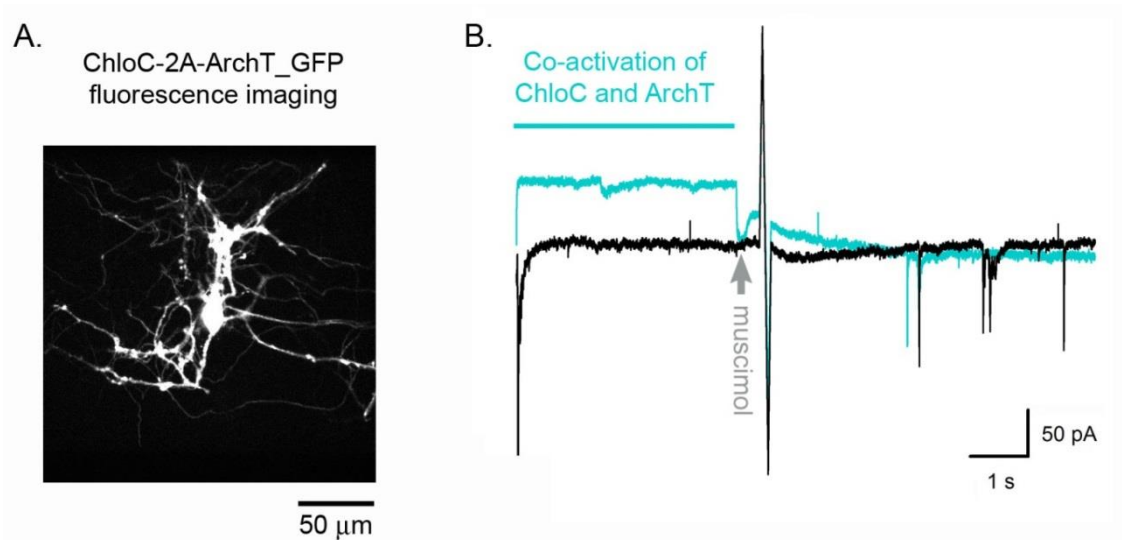


Figure 5.20 Co-expression of ChloC and ArchT using 2A peptide technique. A. Fluorescence imaging for GFP of ChloC-2A-ArchT_GFP expression of 1 example transfected neuron. B. Illumination using green and blue light modulated muscimol event to be more hyperpolarising indicative of a Cl^- extrusion effect.

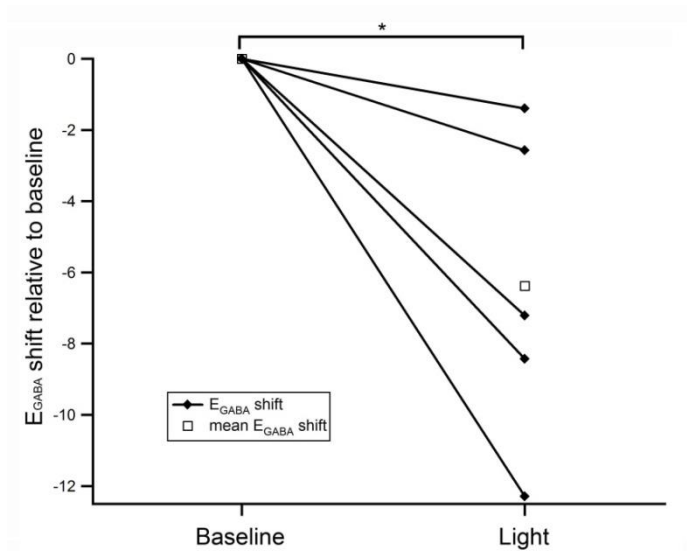


Figure 5.21 Pooled data of E_{GABA} shift by light activation from cells transfected with ChloC-2A-ArchT_GFP. E_{GABA} post light activation for ChloC and ArchT was subtracted by its corresponding baseline E_{GABA} that gave a mean E_{GABA} shift of -6.38 ± 1.99 mV (mean \pm sem, $n=5$; *: $p < 0.04$ paired t-test).

Current clamp recording of ChloC-ArchT Cl⁻ extrusion effect

GABA event modulation by ChloC-ArchT co-activation was also assessed in current clamp mode. ChloC and ArchT were co-expressed on dissociated neuronal cultures using the T2A peptide and gramicidin perforated patch was performed. Recording was made in current clamp mode with a holding current (I_{Hold}) ranging between 0 to -500 pA, aiming for a depolarizing GABA response (upward deflection, figure 5.21A black trace). Muscimol was applied with an interval of 1 minute, with or without prior 5.8 s light activation interchanged. In this mode, light activation shifted the membrane potential by -6.46 ± 1.63 mV (mean \pm sem, n=6), confirming the hyperpolarizing effect of light activation on the E_m .

Two measures were made to assess the GABA event modulation: amplitude of E_m shift elicited by muscimol puff and the E_m at the peak of GABA event. Light activation consistently changed the amplitude of the E_m shift induced by muscimol puff to a more negative value (mean \pm sem: -5.06 ± 1.31 mV, * $p < 0.01$, n=6, paired t-test; figure 5.21&5.22A-B), indicative of a more hyperpolarizing GABA event. This measure however is also affected by the E_m that tends to get more depolarized post hyperpolarizing event by ChloC-ArchT co-activation due to a rebound effect (figure 5.21B).

Additionally, E_m achieved at the peak of muscimol event was also documented. This could give an indication to what potential GABA tends to clamp the cell. This measure however is affected by both E_{GABA} and also the relative conductance for other ions such as Na^+ and K^+ . Light activation gave a mean negative shift of -2.19 ± 0.97 mV at the E_m value reached during the peak of muscimol event; however this was not statistically significant (n=5; ns, $p > 0.05$, paired t-test; figure 5.22C).

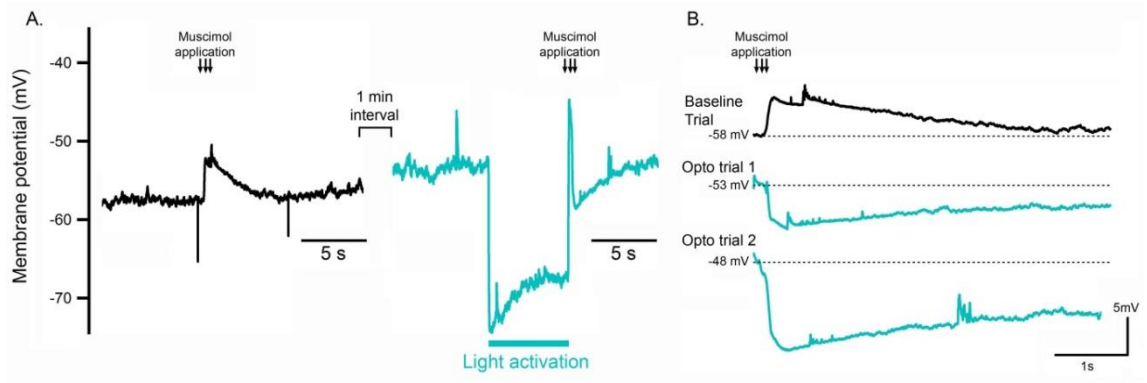


Figure 5.22 Current clamp recording of ChloC-ArchT co-activation effect on GABA activity using the T2A co-expression system. Example traces recorded from a single neuron co-expressing ChloC and ArchT using T2A peptide. A. Gramicidin perforated patch was performed and recording was made on current clamp mode with a current holding of -30 pA. Muscimol was applied with 1 minute interval. Left: The baseline GABA event without any light activation (black trace). Right: GABA event after illumination for ChloC-ArchT co-activation (turquoise). B. Isolated muscimol events without (black) and with prior ChloC-ArchT co-activation (turquoise) showed a change in polarity of the event from depolarizing (black) to hyperpolarizing (turquoise). Note the more depolarized initial E_m prior to muscimol puff for the optogenetic trials.

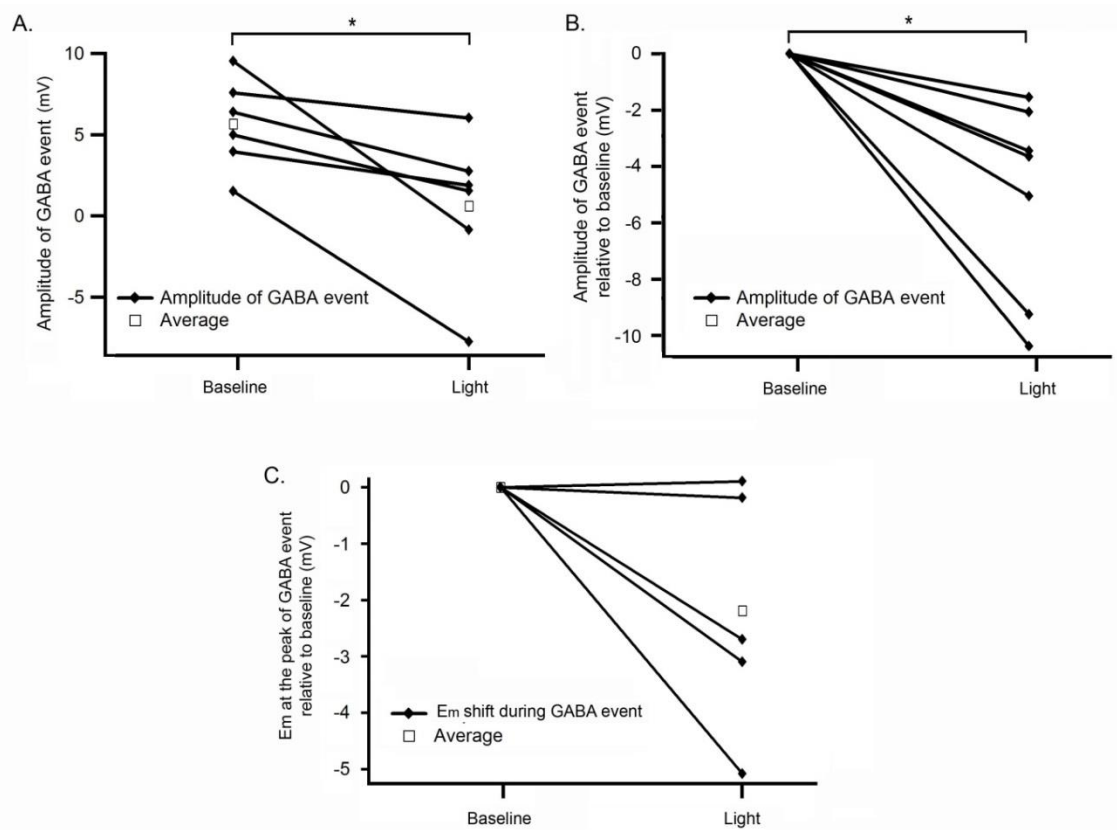


Figure 5.23 Pooled data of current clamp recording showing GABA modulation by ChloC-ArchT co-activation expressed using T2A peptide system. A. Amplitude of GABA event without and with prior ChloC-ArchT activation. B. Amplitude of GABA event post light activation relative to baseline. Light activation consistently showed a negative shift in GABA event amplitude with a mean shift of -5.06 ± 1.31 mV (mean \pm sem, $*p < 0.01$, $n = 6$, paired t-test). This measurement however might be affected by E_m as well. C. E_m at the peak of GABA event triggered by muscimol puff with and without prior ChloC-ArchT activation relative to baseline. There was a slight negative shift trend with a mean of -2.19 ± 0.97 mV (mean \pm sem, $n = 5$; ns, $p > 0.05$, paired t-test), however this is not statistically significant. Note that this is not the accurate E_{GABA} measurement.

5.3. Discussion

5.3.1. Attempts to reverse the orientation of HR

We tried two different strategies to reverse HR orientation in the membrane that could potentially reverse the direction of the Cl⁻ pump: charged residues mutation and protein anchoring. Unfortunately neither strategy managed to reverse HR, with evidence of expression problems for most of the modified proteins. Immunofluorescence staining show aggregates in the cytoplasm suggestive of the protein being retained in the endoplasmic reticulum, leading to a conclusion that the protein failed to be targeted to the membrane (figure 5.5-5.7). This could be due to a lack of ER export signal hence retention of the protein in the ER as originally shown by the wild-type HR (Gradinaru *et al.*, 2008) or due to misfolding of the protein.

Indeed in all these constructs (mutHR-EYFP, mutHR-IRES-EYFP, lepA-GFP-HR, CD8-GFP-HR, CD8-HR-IRES-EYFP), the ER export signal that was introduced by Gradinaru *et al.* (2008) to improve the original HR expression was not included. In our hands, this ER export signal resulted in an improved wild-type HR current with a mean of 163.89 ± 108.94 pA, n=14 compared to the original wild-type HR construct that only gave a mean current of 13.79 ± 4.73 pA, n=6 (chapter 3). This ER export signal (FCYENEV) is originally found in the C-terminal end of an inward-rectifier potassium channel 2.1 (Kir 2.1). Omission of this signal by site directed mutagenesis leads to intracellular protein aggregation of Kir2.1 expression (Gradinaru *et al.*, 2008).

This ER export signal was not incorporated in our construct due to the uncertainty of how this signal actually works, making it difficult to know where exactly to place this within the construct that was designed to have a reversed orientation. This is especially the case because a reversal will swap the position of the originally N_{out}-C_{in} HR into N_{in}-C_{out} HR (figure 5.1&5.2) that also will change the position of the c-terminally located ER export signal. However, even without this signal, wild-type HR still consistently gave a light activated current of about 13.79 ± 4.73 pA. This suggests

that the aggregates of our constructs and the absence of light activated current are likely due to misfolding of the protein rather than a mere lack of ER export signal. However, this is not definitive and could be clarified in the future by adding the ER export signal into the construct in either the C-terminal or N-terminal and assess the quality of the expression and the light activated current.

Finally, reversal of HR Cl⁻ flow without reversing the HR orientation could be another option to explore in the future. As changing orientation of a membrane protein that affects the whole protein might lead to misfolding, another strategy would be by targeting the Cl⁻ pump machinery component of the protein only.

5.3.2. Light activated Cl⁻ channel as a tool to extrude Cl⁻

ChloC variants were selected based on the fact that light activated current was more reliably induced compared to iC1C2. Furthermore the size of iC1C2 current was rather small compared to slow-ChloC. This could be due to the fact that there are more mutations introduced for the construction of iC1C2 (9 nucleotides substitution) that might affect the expression level of the protein on the membrane compared to ChloC and slow-ChloC that only have 2-3 mutations respectively. Additionally, in both ChloC variants the T159C mutation was introduced specifically to optimize the current as it has been shown before that it improves the membrane targeting and retinal binding in the chromophore pocket that might underlie its larger current size (Wietek *et al.*, 2014). However, recently a new version of iC1C2 with an enhanced current named iC1C2 3.0 has been generated, this could be another candidate to be used for this purpose in the future.

In this chapter, some recordings used ChloC while others used slow-ChloC. ChloC is a ChR2 variant that has two point mutations: at E90R, which is believed to affect the ion selectivity of ChR2, and at T159C for membrane targeting improvement. Slow-ChloC was then generated by adding an extra point mutation at D156N that confers the slow kinetic property to the channel (Wietek *et al.*, 2014). The main difference between the two proteins is the kinetic of the channel; ChloC closes almost instantaneously whereas slow-ChloC current outlast the light with a time constant of 10.5s (Wietek *et al.*, 2014). Additionally there is a slight difference in the reversal potential between ChloC and slow-ChloC, -61.8 mV and -68.2 mV respectively. Finally slow-ChloC also

shows a higher light sensitivity and a slightly bigger current compared to ChloC (Wietek *et al.*, 2014). As there are differences between the two, ideally the same experiment should be done with both ChloC and slow-ChloC to compare if one is more suitable for Cl⁻ clearance purpose than other, but due to limitations of time this has not been done.

Wietek J et al (2014) has conducted ion replacement studies to show that the reversal potential for ChloC variants are mainly affected by the concentration of Cl⁻ inside and outside the cell more than other ions such as Na⁺, K⁺, H⁺, or Ca²⁺. However, my results from gramicidin patch recording of cell expressing only slow-ChloC, showed that when GABA was generating IPSCs (inward Cl⁻ flow) with an E_{GABA} of -68.39 mV, slow-ChloC current was actually depolarizing with an E_{slow-ChloC} of -48 mV when measured by introducing voltage ramps during the activation of slow-ChloC by light. However, slow-ChloC activation was still inducing a depolarising shift in E_{GABA} (figure 5.18B), indicating that in regard to Cl⁻, slow-ChloC indeed had the same effect as GABA that in this cell was driving an inwardly directed Cl⁻ flow during activation. This suggests that although ChloC variant reversal potential could also be affected by other ions, evidently it is still conducting a significant flow of Cl⁻.

Both ArchT and ChloC variants have quite broad activation spectra (400 – 650 nm for ArchT and 350 – 500 nm for ChR2 family including the ChloC variants) (Nagel *et al.*, 2003; Han *et al.*, 2011). Testing different wavelength for the opsins activation could give insightful information in choosing the best illumination strategy, especially because for the Cl⁻ clearance purposes the right combination of two opsins current is needed. Experiments done on cells that express both opsins reveal that with both 491 nm and 561 nm or combined, light activation always produce a hyperpolarising current albeit with different amplitude, regardless of the V_{Hold} (figure 5.18C). Basically this could be explained by the heavily overlapping activation curve of the two opsins and the masking effect of large ArchT current (can be up to 1000 pA) that overwhelms the current generated by ChloC variants (maximum current recorded -81 pA). From this experiment, it becomes clear that when co-expressing ArchT and ChloC variants, it may not be possible to activate each opsin independently, at least when using 491 nm or 561 nm light. Hence any future experiment that intends to use ArchT-ChloC variants co-activation should have a single expression of each opsin as control since different wavelength of light is not enough to separate out the activity of the 2 opsins.

First characterisation of Cl⁻ extrusion effect of combined ArchT and ChloC variant activity was done using slow-ChloC. The mean negative shift in E_{GABA} induced was relatively small (-2.67 ± 0.47 mV) and unlike HR Cl⁻ loading effect, this did not change significantly with longer illumination. The small shift could be explained by the fact that the slow-ChloC current outlasts the light for over 10s whereas the ArchT current stops instantaneously. This residual slow-ChloC current post light activation might have a reversed effect on the E_{GABA} due to the lack of the hyperpolarizing ArchT current effect on the E_m . Note that there was 100 ms delay between light illumination and muscimol puff in which Cl⁻ might go in an outward direction without ArchT activation. A precise temporal matching of the currents is likely to be desirable.

The illumination strategy for optogenetic co-activation of ArchT and ChloC variants affects the Cl⁻ clearance effect of the two opsins. Blue light (491 nm) activation of ArchT-slow-ChloC that consistently gave a net hyperpolarizing current of 103.5 ± 27.69 pA (mean \pm sem, n= 5) did not give a consistent direction of E_{GABA} shift: 2 out of 4 cells gave an outward Cl⁻ flow (negative E_{GABA} shift) and the other 2 gave an inward Cl⁻ flow (positive E_{GABA} shift). This suggests that this amplitude of hyperpolarising current is not always enough to shift the E_m to be more negative than the E_{GABA} . Whereas, green (561 nm) or combined green and blue illumination gave a mean hyperpolarising current of 441.38 ± 87.41 pA and 442.79 ± 92.84 pA respectively, and reliably induced a negative shift in E_{GABA} . This further supports the essential need of an ArchT hyperpolarizing effect on the E_m to allow the ChloC variants to exert a Cl⁻ clearance effect on the cell rather than a Cl⁻ loading effect. It should be noted however that these experiments were done in a voltage clamp mode and so the E_m modulation was not perfect.

More control experiments with single expression of ArchT and ChloC variant in E_{GABA} modulation are needed. However, it has been shown before by Raimondo et al (2012) that Arch (which has the same properties as ArchT, except for its light sensitivity) activation does not significantly modulate E_{GABA} . In principle, this should be the same with ArchT effect on E_{GABA} . Additionally, unlike the consistent effect of green-blue light (that gave large ArchT current) on E_{GABA} , blue light activation of the ArchT-slow-ChloC that only showed a small ArchT current, did not give a consistent negative shift in E_{GABA} . This further supports the requirement of both ArchT and ChloC to produce a more consistent outward Cl⁻ flow.

To see whether the ArchT-ChloC variant could impose a bigger negative shift when cells have extra $[Cl^-]_i$ to begin with, I primed the cells by repetitive activation of GABA_A channel by trains of muscimol puffs. This has been shown to have a depolarising effect in the E_{GABA} (Thompson & Gahwiler, 1989a). Indeed, in this situation co-activation of ArchT-ChloC drove more Cl^- out, shown as a bigger mean of negative shift in E_{GABA} (-9.34 ± 1.05 mV) compared to on cells that have not been primed beforehand (mean shift of -2.67 ± 0.47 mV when it was done using ArchT-slow-ChloC). This confirms that ChloC variants are capable of extruding more Cl^- when there is higher Cl^- inside the cell.

Finally, I have shown that we could co-express ChloC and ArchT using the T2A peptide that allows expression of multiple proteins under a single promoter. This technique required a longer expression to achieve a comparable optogenetic current compared to the conventional dual plasmids transfection. The need for longer expression time of the 2A peptide system has been documented before (Tang *et al.*, 2009). However, even when patched 3 - 4 weeks post electroporation, the amplitude of the hyperpolarizing current by the T2A construct was still smaller (mean \pm sem: 57.74 ± 9.99 pA, n=5) than the dual plasmid electroporation of (mean \pm sem: 385.59 ± 90.57 pA, n=7).

This could be explained by the issue of an unbalanced expression level of the different proteins when using 2A peptide. Relatively lower expression of the protein downstream of the 2A peptide has been reported before. Two reasons could underlie the smaller hyperpolarizing current recorded from the ChloC-2A-ArchT_GFP. Firstly, it is due to a lower ArchT level of expression and consequently smaller hyperpolarizing current of ArchT. Secondly, the higher level of ChloC will give a bigger depolarizing current, at least when co-activated together with ArchT, hence counteracting the hyperpolarizing current of ArchT. The second explanation is more likely to underlie the smaller hyperpolarizing current, because when using blue light on the 2 plasmids transfection method, the elicited 103.5 ± 27.69 pA hyperpolarizing current did not show a consistent Cl^- extrusion effect whereas the 2A peptide expression that only gave a hyperpolarizing current of 57.74 ± 9.99 pA seemed to consistently induce a negative shift in E_{GABA} (mean \pm sem: -6.38 ± 1.99 mV n=5; figure 5.18). This negative shift was even bigger than the slow-ChloC-ArchT co-activation by the 2 plasmid transfection method (mean \pm sem: -2.67 ± 0.47 mV n=5; figure 5.8).

To further optimize the co-expression of ChloC and ArchT, a fusion protein strategy should be considered in the future. This will eliminate the unbalanced expression issue as the 2 proteins will be produced as a single entity. Furthermore, this will allow a precise co-localization of the 2 proteins in the membrane in which every one ChloC will be associated with one ArchT side by side. This could potentially give a better Cl^- extrusion effect and furthermore allows a compartmental Cl^- extrusion in subcellular level for instance by spot illumination of only the dendritic spine or axon initial segment, etc. This will not be optimal with other non-stoichiometric co-expression system in which the 2 proteins might not be uniformly distributed across the cell membrane and hence the Cl^- extrusion effect is brought about collectively from the ChloC and ArchT proteins in the entire cell membrane.

Ernst Bamberg has tried to co-express excitatory and inhibitory optogenetic proteins in neurons before by protein fusion strategy. He successful did this by fusing the two proteins using a specific length of linker to assure both proteins are oriented properly and function well (Kleinlogel *et al.*, 2011b). Adopting this linker to combine the ChloC and ArchT for co-expression purpose (figure 5.19) is one possible strategy for co-localization with a strong point of a guaranteed 1:1 expression level of both proteins.

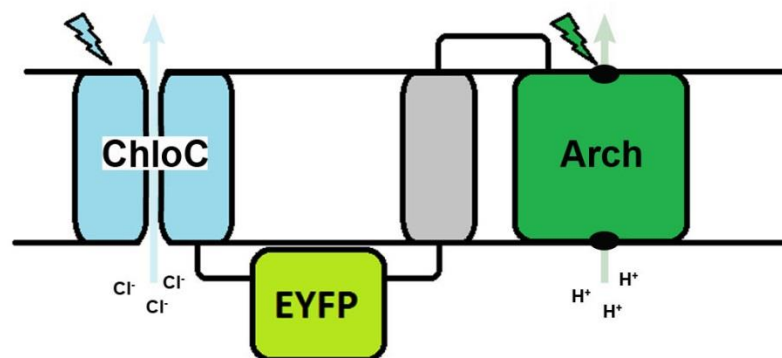


Figure 5.24 Co-expression of ChloC and Arch to extrude chloride. Arch (green) activation hyperpolarises the membrane potential that will provide a driving force for chloride to leave the cell when the ChloC (blue) is light-activated. The two optogenetic proteins are linked together by EYFP and an additional transmembrane helix from the β subunit of the rat gastric H^+, K^+ -ATPase (grey) for expression of a single fusion protein, adopted from (Kleinlogel *et al.*, 2011b).

Finally, I would like to address the issue of how voltage clamp mode recording might not allow strong E_m modulation as actually required to be imposed by ArchT for Cl^- extrusion purpose. This is due to the design of this recording mode that tries to clamp the cell E_m into the desired V_{Hold} by injecting positive and negative current. The fact that we could still measure a consistent negative shift in the E_{GABA} using this mode suggests that the quality of the voltage clamp was poor and hence E_m was still modified sufficiently by ArchT activation, to allow Cl^- extrusion via ChloC. This could happen when the contact between the patching electrode and the internal of the cell is very limited, which gives a relatively high series resistance (R_s). This is indeed the case when doing perforated gramicidin patch clamp recordings. In this situation, the injected current's effect on the voltage shift will shrink due to the high R_s ($V = I \times R$) and voltage clamp becomes less efficient.

Additionally, the efficiency of voltage clamp also diminishes with distance from where the patching electrode is. As optogenetic proteins were distributed widely throughout the cell soma and also the processes, it is likely that ArchT could still hyperpolarize the cell quite efficiently in the processes, with an increasing efficiency further away from the soma where patching electrode was placed. Furthermore, the large instantaneous hyperpolarizing current of ArchT could also overwhelm the V_{Clamp} system, allowing some E_m modulation. Nevertheless, it should be noted that voltage clamp mode could actually attenuate the ArchT effect in E_m modulation and this possibly explains the relatively small effect of slowChloC-ArchT co-activation effect in E_{GABA} .

Current clamp mode (I_{Clamp}) on the other hand is a more suitable option when E_m modulation is desired. I_{Clamp} experiments were then done to assess the Cl^- extrusion effect of ChloC-ArchT co-activation. First, the amplitude of GABA event was measured with and without prior ChloC-ArchT co-activation. A significant change in the amplitude could be observed post light activation with a mean negative shift of -5.06 ± 1.31 mV (mean \pm sem, $*p < 0.01$, $n=6$, paired t-test). This test however could be confounded by the fact that E_m tends to be slightly shifted to a more depolarized level post light activation, due to rebound effect post ArchT hyperpolarization. A second measure was then done by measuring the E_m at the peak of muscimol event. This should be less affected by the initial E_m . A slight negative shift trend post light

activation was shown with a mean of -2.19 ± 0.97 mV (mean \pm sem, n=5; ns, $p>0.05$, paired t-test), however this was not statistically significant.

Based on these two measures derived from the current clamp experiments, there was a suggestion that ChloC-ArchT indeed induced a hyperpolarizing shift in GABA activity. However, this is still not a definitive prove. For the first measure, an important question to ask is whether the depolarized E_m prior to muscimol puff could account for the negative shift in the GABA amplitude post light activation and more experiments are required to clarify this. As for the second measure, the main issue is, although I_{Clamp} is a better set up for ArchT hyperpolarizing effect on the E_m , it is not the best mode to measure the E_{Cl^-} as an indicator of $[Cl^-]_i$. GABA_A activation will bring the cell's E_m close to the E_{GABA} , however it might not always reach the E_{GABA} depending on the conductance for other ions and the leakiness of the cell. This factor was taken into account when E_{GABA} is measured on a V_{Clamp} using ramps. A better design of experiments to clarify this in the future would be to perform illumination for ChloC-ArchT co-activation under current clamp mode while measuring the E_{GABA} under voltage clamp mode.

5.3.3. Reverse HR strategy versus ArchT-ChloC co-activation strategy

The different nature between an electrogenic pump and a channel make HR and light activated Cl^- channel such as ChloC differ in their way of modulating $[Cl^-]_i$. The first one is that electrogenic pump activity is independent of the E_m whereas Cl^- channel driving force is set by E_m as well as E_{Cl^-} . This will give a benefit for the reversion of HR Cl^- flow strategy as a tool to extrude Cl^- , if successful. As HR is an electrogenic pump and not a channel, its activity is not regulated by the E_m . This means that its activity will be less dependent on any synaptic event such as glutamatergic that modulates E_m . In contrast, the ArchT-ChloC strategy will be more likely to be affected by glutamatergic events that shift E_m to be really positive. Note that if E_m is more positive than E_{Cl^-} , opening of any Cl^- channel including ChloC will lead to an inward Cl^- flow. Therefore, glutamatergic activity in principle will attenuate the ArchT-ChloC effect in Cl^- extrusion by setting a

higher starting E_m for ArchT hyperpolarization to shift to be more negative than E_{Cl^-} , creating a smaller driving force for Cl^- extrusion.

Both HR and ChloC activity are affected by Cl^- concentration. As shown by the low Cl^- ACSF experiment of wild-type HR current (figure 5.3), low Cl^- concentration outside does change the driving force of the pump by 70% however it does not completely abolish the current (HR mean current: 30.64 pA) when there is about 9.5 mM Cl^- outside compared to 131.5 mM Cl^- in normal ACSF (HR mean current: 97.95 pA). SlowChloC-ArchT Cl^- extrusion effect was well correlated with the E_{GABA} indicative of the higher initial $[Cl^-]_i$; the bigger the driving force for ChloC activity.

The added benefit of ChloC-ArchT co-activation strategy is that the clearing of chloride will not be associated with depolarisation as the membrane potential is kept hyperpolarised by ArchT. In addition, a chloride channel opening has a shunting effect on the cell shown by a drop in input resistance to almost 50% (Berndt *et al.*, 2014). Theoretically, this strategy will enhance inhibition by its hyperpolarising effect, shunting effect, and also correction of the high $[Cl^-]_i$. Whereas with HR reversion strategy, hypothetically the Cl^- extrusion will be associated with a depolarization. In summary, I suggest that the ChloC-ArchT co-activation approach is a better candidate for correcting Cl^- levels in epileptic tissue.

Chapter 6. General Discussion

6.1. Summary of experimental findings

The first aim of my thesis was to investigate the role of raised $[Cl^-]_i$, a feature of epileptic network that has been documented by many studies before, in the generation of certain epileptic activity. However it has proved difficult to separate this out from other contributing factors in a complex system phenomenon such as a seizure. To address this, I made a novel use of the hyperpolarising optogenetic protein HR (light activated Cl^- inward pump) to artificially load neurons with Cl^- . The ability of HR in modulating $[Cl^-]_i$ was characterised in chapter 3. There I have shown that brief HR activation (2 – 10s) readily induced positive shifts in E_{GABA} , and since GABA is mainly permeable to Cl^- , this strongly indicates that HR activation accumulates Cl^- into the cells. E_{GABA} then recovered back to its initial baseline with a time constant of 8.01 ± 2.85 s in acute brain slices, made from adult mice. This appears to be faster than in dissociated neuronal culture of more immature cells in which $[Cl^-]_i$ recovered with a time constant of 28.1 ± 9.26 s. The faster decay of HR Cl^- loading effect in acute brain slices could be explained by the different age of the cells that consequently affect the different level of KCC2 expression.

Based on this knowledge, in chapter 4 HR was used to load a subset of cells with Cl^- using a 25s ON/5s OFF illumination paradigm, while monitoring any modulation being imposed onto the network event triggered by electrical stimulation during the OFF period. The results from chapter 4 suggest that long repeats of HR Cl^- loading into pyramidal cells alone was not enough to trigger ictal activity even when applying electrical stimulations into the white matter to mimic a thalamic input. This however is sufficient to induce high frequency oscillation (HFO) with a characteristic doubling of frequencies, increased jitter in spike timing, and out-of-phase firing. This is consistent with certain features of HFOs that have been recorded from animal models of epilepsy, and which has been regarded as one of the hallmarks of epileptic foci.

Only when combined with low, sub-epileptic levels of 4-AP (20 μ M) did Cl^- loading rapidly trigger full ictal activity. This suggests that high $[\text{Cl}^-]_i$ has an adjunctive effect in seizure initiation, at least in vitro brain slices. In this situation, when longer Cl^- loading was maintained in the presence of 20 μ M of 4-AP, multiple ictal discharges were triggered and often a spreading-depression like event was triggered, which had a terminating effect on the ictal discharge. This is similar to what is described by Bragin et al (1997) termed afterdischarge terminating oscillation (ATO). This manifested as a depression state that silenced the network transiently. The ATO appeared to be initiated in the HR illumination foci suggesting that this event could be directly or indirectly influenced by Cl^- loading of the neurons.

Lastly, the second aim of my thesis was to design optogenetic tools to extrude Cl^- . This has potential use both as a research tool and clinically as a treatment option for epilepsy, if bioengineering technology advances to allow optogenetic activation for human use. In chapter 5, several different approaches were explored mainly trying to reverse the orientation of HR, and thereby reverse the Cl^- flow direction of this pump to be outwardly directed. A second approach was to couple the effect of hyperpolarizing ArchT current on the E_m and opening of a light activated Cl^- channel to provide both the driving force and the conductance for an outward Cl^- flow. The first approach was not successful, mainly due to membrane localization problem that could be caused by the lack of endoplasmic reticulum (ER) export signal in the cDNA of modified HR or a misfolding of the protein. The second approach on the other hand showed a positive effect as a Cl^- extrusion tool, based on the fact that brief co-activation of ArchT and ChloC consistently shifted E_{GABA} to a more hyperpolarizing level. This shift was well correlated with the baseline $[\text{Cl}^-]_i$, with bigger shift tends to be achieved by cells that had higher initial $[\text{Cl}^-]_i$.

6.2. HR chloride loading effect as a model of raised intraneuronal chloride

HR Cl⁻ loading effect was used as a model of raised intraneuronal chloride. As this could be a good model of Cl⁻ loading via intense GABA_A activation that is also associated with hyperpolarization, this may not be directly comparable to high [Cl⁻]_i induced by co-transporter dysregulation for several reasons.

First, Cl⁻ co-transporters such as NKCC1 and KCC2 are electroneutral (Kaila *et al.*, 2014) meaning that ion movements across the membrane via these co-transporters will not impose abrupt changes in the membrane potential. In contrast, HR Cl⁻ loading is always accompanied by an instantaneous membrane hyperpolarization and so it could impose some downstream consequences such as the activation of HCN channel that gives rise to the depolarising I_H current or the activation of CLC2 channel that gives an outward Cl⁻ flow post hyperpolarisation.

Second, co-transporter dysregulation not only affects a cell's initial [Cl⁻]_i, but moreover it affects the time course of Cl⁻ fluxes in a cell. For instance, when KCC2 was blocked using 100 μM furosemide, HR Cl⁻ loading gave a comparable E_{GABA} shift with control, however the time constant of the HR Cl⁻ loading effect was three times longer compared to baseline. This indicates that when KCC2 function is blocked, the cells' capability in restoring [Cl⁻]_i back to their preferred [Cl⁻]_i is compromised. In the HR Cl⁻ loading experiment, KCC2 was intact, at least initially, and so was the cells' ability in restoring their [Cl⁻]_i back to baseline. However, this process is slow as shown that E_{GABA} was recovering with a mean τ of 8.01 ± 2.85 s post HR priming in adult brain slices. Furthermore, it should be noted that when KCC2 is intact, intraneuronal Cl⁻ accumulation could promote excitability not only by depolarizing GABA, but also by raising K⁺ in the extracellular space (Viitanen *et al.*, 2010). This is because intraneuronal Cl⁻ accumulation increases the driving force for KCC2 activity, which will extrude Cl⁻ together with K⁺ to the extracellular space. Consequently, this could result in an extracellular accumulation of K⁺ that will shift the membrane potential into a more depolarizing level and hence increasing excitability of the cell.

Lastly, the effect of co-transporter dysregulation on $[Cl^-]_i$ is long lasting, while HR Cl^- loading is a transient effect that decays over time. Due to the transient nature of HR Cl^- loading, electrical stimulation was used to induce ripple like activity rather than the spontaneous ripple model that was used by Foffani G., et al (Foffani *et al.*, 2007a). Electrical stimulation was timed to be elicited 0.5s post HR activation to make sure that HR Cl^- loading effect was still close to its maximum. Although this is slightly artificial, the mechanism is still valid, as HFO induced by HR Cl^- loading and the electrical stimulation share the same characteristic as shown by Foffani et al, which will be elaborated in the next section. Furthermore, the effect was also well predicted by the computer model simulation.

6.3. The role of raised $[Cl^-]_i$ in generation of high frequency oscillation

Network events in high gamma range (>80 Hz) could be observed both in healthy and epileptic brains. However, in contrast to activity <250 Hz range that could be both physiological or pathological, network activity in 250-600 Hz range termed fast ripple, has been mainly regarded as epileptic (Alvarado-Rojas *et al.*, 2014). Fast ripples have been shown in patients with mesial temporal lobe epilepsy (Bragin *et al.*, 1999), in neocortical tissues resected from epileptic patients (Roopun *et al.*, 2010), and in animal model of epilepsy (Foffani *et al.*, 2007a). This HFO often precedes seizure onset (Jirsch *et al.*, 2006) and also has been associated with interictal activity in the EEG recording (Schevon *et al.*, 2009).

The results in chapter 4 revealed a direct cause and effect relationship between high $[Cl^-]_i$ and the modulation of high frequency activity (250-600 Hz). When neocortical tissues were challenged with HR Cl^- loading, modulation of the network activity could be observed especially in the high frequency oscillation range (250 -600 Hz). This frequency is roughly the doubling of the frequency of the dominant oscillation (figure 6.1B) as shown in baseline network activity (<250 Hz). This characteristic doubling of frequencies is consistent with the specific feature of epileptic HFO described by Foffani et al (2007) (figure 6.1A). The Cl^- induced high frequency modulation was rapid and reversible when Cl^- loading was terminated.

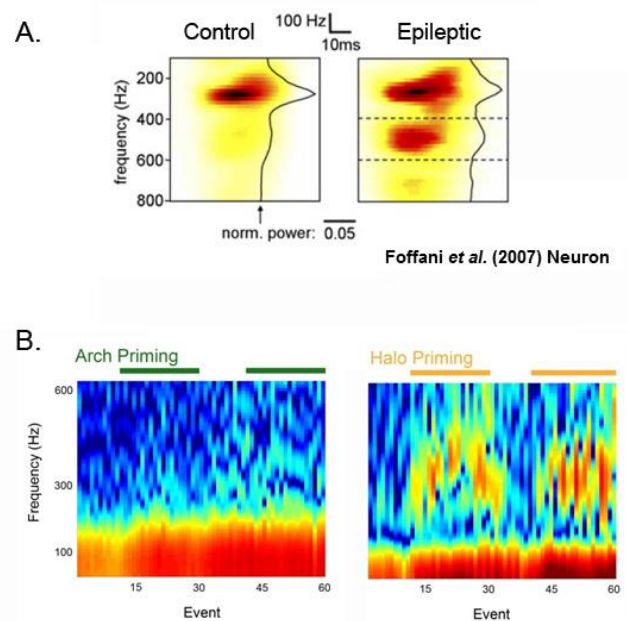


Figure 6.1 Striking resemblance between spontaneous epileptic HFO and HR priming tissue. A. Representative spectrogram showing HFO recorded from healthy animal (left) and epileptic one (right) shown by Foffani et al (Foffani *et al.*, 2007a). Epileptic HFO shows as a second harmonic event or doubling frequency of the baseline event. B. Only HR priming (right) but not ArchT priming (left) resulted in HFO events with a similar second harmonic characteristic that shown in HFO recorded from epileptic animal by Foffani et al.

Likewise, raised intraneuronal chloride too has also been linked to epileptogenic region. Supporting evidence mainly comes from epileptic tissue resected from patients with temporal lobe epilepsy, in which significant reduction of KCC2 expression was found in about 30% of the pyramidal cells (Huberfeld *et al.*, 2007c). They then found that most of the cells that lacked the expression of KCC2 showed a depolarizing event during interictal event whereas all cells that were hyperpolarized expressed KCC2. Similar findings were also found from human epileptic tissues surrounding human glioma and in peritumoral epileptic tissue in mice when injected with human gliomas (Pallud *et al.*, 2014; Campbell *et al.*, 2015).

My result then provides direct evidence that these two phenomena namely raised intraneuronal chloride and HFO, which are associated with epileptogenic area, are actually linked to each other. This result also links the Foffani et al study and Cohen et al study that described the underlying mechanism of epileptic HFO. Cohen et al reported that during HFOs associated with interictal discharges, underlying excitation comes from both glutamatergic activity and GABAergic activity (Cohen *et al.*, 2002). They further showed that during these events interneurons were highly active in a bursting mode, while pyramidal cells showed two different responses; either receiving a small excitation followed by larger hyperpolarisation, or were excited, resulting in their firing at the time of the event. Foffani et al on the other hand suggested that epileptic HFOs arise from a desynchronized mechanism rather than hypersynchrony, of populations of cells that fired out-of-phase of each other (Foffani *et al.*, 2007a). My results from chapter 4 give an explanation that the different populations that fire out-of-phase of each other are determined by their $[Cl^-]_i$, one population with an E_{GABA} below the threshold for action potential, and the other above. Since E_{GABA} dictates whether cells are inhibited or excited during GABA activation, cells with healthy E_{GABA} will only be excited by glutamatergic drive during the refractory period of inhibitory conductance, while cells with depolarizing E_{GABA} can also be excited by GABA during the peak of inhibitory conductance itself. When the mixture of both is present, out-of-phase firing of the 2 different groups results in the generation of HFO. This fits the observation by Cohen et al that during HFO bursts, interneurons fire almost at the same time with some pyramidal cells (pyramidal cells with depolarizing E_{GABA} that fires by GABAergic drive) while some other pyramidal cells were hyperpolarized during the burst preceded by small excitation (pyramidal cells with healthy E_{GABA} that fires by glutamatergic drive with a jitter from the interneuron's burst of action potential).

This mechanism completely relies on interneuronal activity especially fast-spiking interneurons, as explained by the computer model. However, epileptic activity has been recorded before when there is a local loss of inhibition or in a preparation without any synaptic function intact in which ephaptic or gap-junction mediated spread has been implicated (Traub & Bibbig, 2000). This suggests that other mechanisms could exist too.

Furthermore Cl^- loading experiments also showed evidence of increased jitter in spike timing (5 of 8 slices) and even out-of-phase firing (3 out of 8 slices) when spike-phase relationship was assessed according to the dominant oscillation. This also provide an explanation to the puzzling observation of increasing jitter of action potential timing during recruitment of cortical area into a seizure (Netoff & Schiff, 2002), that seemed to contradict the hypersynchrony nature of epilepsy. The computer model further explains how progressive Cl^- loading initially results in increasing jitter in spike timing that after a certain threshold will eventually induce out-of-phase firing. Cl^- loading that positively shifts E_{GABA} but not sufficiently to give an E_{GABA} beyond the threshold for action potential, will result in an increased jitter in spike timing, by broadening the window of opportunity for pyramidal cells to spike as inhibition becomes weaker. However as soon as the E_{GABA} reaches the threshold for action potential, a very high probability of cells to spike in the opposite phase from the baseline was observed, as suddenly GABA is triggering action potential, favouring a hyper-synchrony state.

The question still remains of whether tissues with HFO and raised $[\text{Cl}^-]_i$ are actually indicative of the initiator of seizure activity or rather a secondary local response of tissue to the actual trigger. Answering this is particularly important especially since HFO has been regarded as one of the hallmarks of epileptic foci in clinical setting. It has been documented before that there are two types of HFO which can be recorded from human epileptic patients implanted with multi electrode array (MEA): macrodischarges that are widespread, and microdischarges that instead are very local, affecting only a single electrode (Lee *et al.*, 2005; Schevon *et al.*, 2009). This suggests that it is possible that HFOs could be generated by the initiator (presumably the one with local microdischarge) but also as a secondary response of the tissue towards something else as macrodischarges seemed to be synchronized in wider areas and also 80% of the times are associated with interictal discharges.

Similarly for high $[Cl^-]_i$, evidence has shown that glutamatergic activity could readily trigger GABA release that will rapidly induce an increase of intracellular Cl^- via $GABA_A$ activation (Lee *et al.*, 2005). This suggests that high $[Cl^-]_i$ could be induced as a local response towards an excitatory drive. This initial transient high $[Cl^-]_i$, as a local response towards excitatory drive, could induce changes of co-transporter expression and function that could result in a more persistent high $[Cl^-]_i$ state. Supporting evidence comes from the in vitro low Mg^{2+} model in which after repetitive interictal discharges, reduction of KCC2 expression was observed and it appears to be mediated by calcium activated protease calpain (Puskarjov *et al.*, 2012). Therefore it is possible that later on, this tissue could become more prone to be the initiator, as shown by my results that high $[Cl^-]_i$ state lowered the threshold for 4-AP to induce seizure.

It should be noted that based on the results described in chapter 4, HFO could be associated with Cl^- dysregulation when it shows the characteristic doubling of frequencies. Potentially, this feature could be used as a hallmark for tissues associated with Cl^- dysregulation and might provide an insight whether Cl^- targeted treatment could be useful for certain patients or not. However, so far the observation of the doubling of frequencies feature of epileptic HFO has only been observed in animal model of epilepsy, in which recording was made using a high quality deep penetrating microelectrodes. Whether such a quality of recording could be made in the clinical setting or whether this feature could be captured by non-invasive tools suitable for patients remains to be seen.

Lastly, as $[Cl^-]_i$ clearly modulates activity in the gamma oscillation range by controlling the GABA post-synaptic response of pyramidal cells, it is an interesting question whether Cl^- dysregulation would have a significant impact on information coding and memory processing, given the fact that gamma oscillation has an important role in spike timing dependent plasticity and sensory information processing (Buzsáki & Draguhn, 2004). Furthermore, it is an interesting possibility that cells might use their $[Cl^-]_i$ as a mean to modulate their response to GABA activity that will have implication on synaptic input integration in a single cell level that is still remained to be explored.

6.4. The adjunctive role of raised $[Cl^-]_i$ in seizure initiation

Synaptic inhibition is the key mechanism that restrains the spread of activity and seizure recruitment of a new territory (Prince & Wilder, 1967a; Trevelyan *et al.*, 2006a; Schevon *et al.*, 2012). Altered inhibitory function is therefore regarded as an important facet of epilepsy that could lead to seizure initiation. Raised $[Cl^-]_i$ is one of the factors that could lead to a failure of inhibitory restraint by reducing the driving force for GABA hyperpolarizing current and even switching its polarity to be depolarizing (Thompson & Gahwiler, 1989a; Kaila *et al.*, 1997; Ben-Ari, 2002). However to what extent raised $[Cl^-]_i$ is contributing to seizure initiation has not been fully explored.

Results from chapter 4 as summarised earlier, are consistent with previous study that has shown when full ictal discharges were induced by 50-100 μ M 4-AP application and removal of Mg^{2+} from the bath, GABAergic blockers had a significant reduction effect on seizure activity, which is comparable to the effect of glutamatergic blockers (Lillis *et al.*, 2012). The use of either GABAergic or glutamatergic blockers both resulted in a conversion of full ictal discharges into interictal like burst (Lillis *et al.*, 2012). This indicates that ictal activity depends on both glutamatergic activity and also GABAergic activity.

GABAergic excitatory effect is especially dominant in the clonic phase or the afterdischarge phase of post-tetanic stimulation induced ictal events (Fujiwara-Tsukamoto *et al.*, 2006; Ellender *et al.*, 2014). In this model GABAergic blockers tend to be more potent in abolishing afterdischarges than glutamatergic blockers. Recent study then explained how GABAergic contribution to seizure is mainly imposed by parvalbumin (PV) positive interneurons (Ellender *et al.*, 2014), the soma targeting interneuron that is also known to have the capability to synchronize a wide range of pyramidal cells' activity (Tamas *et al.*, 2000). Using post-tetanic stimulation induced ictal events, Ellender *et al.* showed that when PV was optogenetically activated using ChR2, GABA release from PV cell was actually triggering an afterdischarge rather than inhibiting it. In contrast, when PV cell was inactivated optogenetically by Arch activation, the frequency of afterdischarges was significantly reduced. The idea is that the synchronizing effect of PV cells on the post-synaptic pyramidal cells, together with

high $[Cl^-]_i$ that leads to depolarizing GABA activity, will impose a synchronized excitatory effect on the post-synaptic pyramidal cells manifested as the afterdischarge.

These studies, together with my results, suggest that GABAergic activity is indeed required in a full ictal discharge and furthermore it could actually contribute as an excitatory drive in a seizure when $[Cl^-]_i$ is high. However, equally important, other pathological state is also required for the generation of full ictal activity, as shown that only when 20 μ M 4-AP was added in the bath, high $[Cl^-]_i$ triggered full ictal discharges. Based on the Ellender et al study, it could be speculated that this other pathological state should involve hyper-excitability of PV interneurons, as what might have also been imposed by low concentration of 4-AP in my experiments as well. Note that high $[Cl^-]_i$ could not trigger a seizure just in combination with glutamatergic activity triggered by electrical stimulation. Contrast this with HFO which also requires both glutamatergic and GABAergic activity, but electrical stimulation triggered release of glutamate and GABA are enough to accompany high $[Cl^-]_i$ state to trigger HFO.

It is therefore interesting to explore the exact underlying mechanism of 20 μ M 4-AP's contribution to ictogenesis when combined with Cl^- loading. The first possibility is due to the widespread effect of bath application of 4-AP that affects the entire slices in contrast to electrical stimulation that is relatively focal. A second possibility could be simply because 20 μ M 4-AP provides stronger excitatory drive than an electrical stimulation. Lastly, it could also be explained by the fact that 4-AP blocks potassium channel (Kv3.1 and Kv1.1) that are mainly expressed by fast-spiking interneurons, hence triggering burst firing of these interneurons. It also expressed by pyramidal cells, so could further enhance excitability of the network this way (Martina *et al.*, 1998; Rudy & McBain, 2001). An interesting future work that could be done to answer this is by expressing HR in pyramidal cells and ChR2 in PV cells, and assessing whether focal activation of PV cells while loading the pyramidal cells with Cl^- is enough to trigger ictal discharges.

My finding also shows a clear parallel with recent studies of human brain tissue resected during epilepsy surgery (Huberfeld *et al.*, 2007c; Pallud *et al.*, 2014), which show spontaneously occurring interictal events when bathed in conventional ACSF. These interictal events are sensitive to GABAergic blockade, suggestive of a Cl^- -loaded,

excitatory GABAergic state, but to trigger full ictal events in these slices required excitability to be further enhanced by bathing in raised K^+ (Pallud *et al.*, 2014). Importantly, the subsequent ictal activity appeared to arise out of a fundamentally different type of transient discharge which was not sensitive to GABAergic blockade.

Pallud *et al* has shown that in tissues associated with Cl^- dysregulation, a second pathological state such as raised extracellular K^+ resulted in full ictal discharges. Conversely, my result showed that in tissues that were predisposed to a certain pathological state such as sub-epileptic level of 4-AP, high $[Cl^-]_i$ and hence excitatory GABA, could tip the network activity over the balance into a seizure.

6.5. After discharge terminating oscillation

One incidental finding of the HR Cl^- loading experiment in conjunction with low level of 4-AP was the observation of a characteristic seizure terminating event also known as afterdischarge terminating oscillation (ATO). This pattern of activity has been reported and discussed before as one possible way in which seizures terminate (Bragin *et al.*, 1997). In their study, Bragin *et al* was applying tetanic stimulation onto the perforant path and commissural path in vivo that manifested as seizures that either short lasting (<10s) or long lasting (>30s). In their hand, only long lasting seizures were terminated by the ATO whereas the short lasting seizures tend to terminate abruptly without any sign of ATO or post-ictal depression.

Bragin *et al* has demonstrated that ATO happened when cells' E_m was shifting into a depolarized level, triggering cells to fire intensely, which in the network level manifested as the low amplitude fast oscillation (40-90 Hz). Further depolarization of the cells then prevented sodium channel de-inactivation, leaving cells incapable of firing. This manifests as the sustained potential shift that is followed by a depression state. Activity only recovers after E_m is back to normal. Bragin *et al* also showed that they could successfully mimic ATO by local injection of KCl extracellularly, highlighting the role of high extracellular K^+ in the generation of ATO.

The role of ATO in seizure termination still remains elusive. Especially because ATO is not commonly reported in popular seizure models such as 0 Mg^{2+} , 4-AP, spontaneously developed seizures of organotypic cultures, or chronic model of epilepsy such as the one induced by kainic acid, tetanus toxin, or pilocarpine; although it could possibly occur in these model too. However, several other studies have documented ATO before, to be associated with seizure termination (Somjen *et al.*, 1985; Rafiq *et al.*, 1995; Bragin *et al.*, 1997); it should be noted that in all these studies, seizures were induced by focal application of tetanic stimulation in hippocampus. In these studies, ATO was not recorded in all seizures with long seizures tend to be associated with ATO more than short ones.

Bragin *et al.* (1997) and Somjen G *et al.* (1985) both showed that only long seizures were terminated by ATO; similarly in my results ATO tend to be recorded only after long repeats of HR priming in which most of slices had generated multiple seizures beforehand. This might suggest that although ATO is not the general terminating mechanism that could be applied to all seizures, it is possible that it is a secondary terminating mechanism generated by the network when the first line terminating mechanism fails or when the convulsant persists.

The mechanism of ATO has been mainly explained as the consequence of K^+ accumulation in the extracellular space due to intense firing of cells during seizure (Somjen & Giacchino, 1985; Bragin *et al.*, 1997). However, HR priming induced ATO in my experiment suggests that intracellular Cl^- accumulation could also contribute to the generation of ATO. It is probably not a coincidence that excitatory GABAergic activity (Fujiwara-Tsukamoto *et al.*, 2006; Ellender *et al.*, 2014) and ATO associated seizure (Somjen *et al.*, 1985; Rafiq *et al.*, 1995; Bragin *et al.*, 1997) are both particularly prominent in the focal post tetanic stimulation seizure model, as both may share a common contributing factor, which is the high $[Cl^-]_i$. The most likely explanation would be as Cl^- builds up inside the neurons, the driving force for KCC2 to extrude Cl^- increases (figure 6.2A). As KCC2 extrudes Cl^- together with K^+ , Cl^- clearance leads to a greater K^+ extrusion and hence significantly increases the extracellular K^+ to a level that is sufficient to induce the generation of ATO (figure 6.2B). However it is not impossible that Cl^- by itself could also have a direct effect in the generation of ATO. To what extent extracellular K^+ accumulation and the consequent ATO generation is actually

related to Cl^- clearance is an interesting question that still need to be resolved and this could be explored by repeating the same experiment and using a specific KCC2 blocker.

A recent study has shown using computer modelling how the transition between normal spiking activity to seizure and to spreading depression could be explained by a progressive increase in extracellular K^+ (Wei *et al.*, 2014). Experimentally it has been shown how physiologically, $[\text{K}^+]_o$ is kept low around 3-4 mM, while during seizure this goes up to 8 – 12 mM (Heinemann & Lux, 1977), and may even reach 20 – 40 mM during spreading depression (Somjen & Giacchino, 1985). Wei et al showed that when $[\text{K}^+]_o$ is between 12 – 18 mM, tonic firing behaviour is produced (Wei *et al.*, 2014). This fits with the observation of the ATO or low amplitude fast oscillation (40-90Hz) that precedes the sustained potential shift or depression state (flattening of the recording). This suggests that seizure could be followed by ATO or not depending on the level of extracellular K^+ . Accordingly, the different tendency for different slices to generate ATO post seizure might be related to the local regulation of K^+ , such as ATP or energy supply that is needed by the sodium potassium ATPase pump ($\text{Na}^+\text{K}^+\text{ATPase}$) to bring K^+ back into the cell (Bragin *et al.*, 1997; Wei *et al.*, 2014) or possibly Cl^- loading that might facilitate extracellular K^+ rises via KCC2 activity. To answer these questions, it will be interesting in the future to monitor both internal chloride and external potassium level simultaneously during seizure and ATO to tease out the interplay of these 2 ions that could underlie the generation of ATO and potentially give an important insight for seizure termination.

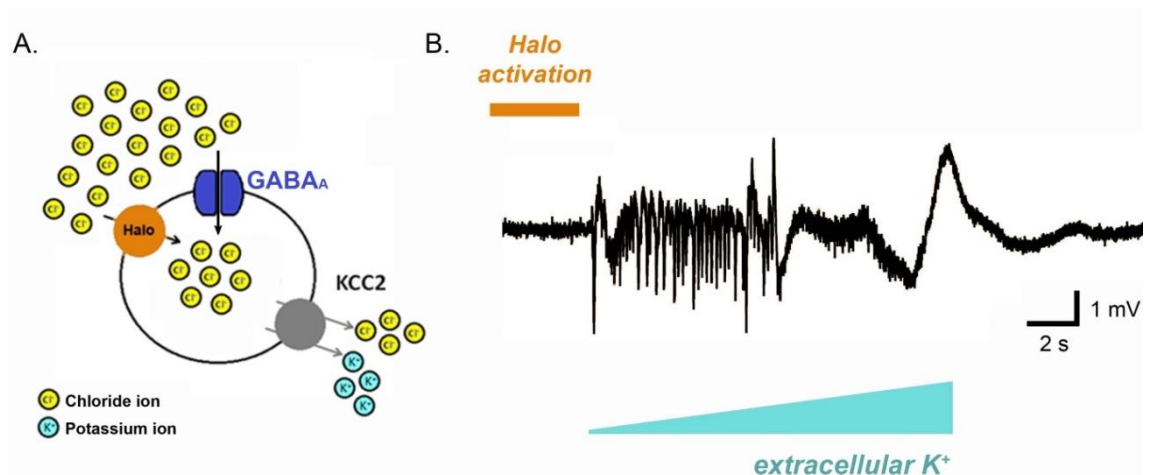


Figure 6.2 Hypothetical underlying mechanism of ATO that terminates an ictal discharge. A. Cl⁻ accumulation, facilitated by HR activation and also via GABA_A activity, increases the driving force for KCC2 Cl⁻ extrusion, which progressively accumulates K⁺ in the extracellular space, as Cl⁻ is being extruded. B. Progressive increase of extracellular K⁺ makes the transition from an ictal discharge into a spreading-depression like event when extracellular K⁺ is sufficiently high to trigger a depolarization block.

Another interesting observation is that some slices, and some area in the brain, tend to generate ATO more easily than others (Somjen *et al.*, 1985; Bragin *et al.*, 1997), as also the case with my observation during the ATO experiments. ATO is very similar to the phenomenon of spreading depression, first described by Leao (Leao, 1944). Spreading depression is a condition of an extreme depolarisation of populations of cell that is associated with ionic imbalances resulting in a silencing of normal on-going activity. Spreading depression has been linked to seizures before (Somjen, 2004). It came back to the first spreading depression recording by Leao (1944), in which he applied tetanic stimuli in vivo to induce a focal seizure but instead of generating seizures, it actually induced the silencing of the network and the flattening of the ECoG. From then on, spreading depression has commonly been induced in vitro and in vivo by the same stimuli that are used to trigger seizures, including electrical stimulation, mechanical injury, alkaline pH, low osmolarity, high extracellular potassium, or even by glutamate (Somjen, 2004). However it has proved difficult to predict whether seizure or spreading depression or both is going to occur (Somjen, 2004). This highlights the overlapping underlying mechanisms behind these two phenomena, and also how

neuronal networks seem to vary in their tendency to go into spreading depression only pathway, seizures only pathway, or seizure that is terminated by ATO.

Parallel to the animal work recording, there seems to be a link between seizure and spreading depression in clinical setting as well. Clinically, cortical spreading depression has been associated with migraine that often started with an aura like phenomenon. It has been shown that sometimes migraines could induce seizures, seizures often followed by post-ictal headache like migraine, also there has been evidence of the usefulness of antiepileptic drug as prophylactic drug for migraine (Rogawski, 2010). Additionally, there were some familial genetic conditions such as mutations with genes encoding for CACNA1A, ATP1A2, and SCN1A that manifested differently in different patients with either seizure, migraine or both (Rogawski, 2010).

In their paper, Bragin et al (1997) also proposed the possibility of glial involvement in the generation of ATO mainly due to the slowly propagating event that is around 0.1-0.2 mm/s (in my experimental data 0.19 mm/s) resembling the speed of calcium wave propagation in the glial network (Cornell-Bell *et al.*, 1990). Glia are likely to be involved mainly due to their role in K^+ buffering. It has also been shown that neuronal activity associated with K^+ release can induce Ca^{2+} waves in the glial gap-junction coupled network (Cornell-Bell *et al.*, 1990). One mechanism of glia K^+ buffering system is by diffusion, where K^+ is absorbed from the extracellular space by the glia where there is a local excess of K^+ , and K^+ then diffuses through the interconnected glial network to the less concentrated area, where it is eventually released back to the extracellular space (Somjen, 2004). Bragin et al then hypothesized that to accumulate K^+ enough to reach the concentration suffice to induce ATO, glial involvement is needed. If Bragin et al's theory of glial K^+ buffering mechanism involved in ATO generation is correct, this could explain why ATO has never been recorded in an in vitro model of epilepsy where the epileptic agent is affecting the entire slice (e.g the 0 Mg^{2+} model or 50-100 μ M 4-AP), and why it only has been recording in focally induced seizures (by electrical stimulation of in my case HR priming). Presumably, the generalised hyper-excitability will raise extracellular K^+ throughout the slice hence glial diffusion mechanism to buffer K^+ could not work due to the lack of K^+ concentration gradient.

6.6. The use of HR to control epilepsy

Earlier studies have tried to use HR as a tool to control epileptic seizures based on its hyperpolarizing effect. These studies showed that HR activation had a significant suppressive effect on seizure activity both in vitro and in vivo that often results in early termination of seizures (Tønnesen *et al.*, 2009; Krook-Magnuson E *et al.*, 2012; Wykes *et al.*, 2012). This might seem to contradict the observation that HR Cl⁻ loading could actually contribute to seizure initiation when combined with sub-epileptic level of 4-AP as described in chapter 4.

Two different illumination paradigms have been used by two different studies that were done on in vivo chronic model of epilepsy. The first one was expressing the original HR protein (NpHR) and activation done by a 20s ON/20s OFF illumination paradigm (Wykes *et al.*, 2012). The second one was expressing the enhanced HR protein (eNpHR3.0) and activation was done using a closed-loop paradigm in which computer algorithm was used to detect seizure initiation that automatically activates light illumination for 5,10, or 30s (Krook-Magnuson E *et al.*, 2012).

There are several possible explanations how HR could show a suppressive effect rather than promoting seizure in the first system. Firstly, Wykes et al used the original HR protein which drives a relatively small current. In chapter 3, I showed that original HR protein gives a markedly smaller current compared to the enhanced version (original HR: 13.79 ± 4.73 pA, enhanced HR: 163.89 ± 108.94 pA) and consequently the HR priming induced depolarizing shift in E_{GABA} (original HR: 1.03 ± 0.18 mV/s, enhanced HR: 6.95 ± 1.5 mV/s). It should be noted however that this E_{GABA} shift was calculated with the orange-blue co-illumination paradigm in which HR current was stabilized for a longer time.

On the other hand in their study, orange light only was used for 20 s long HR activation. Result from chapter 3 shows that this illumination paradigm will result in a decaying HR current over the duration of illumination. Based on this, it is possible that Cl⁻ loading effect in this study was relatively small and so the hyperpolarizing effect of HR undermining the mild Cl⁻ accumulation issue.

The second study (Krook-Magnuson E *et al.*, 2012) on the other hand was using the enhanced HR protein that has larger current and Cl^- loading effect. However, in their study, a close-loop illumination paradigm was used, in which light activation is only delivered when a computer algorithm detects a seizure initiation. This means that HR was only activated whenever seizure had already been initiated. It has been shown before that Cl^- rises within the pyramidal cells almost instantaneously when the seizure starts (Lillis *et al.*, 2012) and so with the close-loop paradigm HR was only activated whenever Cl^- accumulation has already happened. My result indeed suggests that Cl^- loading could lead to seizure initiation, however whether HR Cl^- loading can do further harm when seizure has been initiated is unknown. E_m and $[\text{Cl}^-]_i$ are dynamic in the neuronal network especially during seizure and depending on these 2 factors further Cl^- influx that imposes hyperpolarizing effect on E_m but depolarizing shift in E_{GABA} could potentially be promoting or suppressing seizure activity. Additionally, these 2 studies were done in vivo in which Cl^- dynamics have not been explored.

6.7. A novel use of optogenetic tools to extrude Cl^-

In chapter 5, I showed that co-activation of ArchT and ChloC consistently imposed a hyperpolarizing shift in the E_{GABA} indicative of a Cl^- extrusion effect. Ultimately, we would like to assess the potential therapeutic effect of ArchT-ChloC Cl^- extrusion in a context of epilepsy. Since seizures are network phenomena, the next aim is to apply this strategy in the network level. Ideally a set protocol that guarantees an optimised outward flow of Cl^- is needed especially when intended to be used for network activity studies where monitoring $[\text{Cl}^-]_i$ in all cells is not trivial. Optimization could be achieved by finding the best combination of the light activated Cl^- channel and the Cl^- independent hyperpolarising tool, finding the best co-expression system, and assessing the best illumination paradigm.

To date, the available light activated Cl^- channels are iC1C2 and the bistable version called SwiChR_{CT}, and two variants of ChloC with fast or slow kinetics respectively (Berndt *et al.*, 2014; Wietek *et al.*, 2014). At least in our hand, the light activated current of iC1C2 was variable and rather small and so ChloC is more favourable. However there is a new version of iC1C2 channel namely iC1C23.0 that has an

improved membrane expression and consequently the light activated current that could also be a good candidate to be tested in the future (*unpublished* – Karl Deisseroth, personal communication, August 7, 2014). The slow kinetic versions are less suitable for this purpose. This is due to the fact that the residual current post light termination by the light activated Cl⁻ channel might not give a Cl⁻ extrusion effect since ArchT hyperpolarizing effect does not outlast the duration of illumination as well.

As for the Cl⁻ independent hyperpolarising tool, this mainly comes from the light-driven outward proton pump family such as Mac, bacteriorhodopsins (BR), or archeorhodopsins (Arch or ArchT). ArchT makes a really good, Cl⁻ independent, hyperpolarising tool to be coupled with the Cl⁻ channel, for several reasons. Firstly is the really good level of expression of the protein that results in a large light activated current (up to 900 pA), and with the improved light sensitivity of almost three times than the original version of Arch. That significantly enhances the photocurrent, when using light with the power of 1-10 mW/mm².

Additionally, Wietek et al has described that external binding of H⁺ enhances the conductance of the ChloC without the transport of H⁺ itself (Wietek *et al.*, 2014). This suggests that by using ArchT that is an outward H⁺ pump hence provides an external binding of H⁺ to the ChloC might actually optimize the conductance of the ChloC.

Co-localization of multiple proteins can be achieved mainly in 2 different ways, as a fused protein or by bicistronic expression system such as the use of internal ribosomal entry site (IRES) or a self-cleaving 2A peptide (Chan *et al.*, 2011; Kleinlogel *et al.*, 2011b). Only the former but not the latter could provide a stable 1:1 expression of the different proteins. 2A peptide has been used to co-express ChloC-ArchT and there were evidence that this system could induce a Cl⁻ extrusion effect on cells during illumination. However it was apparent that the hyperpolarizing current generated during illumination was markedly smaller compare to the 2 plasmids transfection. One possibility is that there is lower expressions of the second protein compared to the first one, and so for this case, less ArchT expression compared to ChloC.

One way to further improve this is to use the fusion strategy so that both ChloC and ArchT are expressed as a single entity. Theoretically, this would maximize the effect of ArchT by localizing it to ChloC and hence optimizing the Cl⁻ extrusion effect of ChloC-ArchT co-activation. Furthermore fusion protein of ChloC and ArchT will also allow a compartmental Cl⁻ extrusion in subcellular level. In contrary to the bicistronic expression system or dual plasmids transfection system, fusion protein will allow a precise stoichiometric side by side expression of the two proteins, assuring that every ChloC protein will be associated with a single ArchT protein. This will be a more reliable way to exert a Cl⁻ extrusion effect in a more confined area, compared to bicistronic expression or dual plasmids transfection system in which the 2 proteins will be distributed quite randomly along the cell membrane. It has been reported before that there are subcellular differences in Cl⁻ concentration within the cytoplasm. For instance, axon initial segment has been shown to have higher Cl⁻ that might affect the post-synaptic activity of chandelier cell interneuron that specifically innervates this region (Szabadics *et al.*, 2006). Another example is that there is an evidence of transient Cl⁻ increase in the dendritic spine when glutamate is applied (Waseem *et al.*, 2010). Compartmental Cl⁻ extrusion might be useful to investigate the implication of Cl⁻ subcellular differences.

Finally, the best illumination paradigm should also be investigated to achieve the optimal Cl⁻ extrusion effect from this strategy. This is especially important when trying to use it in the seizure context in which optimal Cl⁻ extrusion and hyperpolarization is probably required to exert a therapeutic effect. It should be noted that there might be differences between how a light activated channel and a light activated pump work in modulating ion level as this affect what is the best illumination paradigm to be used.

The size of current passing through a channel or in this case ChloC depends on the reversal potential for the permeable ion (Cl⁻) and the V_m. While the role of light in this case is only to open the channel to provide a conductance for the ion flow but not directly regulating the amount of ion that flows through. Once the Cl⁻ reversal potential is achieved, no more Cl⁻ flow will take place even when the channel still open. On the other hand, light activated pump such as HR works by using about 20% of a photon energy to translocate one Cl⁻ ion into the cell (Pfisterer *et al.*, 2009). This means that the amount of light will directly affect the number of ion being

translocated and the more photons from light hits the protein the more Cl^- being translocated. Note however that this is also affected by the availability of the trans-retinal (the ready to use form of the chromophore that converts the light into the energy needed for the Cl^- transport). Based on this, it is known that unlike HR, longer illumination does not always result in more Cl^- flow through a Cl^- channel such as ChloC. This is also supported by the results from chapter 5 that shows no correlation between ChloC-ArchT Cl^- extrusion and duration of illumination, but instead showed better correlation with the baseline level of $[\text{Cl}^-]_i$.

Similarly to HR, ArchT is a light activated pump in which the number of H^+ ions extruded depends on the amount of light. However, for the Cl^- extrusion purpose ArchT is used to modulate V_m rather than to modulate ion concentration. Just like HR, the ArchT current also decays with time (chapter 5), possibly explained by the reduced amount of ready-to-use form of the chromophore, and so the longer the illumination the weaker E_m modulation is being imposed by ArchT. Together, it suggests that a long duration of illumination is not a favourable approach to optimize the Cl^- extrusion effect of ChloC-ArchT co-activation. Rather, multiple repeats of short illumination are more likely to exert a stronger Cl^- extrusion effect. Further investigation is needed to select the best illumination paradigm for this purpose.

Finally, the ultimate goal will be to assess the therapeutic effect of ChloC-ArchT Cl^- extrusion in the context of epilepsy. ChloC-ArchT is potentially useful for epilepsy in 2 different ways; acutely as an on-demand control when seizures take place, and chronically to reduce the probability of having more seizures. The acute effect of ChloC-ArchT Cl^- extrusion effect hypothetically could outperform the use of HR to stop seizures for several reasons. Firstly, ChloC-ArchT co-activation gives a comparable hyperpolarizing current with HR but without loading cells with Cl^- . Secondly, Cl^- extrusion effect of ChloC-ArchT co-activation would shift E_{GABA} to a more hyperpolarized level and hence boosting the inhibitory effect of GABA during the course of a seizure. Lastly, ChloC activation will have a shunting effect as when a channel opens cells becomes leakier; this also will have an extra inhibitory effect to the cells.

Chronically, we also hypothesize that ChloC-ArchT Cl^- extrusion might have a positive effect on epileptogenesis and ultimately reducing the seizure frequency. This is based on the adjunctive effect of high $[\text{Cl}^-]_i$ in seizure initiation as shown that it lowered the threshold for 4-AP to induce seizure. If we believe that high $[\text{Cl}^-]_i$ leads to a higher propensity for seizure initiation it could be implied that Cl^- extrusion would then have an opposite effect that is reducing the propensity for seizure generation.

So far the use of optogenetic to control epilepsy has focused mainly on seizure termination and the long term effect on seizure frequency has never been assessed. The use of ChloC-ArchT Cl^- extrusion will be a novel way of using optogenetic tools to control epilepsy that goes beyond seizure termination but more importantly to actually prevent the generation of more subsequent seizures.

6.8. The prospect of gene therapy and optogenetics as a treatment for epilepsy

Approximately, 65 million people or 1% of the world population suffer from epilepsy (Moshé *et al.*, 2014). Patients with epilepsy often have to face a life-long health and socioeconomic burden. This is particularly devastating for the 30% of the patients who do not respond to the available anti-epileptic medication. The number of treatment options available for this group of patients is limited and often show a relatively low efficacy (Kullmann *et al.*, 2014; Moshé *et al.*, 2014).

One of the most promising candidates as a new treatment option for the pharmacoresistant patients of epilepsy is gene therapy. In general, gene therapy is preferable as it allows region specific and cell-type specific modulation of neuronal excitability (Kullmann *et al.*, 2014). Research has focussed on the viral gene therapy. Lentiviral and adeno-associated viruses (AAV) vectors are the most common ones to be used to deliver the target gene into the cells, for the expression of the desired proteins. Both of these viruses are considered to be safe for this purpose based on prior animal research (Kullmann *et al.*, 2014). Target genes that have been tested vary from endogenous genes such as human potassium channel protein (Kv1.1), to exogenous or engineered genes such as genes encoding for optogenetic proteins and designer receptor exclusively activated by a designer drug (DREADD) proteins (Krook-Magnuson *et al.*, 2012; Wykes *et al.*, 2012; Kätzel *et al.*, 2014).

Overexpression of endogenous protein Kv1.1 has been proven effective in reducing the excitability of pyramidal cells in the epileptic foci of animal model of epilepsy (Wykes *et al.*, 2012). However, in this situation, the effect of Kv1.1 overexpression would persist regardless of the excitability state of the tissue. The desire for a temporally controlled modulation of neuronal excitability, which suits the transient nature of epileptic seizure, leads to the concept of using DREADDs or optogenetic proteins where neuronal modulation only takes place when a certain chemical agent or light are presented respectively (Deisseroth *et al.*, 2006; Armbruster *et al.*, 2007; Pei *et al.*, 2008).

DREADDs are engineered receptors that could only be activated by an artificial ligand; there are both excitatory and inhibitory DREADDs (Armbruster *et al.*, 2007; Pei *et al.*, 2008). This technology allows transient modulation of neuronal activity, whenever the specific ligand is presented. The activation of inhibitory DREADD receptor in pyramidal cells has also been shown to be effective in suppressing seizure activity in animal model of epilepsy (Kätzel *et al.*, 2014). Despite the possibility of a limited temporal control over neuronal activity, it is apparent that there is always a delay between the times when the drug is administered to the times when the receptors' action actually take place. In this aspect, optogenetics stands out as a better option, as neuronal activity could be controlled with milliseconds precision (Deisseroth *et al.*, 2006). As discussed earlier in chapter 1, several different groups have provided evidence that show seizure suppressive effect of different optogenetic approach to control epileptic seizures in animal model of epilepsy, by only short activation of the proteins (Krook-Magnuson E *et al.*, 2012; Wykes *et al.*, 2012).

The translation of these different approaches into clinical practice however is not an easy matter. The main issue to address for gene therapy is the safety of the viral vectors gene delivery and the possible long term consequences of overexpressing a certain gene on the expression of other endogenous genes (Kullmann *et al.*, 2014). Extra challenges have to be overcome when temporal control is desired. With DREADDs technology, limited temporal control is made possible, but extra safety issue has to be clarified such as the potential non-specific effect of the artificial ligand on the endogenous receptors. Additionally, in animal model, the seizure suppressive effect was only observed 10 minutes after drug delivery (Kätzel *et al.*, 2014), suggesting that

this approach might not be applicable as an on-demand control for short epileptic seizures, although this could still be advantageous for patients with status epilepticus or to hinder epileptogenesis in a long run.

So far, optogenetics is the only technique that allows for a high temporal precision of neuronal activity modulation. However, to translate this into human application, an extra hurdle has to be overcome, which is to deliver light into the epileptic focus. This system has to be biocompatible, energetically efficient, and as less invasive as possible. Some advancement has been made over these recent years towards achieving this such as improving light sensitivity of the opsins (Han *et al.*, 2011; Zhang *et al.*, 2011), designing opsins activated by red light that has better optical penetrance for the brain tissue (Zhang *et al.*, 2008; Chuong *et al.*, 2014) and the continuing development of biocompatible micro-LEDs or lasers as light sources specifically design for optogenetics (Degenaar *et al.*, 2009). Until these issues are fully addressed, optogenetics remain a mere research tool, which even so is still really valuable for the neuroscience field. Further investigation is also needed to evaluate whether it is necessary to take the extra mile in overcoming all the technical difficulties associated with optogenetics, in exchange for a better temporal control, when more achievable options such as endogenous genes therapy or DREADDs technique are available.

6.9. Conclusion

High intraneuronal Cl^- has been associated with epileptogenic area before. In this project I have shown that when high $[\text{Cl}^-]_i$ state was induced in healthy tissues, epileptic high frequency oscillation was generated, which showed some unique features such as doubling of frequency, increased jitter in spike timing, and out of phase firing. These are consistent with the characteristic of epileptic HFO commonly recorded from epileptic tissue taken from animal model of epilepsy. However it was evident that high $[\text{Cl}^-]_i$ on its own has never triggered a full ictal discharge in vitro. Further exploration then showed that although high $[\text{Cl}^-]_i$ alone was not triggering seizure, however it lowered the seizure threshold for the convulsant 4-AP to develop full ictal discharges. This highlights the adjunctive effect of high $[\text{Cl}^-]_i$ in seizure initiation. Realizing the important contribution of high $[\text{Cl}^-]_i$ in ictogenesis, a way to extrude Cl^- was explored mainly focussed on the optogenetic technology. Combining the ArchT hyperpolarizing effect and the opening of light activated Cl^- channel ChloC, Cl^- extrusion with high temporal control was made possible. This provides a new strategy of utilizing optogenetics to control epilepsy, to be tested in the future.

Appendix

Sequence of ChloC-T2A-ArchT_GFP

atggattatggaggcgccctgagtgccgttgggcgcgagctgctatttgaacgaaccagtagtctgcaatggctctgtact
tgtcctgaggaccagtgttactgcgctggctggattgagtcgctggcacaacgggtgccaaacggcgtcgaacgtgct
gcaatggcttgctgctggcttctccatcctactgcttatgttttacgctaccaaacatggaagtcaacctgaggctgggagg
agatctatgtgtgctatcaggatggcaaggtgattctcgagttcttctcgagtttaagaacctgcatgctgtatctag
ccacaggccaccgctccagtgggttgcgttacgccagtggttctcacctgccgggtcattctcattcacctgtcaaacctg
acgggcttgccaacgactacagcaggcgcacatgggtctgcttgtgtctgatattggctgtattgtgtggggcgccacttc
cgccatggccaccggatacgtcaaggtcatcttcttctgctgggtctgtgttatgggtgtaaacacgttctttacgctgcca
ggcctacatcgagggttaccacaccgtgccgaagggccgggtgctgccaggtggtgactggcatggcttggcttcttctgat
catggggtatgttcccatcctgttcatcctcgccccgagggtctcgctgctgagcgtgtacggctccaccgtcggccac
accatcattgacctgatgtcgaagaactgctgggtctgctcgccactacctgcgctgctgatccacgagcatatcctcat
ccacggcgacattcgcaagaccaccaaattgaacattgggtggcactgagattgaggtcgagacgctgggtggaggacgagg
ccgaggctggcgctgtaaccgctggccgagggcagaggaagtcttctaacaatgcggtgacgtggaggagaatcccgccct
gcaccgggatccgccaccatggacccatcgtctgagggcaggatacagctgctggcgacggaaggccagagacct
gtggctgggaatcggaacctgctgatgctgatcgccaccttacttcatctgaagggctggggcgtgaccgacaagga
ggccaggagtagtacagcatcacaatcctggtgccggcatcgccagcgcctacctgagcatgttcttggcatcggc
ctgaccgaggtgaccgtggccggcgaggtgctggacatctactacgccagatacggcactggctgttaccacccttgc
ttctgctgacctggccctgctggtaaggtggacaggggtgagcatcggaacctggtgggagtgagcgcctgatgatcgt
gaccggcctgatcgccgacctgagccacccccactggctaggtacagctggtggctgtcagccatctgatgatcgtg
gtgctgtacttctggctaccagcctgagggtgctgtaaggagaggggaccagaggtggctagcaccttaacacctg
accgacctggtgctggtgctgtggaccgctacccatcctgtggatcatcggaaccgagggagctggagtggtgggactgg
gaatcgagacctgctgttcatggtgctggacgtgaccgcaaaagtgggcttccgcttcatcctgctgaggagcagggccat
cctggcgacaccgagggccccgagccccgaccgtagtagcagtgagcaagggcgaggagctgttaccggggtggtgc
ccatcctggtcgagctggacggcgacgtaaacggccacaagttcagcgtgtccggcgagggcgagggcgatgccacctac
ggcaagctgacctgaagttcatctgcaccaccggcaagctgccgctgcccctggcccacctctgaccacctgacctag
gcgtgagtgctttagccgctacccgaccacatgaagcagcacgacttctcaagtcgcatgcccgaaggctacgtcca
ggagcgcacatcttctcaaggacgacggcaactacaagaccgctggcggaggtgaagttcgagggcgacacctggtga
accgcatcgagctgaaggcatcacttcaaggagacggcaacatcctggggcacaagctggagtacaactacaacag
ccacaacgtctatatcatggccgacaagcagaagaaggcatcaaggtgaacttcaagatccgccacaacatcgaggacg
gcagcgtgagctcgccgacctaccagcagaacccccatcgccgacggccccgtgctgctgcccgacaacctacc
tgagcaccagtcgcccctgagcaaagacccaacgagaagcgcgatcacatggtcctgctggagttcgtgaccgcccgcg
ggatcactctcgcatggacgagctgtacaagtaagaattcgatatcaagctt

References

- Alvarado-Rojas, C., Huberfeld, G., Baulac, M., Clemenceau, S., Charpier, S., Miles, R., de la Prida, L.M. & Le Van Quyen, M. (2014) Different mechanisms of ripple-like oscillations in the human epileptic subiculum. *Annals of Neurology*.
- Armbruster, B.N., Li, X., Pausch, M.H., Herlitze, S. & Roth, B.L. (2007) Evolving the lock to fit the key to create a family of G protein-coupled receptors potently activated by an inert ligand. *Proceedings of the National Academy of Sciences*, **104**, 5163-5168.
- Armstrong, C., Krook-Magnuson, E., Oijala, M. & Soltesz, I. (2013) Closed-loop optogenetic intervention in mice. *Nat. Protocols*, **8**, 1475-1493.
- Balakrishnan, V., Becker, M., Löhrke, S., Nothwang, H.G., Güresir, E. & Friauf, E. (2003) Expression and Function of Chloride Transporters during Development of Inhibitory Neurotransmission in the Auditory Brainstem. *The Journal of Neuroscience*, **23**, 4134-4145.
- Bartos, M., Vida, I. & Jonas, P. (2007) Synaptic mechanisms of synchronized gamma oscillations in inhibitory interneuron networks. *Nat Rev Neurosci*, **8**, 45-56.
- Ben-Ari, Y. (2002) Excitatory actions of gaba during development: the nature of the nurture. *Nat Rev Neurosci*, **3**, 728-739.
- Berndt, A., Lee, S.Y., Ramakrishnan, C. & Deisseroth, K. (2014) Structure-Guided Transformation of Channelrhodopsin into a Light-Activated Chloride Channel. *Science*, **344**, 420-424.
- Bormann, J., Hamill, O.P. & Sakmann, B. (1987) Mechanism of anion permeation through channels gated by glycine and gamma-aminobutyric acid in mouse cultured spinal neurones. *The Journal of Physiology*, **385**, 243-286.
- Bouchard, R. & Fedida, D. (1995) Closed- and open-state binding of 4-aminopyridine to the cloned human potassium channel Kv1.5. *Journal of Pharmacology and Experimental Therapeutics*, **275**, 864-876.
- Bowery, N.G., Hill, D.R., Hudson, A.L., Doble, A., Middlemiss, D.N., Shaw, J. & Turnbull, M. (1980) (-)Baclofen decreases neurotransmitter release in the mammalian CNS by an action at a novel GABA receptor. *Nature*, **283**, 92-94.

- Bragin, A., Engel, J., Wilson, C.L., Fried, I. & Buzsáki, G. (1999) High-frequency oscillations in human brain. *Hippocampus*, **9**, 137-142.
- Bragin, A., Jando, G., Nadasdy, Z., Hetke, J., Wise, K. & Buzsaki, G. (1995) Gamma (40-100 Hz) oscillation in the hippocampus of the behaving rat. *The Journal of Neuroscience*, **15**, 47-60.
- Bragin, A., Mody, I., Wilson, C.L. & Engel, J., Jr. (2002a) Local generation of fast ripples in epileptic brain. *J Neurosci*, **22**, 2012-2021.
- Bragin, A., Penttonen, M. & Buzsáki, G. (1997) Termination of Epileptic Afterdischarge in the Hippocampus. *The Journal of Neuroscience*, **17**, 2567-2579.
- Bragin, A., Wilson, C.L., Staba, R.J., Reddick, M., Fried, I. & Engel, J., Jr. (2002b) Interictal high-frequency oscillations (80-500 Hz) in the human epileptic brain: entorhinal cortex. *Ann Neurol*, **52**, 407-415.
- Buzsaki, G. (2006) *Rhythms of the Brain*, New York.
- Buzsáki, G. & Draguhn, A. (2004) Neuronal Oscillations in Cortical Networks. *Science*, **304**, 1926-1929.
- Buzsaki, G., Horvath, Z., Urioste, R., Hetke, J. & Wise, K. (1992) High-frequency network oscillation in the hippocampus. *Science*, **256**, 1025-1027.
- Buzsáki, G., Kaila, K. & Raichle, M. (2007) Inhibition and Brain Work. *Neuron*, **56**, 771-783.
- Cammarota, M., Losi, G., Chiavegato, A., Zonta, M. & Carmignoto, G. (2013) Fast spiking interneuron control of seizure propagation in a cortical slice model of focal epilepsy. *The Journal of Physiology*, **591**, 807-822.
- Campbell, S.L., Robel, S., Cuddapah, V.A., Robert, S., Buckingham, S.C., Kahle, K.T. & Sontheimer, H. (2015) GABAergic disinhibition and impaired KCC2 cotransporter activity underlie tumor-associated epilepsy. *Glia*, **63**, 23-36.
- Cardin, J.A., Carlen, M., Meletis, K., Knoblich, U., Zhang, F., Deisseroth, K., Tsai, L.-H. & Moore, C.I. (2009) Driving fast-spiking cells induces gamma rhythm and controls sensory responses. *Nature*, **459**, 663-667.

- Cardin, J.A., Carlen, M., Meletis, K., Knoblich, U., Zhang, F., Deisseroth, K., Tsai, L.-H. & Moore, C.I. (2010) Targeted optogenetic stimulation and recording of neurons in vivo using cell-type-specific expression of Channelrhodopsin-2. *Nat. Protocols*, **5**, 247-254.
- Chan, H.Y., Sivakamasundari, V., Xing, X., Kraus, P., Yap, S.P., Ng, P., Lim, S.L. & Lufkin, T. (2011) Comparison of IRES and F2A-Based Locus-Specific Multicistronic Expression in Stable Mouse Lines. *PLoS ONE*, **6**, e28885.
- Chow, B.Y., Han, X., Dobry, A.S., Qian, X., Chuong, A.S., Li, M., Henninger, M.A., Belfort, G.M., Lin, Y., Monahan, P.E. & Boyden, E.S. (2010) High-performance genetically targetable optical neural silencing by light-driven proton pumps. *Nature*, **463**, 98-102.
- Chuong, A.S., Miri, M.L., Busskamp, V., Matthews, G.A.C., Acker, L.C., Sorensen, A.T., Young, A., Klapoetke, N.C., Henninger, M.A., Kodandaramaiah, S.B., Ogawa, M., Ramanlal, S.B., Bandler, R.C., Allen, B.D., Forest, C.R., Chow, B.Y., Han, X., Lin, Y., Tye, K.M., Roska, B., Cardin, J.A. & Boyden, E.S. (2014) Noninvasive optical inhibition with a red-shifted microbial rhodopsin. *Nat Neurosci*, **17**, 1123-1129.
- Cohen, I., Navarro, V., Clemenceau, S., Baulac, M. & Miles, R. (2002) On the Origin of Interictal Activity in Human Temporal Lobe Epilepsy in Vitro. *Science*, **298**, 1418-1421.
- Coombs, J.S., Eccles, J.C. & Fatt, P. (1955) The specific ionic conductances and the ionic movements across the motoneuronal membrane that produce the inhibitory post-synaptic potential. *The Journal of Physiology*, **130**, 326-373.
- Cornell-Bell, A.H., Finkbeiner, S.M., Cooper, M.S. & Smith, S.J. (1990) Glutamate induces calcium waves in cultured astrocytes: long-range glial signaling. *Science*, **247**, 470-473.
- Craig, M.T. & McBain, C.J. (2014) The emerging role of GABAB receptors as regulators of network dynamics: fast actions from a 'slow' receptor? *Current Opinion in Neurobiology*, **26**, 15-21.
- Degenaar, P., Grossman, N., Memon, M.A., Burrone, J., Dawson, M., Drakakis, E., Neil, M. & Nikolic, K. (2009) Optobionic vision - a new genetically enhanced light on retinal prosthesis. *Journal of Neural Engineering*, **6**.
- Deisseroth, K., Feng, G., Majewska, A.K., Miesenböck, G., Ting, A. & Schnitzer, M.J. (2006) Next-Generation Optical Technologies for Illuminating Genetically Targeted Brain Circuits. *The Journal of Neuroscience*, **26**, 10380-10386.

- Dibb, N.J. & Wolfe, P.B. (1986) *lep* Operon Proximal Gene Is Not Required for Growth or Secretion by *Escherichia coli*. *Journal of Bacteriology*, **166**, 83-87.
- Dichter, M. & Spencer, W.A. (1969) Penicillin-induced interictal discharges from the cat hippocampus. I. Characteristics and topographical features. *J Neurophysiol*, **32**, 649-662.
- Douin, V., Bornes, S., Creancier, L., Rochaix, P., Favre, G., Prats, A.-C. & Couderc, B. (2004) Use and comparison of different internal ribosomal entry sites (IRES) in tricistronic retroviral vectors. *BMC Biotechnology*, **4**, 16.
- Dzhala, V.I., Kuchibhotla, K.V., Glykys, J.C., Kahle, K.T., Swiercz, W.B., Feng, G., Kuner, T., Augustine, G.J., Bacskai, B.J. & Staley, K.J. (2010a) Progressive NKCC1-dependent neuronal chloride accumulation during neonatal seizures. *J Neurosci*, **30**, 11745-11761.
- Dzhala, V.I., Kuchibhotla, K.V., Glykys, J.C., Kahle, K.T., Swiercz, W.B., Feng, G., Kuner, T., Augustine, G.J., Bacskai, B.J. & Staley, K.J. (2010b) Progressive NKCC1-Dependent Neuronal Chloride Accumulation during Neonatal Seizures. *The Journal of Neuroscience*, **30**, 11745-11761.
- Ebihara, S., Shirato, K., Harata, N. & Akaike, N. (1995) Gramicidin-perforated patch recording: GABA response in mammalian neurones with intact intracellular chloride. *The Journal of Physiology*, **484**, 77-86.
- Ellender, T.J., Raimondo, J.V., Irlke, A., Lamsa, K.P. & Akerman, C.J. (2014) Excitatory Effects of Parvalbumin-Expressing Interneurons Maintain Hippocampal Epileptiform Activity via Synchronous Afterdischarges. *The Journal of Neuroscience*, **34**, 15208-15222.
- Engel Jr, J., Bragin, A., Staba, R. & Mody, I. (2009) High-frequency oscillations: What is normal and what is not? *Epilepsia*, **50**, 598-604.
- Englot, D.J., Chang, E.F. & Auguste, K.I. (2011) Vagus nerve stimulation for epilepsy: a meta-analysis of efficacy and predictors of response. *Journal of Neurosurgery*, **115**, 1248-1255.
- Farrant, M. & Nusser, Z. (2005) Variations on an inhibitory theme: phasic and tonic activation of GABAA receptors. *Nat Rev Neurosci*, **6**, 215-229.

- Fisher, R., Salanova, V., Witt, T., Worth, R., Henry, T., Gross, R., Oommen, K., Osorio, I., Nazzaro, J., Labar, D., Kaplitt, M., Sperling, M., Sandok, E., Neal, J., Handforth, A., Stern, J., DeSalles, A., Chung, S., Shetter, A., Bergen, D., Bakay, R., Henderson, J., French, J., Baltuch, G., Rosenfeld, W., Youkilis, A., Marks, W., Garcia, P., Barbaro, N., Fountain, N., Bazil, C., Goodman, R., McKhann, G., Babu Krishnamurthy, K., Papavassiliou, S., Epstein, C., Pollard, J., Tonder, L., Grebin, J., Coffey, R., Graves, N. & the, S.S.G. (2010) Electrical stimulation of the anterior nucleus of thalamus for treatment of refractory epilepsy. *Epilepsia*, **51**, 899-908.
- Fisher, R.S., Acevedo, C., Arzimanoglou, A., Bogacz, A., Cross, J.H., Elger, C.E., Engel, J., Forsgren, L., French, J.A., Glynn, M., Hesdorffer, D.C., Lee, B.I., Mathern, G.W., Moshé, S.L., Perucca, E., Scheffer, I.E., Tomson, T., Watanabe, M. & Wiebe, S. (2014) ILAE Official Report: A practical clinical definition of epilepsy. *Epilepsia*, **55**, 475-482.
- Foffani, G., Uzcategui, Y.G., Gal, B. & Menendez de la Prida, L. (2007a) Reduced Spike-Timing Reliability Correlates with the Emergence of Fast Ripples in the Rat Epileptic Hippocampus. *Neuron*, **55**, 930-941.
- Foffani, G., Uzcategui, Y.G., Gal, B. & Menendez de la Prida, L. (2007b) Reduced spike-timing reliability correlates with the emergence of fast ripples in the rat epileptic hippocampus. *Neuron*, **55**, 930-941.
- Fujiwara-Tsukamoto, Y., Isomura, Y. & Takada, M. (2006) Comparable GABAergic Mechanisms of Hippocampal Seizurelike Activity in Posttetanic and Low-Mg²⁺ Conditions. *Journal of Neurophysiology*, **95**, 2013-2019.
- Gagnon, M., Bergeron, M.J., Lavertu, G., Castonguay, A., Tripathy, S., Bonin, R.P., Perez-Sanchez, J., Boudreau, D., Wang, B., Dumas, L., Valade, I., Bachand, K., Jacob-Wagner, M., Tardif, C., Kianicka, I., Isenring, P., Attardo, G., Coull, J.A.M. & De Koninck, Y. (2013) Chloride extrusion enhancers as novel therapeutics for neurological diseases. *Nat Med*, **19**, 1524-1528.
- Galarreta, M. & Hestrin, S. (1999) A network of fast-spiking cells in the neocortex connected by electrical synapses. *Nature*, **402**, 72-75.
- Gassmann, M. & Bettler, B. (2012) Regulation of neuronal GABAB receptor functions by subunit composition. *Nat Rev Neurosci*, **13**, 380-394.
- Gibson, J.R., Beierlein, M. & Connors, B.W. (1999) Two networks of electrically coupled inhibitory neurons in neocortex. *Nature*, **402**, 75-79.

- Glykys, J., Dzhala, V., Egawa, K., Balena, T., Saponjian, Y., Kuchibhotla, K.V., Bacskai, B.J., Kahle, K.T., Zeuthen, T. & Staley, K.J. (2014a) Local Impermeant Anions Establish the Neuronal Chloride Concentration. *Science*, **343**, 670-675.
- Glykys, J., Dzhala, V., Egawa, K., Balena, T., Saponjian, Y., Kuchibhotla, K.V., Bacskai, B.J., Kahle, K.T., Zeuthen, T. & Staley, K.J. (2014b) Response to Comments on “Local impermeant anions establish the neuronal chloride concentration”. *Science*, **345**, 1130.
- Gradinaru, V., Thompson, K. & Deisseroth, K. (2008) eNpHR: a Natronomonas halorhodopsin enhanced for optogenetic applications. *Brain Cell Bio*, **36**, 129-139.
- Grenier, F., Timofeev, I. & Steriade, M. (2003) Neocortical Very Fast Oscillations (Ripples, 80–200 Hz) During Seizures: Intracellular Correlates. *Journal of Neurophysiology*, **89**, 841-852.
- Guo, L., Rivero, D., Dorado, J., Rabuñal, J.R. & Pazos, A. (2010) Automatic epileptic seizure detection in EEGs based on line length feature and artificial neural networks. *Journal of Neuroscience Methods*, **191**, 101-109.
- Haikala, V., Joesch, M., Borst, A. & Mauss, A.S. (2013) Optogenetic Control of Fly Optomotor Responses. *The Journal of Neuroscience*, **33**, 13927-13934.
- Hájos, N., Pálhalmi, J., Mann, E.O., Németh, B., Paulsen, O. & Freund, T.F. (2004) Spike Timing of Distinct Types of GABAergic Interneuron during Hippocampal Gamma Oscillations In Vitro. *The Journal of Neuroscience*, **24**, 9127-9137.
- Han, X. & Boyden, E.S. (2007) Multiple-color optical activation, silencing, and desynchronization of neural activity, with single-spike temporal resolution. *PLoS One*, **2**, e299.
- Han, X., Chow, B.Y., Zhou, H., Klapoetke, N.C., Chuong, A., Rajimehr, R., Yang, A., Baratta, M.V., Winkle, J., Desimone, R. & Boyden, E.S. (2011) A high-light sensitivity optical neural silencer: development, and application to optogenetic control of nonhuman primate cortex. *Frontiers in Systems Neuroscience*, **5**.
- Hasenstaub, A., Shu, Y., Haider, B., Kraushaar, U., Duque, A. & McCormick, D.A. (2005) Inhibitory postsynaptic potentials carry synchronized frequency information in active cortical networks. *Neuron*, **47**, 423-435.

- He, C., Chen, F., Li, B. & Hu, Z. (2014) Neurophysiology of HCN channels: From cellular functions to multiple regulations. *Progress in Neurobiology*, **112**, 1-23.
- Heinemann, U. & Lux, H.D. (1977) "Ceiling" of stimulus induced rises in extracellular potassium concentration in cerebral cortex of cats. *Brain Research*, **120**, 231-250.
- Hendry, S.H., Schwark, H.D., Jones, E.G. & Yan, J. (1987) Numbers and proportions of GABA-immunoreactive neurons in different areas of monkey cerebral cortex. *The Journal of Neuroscience*, **7**, 1503-1519.
- Hennecke, M., Kwissa, M., Metzger, K., Oumard, A., Kröger, A., Schirmbeck, R., Reimann, J. & Hauser, H. (2001) Composition and arrangement of genes define the strength of IRES-driven translation in bicistronic mRNAs. *Nucleic Acids Research*, **29**, 3327-3334.
- Hines, M.L. & Carnevale, N.T. (2001) NEURON: a tool for neuroscientists. *Neuroscientist*, **7**, 123-135.
- Huberfeld, G., Menendez de la Prida, L., Pallud, J., Cohen, I., Le Van Quyen, M., Adam, C., Clemenceau, S., Baulac, M. & Miles, R. (2011) Glutamatergic pre-ictal discharges emerge at the transition to seizure in human epilepsy. *Nat Neurosci*, **14**, 627-634.
- Huberfeld, G., Wittner, L., Clemenceau, S., Baulac, M., Kaila, K., Miles, R. & Rivera, C. (2007a) Perturbed chloride homeostasis and GABAergic signaling in human temporal lobe epilepsy. *J Neurosci*, **27**, 9866-9873.
- Huberfeld, G., Wittner, L., Clemenceau, S., Baulac, M., Kaila, K., Miles, R. & Rivera, C. (2007b) Perturbed Chloride Homeostasis and GABAergic Signaling in Human Temporal Lobe Epilepsy. *The Journal of Neuroscience*, **27**, 9866-9873.
- Huberfeld, G., Wittner, L., Clemenceau, S.p., Baulac, M., Kaila, K., Miles, R. & Rivera, C. (2007c) Perturbed Chloride Homeostasis and GABAergic Signaling in Human Temporal Lobe Epilepsy. *The Journal of Neuroscience*, **27**, 9866-9873.
- Ibarz, J.M., Foffani, G., Cid, E., Inostroza, M. & Menendez de la Prida, L. (2010a) Emergent dynamics of fast ripples in the epileptic hippocampus. *J Neurosci*, **30**, 16249-16261.

- Ibarz, J.M., Foffani, G., Cid, E., Inostroza, M. & Menendez de la Prida, L. (2010b) Emergent Dynamics of Fast Ripples in the Epileptic Hippocampus. *The Journal of Neuroscience*, **30**, 16249-16261.
- Ilie, A., Raimondo, J.V. & Akerman, C.J. (2012) Adenosine Release during Seizures Attenuates GABAA Receptor-Mediated Depolarization. *The Journal of Neuroscience*, **32**, 5321-5332.
- Isomura, Y., Sugimoto, M., Fujiwara-Tsukamoto, Y., Yamamoto-Muraki, S., Yamada, J. & Fukuda, A. (2003) Synaptically Activated Cl⁻ Accumulation Responsible for Depolarizing GABAergic Responses in Mature Hippocampal Neurons. *Journal of Neurophysiology*, **90**, 2752-2756.
- Jack, J.J.B., Noble, D. & Tsien, R.W. (1975) *Electric Current Flow in Excitable Cells*. Oxford University Press, Oxford.
- Jackson, J.H. (1879) Lectures on the Diagnosis of Epilepsy. *British Medical Journal*, **1**, 109-112.
- Jiang, M. & Chen, G. (2006) High Ca²⁺-phosphate transfection efficiency in low-density neuronal cultures. *Nat. Protocols*, **1**, 695-700.
- Jin, X., Huguenard, J.R. & Prince, D.A. (2005) Impaired Cl⁻ Extrusion in Layer V Pyramidal Neurons of Chronically Injured Epileptogenic Neocortex. *Journal of Neurophysiology*, **93**, 2117-2126.
- Jirsch, J.D., Urrestarazu, E., LeVan, P., Olivier, A., Dubeau, F. & Gotman, J. (2006) High-frequency oscillations during human focal seizures. *Brain*, **129**, 1593-1608.
- Jiruska, P., Csicsvari, J., Powell, A.D., Fox, J.E., Chang, W.C., Vreugdenhil, M., Li, X., Palus, M., Bujan, A.F., Dearden, R.W. & Jefferys, J.G. (2010) High-frequency network activity, global increase in neuronal activity, and synchrony expansion precede epileptic seizures in vitro. *J Neurosci*, **30**, 5690-5701.
- Kahle, K.T., Staley, K.J., Nahed, B.V., Gamba, G., Hebert, S.C., Lifton, R.P. & Mount, D.B. (2008) Roles of the cation-chloride cotransporters in neurological disease. *Nat Clin Pract Neuro*, **4**, 490-503.
- Kaila, K., Lamsa, K., Smirnov, S., Taira, T. & Voipio, J. (1997) Long-Lasting GABA-Mediated Depolarization Evoked by High-Frequency Stimulation in Pyramidal Neurons of Rat Hippocampal Slice Is Attributable to a Network-Driven,

Bicarbonate-Dependent K⁺ Transient. *The Journal of Neuroscience*, **17**, 7662-7672.

Kaila, K., Price, T.J., Payne, J.A., Puskarjov, M. & Voipio, J. (2014) Cation-chloride cotransporters in neuronal development, plasticity and disease. *Nat Rev Neurosci*, **15**, 637-654.

Kaila, K., Voipio, J., Paalasmaa, P., Pasternack, M. & Deisz, R.A. (1993) The role of bicarbonate in GABAA receptor-mediated IPSPs of rat neocortical neurones. *The Journal of Physiology*, **464**, 273-289.

Kapfer, C., Glickfeld, L.L., Atallah, B.V. & Scanziani, M. (2007) Supralinear increase of recurrent inhibition during sparse activity in the somatosensory cortex. *Nat Neurosci*, **10**, 743-753.

Kätzel, D., Nicholson, E., Schorge, S., Walker, M.C. & Kullmann, D.M. (2014) Chemical-genetic attenuation of focal neocortical seizures. *Nat Commun*, **5**.

Klausberger, T. & Somogyi, P. (2008) Neuronal Diversity and Temporal Dynamics: The Unity of Hippocampal Circuit Operations. *Science*, **321**, 53-57.

Kleinlogel, S., Feldbauer, K., Dempsey, R.E., Fotis, H., Wood, P.G., Bamann, C. & Bamberg, E. (2011a) Ultra light-sensitive and fast neuronal activation with the Ca²⁺-permeable channelrhodopsin CatCh. *Nat Neurosci*, **14**, 513-518.

Kleinlogel, S., Terpitz, U., Legrum, B., Gokbuget, D., Boyden, E.S., Bamann, C., Wood, P.G. & Bamberg, E. (2011b) A gene-fusion strategy for stoichiometric and co-localized expression of light-gated membrane proteins. *Nat Meth*, **8**, 1083-1088.

Kouyama, T., Kanada, S., Takeguchi, Y., Narusawa, A., Murakami, M. & Ihara, K. (2010) Crystal Structure of the Light-Driven Chloride Pump Halorhodopsin from *Natronomonas pharaonis*. *Journal of Molecular Biology*, **396**, 564-579.

Krook-Magnuson E, Caren Armstrong, Oijala, M. & Soltesz, I. (2012) On-demand optogenetic control of spontaneous seizures in temporal lobe epilepsy. *Nature communications*, **4**.

Kullmann, D.M., Schorge, S., Walker, M.C. & Wykes, R.C. (2014) Gene therapy in epilepsy - is it time for clinical trials? *Nat Rev Neurol*, **10**, 300-304.

- Le Van Quyen, M., Bragin, A., Staba, R., Crépon, B., Wilson, C.L. & Engel, J. (2008) Cell Type-Specific Firing during Ripple Oscillations in the Hippocampal Formation of Humans. *The Journal of Neuroscience*, **28**, 6104-6110.
- Leao, A.A.P. (1944) Spreading depression of activity in the cerebral cortex. *J. Neurophysiol*, **7**, 359-390.
- Ledri, M., Madsen, M.G., Nikitidou, L., Kirik, D. & Kokaia, M. (2014) Global Optogenetic Activation of Inhibitory Interneurons during Epileptiform Activity. *The Journal of Neuroscience*, **34**, 3364-3377.
- Lee, H., Chen, C.X.-Q., Liu, Y.-J., Aizenman, E. & Kandler, K. (2005) KCC2 expression in immature rat cortical neurons is sufficient to switch the polarity of GABA responses. *European Journal of Neuroscience*, **21**, 2593-2599.
- Lillis, K.P., Kramer, M.A., Mertz, J., Staley, K.J. & White, J.A. (2012) Pyramidal cells accumulate chloride at seizure onset. *Neurobiology of Disease*, **47**, 358-366.
- Löscher, W. & Köhling, R. (2010) Functional, metabolic, and synaptic changes after seizures as potential targets for antiepileptic therapy. *Epilepsy & Behavior*, **19**, 105-113.
- Löscher, W., Puskarjov, M. & Kaila, K. (2013) Cation-chloride cotransporters NKCC1 and KCC2 as potential targets for novel antiepileptic and antiepileptogenic treatments. *Neuropharmacology*, **69**, 62-74.
- Lovett-Barron, M., Turi, G.F., Kaifosh, P., Lee, P.H., Bolze, F., Sun, X.-H., Nicoud, J.-F., Zemelman, B.V., Sternson, S.M. & Losonczy, A. (2012) Regulation of neuronal input transformations by tunable dendritic inhibition. *Nat Neurosci*, **15**, 423-430.
- Luhmann, H.J., Kirischuk, S. & Kilb, W. (2014a) Comment on "Local impermeant anions establish the neuronal chloride concentration". *Science*, **345**, 1130.
- Luhmann, H.J., Kirischuk, S., Sinning, A. & Kilb, W. (2014b) Early GABAergic circuitry in the cerebral cortex. *Current Opinion in Neurobiology*, **26**, 72-78.
- Maccaferri, G., Mangoni, M., Lazzari, A. & DiFrancesco, D. (1993) Properties of the hyperpolarization-activated current in rat hippocampal CA1 pyramidal cells. *Journal of Neurophysiology*, **69**, 2129-2136.

- Madisen, L., Mao, T., Koch, H., Zhuo, J.M., Berenyi, A., Fujisawa, S., Hsu, Y.W., Garcia, A.J., 3rd, Gu, X., Zanella, S., Kidney, J., Gu, H., Mao, Y., Hooks, B.M., Boyden, E.S., Buzsaki, G., Ramirez, J.M., Jones, A.R., Svoboda, K., Han, X., Turner, E.E. & Zeng, H. (2012) A toolbox of Cre-dependent optogenetic transgenic mice for light-induced activation and silencing. *Nat Neurosci*, **15**, 793-802.
- Markram, H., Toledo-Rodriguez, M., Wang, Y., Gupta, A., Silberberg, G. & Wu, C. (2004) Interneurons of the neocortical inhibitory system. *Nat Rev Neurosci*, **5**, 793-807.
- Martina, M., Schultz, J.H., Ehmke, H., Monyer, H. & Jonas, P. (1998) Functional and Molecular Differences between Voltage-Gated K⁺ Channels of Fast-Spiking Interneurons and Pyramidal Neurons of Rat Hippocampus. *The Journal of Neuroscience*, **18**, 8111-8125.
- Miles, R., Toth, K., Gulyas, A.I., Hajos, N. & Freund, T.F. (1996) Differences between somatic and dendritic inhibition in the hippocampus. *Neuron*, **16**, 815-823.
- Moshé, S.L., Perucca, E., Ryvlin, P. & Tomson, T. (2014) Epilepsy: new advances. *The Lancet*.
- Nagel, G., Szellas, T., Huhn, W., Kateriya, S., Adeishvili, N., Berthold, P., Ollig, D., Hegemann, P. & Bamberg, E. (2003) Channelrhodopsin-2, a directly light-gated cation-selective membrane channel. *Proceedings of the National Academy of Sciences*, **100**, 13940-13945.
- Nardou, R., Ben-Ari, Y. & Khalilov, I. (2009) Bumetanide, an NKCC1 Antagonist, Does Not Prevent Formation of Epileptogenic Focus but Blocks Epileptic Focus Seizures in Immature Rat Hippocampus. *Journal of Neurophysiology*, **101**, 2878-2888.
- Nardou, R., Yamamoto, S., Chazal, G., Bhar, A., Ferrand, N., Dulac, O., Ben-Ari, Y. & Khalilov, I. (2011) Neuronal chloride accumulation and excitatory GABA underlie aggravation of neonatal epileptiform activities by phenobarbital. *Brain*, pp. 987-1002.
- Netoff, T.I. & Schiff, S.J. (2002) Decreased Neuronal Synchronization during Experimental Seizures. *The Journal of Neuroscience*, **22**, 7297-7307.
- Nicoll, R.A., Malenka, R.C. & Kauer, J.A. (1990) Functional comparison of neurotransmitter receptor subtypes in mammalian central nervous system. *Physiological Reviews*, **70**, 513-565.

- Pallud, J., Le Van Quyen, M., Bielle, F., Pellegrino, C., Varlet, P., Labussiere, M., Cresto, N., Dieme, M.-J., Baulac, M., Duyckaerts, C., Kourdougli, N., Chazal, G., Devaux, B., Rivera, C., Miles, R., Capelle, L. & Huberfeld, G. (2014) Cortical GABAergic excitation contributes to epileptic activities around human glioma. *Science Translational Medicine*, **6**, 244ra289.
- Pascale, M.C., Malagolini, N., Serafini-Cessi, F., Migliaccio, G., Leone, A. & Bonatti, S. (1992) Biosynthesis and oligosaccharide structure of human CD8 glycoprotein expressed in a rat epithelial cell line. *Journal of Biological Chemistry*, **267**, 9940-9947.
- Paz, J.T., Davidson, T.J., Frechette, E.S., Delord, B., Parada, I., Peng, K., Deisseroth, K. & Huguenard, J.R. (2012) Closed-loop optogenetic control of thalamus as a tool for interrupting seizures after cortical injury. *Nature Neuroscience*, **16**, 64-70.
- Paz, J.T., Davidson, T.J., Frechette, E.S., Delord, B., Parada, I., Peng, K., Deisseroth, K. & Huguenard, J.R. (2013) Closed-loop optogenetic control of thalamus as a tool for interrupting seizures after cortical injury. *Nat Neurosci*, **16**, 64-70.
- Pei, Y., Rogan, S.C., Yan, F. & Roth, B.L. (2008) Engineered GPCRs as Tools to Modulate Signal Transduction. *Physiology*, **23**, 313-321.
- Peron, S. & Svoboda, K. (2011) From cudgel to scalpel: toward precise neural control with optogenetics. *Nat Meth*, **8**, 30-34.
- Pfeffer, C.K., Stein, V., Keating, D.J., Maier, H., Rinke, I., Rudhard, Y., Hentschke, M., Rune, G.M., Jentsch, T.J. & Hübner, C.A. (2009) NKCC1-Dependent GABAergic Excitation Drives Synaptic Network Maturation during Early Hippocampal Development. *The Journal of Neuroscience*, **29**, 3419-3430.
- Pfeffer, C.K., Xue, M., He, M., Huang, Z.J. & Scanziani, M. (2013) Inhibition of inhibition in visual cortex: the logic of connections between molecularly distinct interneurons. *Nat Neurosci*, **16**, 1068-1076.
- Pfisterer, C., Gruia, A. & Fischer, S. (2009) The Mechanism of Photo-energy Storage in the Halorhodopsin Chloride Pump. *Journal of Biological Chemistry*, **284**, 13562-13569.
- Plotkin, M.D., Kaplan, M.R., Peterson, L.N., Gullans, S.R., Hebert, S.C. & Delpire, E. (1997) Expression of the Na(+)-K(+)-2Cl⁻ cotransporter BSC2 in the nervous system. *American Journal of Physiology*, **272**, C173-C183.

- Pouille, F., Watkinson, O., Scanziani, M. & Trevelyan, A.J. (2013) The contribution of synaptic location to inhibitory gain control in pyramidal cells. *Physiological Reports*, **1**.
- Prince, D.A. & Wilder, B. (1967a) Control mechanisms in cortical epileptogenic foci*: "surround" inhibition. *Archives of Neurology*, **16**, 194-202.
- Prince, D.A. & Wilder, B.J. (1967b) Control mechanisms in cortical epileptogenic foci. "Surround" inhibition. *Arch Neurol*, **16**, 194-202.
- Puskarjov, M., Ahmad, F., Kaila, K. & Blaesse, P. (2012) Activity-Dependent Cleavage of the K-Cl Cotransporter KCC2 Mediated by Calcium-Activated Protease Calpain. *The Journal of Neuroscience*, **32**, 11356-11364.
- Rafiq, A., Zhang, Y.F., DeLorenzo, R.J. & Coulter, D.A. (1995) Long-duration self-sustained epileptiform activity in the hippocampal-parahippocampal slice: a model of status epilepticus. *Journal of Neurophysiology*, **74**, 2028-2042.
- Raimondo, J.V., Kay, L., Ellender, T.J. & Akerman, C.J. (2012) Optogenetic silencing strategies differ in their effects on inhibitory synaptic transmission. *Nat Neurosci*, **15**, 1102-1104.
- Rapp, M., Seppälä, S., Granseth, E. & von Heijne, G. (2007) Emulating Membrane Protein Evolution by Rational Design. *Science*, **315**, 1282-1284.
- Ricka, J. & Tanaka, T. (1984) Swelling of ionic gels: quantitative performance of the Donnan theory. *Macromolecules*, **17**, 2916-2921.
- Rivera, C., Voipio, J. & Kaila, K. (2005) Two developmental switches in GABAergic signalling: the K⁺-Cl⁻ cotransporter KCC2 and carbonic anhydrase CAVII. *The Journal of Physiology*, **562**, 27-36.
- Rivera, C., Voipio, J., Payne, J.A., Ruusuvuori, E., Lahtinen, H., Lamsa, K., Pirvola, U., Saarma, M. & Kaila, K. (1999) The K⁺/Cl⁻ co-transporter KCC2 renders GABA hyperpolarizing during neuronal maturation. *Nature*, **397**, 251-255.
- Rivera, C., Voipio, J., Thomas-Crusells, J., Li, H., Emri, Z., Sipilä, S., Payne, J.A., Minichiello, L., Saarma, M. & Kaila, K. (2004) Mechanism of Activity-Dependent Downregulation of the Neuron-Specific K-Cl Cotransporter KCC2. *The Journal of Neuroscience*, **24**, 4683-4691.

- Rogawski, M.A. (2010) Migraine and epilepsy: Shared mechanisms? *Epilepsia*, **51**, 80-80.
- Roopun, A.K., Simonotto, J.D., Pierce, M.L., Jenkins, A., Nicholson, C., Schofield, I.S., Whittaker, R.G., Kaiser, M., Whittington, M.A., Traub, R.D. & Cunningham, M.O. (2010) A nonsynaptic mechanism underlying interictal discharges in human epileptic neocortex. *Proceedings of the National Academy of Sciences*, **107**, 338-343.
- Rudy, B., Fishell, G., Lee, S. & Hjerling-Leffler, J. (2011) Three groups of interneurons account for nearly 100% of neocortical GABAergic neurons. *Developmental Neurobiology*, **71**, 45-61.
- Rudy, B. & McBain, C.J. (2001) Kv3 channels: voltage-gated K⁺ channels designed for high-frequency repetitive firing. *Trends in Neurosciences*, **24**, 517-526.
- Sanchez-Vives, M.V. & McCormick, D.A. (2000) Cellular and network mechanisms of rhythmic recurrent activity in neocortex. *Nat Neurosci*, **3**, 1027-1034.
- Santoro, B., Hu, L., Liu, H., Saponaro, A., Pian, P., Piskorowski, R.A., Moroni, A. & Siegelbaum, S.A. (2011) TRIP8b Regulates HCN1 Channel Trafficking and Gating through Two Distinct C-Terminal Interaction Sites. *The Journal of Neuroscience*, **31**, 4074-4086.
- Schevon, C.A., Trevelyan, A.J., Schroeder, C.E., Goodman, R.R., McKhann, G. & Emerson, R.G. (2009) Spatial characterization of interictal high frequency oscillations in epileptic neocortex. *Brain*, **132**, 3047-3059.
- Schevon, C.A., Weiss, S.A., Jr, G.M., Goodman, R.R., Yuste, R., Emerson, R.G. & Trevelyan, A.J. (2012) Evidence of an inhibitory restraint of seizure activity in humans. *Nature communications*, **3**.
- Schwartz, T.H. & Bonhoeffer, T. (2001) In vivo optical mapping of epileptic foci and surround inhibition in ferret cerebral cortex. *Nat Med*, **7**, 1063-1067.
- Seppala, S., Slusky, J.S., Lloris-Garcera, P., Rapp, M. & von Heijne, G. (2010) Control of Membrane Protein Topology by a Single C-Terminal Residue. *Science*, **328**, 1698-1700.
- Shepherd, G.M. (2004) *The Synaptic Organisation of the Brain*.

- Sik, A., Penttonen, M., Ylinen, A. & Buzsáki, G. (1995) Hippocampal CA1 interneurons: an in vivo intracellular labeling study. *The Journal of Neuroscience*, **15**, 6651-6665.
- Skaggs, W.E., McNaughton, B.L., Permenter, M., Archibeque, M., Vogt, J., Amaral, D.G. & Barnes, C.A. (2007) EEG Sharp Waves and Sparse Ensemble Unit Activity in the Macaque Hippocampus. *Journal of Neurophysiology*, **98**, 898-910.
- Somjen, G.G. (2004) *Ions in the brain*. Oxford University Press, New York.
- Somjen, G.G., Aitken, P.G., Giacchino, J.L. & McNamara, J.O. (1985) Sustained potential shifts and paroxysmal discharges in hippocampal formation. *Journal of Neurophysiology*, **53**, 1079-1097.
- Somjen, G.G. & Giacchino, J.L. (1985) Potassium and calcium concentrations in interstitial fluid of hippocampal formation during paroxysmal responses. *Journal of Neurophysiology*, **53**, 1098-1108.
- Sommer, N., Junne, T., Kalies, K.-U., Spiess, M. & Hartmann, E. (2013) TRAP assists membrane protein topogenesis at the mammalian ER membrane. *Biochimica et Biophysica Acta (BBA) - Molecular Cell Research*, **1833**, 3104-3111.
- Staba, R.J., Wilson, C.L., Bragin, A., Fried, I. & Engel, J., Jr. (2002) Quantitative analysis of high-frequency oscillations (80-500 Hz) recorded in human epileptic hippocampus and entorhinal cortex. *J Neurophysiol*, **88**, 1743-1752.
- Staley, K.J. & Mody, I. (1992) Shunting of excitatory input to dentate gyrus granule cells by a depolarizing GABA_A receptor-mediated postsynaptic conductance. *Journal of Neurophysiology*, **68**, 197-212.
- Staley, K.J., Soldo, B.L. & Proctor, W.R. (1995) Ionic mechanisms of neuronal excitation by inhibitory GABA_A receptors. *Science*, **269**, 977-981.
- Sukhotinsky, I., Chan, A.M., Ahmed, O.J., Rao, V.R., Gradinaru, V., Ramakrishnan, C., Deisseroth, K., Majewska, A.K. & Cash, S.S. (2013) Optogenetic Delay of Status Epilepticus Onset in an In Vivo Rodent Epilepsy Model. *PLoS ONE*, **8**, e62013.
- Szabadics, J., Varga, C., Molnár, G., Oláh, S., Barzó, P. & Tamás, G. (2006) Excitatory Effect of GABAergic Axo-Axonic Cells in Cortical Microcircuits. *Science*, **311**, 233-235.

- Tamas, G., Buhl, E.H., Lorincz, A. & Somogyi, P. (2000) Proximally targeted GABAergic synapses and gap junctions synchronize cortical interneurons. *Nat Neurosci*, **3**, 366-371.
- Tang, W., Ehrlich, I., Wolff, S.B.E., Michalski, A.-M., Wölfel, S., Hasan, M.T., Lüthi, A. & Sprengel, R. (2009) Faithful Expression of Multiple Proteins via 2A-Peptide Self-Processing: A Versatile and Reliable Method for Manipulating Brain Circuits. *The Journal of Neuroscience*, **29**, 8621-8629.
- Tate, C.G. (2010) Membrane Protein Gymnastics. *Science*, **328**, 1644-1645.
- Thompson, S.M. & Gähwiler, B.H. (1989a) Activity-dependent disinhibition. I. Repetitive stimulation reduces IPSP driving force and conductance in the hippocampus in vitro. *Journal of Neurophysiology*, **61**, 501-511.
- Thompson, S.M. & Gähwiler, B.H. (1989b) Activity-dependent disinhibition. III. Desensitization and GABAB receptor-mediated presynaptic inhibition in the hippocampus in vitro. *Journal of Neurophysiology*, **61**, 524-533.
- Töllner, K., Brandt, C., Töpfer, M., Brunhofer, G., Erker, T., Gabriel, M., Feit, P.W., Lindfors, J., Kaila, K. & Löscher, W. (2014) A novel prodrug-based strategy to increase effects of bumetanide in epilepsy. *Annals of Neurology*, **75**, 550-562.
- Tønnesen, J., Sørensen, A.T., Deisseroth, K., Lundberg, C. & Kokaia, M. (2009) Optogenetic control of epileptiform activity. *Proceedings of the National Academy of Sciences*, **106**, 12162-12167.
- Traub, R.D. & Bibbig, A. (2000) A Model of High-Frequency Ripples in the Hippocampus Based on Synaptic Coupling Plus Axon–Axon Gap Junctions between Pyramidal Neurons. *The Journal of Neuroscience*, **20**, 2086-2093.
- Traub, R.D., Bibbig, A., LeBeau, F.E.N., Buhl, E.H. & Whittington, M.A. (2004) Cellular Mechanisms of Neuronal Population Oscillations in the Hippocampus in vitro. *Annual Review of Neuroscience*, **27**, 247-278.
- Traub, R.D., Jefferys, J.G.R. & Whittington, M.A. (1999) *Fast oscillations in cortical circuits*. Massachusetts Institute of Technology.
- Trevelyan, A.J. (2009) The direct relationship between inhibitory currents and local field potentials. *J Neurosci*, **29**, 15299-15307.

- Trevelyan, A.J., Baldeweg, T., van Drongelen, W., Yuste, R. & Whittington, M. (2007a) The source of afterdischarge activity in neocortical tonic-clonic epilepsy. *J Neurosci*, **27**, 13513-13519.
- Trevelyan, A.J., Sussillo, D., Watson, B.O. & Yuste, R. (2006a) Modular Propagation of Epileptiform Activity: Evidence for an Inhibitory Veto in Neocortex. *The Journal of Neuroscience*, **26**, 12447-12455.
- Trevelyan, A.J., Sussillo, D., Watson, B.O. & Yuste, R. (2006b) Modular propagation of epileptiform activity: evidence for an inhibitory veto in neocortex. *J Neurosci*, **26**, 12447-12455.
- Trevelyan, A.J., Sussillo, D. & Yuste, R. (2007b) Feedforward Inhibition Contributes to the Control of Epileptiform Propagation Speed. *The Journal of Neuroscience*, **27**, 3383-3387.
- Viitanen, T., Ruusuvuori, E., Kaila, K. & Voipio, J. (2010) The K⁺-Cl⁻ cotransporter KCC2 promotes GABAergic excitation in the mature rat hippocampus. *The Journal of Physiology*, **588**, 1527-1540.
- Voipio, J., Boron, W.F., Jones, S.W., Hopfer, U., Payne, J.A. & Kaila, K. (2014) Comment on "Local impermeant anions establish the neuronal chloride concentration". *Science*, **345**, 1130.
- von Heijne, G. (1992) Membrane protein structure prediction: Hydrophobicity analysis and the positive-inside rule. *Journal of Molecular Biology*, **225**, 487-494.
- Wang, X., Zhang, C., Szábo, G. & Sun, Q.-Q. (2013) Distribution of CaMKII α expression in the brain in vivo, studied by CaMKII α -GFP mice. *Brain Research*, **1518**, 9-25.
- Waseem, T., Mukhtarov, M., Buldakova, S., Medina, I. & Bregestovski, P. (2010) Genetically encoded Cl-Sensor as a tool for monitoring of Cl-dependent processes in small neuronal compartments. *Journal of Neuroscience Methods*, **193**, 14-23.
- Wei, Y., Ullah, G. & Schiff, S.J. (2014) Unification of Neuronal Spikes, Seizures, and Spreading Depression. *The Journal of Neuroscience*, **34**, 11733-11743.
- Wiebe, S., Blume, W.T., Girvin, J.P. & Eliasziw, M. (2001) A Randomized, Controlled Trial of Surgery for Temporal-Lobe Epilepsy. *New England Journal of Medicine*, **345**, 311-318.

- Wietek, J., Wiegert, J.S., Adeishvili, N., Schneider, F., Watanabe, H., Tsunoda, S.P., Vogt, A., Elstner, M., Oertner, T.G. & Hegemann, P. (2014) Conversion of Channelrhodopsin into a Light-Gated Chloride Channel. *Science*, **344**, 409-412.
- Wilson, M.A. & McNaughton, B.L. (1994) Reactivation of hippocampal ensemble memories during sleep. *Science*, **265**, 676-679.
- Wykes, R.C., Heeroma, J.H., Mantoan, L., Zheng, K., MacDonald, D.C., Deisseroth, K., Hashemi, K.S., Walker, M.C., Schorge, S. & Kullmann, D.M. (2012) Optogenetic and Potassium Channel Gene Therapy in a Rodent Model of Focal Neocortical Epilepsy. *Science Translational Medicine*, **4**, 161ra152.
- Yamada, J., Okabe, A., Toyoda, H., Kilb, W., Luhmann, H.J. & Fukuda, A. (2004) Cl⁻ uptake promoting depolarizing GABA actions in immature rat neocortical neurones is mediated by NKCC1. *The Journal of Physiology*, **557**, 829-841.
- Zhang, F., Gradinaru, V., Adamantidis, A.R., Durand, R., Airan, R.D., Lecea, L.d. & Deisseroth, K. (2010) Optogenetic interrogation of neural circuits: technology for probing mammalian brain structures. *Nature Protocols*, **5**, 439-455.
- Zhang, F., Prigge, M., Beyriere, F., Tsunoda, S.P., Mattis, J., Yizhar, O., Hegemann, P. & Deisseroth, K. (2008) Red-shifted optogenetic excitation: a tool for fast neural control derived from *Volvox carteri*. *Nat Neurosci*, **11**, 631-633.
- Zhang, F., Vierock, J., Yizhar, O., Fenno, L.E., Tsunoda, S., Kianianmomeni, A., Prigge, M., Berndt, A., Cushman, J., Polle, J., Magnuson, J., Hegemann, P. & Deisseroth, K. (2011) The Microbial Opsin Family of Optogenetic Tools. *Cell*, **147**, 1446-1457.
- Zhang, X.-B. (2013) Cellular Reprogramming of Human Peripheral Blood Cells. *Genomics, Proteomics & Bioinformatics*, **11**, 264-274.
- Zhang, Z.J., Koifman, J., Shin, D.S., Ye, H., Florez, C.M., Zhang, L., Valiante, T.A. & Carlen, P.L. (2012) Transition to Seizure: Ictal Discharge Is Preceded by Exhausted Presynaptic GABA Release in the Hippocampal CA3 Region. *The Journal of Neuroscience*, **32**, 2499-2512.
- Zhao, S., Cunha, C., Zhang, F., Liu, Q., Gloss, B., Deisseroth, K., Augustine, G.J. & Feng, G. (2008) Improved expression of halorhodopsin for light-induced silencing of neuronal activity. *Brain Cell Biol*, **36**, 141-154.

